Advanced Neutron Moderators for the ESS

Schönfeldt, Troels

Publication date:
2016

Document Version
Publisher's PDF, also known as Version of record

Advanced Neutron Moderators for the ESS

Ph.d. Thesis by Troels Schönfeldt

October 2016

Abstract (Danish)

Termiske og kolde neutroner benyttes i en bred vifte af eksperimenter til undersøgelse af materialeegenskaber på længdeskalaer under 1 mikrometer. Neutroner bliver typisk produceret på reaktorer eller spallations kilder,og bliver kølet til termiske og kolde energier i neutron moderatorer. Den største forøgelse i termisk og kold intensitet opnås ved at opskallere effekt-tætheden ved reaktorer eller effekten af protonstråle ved spallations kilder. Reaktorudviklingen nåede sit maksimum i 1960erne med opførelsen af de kontinuerte, kompakte, høj-effekt-tæthed reaktorer ILL i Grenoble og HFIR i Oak Ridge. Disse kilder er de mest intense neutronkilder til dato. Kort-puls kilderne SNS og J-PARC er de kraftigste spallations kilder i verden; på trods af, at de er mindre intense end ILL og HFIR, leverer disse kilder flere brugbare neutroner, grundet deres kort-puls stråle struktur.

Denne afhandling fokuserer på den Europæiske Spallations Kilde (ESS), som er under opførelse i Lund, Sverige. ESS bliver en lang-puls spallations kilde (2,86 ms) drevet af en 5-MW protonstråle som skydes på et roterende wolfram hjul. ESS bliver verdens mest intense neutron kilde, målt i brillians, og vil være den første spallations kilde som bliver i stand til at udkonkurrere reaktorkilder i integreret intensitet af termiske og kolde neutroner.

På moderne faciliteter bruger eksperimenter mindre end en ud af en million neutroner som bliver skabt i kilden. Meget af denne ineffektivitet kan tillægges moderator systemet. Imperfektionerne i moderator systemet kommer fra isotropien af neutronierne i opbremsnings- og termaliserings-processerne, samt for tidlig undslippelse fra systemet, neutron absorption samt suboptimale geometriske konfigurationer. Ineffektiviteten af moderator systemer indikerer en potentielt gevinst i effektiviteten af neutron kilder, hvilket afføder en stor interesse i moderator udvikling. Mange faciliteter har foreslået og implementeret avancerede moderator koncepter. Emnet for denne afhandling er studier af disse avancerede moderator-koncepter.

Kapitel 1 til 6 giver en hurtig gennemgang af den historiske udvikling af neutronkilder, herunder ESS. Derpå bliver bliver den drivende fysik og de bagvedliggende principper for neutronkilder og avancerede moderatorer gennemgået. **Kapitel 7 til 10** (uddybet nedenfor) præsentere nyskabende arbejde i form af tre artikler (to publiceret og en indsendt) og to konferencebidrag.

Kapitel 7 består af to konferencebidrag og beskriver udviklingen af ESS moderator systemet, fra det forslåede design i den Tekniske Design Report (TDR) til den nye udgangspunkts moderator (accepteret i marts 2015), kendt som sommerfugl-moderatoren. Denne afhandling opridser udviklingsprocessen fra det oprindelige TDR design via det såkaldte pandekage-design til det endelige sommerfugle-design og præsenterer de relaterede nøgleresultater. Ultimativt vises det, at det nye design og den relaterede optimering resulterer i en signifikant forøgelse af den kolde og termiske brillans relativt til TDR designet.

Kapitel 8 er et studie, hvor MCNPX simulationer bliver overført til ROOT og analyseret. Der udvikles en metode til at rekonstruere den fulde emissions-fordeling af brilliansen fra moderatorsystemet. Studiet undersøger såvel pandekage- som sommerfugldesignet (sidstnævnte dog i et appendix). Brillans fordelingen bliver tilpasset til analytiske funktioner, som er blevet implementeret i McStas. Dette muliggør meget mere præcise forudsigelser til forventningerne fra ESS, hvilke er et centralt krav til eksper-

imenter ved ESS, men muliggør desuden signifikant bedre optimeringer af eksperimenter forud for deres udføresel. Disse forbedringer forventes at bidrage signifikant til kvaliteten af ESS.

Kapitel 9 forslår en ny type bred-spektrum moderator. Dette koncept baserer sig på tungmetallers begrænsede evne til at moderere. Artiklen undersøger konceptet ved hjælp af studier af beriget ^{208}Pb. Det vises, at dette materiales manglende evne til at moderere neutroner kan udnyttes til at designe en moderator, som reflekterer neutroner fra omkringliggende moderatorer med forskellige spektre, uden at ændre betydeligt på neutronernes energi. Dette medføre, at bly-elementet vil udstråle et bredt neutron spektrum. Da bly desuden kan anvendes som reflektor-filter, kan geometrien konfigureres således, at bred-spektrum bly moderatoren også virker som et reflektor filter for en kold moderator placeret bag den. Dette giver en yderligere forøgelse af neutroner med energi under Bragg-kanten for bly, uden at det brede spektrum ofres.

Kapitel 10 er en eksperimentalt artikel. Eksperimentet blev udført i forbindelse med LENS kollaborationen. Eksperimentet undersøger enkrystal reflektor-filter konceptet, der muliggør at et reflektor-filter kan transmittere neutroner i det termiske energy område, grundet den delta-funktion lignende Braggkant i et enkrystal. Eksperimentet sammenligner enkrystal safir, safir pulver og vakuum. Safir blev anvendt, fordi ingen andre enkeltkrystaller var til rådighed indenfor eksperimentets tids- og pris-rammer. Desværre resulterer safir ikke i en nævneværdig forøgelse af neutroner, men eksperimentet viser at et enkrystal reflektor-filter kan anvendes i praksis og indikerer desuden at et sådant filter vil forøge antallet af termiske neutroner, som ville være tabt med et konventionelt reflektor-filter.

Abstract

Thermal and cold neutrons are used in a wide array of different experiments investigating the sub-micrometer properties of matter. Neutrons are typically produced at reactor or spallation sources and subsequently cooled to the wanted thermal or cold energy levels by employing neutron moderators. The main increases in thermal and cold intensity are achieved by upscaling the power density of reactors or proton beam power of spallation sources. Reactor development saturated in the 1960s with the construction of the continuous, compact, high-power-density reactors HFIR, Oak Ridge, and ILL, Grenoble. Today these sources are still the most intense neutron sources. The short-pulsed sources SNS and J-PARC are the most powerful spallation sources in the world; although less intense than ILL and HFIR, these sources provide more useful neutrons because of their pulsed beam structure.

This thesis focuses on the European Spallation Source (ESS), which is currently being constructed in Lund, Sweden. The ESS will be a long-pulsed spallation source (pulse length 2.86 ms) driven by a 5-MW proton beam impinging on a rotating tungsten target. The ESS will be the world's most intense neutron source in terms of brightness, but it will also be the first spallation source to outperform reactors in terms of the integrated intensity of thermal and cold neutrons.

Experiments at modern facilities use less than one millionth of the neutrons created in neutron source. Much of this inefficiency can be attributed to the moderator system. The imperfections of moderator systems originate from the highly isotropic slowing-down and thermalizing processes, premature leakage (fast neutron escape), neutron absorption and suboptimal geometrical configurations. The inefficiency of moderator systems implies a potential gain in efficiency for neutron sources, which generates an interest in moderator development. Many facilities have proposed and applied advanced moderator concepts to better utilize the produced neutrons. The topic of this thesis is the study of these advanced moderator concepts..

Chapters 1 to 6 briefly summarize the historical development of neutron sources. The ESS is briefly introduced. Then the governing physics is outlined as well as the main principles behind neutron sources and advanced moderators. **Chapters 7 to 10** (further detailed below) present novel work in the form of three papers (two published articles, one submitted) and two conference proceedings.

Chapter 7 comprises two conference proceedings and describes the development from the moderator system at the ESS suggested in the Technical Design Report (TDR) to the new moderator baseline (accepted in March 2015), known as the butterfly moderator. The chapter outlines the development process from TDR through the pancake moderator and to the butterfly moderator, and presents various key results. Ultimately, it is shown how this redesign and optimization results in a significant increase in cold and thermal brightness relative to the TDR proposal.

Chapter 8 is a study in which MCNPX simulations are transferred to ROOT and analyzed. A method for reconstructing the full emission distribution of the moderator brightness is developed. The ESS pancake moderator (and butterfly moderator in the sub-appendix) is studied. The brightness distributions are fitted to analytical functions that have been implemented in McStas. This enables more precise predictions of the expectations from ESS, which is not only a key requirement for experiments at ESS but also enables neutron instruments to be significantly better optimized before their

construction. This, in turn, is expected to contribute significantly to the overall quality of the ESS.

Chapter 9 suggests a novel type of broad-spectrum moderator. This moderator concept is based on the idea that heavy metals, such as lead and bismuth, are inefficient moderator materials. The article investigates this idea through enriched ^{208}Pb. The article shows that the inability of these materials to moderate can be exploited to design a moderator that reflects neutrons from surrounding moderators of different spectral temperatures, with little change in energy. This results in the emission of a broad neutron spectrum (or multiple spectra) from the lead element. Since lead can also serve as a reflector filter, the geometry can be configured such that the broad-spectrum lead moderator acts as a reflector filter for a cold moderator positioned behind it, thus increasing the neutron yield below the lead Bragg edge whilst still producing a broad spectrum of neutrons.

Chapter 10 is an experimental paper carried out in the framework of the LENS collaboration. The experiment investigates the concept of a single-crystal reflector filter – a reflector filter that also transmit neutrons in the thermal energy range because of the delta-function-like Bragg edge in a single crystal. The experiment compares single-crystal sapphire, sapphire powder and void. Sapphire was used, since no other single-crystal candidates (diamond, pyrolytic graphite and lithium fluoride) could be obtained within the cost and time constraints of the experiment. Unfortunately, sapphire does not notably increase neutron yield, but the experiment proves the viability of a single-crystal reflector filter and indicates a potential regain of the thermal neutrons lost to a conventional reflector filter, with little or no loss of the cold neutrons below the Bragg edge.

Acknowledgements

First and foremost I thank my good friend and colleague Esben B. Klinkby, who has greatly contributed to my work throughout this PhD study. Through collaboration, conversation and bouncing of ideas, Esben has significantly improved the quality, and enjoyment, of my study and my work and has been involved in every aspect of it.

I thank my colleagues Konstantin Batkov and Alan Takibayev from the neutronics group at the ESS for providing tools, models and general knowledge of the ESS and for our enriching weekly discussions. It has been a pleasure working with you. Erik Nonbøl from the neutronics team of the Center for Nuclear Technologies of the Technical University of Denmark has also been a great asset through his experience in and knowledge of neutronics and reactors.

I am very grateful to the entire neutronics community for welcoming me into this field. I especially thank the LENS collaboration for welcoming me and providing me with the opportunity to participate in our exciting experiments. In particular, I thank Erik Iverson and Günter Muhrer for their patient and inspiring guidance throughout this project. Their enthusiasm, experience and knowledge have been highly valued, and our intense discussions have significantly improved the quality of this study. I am also grateful to David Baxter, Franz X. Gallmeier, Thomas Hügle and Michael Mocko for contributing to my work through our experimental collaboration and regular meetings and for the tours they have enabled at their home facilities. Although Tom Rinckel was not an active part of the LENS collaboration, I recognize his key role in facilitating our experiments at LENS.

At the ESS, I also thank Ferenc Mezei and Eric Pitcher for their experience and inspiration, which has been highly valuable. Their professional support, along with the neutronics team and the staff at ESS, especially Daniel Lyngh and the team of moderator engineers, has been essential for implementing the butterfly moderator concept at the ESS and thus enabling a key part of this project and this thesis. I also acknowledge the importance of the extensive work by Mads Bertelsen in this implementation process.

On a personal level, I thank those close to me, friends, family and Ølsnedkeren, for supporting me through this project. I also thank the crew at Seaborg Technologies for providing excitement through the somewhat dull finalizing phase of this study.

Last, but not least, I profoundly thank my great supervisors: Bent Lauritzen, Peter K. Willendrup and Luca Zanini. You have provided me with this great opportunity, for which I express my sincerest gratitude. I have appreciated your outstanding supervision, each of you with a unique perspective. You have my reverential respect for providing me with this foundation from which to take off.

Funding provided by the European Spallation Source and Center for Nuclear Technologies of the Technical University of Denmark enabled this project. Seaborg Technologies provided my salary in the final year of this project.

Contents

1 Introduction to this thesis **1**

1.1 Motivation for an advanced moderator 1

1.2 Outline of this thesis 2

1.3 My contribution to the field 2

1.3.1 Flat moderators and the butterfly moderator (Chapter 7) 2

1.3.2 Interfacing from moderator to instrument (Chapter 8) 5

1.3.3 The non-moderating bi-spectral moderator (Chapter 9) 7

1.3.4 Experimental development of moderators (Chapter 10) 9

2 European Spallation Source **11**

2.1 Accelerator 11

2.2 Target station 11

2.3 Instrument suite 14

3 Spallation **17**

3.1 Spallation process 17

3.2 Spallation neutron sources 20

3.2.1 Considerations for the best target material 20

4 Moderator neutronics **25**

4.1 Kinematic elastic scattering – slowing neutrons down 25

4.2 Scattering of neutrons by matter 26

4.2.1 Scattering intensity 27

4.2.2 Momentum transfer 29

4.2.3 Thermalization 34

4.2.4 Cold moderators 36

5 Designing advanced moderators **41**

5.1 Figure of merit 41

5.2 The basics of moderators 43
5.2.1 Pre-moderators and reflectors 44
5.2.2 Quick guide for moderator designers 45
5.2.3 Cooling and engineering 46
5.2.4 Wing versus slab geometry 47
5.3 Cavities, grooves and re-entrant holes 48

6 State-of-the-art moderator concepts 51
6.1 Convoluted moderator 51
6.2 Reflector filters 52
6.3 Single-crystal reflector filters 53
6.4 Decoupled and poisoned moderators 54
6.4.1 Note on time resolution 54
6.4.2 Decoupling and poisoning 55
6.5 Backscattering moderator 55
6.6 Pellets 56
6.7 Flux trap 56
6.8 Bispectral moderators 57
6.9 Parahydrogen moderators 58
6.9.1 Flat moderators 60

7 Disc-shaped and butterfly moderators 63
7.1 Development of the butterfly moderator 72
7.2 Estimating the neutron background 82

8 Neutron extraction at the ESS 85

9 A bispectral moderator using lead 123

10 Single-crystal reflector filter experiment 129

11 Summary 137

Chapter 1

Introduction to this thesis

1.1 Motivation for an advanced moderator

The insatiable desire for more cold and thermal neutrons for science applications has driven the development of neutron sources since Enrico Fermi et al. discovered the concept of moderation and the thermal neutron reactions [1].

The task of supplying cold and thermal neutrons for experiments has three parts: neutron sources, neutron moderators and neutron instrumentation. This thesis focuses on advanced neutron moderators.

The best neutron sources today are compact high-power density reactors dedicated to neutron research and high-power spallation sources driven by state-of-the-art accelerators. Throughout history, neutron availability has mainly increased from the development of neutron reactors or spallation sources. The development of reactor sources peaked in the late 1960s with the high-flux isotope reactor (HFIR [2]) and Institut Laue-Langevin high-flux reactor (ILL [3]), which maximized the compactness and pushed the limits of power density. Since then, spallation sources have exceeded reactor sources in terms of "effective neutron flux", and the coming commissioning of the European Spallation Source (ESS) will enable spallation sources to take the lead in terms of time-averaged flux – despite being a pulsed source [4].

Although making reactors more compact and scaling up spallation neutron sources has resulted in most of the increase in neutron availability, moderators are key in producing thermal and cold neutrons. Throughout history, moderators have developed slowly, with few large (more than a factor of 2) steps forward. Knowledge of moderator materials, favorable geometrical configurations and using advanced moderator concepts are essential in increasing useful neutron production. Further, development in neutron optics, detectors and related instrumentation equipment and techniques has facilitated much better exploitation of the available neutrons, thus contributing significantly to the quality and efficiency of experiments.

Despite the development of moderators and instruments, experiments still only use less than one millionth [5] of the neutrons created at the source. As a result there exist significant potential for improvement. For instance, a successful concept for a directional moderator could potentially gain many orders of magnitude in useful neutrons.

The neutron moderator is the device between the neutron source and the neutron

instrument. Its role is to reduce the kinetic energy of the neutrons to the energy required for the applications of interest. For neutron scattering, this energy is in the meV-range. In the discovery the thermal neutron reaction it was realized that hydrogenous materials play a key role in moderation [1]. Today, most moderators are still composed of hydrogenous materials.

1.2 Outline of this thesis

Chapters 2 to 6 briefly introduce the ESS, spallation physics, moderator neutronics, moderator design and state-of-the-art advanced moderator concepts. I mainly present my contribution to this field in Chapters 7 to 10 and briefly outline this in the sections below.

For more information on neutron sources, and their use, implementation and physics, I recommend Filges & Goldenbaum's "Handbook of spallation research" [6] and Carpenter & Yelon's chapter "Neutron sources" in "Neutron scattering" (Methods in Experimental Physics, Volume 23) [7]. For more specific details on moderator physics, I recommend consulting Carpenter's essay "Neutron production, moderation, and characterization of sources" [8] and Muhrer's article "Urban legends of thermal moderator design" [9]. Enrico Fermi's original notes from 1936 on neutron physics [1] are also worth reading.

1.3 My contribution to the field

The novel work of this thesis is presented in three papers (two published and one submitted) and two conference proceedings, divided into four chapters (Chapters 7 to 10), each focusing on different aspects of moderator physics and design: technical work, developing methods, developing new concepts and experimentally verifying new concepts. More specifically, the four topics are:

- designing, optimizing and developing the new baseline moderator system of the ESS (Chapter 7);
- developing methods and tools for the neutron science community, including important interfacing between moderators and instruments (Chapter 8);
- a novel concept for producing inherently bispectral moderators – using the poor moderating properties of heavy elements (Chapter 9); and
- experimental work on advanced moderator concepts carried out under the Low Energy Neutron Source (LENS) collaboration, at Indiana University (Chapter 10).

These chapters are presented in more detail below.

1.3.1 Flat moderators and the butterfly moderator (Chapter 7)

The work carried out as part of this thesis revolves around the ESS: a long-pulse source currently being constructed in Lund, Sweden. With its 5 MW proton beam power, the

ESS will be the most powerful spallation source ever built. The ESS will free neutrons from heavy nuclei through spallation, driven by a 2 GeV proton beam impinging on a rotating tungsten wheel. The ESS technical design report (TDR) [4] presented the initial design for the ESS moderators. Figure 1.1 shows the geometrical configuration. The TDR configuration cools neutrons down to thermal and cold energy in two moderator systems: one above and one below the target. Neutron scattering instruments will extract thermal and cold neutrons 2 m from the moderator and transport them to experiments placed up to 200 m away using neutron optics.

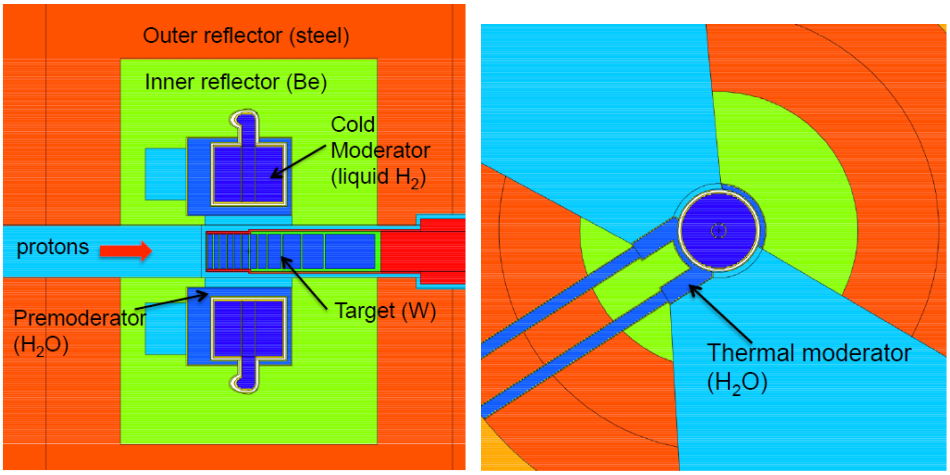

(a) TDR side view (b) TDR top view

Figure 1.1: Vertical and horizontal cross-section of the TDR moderator configuration for ESS. Two 12 cm tall moderator systems are positioned above and below the target. Each moderator system comprises a room-temperature water moderator and a 20 K cold parahydrogen moderator. Both the water and the parahydrogen moderator can be viewed from 2×60° beam openings for each of the two moderator systems, yielding a total of 240° opening view for experiments. Source: [4].

Batkov et al. [10] initiated the investigation of flat moderators at the ESS with a potential increase in cold brightness larger than a factor of 2. To study this option in detail and possibly change the TDR configuration, investigations began in both the science division and neutronics group. Figure 1.3 shows a side view of one of the early models being investigated; Figure 1.4a shows a horizontal cross-section.

Within this PhD project, I was involved in investigating and optimizing with the aim of assessing how to implement a flat moderator at the ESS. In this process, I identified one issue with the flat moderator in relation to the work presented in Chapter 8. With the disc-shaped flat moderator, the thermal moderator was positioned far away from the cold hotspot (the maximum in cold neutron intensity - see more in Chapter 7 and 8) to be efficient for bispectral extraction using a mirror. This is problematic, since the possibility of bispectral extraction is a fundamental requirement for the ESS [4]. Further, it was discovered that the emission distribution of neutrons from the thermal moderator extensions was decreasing on a centimeter scale (Chapter 8).

At the ESS, these issues were finally solved by redesigning the moderator system as a butterfly moderator system, a concept I envisioned and initially investigated within this PhD project based on concepts and development carried out by the ESS neutronics group. The butterfly moderator is still a flat moderator concept, but in contrast to

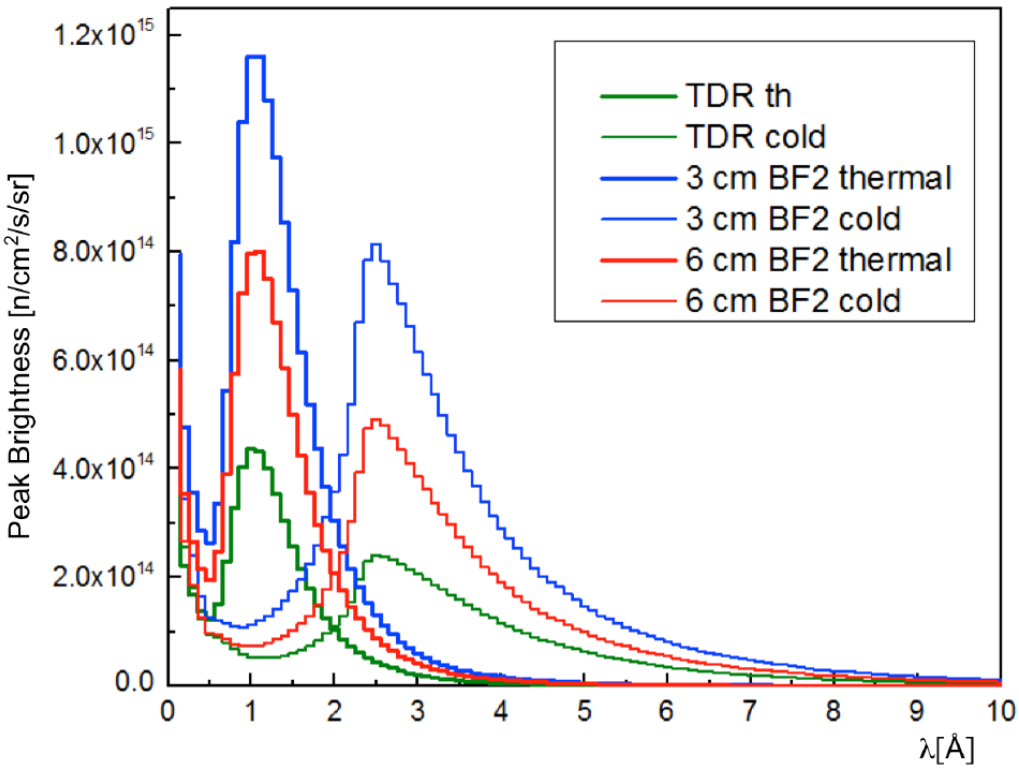

Figure 1.2: Comparison between the TDR moderator brightness spectrum and the butterfly moderator (BF) spectrum, in a 3 cm tall and a 6 cm tall configuration. From Chapter 7.

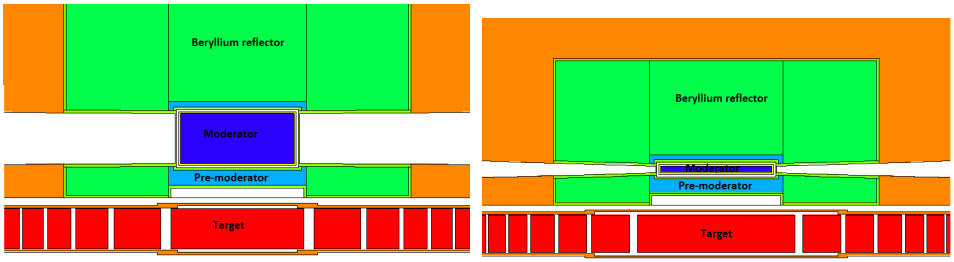

(a) Tall moderator (10 cm) (b) Flat moderator (1.5 cm)

Figure 1.3: Vertical cross-section of the flat and tall moderator geometrical configurations, illustrated here using a disc-shaped moderator, as seen in Figure 1.4a.

the disc-shaped moderator, the ambient-temperature water moderator is positioned centrally, with two cold moderators on each side (Figure 1.4b). The butterfly not only facilitates bispectral extraction but also preserves the high cold brightness from the disc-shaped moderators and significantly increases the thermal brightness in its currently planned configuration. The resulting brightness spectrum from a 3 cm and a 6 cm tall butterfly moderator is observed in Figure 1.2 compared to the TDR moderator configuration.

The ESS finally accepted the butterfly moderator as the new baseline in March 2015 [11, 12, 13]. The moderator system will comprise two butterfly moderators: a flat (3 cm tall) moderator above the target, resulting in a brightness factor of about 2.5

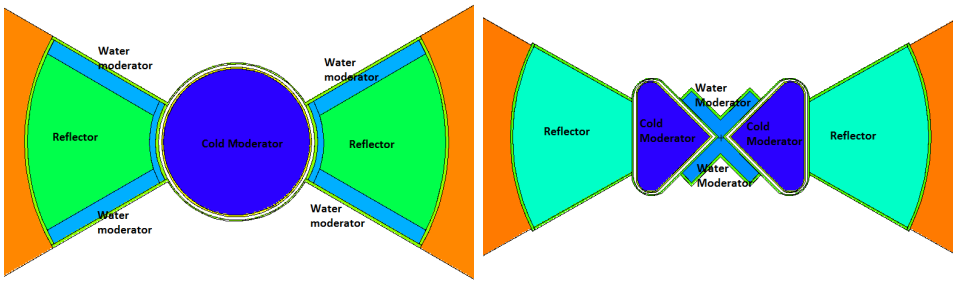

(a) Disc-shaped moderator (b) Butterfly moderator

Figure 1.4: Horizontal cross-section of the disc-shaped moderator and the butterfly moderator. In the disc-shaped moderator, the instrument extracts thermal neutrons from the water wings on the side of the cold moderator, and the butterfly has the water moderator positioned centrally and the cold parahydrogen moderators as its wings.

compared with the TDR moderator and a taller (6 cm tall) moderator below the target. The taller moderator still yields a factor of 1.6 in brightness but has an overall greater neutron emission because the emission surface is larger.

Chapter 7 includes two conference proceedings. The first is from the 21st Meeting of the International Collaboration on Advanced Neutron Sources (ICANS XXI, Mito, Japan, October 2014) and describes the development from the moderator system suggested in the TDR [4] to the disc-shaped flat moderator, originally suggested by Batkov et al. [10]. The second proceeding is from the Twelfth International Topical Meeting on Nuclear Applications of Accelerators (AccApp '15, Washington, DC, November 2015) and describes the development of the butterfly moderator and compares it with the TDR and the flat moderator.

1.3.2 Interfacing from moderator to instrument (Chapter 8)

The ESS has a fundamental principle that all experiments should undergo detailed simulation before the final instrument or experiment is designed and manufactured. To access the performance of various instrument design options, instrument designers typically apply Monte Carlo ray-tracing codes, such as McStas [14], to explore various instrument configurations and predict experimental results. These codes typically assume that the moderator emits neutrons homogeneously over its surface. However, this assumption is not true, especially when using parahydrogen, as the ESS will do. Figure 1.6 and 1.5 demonstrate this, showing surface images of a flat and a tall moderator as observed from an instrument at 2 m. The simulations are produced in Monte Carlo N-Particle eXtended (MCNPX) 2.7.0 [15].

Before the study presented in Chapter 8 was conducted, various tools were developed in the community coupling MCNPX to the Monte Carlo ray-tracing code, McStas. This can be done through a surface source write (SSW) card, which is part of MCNPX. The SSW writes the position, direction, energy, time, particle type and weight-factor to a file for every particle crossing a specific surface. This information can be passed to McStas, which can continue the transport down through the instruments [16]. McStas typically require billions of individual neutron simulations, and usually only a tiny fraction of the energy spectrum is of interest. In addition, only a tiny fraction of the neutrons leaving the moderator travel in the direction of the instrument, which

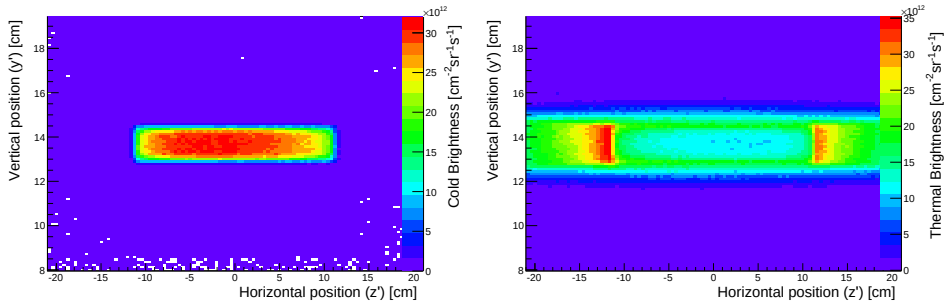

(a) Cold neutrons (b) Thermal neutrons

Figure 1.5: Image of the moderator surface of the 1.5 cm disc-shaped moderator for cold ($E < 5$ meV) (left) and thermal (20 meV$< E < 100$ meV) (right) neutrons

results in unreachable statistical demands using this method. Several terabytes of data storage is typically required and weeks of computer time in MCNPX simulations on a modern computer cluster. Although this method is highly precise, it is too impractical for general purpose analysis.

The methods and tools developed by Klinkby et al. [16] can also be used to translate MCNPX simulations, again through the SSW card, into ROOT [17]. The translation tool is available from Borghi & Batkov (see [18]). ROOT is an object oriented scientific analysis framework developed at the European Organization for Nuclear Research (CERN) that is used throughout the particle physics community.

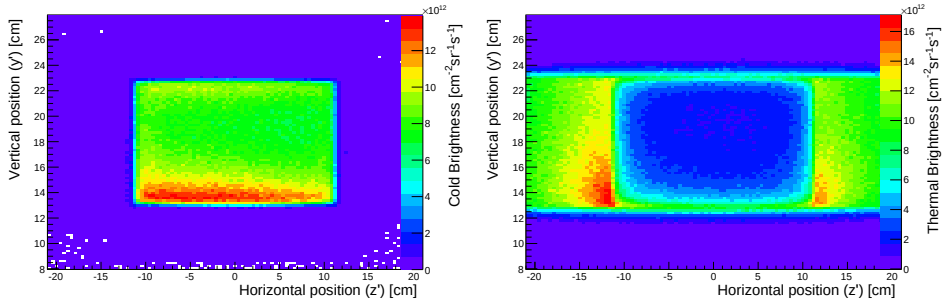

(a) Cold neutrons (b) Thermal neutrons

Figure 1.6: Image of the moderator surface of a 10 cm tall moderator for cold ($E <$ 5 meV) (left) and thermal (20 meV$< E < 100$ meV) (right) neutrons

This PhD project started out using this SSW to ROOT tool and studied many details in the ESS moderator system. The first discovery was that the cold ESS spectrum implemented in McStas was slightly incorrect for the cold parahydrogen moderators. This was initially observed for the TDR geometry design but also applies to the later disc-shaped and butterfly moderator design. The original McStas implementation was based on a Maxwellian spectrum distribution, and was corrected using a fudge function. I developed a more descriptive function which was incorporate into McStas, and this new function was implemented in McStas. This function was first presented on a poster at the International Conference on Neutron Scattering (ICNS) in Edinburgh, Scotland in July 2013 and later at a presentation at AccApp '13 in Bruges, Belgium in August 2013 [19]. The mathematical formalism is best described in the proceedings of ICANS

XXI [20].

The work presented at ICNS and AccApp also demonstrated another important observation, which I also observed using the SSW to ROOT tool as part. Not only does the parahydrogen moderator emit neutrons inhomogeneously from its surface (which was expected based on Kai et al. [21]); the thermal neutrons also had a non-flat distribution. One important feature was that, from certain extraction positions, in the 60° extraction opening (used in the TDR geometrical configuration), the peak thermal brightness originated from the reflector wall on the opposite side of the cold moderator from the thermal moderator. In fact, the global thermal brightness maximum originated from this reflector wall. I first showed this in the AccApp '13 conference proceedings [19] through 2D position-direction and wavelength-direction plots. Direction here corresponds to the term divergence, often used within the field of neutron instrumentation.

The SSW to ROOT approach was further developed into a picture description, as observed in Figure 1.6 and 1.5. Position, momentum and time are logged for each neutron impinging on a small area on the extraction surface: that is, the 12 cm tall and 60° or 120° wide cylindrical surface 2 m from the moderator center. These neutrons are then projected backward along their own trajectories to a surface intersection with the moderator surface. This effectively produces a picture of the moderator and its vicinity as observed from the point on the extraction surface.

An important effect discovered using the image approach was that the number of thermal neutrons per unit area, from the thermal moderator extensions next to the disc-shaped moderator, declined on a centimetre scale. Ultimately, this discovery became one of the key arguments in deciding to use the butterfly moderator instead of the disc-shaped moderator as the new ESS baseline, since the butterfly has a more uniform thermal distribution across the moderator surface.

Chapter 8 includes a manuscript [22] submitted to Journal of Neutron Research. It describes the details of a method for extracting full spatial information on brightness using the SSW to ROOT and image approaches. The full brightness distribution is averaged into one-dimensional brightness distributions that are fitted to functional forms. A method for reconstructing the full neutron brightness distribution from the one-dimensional functions is presented, based on the assumption that the full brightness distribution factorizes and is uncorrelated. This has been done for both the disc-shaped flat moderator system of different heights observed from a central extraction angle and the 3 cm tall butterfly moderator system observed from different angles. The results have been implemented into McStas and other ray-tracing codes.

1.3.3 The non-moderating bi-spectral moderator (Chapter 9)

Some instruments require a broad neutron spectrum or even two spectra. Such a spectrum can be achieved by using bispectral extraction [23, 24, 25]. In bispectral extraction, an instrument focuses on a thermal moderator located next to a cold moderator. A mirror is placed in front of the instrument guide, which reflects some of the cold neutrons into the instrument while transmitting some of the thermal neutrons. The ESS requires that bispectral extraction be possible [4].

One challenge for bispectral extraction, however, is that mirrors are not perfect in reflection or in transmission. Thus, bispectral extraction reduces both cold and thermal

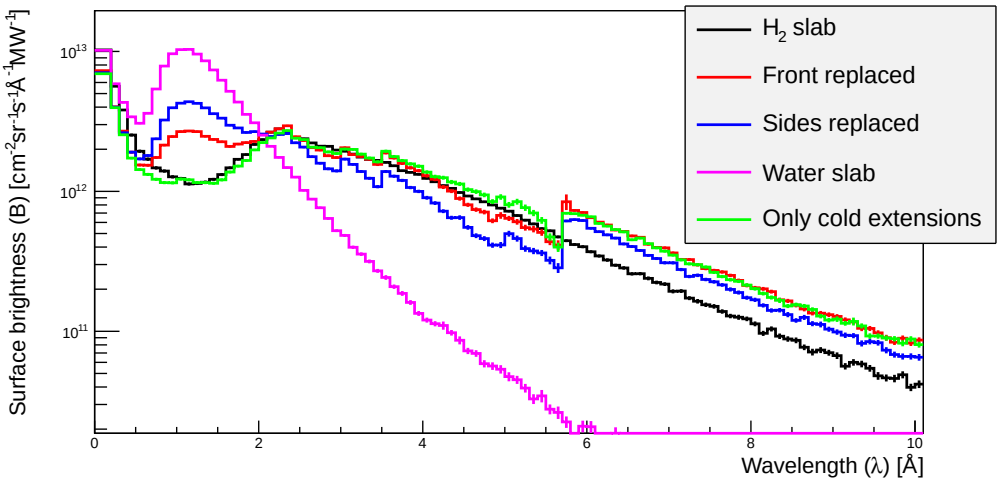

Figure 1.7: Results of simulations on a broad-spectrum moderator in which ortho-hydrogen replaces different amounts of water around an enriched piece of lead (see Chapter 9 for the details). Simulations of a 3 cm thick room-temperature water slab and a 5 cm thick 20 K hydrogen slab ("H_2 slab") are shown as reference.

neutrons compared with cold-only or thermal-only extraction. Another problem with bispectral extraction is that mirrors can suffer radiation damage or otherwise fail; in this case, the instrument is left with thermal neutrons only.

Producing a moderator with a very broad spectrum would make bispectral extraction redundant. One idea for such a moderator is the composite moderator [26, 27]. However, bispectral extraction outperforms this moderator concept (explained later in Section 6.8).

Chapter 9 presents an article published in Nuclear Instruments and Methods in Physics A [28]. The article presents a novel moderator concept I developed within this PhD project. The article shows that using the poorly moderating properties of heavy elements, in particular enriched ^{208}Pb, enables a direct bispectral moderator to be designed. Lead can also serve as a reflector filter, so if positioned in front of a cold moderator with other moderators around it, it will produce a bispectral spectrum while enhancing the very cold part of the spectrum compared with a conventional moderator. Figure 1.7 shows some simulated results.

Note that lead is not a better reflector filter than beryllium in the cold neutron region above the Bragg edge ([28]). However, beryllium cannot be used to produce a bispectral spectrum. Note also that lead and other heavy elements have significant (γ,n) cross-section and therefore emit a higher fraction of fast neutrons, which contribute to the background. However, in modern instruments, the neutrons are bent out of the line of sight of the moderator using mirrors, and since the fast neutrons do not reflect in the mirrors, these fast neutrons are less of a concern in modern instruments.

Although this thesis does not investigate this, the combined lead bispectral moderator and reflector filter could be used in conjunction with the single-crystal reflector filter (Chapter 10) using single-crystal enriched lead.

1.3.4 Experimental development of moderators (Chapter 10)

Several experiments have been carried out within this PhD project as part of collaboration built around the Low Energy Neutron Source (LENS) at Indiana University. The collaboration comprises neutronic experts from several international facilities, including the Spallation Neutron Source (SNS), the ESS and the Manuel Lujan, Jr., Neutron Scattering Center at the Los Alamos Neutron Science Center (LANCE). The experiments have been carried out at the LENS facility in Indiana using their highly flexible and easily exchangeable moderator system [29, 30].

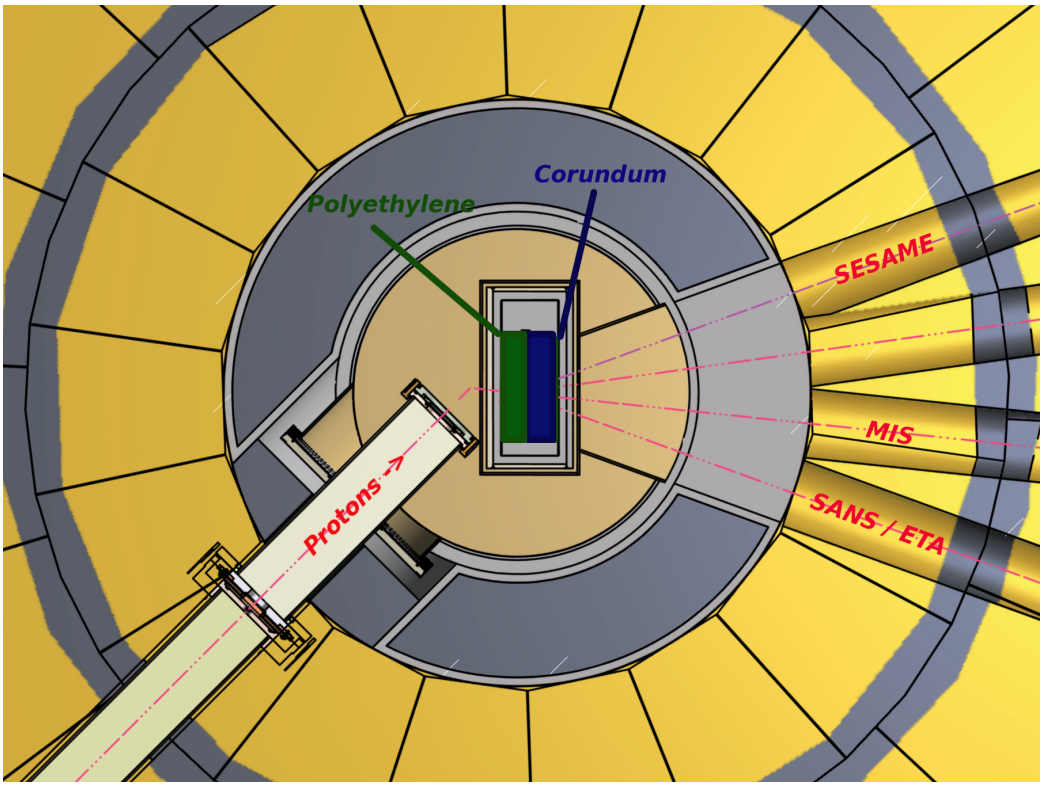

Figure 1.8: Horizontal cross-section of the LENS moderator system. A single-crystal sapphire reflector filter is positioned in front of a polyethylene moderator.

The first experimental participation within this PhD project was in 2012, when the LENS collaboration tested a convoluted moderator using water and single-crystal silicon. The experiment followed up an earlier experiment on convoluted moderators using polyethylene and silicon. The results from this experiment have not yet been published and are not included in this thesis.

The next experiment was an experiment on a single-crystal reflector filter. G. Muhrer ([31]) conceived the idea of a single-crystal reflector filter, which is based on the fact that the Bragg edges in a single crystal are delta-function-like (neutrons must fulfil the Bragg condition). This results in transmission of both cold- and intermediate-wavelength neutrons through a single-crystal reflector filter (a conventional polycrystalline filter transmits only very-long-wavelength neutrons above the Bragg edge and suppresses the intermediate-wavelength neutrons). Figure 1.8 shows the experimental mock-up. An article published in Nuclear Instruments and Methods in Physics A (830, 2016) summarizes the results of this experiment. This article is presented in

Chapter 10.

In addition, an experiment assessing triphenylmethane and deuterated triphenylmethane as moderator materials was carried out within this PhD project through the LENS collaboration. Further, David Baxter and I carried out simple precursor experiments on high-albedo nanodiamonds at LENS (during the calibration in preparation for the experiment presented in Chapter 10). The results from these experiments are still being analyzed and have thus not been published. These results are not shown or discussed further in this thesis.

Chapter 2

European Spallation Source

The ESS is a large-scale research facility being constructed outside Lund, Sweden [4], with the first protons on the target planned in 2019. The ESS will be the most powerful neutron source ever built. Overall, the ESS comprises three elements: an accelerator, a target station and an instrument suite.

2.1 Accelerator

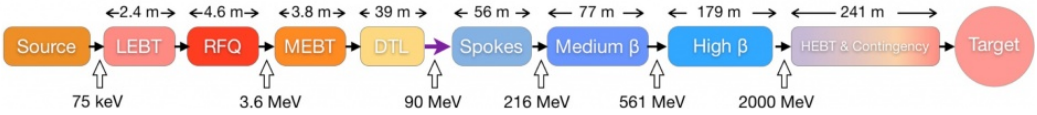

Figure 2.1: Layout of the ESS accelerator. Source: European Spallation Source (https://europeanspallationsource.se/accelerator).

The more than 600 m long state-of-the-art accelerator will deliver a high-power proton beam to the target station. Through a series of radio-frequency cavities, protons will be accelerated to an energy of 2 GeV. The beam will mainly be confined and guided by superconducting magnets. The accelerator is planned to bombard the target with $1.56{\cdot}10^{16}$ protons per second, bunched in 2.86-ms pulses at 14 Hz. With these characteristics, the accelerator will deliver an average of 5 MW of beam power to the target, which will make it the worlds most powerful accelerator. Figure 2.1 shows a sketch of the acceleration scheme.

2.2 Target station

Centrally at the ESS is the target monolith, which contains the neutron source itself. In the center of the monolith is the target, a 10 cm tall tungsten wheel with a radius of 125 cm that rotates in phase with the proton beam bunches and is cooled by helium flowing at high speed [4]. The 2 GeV protons from the accelerator impinging on this tungsten wheel produce neutrons by spallation. The next chapter explains this in more detail.

The neutrons created in the target have energies exceeding 100 keV and are typically

denoted fast or high energy neutrons. To be useful for experiments, these fast neutrons must be slowed down to energy below 100 meV or even below a few meV depending on the experiment. These energies of interest are in the same range as the energies of atoms in a cold or ambient-temperature (thermal) material. Thus the fast neutrons can be "thermalized" to these meV range energies through repetitive collisions with atoms in a room temperature thermal or cold material - for this reason these meV-range neutrons are called thermal and cold neutrons. At ESS the thermalization processes take place in two moderator systems positioned above and below the target. The moderator systems comprise a 300 K water moderator, referred to as the thermal moderator, and a cold moderator of liquid pressurized para-hydrogen at 20 K. Each moderator has two 120° openings, where neutrons are emitted towards the neutron-scattering instruments. The entire system is designed such that each instrument can view both the cold and the thermal moderator. The thermal moderator vessel is constructed to surround the cold moderator, acting as a pre-moderator (explained later). Each moderator is surrounded by a 30 cm tall block of beryllium with a 30 cm radius: the reflector. The reflector significantly increases the number of neutrons emitted from the moderators (Table 5.1). Around the beryllium reflector is a bulk volume of steel called the outer reflector. The outer reflector shields the area around the inner reflector from neutrons and γ-radiation, but also reflects some neutrons back into the inner beryllium reflector and moderator system. Together, the target, the moderator and the reflector system (TMR) comprise the heart of the facility. Figure 2.2 shows a drawing, and Figure 2.3 shows an MCNPX vertical cross-section.

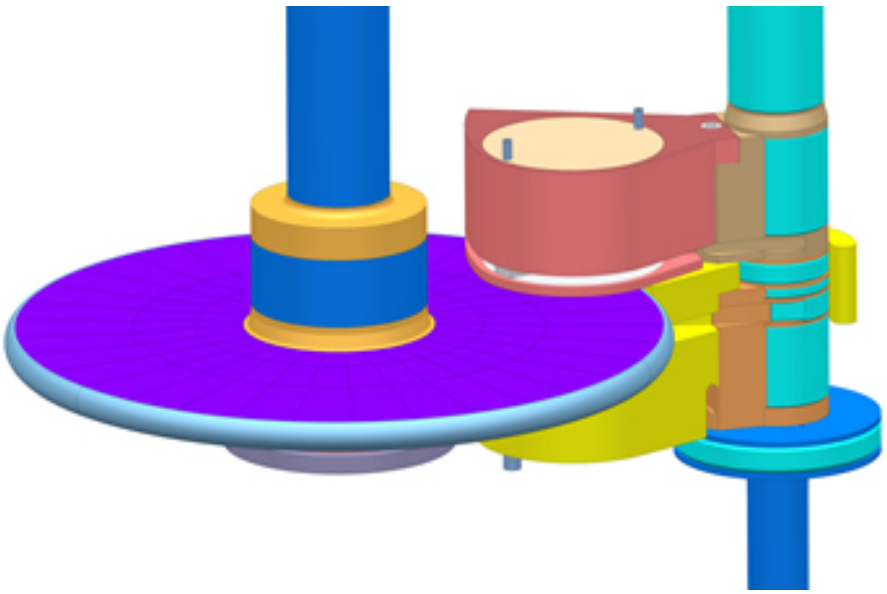

Figure 2.2: The TMR system at the ESS. The vertical axes leads to the ground level and embeds the cooling system for the target (left) and moderators (right). The moderator plugs (yellow and red) can be twisted on the axis such that they can be pulled up and replaced individually without having to move the target. From [32]

The TMR is surrounded by a cylindrical block with a 5.5 m radius made from 6000 tons of steel. This acts as shielding from the neutrons, photons and other radiation created in the TMR. The block and its content are known as the target monolith.

With the high-power beam delivered from accelerator, the TMR produces substantial

heat, especially in the target. Once protons enter the target, they start slowing down through ionization ([33]) and nuclear interactions, which causes heating. When a proton hits a tungsten nucleus, the nucleus becomes excited and starts emitting high-energy photons, neutrons and other residual particles (pions, muons and others). These disperse in the TMR and disseminate their energy over a larger area. Using MCNPX and the ESS target station model, it can be calculated that about 18% of the proton energy is converted into mass, usually in the form of binding energy or by creating pions.

Many of the higher-energy residuals, especially muons but also high-energy neutrons, tend to be forward directed and travel through the target ([34]). Photons and MeV-range neutrons (most of the neutrons) are more evenly distributed in direction, and many fly into the moderator and reflector ([6]). The photons deliver much of their energy as ionizing energy by forming an electromagnetic shower ([33]). This occurs mostly in the heavier materials, such as the target itself, the target steel casing and the outer steel reflector, but also in structural elements, such as piping and moderator cans made from aluminium. The kinetic energy of the fast neutrons is also converted into heat in the slowing-down process: this is typically about 1 MeV per neutron. The neutrons lose their kinetic energy through interaction with different material, the energy is deposited as heat in the material. Some neutrons result in new neutrons, mainly from the (n,2n) reaction. This reaction is especially dominant in the beryllium reflector and results in additional heating and more MeV-range neutrons. Some neutrons are absorbed in the slowing-down process, especially in the steel and the tungsten, and this process converts energy to mass and emits additional high-energy gamma radiation.

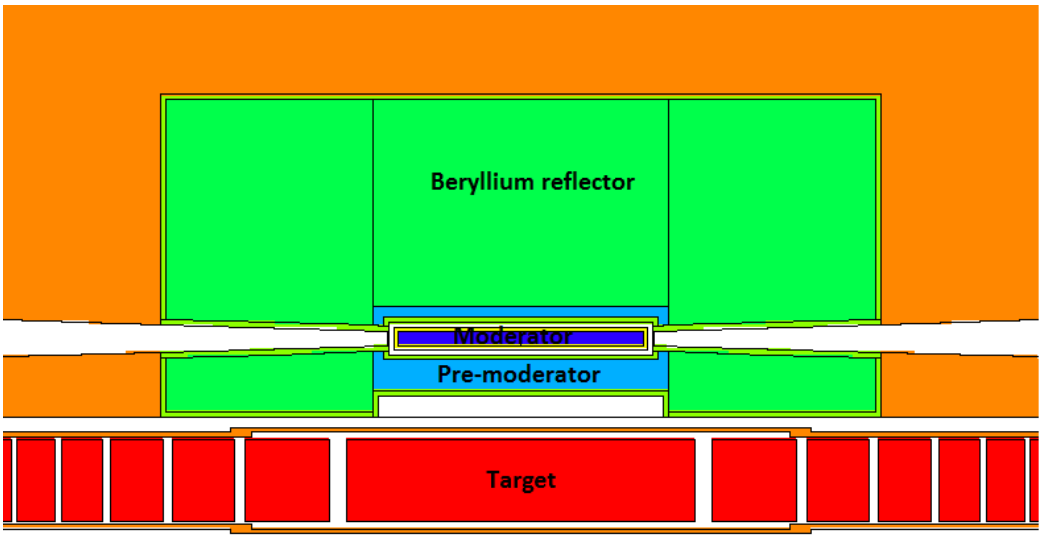

Figure 2.3: Vertical cross-section of the TMR, here featuring a disc-shaped flat moderator.

The spallation products (and fission products) in the target are usually highly radioactive and will begin alpha or beta decay towards stability. Similarly, the nuclei that have absorbed neutrons will typically be unstable and undergo beta decay. The decay causes residual heating (heating after the beam has been switched off) and, for beta decay, also emits some energy through neutrinos, which leave the target monolith without interacting.

From each 2 GeV proton, the TMR converts about 1.6 GeV into heat, mainly in the target, and 40 MeV disappears with neutrinos and 360 MeV is converted into mass, again mainly in the target [35, 36]. The energy converted into mass results in significant residual heat build-up in the target over its lifetime. While operating, a section of the target that was rotated out of the beam 1 second earlier emits about 10^{12} high-energy gamma rays per second per cm^3 [35]. A fraction of the energy escapes the TMR plug and is distributed over the outer monolith, which can be cooled passively. All the TMR parts need active cooling [4].

The target is cooled by using high-pressure helium gas at high flow speed; this is challenging [4]. However, despite the significantly lower energy deposition in the reflector and moderator, these still need significant cooling. In particular, the cold hydrogen moderators are challenging, because they need to be kept at 20 K. In the TDR ([4]), the energy deposition in the cold hydrogen moderator was estimated to be 20 kW in each moderator bucket, whereas more detailed simulations in the flat moderator and the butterfly moderator (Chapter 7) show only about 10 kW of energy deposition in each cold moderator system (including the piping and the moderator's aluminium vessel). To cool the cold moderator, the ESS will host a large cryoplant (see more in [37]), which is a significant cost factor for the target station. A series of water coolant loops near 300 K cool the water moderator, the beryllium reflector, the outer steel reflector and other critical components.

Because of the intense radiation on the reflectors, moderators and target, these components need to be replaced regularly. The entire monolith is therefore designed such that the moderator–reflector plugs can be retracted and replaced about once every 6 months, with the shortest possible shutdown of the facility. The target will be replaced every 2 years, and this will require a longer shutdown of the facility [4].

2.3 Instrument suite

At the ESS, instruments will be given a beam opening, or beam extraction port, where neutron extraction devices can be inserted; for most instruments, this opening will be about 5° wide in the horizontal plane. With the two 120° horizontal openings from the moderator, this enables a maximum of 48 instruments. However, currently only 22 instruments are being planned. Figure 2.4 shows an overview of the instrument suite.

The neutrons are transported using advanced neutron guide systems, which use neutron super-mirrors to reflect neutrons along the guide. Neutron super-mirrors comprise ultra thin alternating layer substrates of various materials with differences in refractive index to neutrons. The interference between layers causes total external reflection at a much wider critical angle of incidence than a single-layer mirror [39].

The instruments at the ESS only use thermal and/or cold neutrons and consider fast or epithermal neutrons plus high-energy photon noise, also denoted background. At the ESS, most of the guides are bent such that the moderator is out of the line of sight from the experiment. Since super-mirrors in the guides reflect thermal and cold neutrons and transmit neutrons and gamma rays of higher energy, these curved guides significantly reduce the background.

Many experiments use choppers, which are typically large rotating wheels made from

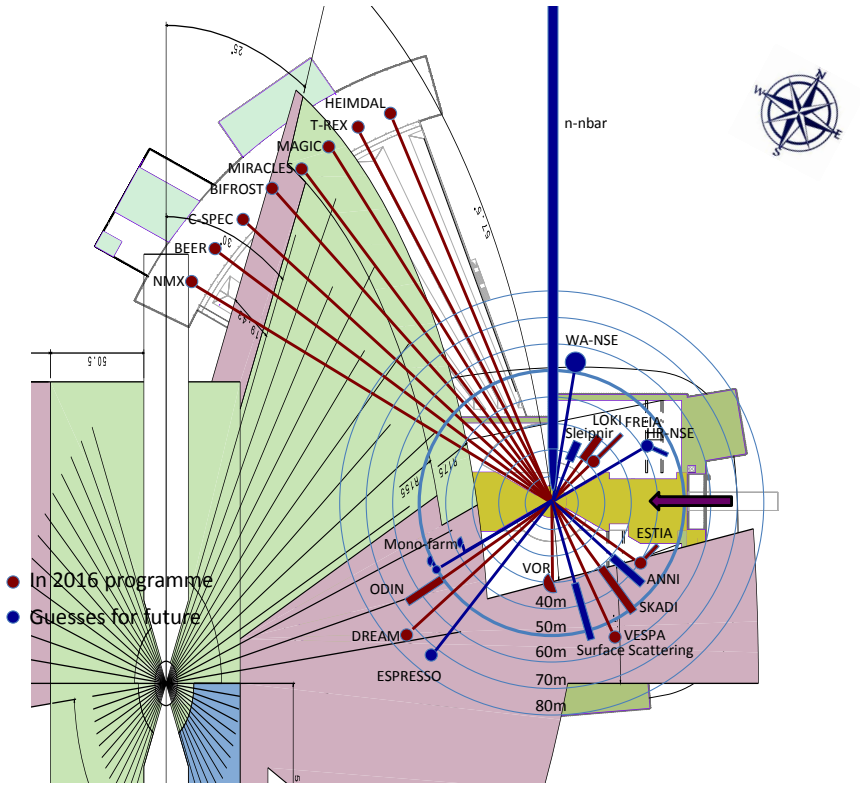

Figure 2.4: ESS instrument suite surrounding the target monolith, with the accelerator entering from the top right. Source: [38].

absorbing material with a cutout or hole in the absorber (see e.g. [40]). This allows neutrons to be transmitted through the chopper rapidly in times-structured bunches. These choppers cut up the neutron pulse into pulses of shorter duration, which enables better energy resolution through time of flight measurements and reduces background.

Instrument design and construction is not the topic of this thesis. The TDR [4] describes the planned ESS instruments in detail. Detailed studies of how the changeover from the tall bucket-like TDR moderator design to the disc-shaped flat design and butterfly moderator designs affects the instruments can be found in [41, 42, 43].

Chapter 3

Spallation

The work in this thesis revolves around the European Spallation Source (ESS), which, as indicated by the name, is a spallation source. In recent years, spallation sources have become the most efficient neutron sources ([44]) in terms of peak birghtness (see section 5.1, which can be considered a measure of useful neutron flux.

This chapter focuses on the spallation process, spallation sources and target materials. The details on the modeling of the spallation process are omitted. Filges & Goldenbaum [6] provide more information on modeling of the spallation process.

Glenn T. Seaborg first proposed the spallation process in his PhD dissertation in 1937 [45, 46, 47] before fission was discovered [48]. John M. Carpenter developed the first accelerator-induced spallation source in the 1970s, with the first neutrons produced in 1981 [49]. Figure 3.1 illustrates the spallation process.

3.1 Spallation process

Spallation is the governing process when a hadron interacts with a nucleus, in the kinetic energy range of a few tens of MeV to about 10 GeV, when multi-fragmentation and vaporization takes over [6]. In the energy regime of interest here, a hadron refers to any free proton, neutron, charged pion and, in rare cases, more exotic particles such as kaons.

The spallation process can be divided into three subsequent phases [6]:

- an intranuclear cascade (INC);
- an evaporation phase (including both evaporation and high-energy fission); and
- a residual de-excitation phase.

Several models describe the INC. Most of these are derived from the Bertini model [50, 51, 52]. Filges & Goldenbaum [6] have summarized this. The spallation process is ilustrated in Figure 3.1. According to the Bertini model, the INC is formed by interactions between a hadron traversing and the individual nucleons in the nucleus, described by a Fermi-Dirac gas. At this energy, the main relevant nucleon species are protons and neutrons and pions. At each interaction point, the hadron transfers some energy to the nucleon, which might become a free hadron and start a secondary

cascade. The INC process continues until all hadrons have come to a stop or have left the nucleus.

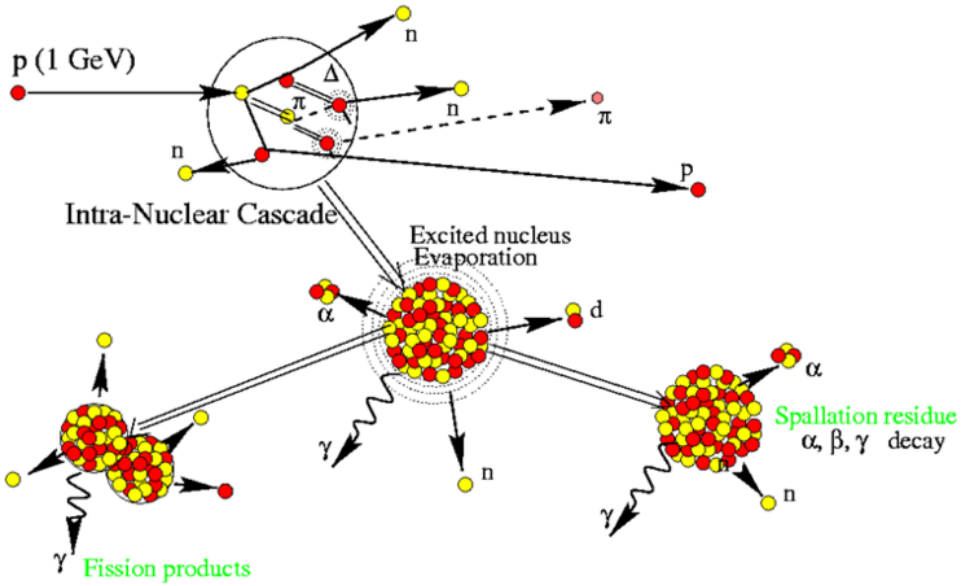

Figure 3.1: Illustration of the spallation process. Source: Mank et al. [53].

The free hadrons that have left the nucleus will traverse onwards in the material. Some have enough energy to result in subsequent spallation. Thus, a hadron with sufficient energy can form a cascade of spallations in a material, an inter nuclear cascade.

After the INC, the nucleus is left highly excited and will start a de-excitation process. The most common de-excitation process is evaporation: emitting a nucleon. Especially for heavier elements, more neutrons than protons evaporate. Occasionally, heavier residual particles, such as a deuteron or helium nucleus, evaporate.

During the evaporation phase, the a fraction (depending on the isotope) of the excited nuclei undergo high-energy fissions instead of nucleon evaporation. Like thermal and fast fission, high-energy fission breaks the excited nuclei into two separate fragments but, unlike thermal and fast fission, these fragments are typically of equal mass. The likelihood of high-energy fission increases with mass number. Thus, this happens rarely in tungsten spallation, whereas it is fairly common in lead. High-energy fission emits more fission neutrons than "regular" fission but fewer than the average number evaporated from spallation without fission.

The last phase of spallation is the residual de-excitation phase. The last couple of nucleons rearrange to bring the nucleus into its ground state, which typically results in the emission of high-energy photons. After the spallation, where more neutrons than protons are emitted emitted, the nucleus is typically left as a relatively proton-rich unstable isotope (neutron rich in fission) that will start decaying via β^+ (β^- in fission).

According to Carpenter & Yelon [7], Bauer [55] and Hilborn et al. [56], the neutron yield from spallation by an impinging proton beam, with energy E, for a heavy element can be approximated by the empirical formula $Y(A, E) = \alpha(A + 20)(E_p - \beta)$, where α is 0.1 GeV^{-1} for the non-fissile heavy elements and 0.19 GeV^{-1} for ^{238}U. β is the

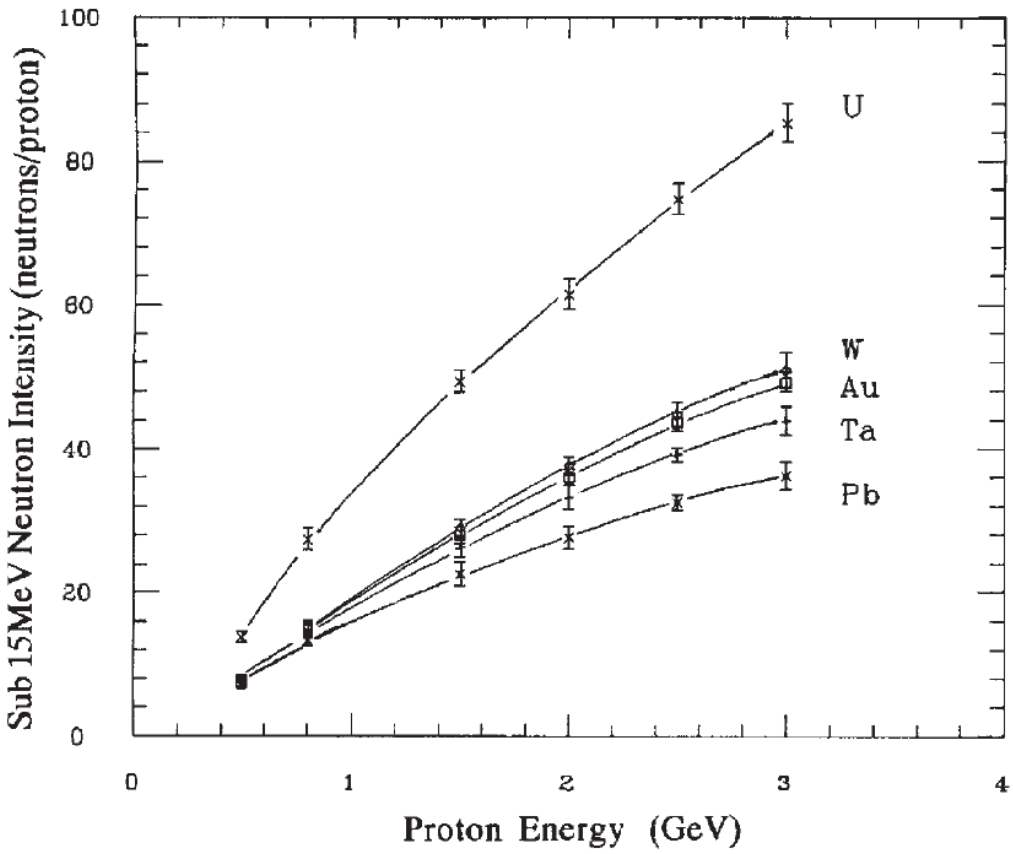

Figure 3.2: Production of neutrons by spallation in a 5 cm radius and 35 cm long cylindrical target comprising various materials irradiated with protons of different energy. Source: Watanabe [54].

spallation limit that fits well to 0.12 GeV. Since the fast fission energy limit is below the spallation energy limit, this secondary fission results in a significant increase in neutron yield per proton in very heavy target materials, such as depleted uranium. Figure 3.2 shows the neutron yield per proton in various spallation targets at different proton energy (including fission, as explained below).

Making use of fission in a spallation neutrons source, is challenging for two reasons ([6, 57]):

- While producing more neutrons per proton, fission does not produce many neutrons per unit energy released and thus requires more cooling per neutron, which is ultimately the upper limit for any neutron source ().

- The fission fragments are typically neutron-rich isotopes. Some of these isotopes emit delayed neutrons and have lifetimes between a few microseconds and several minutes, which can contribute significantly to background in experiments (for pulsed sources, timing is essential).

3.2 Spallation neutron sources

A spallation neutron source is realized by aiming an accelerator at a good spallation target material. The protons are typically accelerated to some hundreds of MeV or a couple of GeV (the Japan Proton Accelerator Research Complex (J-PARC) operates at 3 GeV) and collide with the target. There are several requirements for the optimal target material ([58, 6]).

- It should have as high density as possible, to minimize the hotspot size of neutron emission, which makes the moderator systems more efficient.
- It should be as heavy an element as possible and yet light enough not to produce too much high-energy fission. In particular, it should be light enough not to undergo significant fractions of fast or thermal fission.
- It should have excellent material properties: chemical stability; resistance to radiation; low brittleness; corrosion resistance; a high melting point (except for liquid targets, such as mercury); and high heat conductivity.
- It should have good neutronic qualities: low absorption, such that thermal neutrons can scatter through the target.

The most commonly used targets for low-power sources are tantalum and tungsten, whereas high-power sources use liquid mercury (J-PARC [59] and SNS [60]) or lead canned in zircaloy (Swiss Spallation Neutron Source (SINQ)). The ESS will use a rotating tungsten wheel.

Tantalum has historically been used mainly because of its high corrosion resistance, chemical stability and radiation resistance, which simplifies target engineering. Tantalum has significant residual decay heat, which can become problematic with high-power sources. Tungsten has higher neutron richness and higher density and thus a higher neutron yield per proton with a smaller hotspot size. However, tungsten has problems with corrosion and cannot be water-cooled without cladding. In the transition to higher-power sources, more cooling is required, which leads to the idea of using liquid mercury, where the heated target material itself can be transported out of the hotspot and cooled elsewhere.

Mercury has a density of 13.54 $\mathrm{g{\cdot}cm^{-3}}$ (at room temperature), which is significantly lower than tungsten (19.25 $\mathrm{g{\cdot}cm^{-3}}$). However, to be fair, tungsten requires embedded cooling channels, and thus maximum density is not achieved. For example, at the ESS, the expected target tungsten density is $\approx 78\%$ of the theoretical density: 15.02 $\mathrm{g{\cdot}cm^{-3}}$ [4] – which is close to, but better than, the density of mercury. Table 3.1 summarizes various target materials.

3.2.1 Considerations for the best target material

During this study I have gained knowledge on materials and issues at spallation sources and target-moderator-reflector system design. This subsection outlines some of my considerations for a target material, and proposes the idea of using enriched platinum.

Revisiting the list of target requirements shows that platinum is the perfect match. It is heavier and more neutron rich than tungsten; it is more chemically stable and has

better corrosion resistance than tantalum; it is one of the most ductile elements; and it has excellent heat conductivity and a high melting point. In addition, the absorption cross-section is about half that of tungsten and tantalum and one 37th that of mercury; this is not fantastic by itself, since it is still 10 barn (for 2200 $m \cdot s^{-1}$ thermal neutrons [61]). However, the second heaviest stable isotope of platinum, ^{196}Pt, has an abundance at 25.2% and has absorption cross-sections of 0.72 barn. Low-absorption cross-section highly enriched platinum would open up new possibilities in designing target moderator reflector systems. Thermalized neutrons can migrate through or reflect on the target, whereas conventional target materials are thermal neutron sinks absorbing many of the thermal neutrons.

One could argue that osmium or iridium (both heavier than platinum) would be good target materials. However, iridium is an odd proton number isotope and thus has a very high absorption cross-section (≈400 barn at 2200 ms^{-1} [61]). In fact, it has a fast neutron cross-section of a few barn. Thus, iridium absorbs many of the spallation neutrons even before they leave the target – and there are no good enrichment options. Osmium's absorption cross-section is comparable to that of tungsten, but it has no good enrichment option. Osmium is better than tungsten as a target material, but several years of world production would be required for an osmium target the size of the ESS target, and thus it is probably not viable.

	Cold brightness (E<20 meV) [$10^{13} cm^{-2} sr^{-1} s^{-1}$]	Thermal brightness (20 meV<E<100 meV) [$10^{13} cm^{-2} sr^{-1} s^{-1}$]	Target offset [cm]
Conventional targets			
Tungsten	4.716±0.012	2.835±0.022	12.75
Tantalum	4.093±0.011	2.456±0.021	13.75
Mercury	4.641±0.012	2.670±0.022	13.50
Depleted Uranium†	8.446±0.017	5.100±0.031	13.50
Alternative targets			
Platinum	5.004±0.012	3.048±0.023	12.25
Osmium	5.362±0.013	3.232±0.024	11.75
Iridium	4.341±0.011	2.675±0.021	11.25
Enriched tungsten	5.070±0.013	2.972±0.023	12.75
Enriched platinum	5.269±0.012	3.186±0.024	12.50
Zircaloy container			
Enriched tungsten	5.231±0.013	3.106±0.024	12.75
Enriched platinum	5.598±0.013	3.357±0.025	13.00

Table 3.1: Summary of some spallation target materials in the ESS butterfly geometry (explained in Chapters 7 and 8 and shown in Figure 3.3). The target offset is the "optimal" distance from the target material front phase (beam entrance point) and the moderator center position. Note that the geometrical configuration of the moderator and reflector is optimized for the conventional tungsten target [4].
† *Depleted uranium (0.3%^{235}U) has a significant delayed neutron fraction, and 2.54 times more heat is produced per proton in this target (in this mock-up) compared with the other targets, which are comparable in heat production.*

Table 3.1 shows the results for various target materials. The simulations are produced in the ESS butterfly geometry (Figure 3.3 and are explained in detail in Chapter 7).

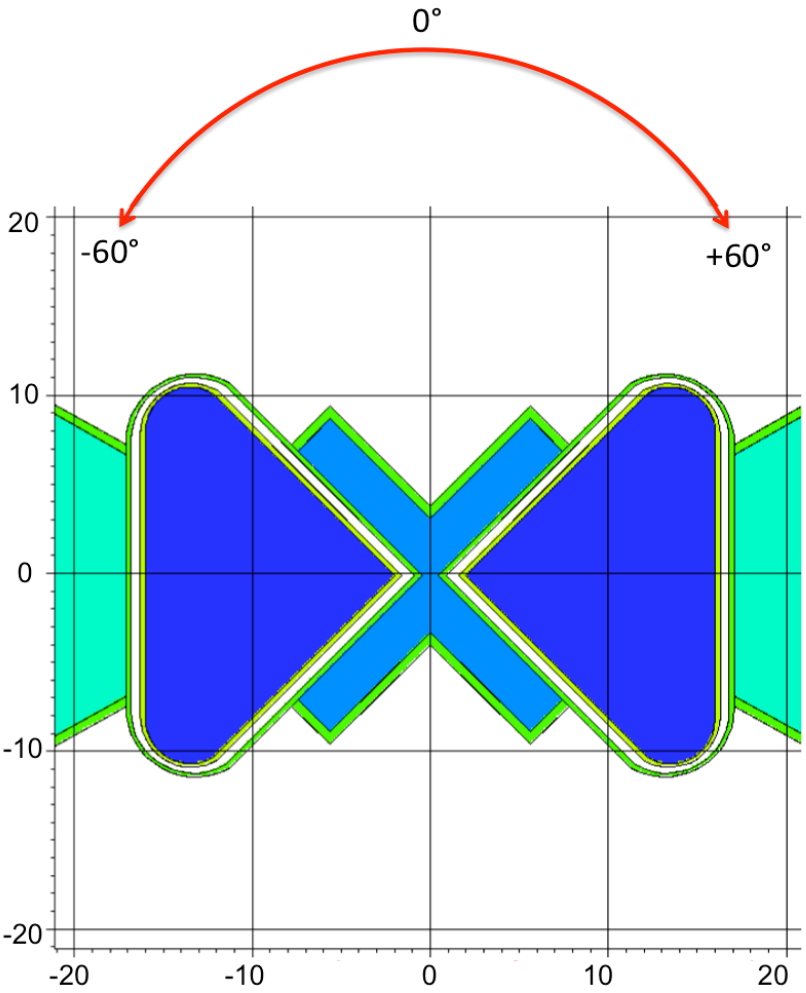

Figure 3.3: The butterfly geometry. A central room-temperature water "cross" provides thermal neutrons while two cold parahydrogen wings deliver cold neutrons for instruments positioned in 2×120° beam extraction windows.

Cold and thermal brightness are measured from a central instrument (i.e. perpendicular to the proton beam). The optimal target position is the point where the two cold wings emit the same brightness (Figure 3.4). The results in Table 3.1 were produced by changing the target material and moving the target to its new "optimal" position (translation along the proton beam direction) in the geometrical configuration for the ESS butterfly [62].

When enriched materials are used as the target material, the steel target container becomes the major source of absorption. Thus, in this case, the container should be replaced with a less absorbent material, such as zircaloy.

The solid target materials are simulated as helium-cooled targets with 78% filling factor (that is, homogeneous using 78% theoretical density); the liquid target, mercury, is at its theoretical density. Platinum cross-sections were taken from Hendricks et al. [63]. Table 3.1 shows that a platinum target contained in zirconium housing has 20% higher brightness than the current tungsten target (conventional tungsten), even in this mock-up – which is optimized for a tungsten target.

In addition to the 20% gain in switching from tungsten to enriched platinum comes a long list of potential gains, which are not investigated here. However, intuitively, one could imagine the following.

- Platinum has higher density, and the target height could therefore be reduced, and thus the moderator could be moved closer to the target center, which is known to increase brightness.
- The platinum target could also be water cooled, since platinum is highly corrosion resistant (tungsten is not, and the ESS therefore cools with helium). This could increase the filling factor, which would increase the brightness significantly.
- A water-cooled target could act as a pre-moderator (explained later); thus, the dedicated pre-moderator thickness could be reduced or could be removed entirely, bringing the moderator even closer to the target – resulting in a brightness gain.
- One could also imagine a significant gain from optimization aimed at improving the cross-talking of neutrons between the top and bottom moderator system, which would be enabled because of the low absorption in enriched platinum.
- With the higher density, a platinum target could either be reduced in diameter or even made stationary, which would reduce the interference between the target and the beam extraction windows, enabling more reflector/shielding, resulting in less background neutrons and more useful neutrons.

Platinum has never been used as a target material, probably because of its high price. However, the price of the ESS facility is on the order of €2 billion, and the accelerator alone is about half of that. Naively, the 20% higher neutron yield in enriched platinum can be translated to a value: €400 million. An online search and using a simple model for separation work units shows that the price of enriched platinum is about €700,000 per litre. Even with a large rotating-wheel-type target such at the ESS target, the price would be less than €100 million. Further, if the target were produced by using such an expensive material, it is considerable that the target would be made stationary. A stationary target has been investigated and shown feasible for a water-cooled tantalum target [64]. For a stationary platinum target, the price would be about €3 million to €5 million.

Enriched tungsten (99% ^{184}W – 1.7 barn at 2200 ms^{-1} [61]), also included in Table 3.1, could be a cost-effective alternative to platinum.

No detailed study on platinum cross-sections or platinum's physical ability as a target material (such as behaviour under irradiation) has been found in literature searches. Thus, building a platinum target facility would naturally require an extensive research, development and licensing effort.

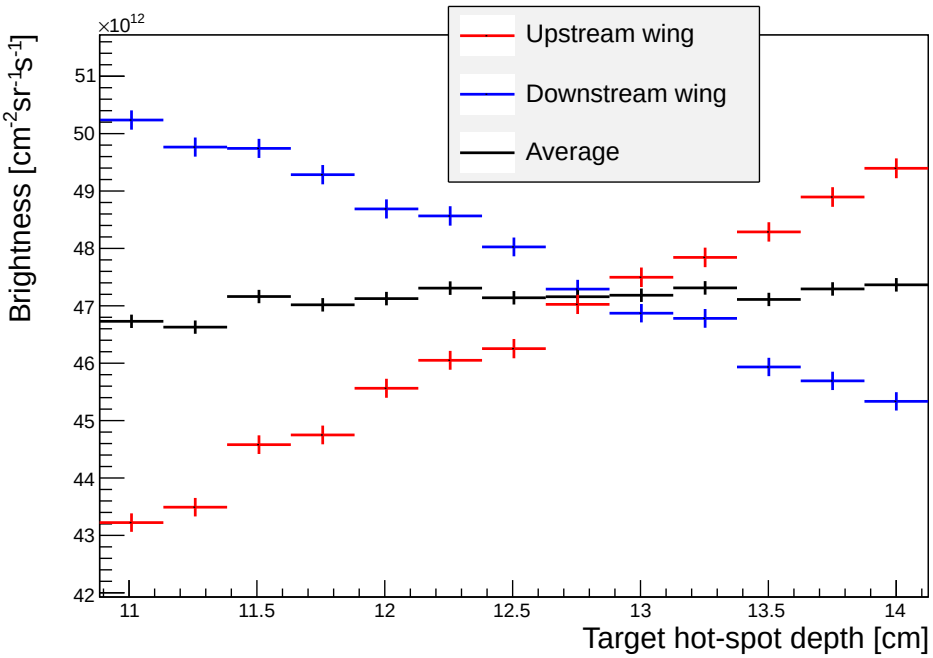

Figure 3.4: Target hotspot depth: the distance from the target front face to the moderator center axis in the ESS butterfly moderator system. The left and right wings in the butterfly moderator system resemble two individual cold moderators. The optimal target position is such that the target hotspot is in the middle of the two wings.

Chapter 4

Moderator neutronics

4.1 Kinematic elastic scattering – slowing neutrons down

The simplest form of interaction between a neutron and a nucleus is kinematic elastic scattering, in which the mass of the system is conserved, $E_i = E_o$ for the sum of the energy of the neutron and nucleus (to be differentiated from total elastic scattering, in which the magnitude of the momentum vector of the neutron is conserved: $|p_i| = |p_o|$). Kinematic elastic scattering is well described by the so-called free gas model, the text below is based on [57, 65]. In kinematic scattering between two particles with mass $m_n = 1$ and $M \approx A$ (in which A is the mass number of the nucleus), one yields the relationship between the neutron's incoming energy, E_i, and outgoing energy, E_o, as a function of the scattering angle, θ:

$$\frac{E_o}{E_i} = \frac{M^2 + m_n^2 + 2Mm_n \cos\theta}{(M + m_n)^2} \approx \frac{A^2 + 1 + 2A\cos\theta}{(A+1)^2}. \tag{4.1.0.1}$$

The function has a maximum (in terms of energy transfer) for $A = 1$, that is, hydrogen, where a backscattering ($\theta = 180°$) neutron will lose all its energy in one single collision.

Another important quantity is the average energy loss per collision, which can be shown to be:

$$< E_o > \approx \frac{1}{2}E_i \left(1 - \frac{1 + A^2 - 2A}{1 + A^2 + 2A}\right) = \frac{1}{2}E_i(1 - \alpha), \tag{4.1.0.2}$$

where $\alpha = \left(\frac{A-1}{A+1}\right)^2$ is commonly referred to as the collision parameter. This equation shows that neutrons colliding with hydrogen also have the greatest average energy transfer of any nucleus of $< E_o >= \frac{1}{2}E_i$.

Based on equation 4.1.0.2, the energy after a collision is proportional to the neutron's incident energy. Thus, it is favorable to examine the logarithmic energy decrement per collision, $\xi =< \ln E_i - \ln E_o >$, which turns out to be constant for a given nucleus:

$$\xi = 1 + \frac{(A-1)^2}{2A} \ln \frac{A-1}{A+1} \tag{4.1.0.3}$$

ξ can be calculated for materials comprising different nuclei by simply averaging over all nuclei, weighting by the scattering cross-section, σ_s. Based on ξ, three quantities

highly important to moderator neutronics can be calculated: the slowing-down power, S, the average number of collisions needed, N, and the moderation ratio, M.

The slowing-down power is given by:

$$S = \xi \rho_A \sigma_s = \xi \Sigma_s, \tag{4.1.0.4}$$

where ρ_A is the number density (or atom density) and $\Sigma_s = \rho_A \sigma_s$ is the macroscopic scattering cross-section.

Material	ρ [barn cm^{-1}]	Σ_s [cm^{-1}]	Σ_a [cm^{-1}]	S	M	N
Liquid H_2	0.042	0.86	1.40×10^{-6}	0.864	62	17.5
Liquid D_2	0.042	0.15	2.19×10^{-6}	0.106	48496	24
Be	0.044	0.28	3.36×10^{-5}	0.057	170	84
C	0.050	0.23	1.76×10^{-4}	0.037	211	111
Al	0.060	0.09	1.39×10^{-2}	6.54×10^{-3}	0.47	242
Si	0.050	0.09	8.53×10^{-3}	6.61×10^{-3}	0.76	250
Pb	0.033	0.37	5.64×10^{-3}	3.53×10^{-3}	0.63	1817
^{208}Pb	0.033	0.37	1.58×10^{-5}	3.57×10^{-3}	226	1826
H_2O	0.100	1.50	2.22×10^{-2}	1.061	48	25
D_2O	0.125	0.45	1.23×10^{-5}	0.242	19745	33
CH_4	0.124	2.19	3.32×10^{-2}	1.823	55	21
$(CH_2)_xH_2$	0.124	1.95	2.78×10^{-2}	1.403	51	24
$(C_6H_5)_3CH$	0.087	1.11	1.36×10^{-2}	0.604	44	32
$(C_6D_5)_3CD$	0.086	0.43	3.57×10^{-4}	0.178	500	42
Al_2O_3	0.118	0.35	1.09×10^{-2}	0.035	3.2	173

Table 4.1: Summary of selected moderator materials, showing macroscopic elastic scattering (near 1 eV) and absorption cross-section at (2200 m/s or ≈25.3 eV), slowing–down power, S, moderating ratio, M, and average number of collisions needed, N. Calculated based on ENDF/B.-VII.1 cross section [66] and [61].

Given the macroscopic absorption cross-section, Σ_a, the moderating ratio (that is, the number of neutrons moderated per neutron absorbed) can be defined as:

$$M = \frac{S}{\Sigma_a} = \frac{\xi \Sigma_s}{\Sigma_a}. \tag{4.1.0.5}$$

Based on ξ, the average number of collisions, N, needed to slow down a neutron from its creation energy, E_c, typically about 1 MeV, to thermal energy, E_t, about 25 meV, can also be calculated using:

$$N = \frac{\ln E_c - \ln E_t}{\xi}. \tag{4.1.0.6}$$

Table 4.1 summarizes selected moderator candidates.

4.2 Scattering of neutrons by matter

In kinematic elastic scattering as described above, the neutron has significantly higher energy than the kinetic energy of the atom and the binding energy of the material.

Thus, the scattering interaction can be considered the kinematic scatter between two free particles of which the nuclei is at rest.

However, at thermal and especially cold neutron energy, the momentum of the atom must be considered; in fact, the neutron might scatter on a moving atom and gain energy from the interaction. Further, the binding energy of the molecules or material cannot be neglected, nor can the quantum states of matter at thermal or cold energy, and many interactions are inelastic scattering processes. In the thermal and cold energy regime, the neutron does not simply interact with the nucleus, but instead interacts with molecules or materials. In the same energy regime, the neutron wavelength $\lambda = \frac{2\pi\hbar}{p}$ (in which p is the neutron's momentum) approaches the characteristic distances between atoms in matter, enabling the neutron to scatter coherently.

In this low-energy regime, quantum mechanics governs neutron scattering. The next subsections examine some of the important physics behind the main processes relevant to moderator neutronics, but without digging deeply into the underlying quantum mechanics.

4.2.1 Scattering intensity

In neutron scattering, the neutron momentum typically described as a wave vector $\mathbf{k}$ whose magnitude is given by:

$$\mathbf{k} = \mathbf{p}/\hbar, \tag{4.2.1.1}$$

where $\mathbf{p}$ momentum vector of the neutron. When a neutron scatters in matter, the wave vector changes, and the wave vector after a collision is denoted $\mathbf{k'}$. The scattering angle, 2θ, can be derived from $\mathbf{k}$ and $\mathbf{k'}$ by the relationship $2\theta = 2\sin^{-1}\left(\frac{\mathbf{k}-\mathbf{k'}}{2k}\right)$. Another useful quantity is the scattering vector $\mathbf{Q} = \mathbf{k} - \mathbf{k'}$. Figure 4.1 illustrates the relationship between $\mathbf{k}$, $\mathbf{k'}$, $\mathbf{Q}$ and 2θ.

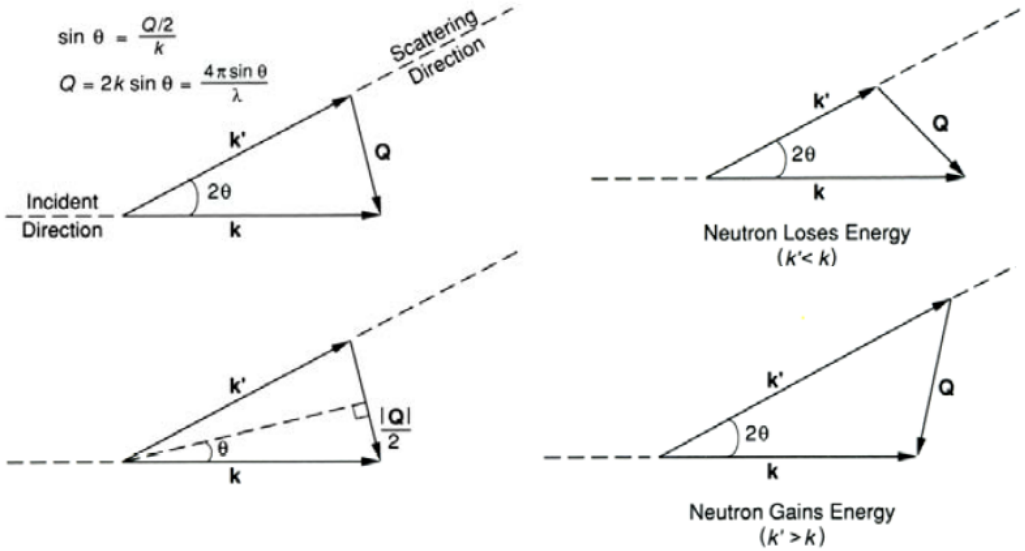

Figure 4.1: Illustration of the relationship between the wave vector $\mathbf{k}$ and $\mathbf{k'}$, momentum transfer Q and the scattering angle 2θ in the scattering processes in total elastic scattering (left) and inelastic scattering (right). Source: Pynn [67]

All scattering processes can be described as the scattering intensity $I(\mathbf{Q},\omega)$ for neutrons as a function the scattering vector $\mathbf{Q}$ and the angular frequency $\omega = \frac{E}{\hbar}$, where E is the energy of the neutron.

The Born approximation says that the scattering amplitude can be found as $\psi(\mathbf{k},\mathbf{k'}) = \left|\int e^{i\mathbf{k}\cdot\mathbf{r}} V(\mathbf{r}) e^{i\mathbf{k}\cdot\mathbf{r}} d^3\mathbf{r}\right|^2 = \left|\int e^{i\mathbf{Q}\cdot\mathbf{r}} V(\mathbf{r}) d^3\mathbf{r}\right|^2$, where $V(\mathbf{r})$ is a potential at position $\mathbf{r}$ [68]. In 1954, Van Hove ([69]) used the Born approximation and showed that the scattering intensity can be written in terms of the time-dependent correlation between atom pairs in the scattering medium. Van Hove started from Fermi's pseudo-potential, which says $V(\mathbf{r}) = \frac{2\pi\hbar^2}{m} b\delta(\mathbf{r})$, where m is the neutron mass, b is the neutron scattering length on the atom and $\delta(\mathbf{r})$ is the Dirac delta function [1]. By using this potential for an assembly of nuclei at position $\mathbf{r}$, van Hove showed that the scattering intensity in a material is given by:

$$I(\mathbf{Q},\omega) = \frac{2\pi}{\hbar}\frac{\mathbf{k}}{\mathbf{k'}} \sum_{i,j} b_i b_j \int_{-\infty}^{\infty} \left\langle e^{-i\mathbf{Q}\cdot\mathbf{r}_i(0)} e^{-i\mathbf{Q}\cdot\mathbf{r}_j(t)} \right\rangle e^{-i\omega t} dt, \tag{4.2.1.2}$$

where i,j is the i'th and j'th atom, t is time and $\langle\rangle$ indicates a thermodynamic average.

By defining:

$$A_{ij} = \frac{2\pi}{\hbar}\frac{\mathbf{k}}{\mathbf{k'}} \int_{-\infty}^{\infty} \left\langle e^{-i\mathbf{Q}\cdot\mathbf{r}_i(0)} e^{-i\mathbf{Q}\cdot\mathbf{r}_j(t)} \right\rangle e^{-i\omega t} dt, \tag{4.2.1.3}$$

the scattering law can be written as:

$$I(\mathbf{Q},\omega) = \sum_{i,j} b_i b_j A_{ij}. \tag{4.2.1.4}$$

This can be simplified by averaging over the scattering lengths b_i and b_j, which gives:

$$\sum_{i,j} \langle b_i b_j \rangle A_{ij} = \sum_{i,j} \langle b \rangle^2 A_{ij} + \sum_i \left(\langle b^2 \rangle - \langle b \rangle^2 \right) A_{ii}. \tag{4.2.1.5}$$

In this equation, the second term contains only the index i. Thus, it represents the neutrons that are scattered by a single nucleus without interference from other nuclei in the scattering medium: it is the incoherent scattering term. The scattering already covered in section 4.1 is in fact incoherent elastic scattering, which is described later.

The first term depends on both indices i and j and thus is interaction between more than one atom, also denoted coherent scattering. The scattering lengths for different atoms are typically defined as an incoherent scattering length $b_{inc} = \sqrt{\langle b^2 \rangle - \langle b \rangle^2}$ and a coherent scattering length $b_{coh} = b$.

From a moderator neutronics perspective, it is not important whether a scattering interaction is coherent or incoherent, and thus b_{coh} and b_{inc} are not of high importance. The more interesting quantity is the cross-section $\sigma = 4\pi b^2$. From the cross-section, we can calculate the intensity I of a neutron beam after traveling a distance x through a material as:

$$I = I_0 e^{-\sigma\rho_A \cdot x}, \tag{4.2.1.6}$$

where ρ_A is the number density of the material and I_0 is the initial beam intensity. This is also known as attenuation.

This formula for attenuation means that neutrons scatter more frequently as the cross-section of an atom increases and the density of the material increases. In moderator design, this is a double-edged sword. On the one hand, as many scatters as possible are needed in as little space as possible to slow the neutrons down to useful energy levels while not dispersing them too much. On the other hand, the moderator also needs to emit the neutrons once they have reached the desired energy. The following sections and chapters provide much more on this dilemma and suggested solutions.

4.2.2 Momentum transfer

Besides the cross-section, another key element of moderator neutronics is the magnitude of the momentum transfer in a collision. The detailed mechanisms are not covered here but are available in the literature [70, 71, 72, 73].

In general, scattering processes can be divided into three classes:

- total elastic scattering, in which the neutron energy is conserved, $|\mathbf{k}| - |\mathbf{k'}| = 0$;
- kinematic elastic scattering, in which the system mass is conserved; and
- inelastic scattering, in which the mass plus the energy of the system is conserved.

Total elastic scattering and inelastic scattering are covered below. Kinematic elastic scattering was already covered in section 4.1, assuming that the atom was at rest. The assumption of an atom at rest is no longer valid for thermal and cold neutron energy, as these energies resemble the energy levels of atoms in a cold or ambient room-temperature material. A neutron with low energy can scatter on a moving atom and gain energy from the collision. This is classical kinematics and is not covered here.

Note that, in the neutron-scattering community, total elastic scattering is commonly referred to simply as elastic scattering and kinematic elastic scattering as inelastic scattering. However, this definition provides no means to distinguish between kinematic elastic scattering and inelastic scattering. Fast neutrons are not very important for instruments thus this is not a big issue, but fast neutrons are very important for moderator neutronics and therefore this definition is problematic from a moderator neutronics point of view.

Total elastic scattering

Total elastic scattering is a neutron interaction in which the neutron's energy is conserved but where its direction of motion changes. All total elastic interactions are coherent. There are three common total elastic processes: diffraction, refraction and reflection. Similar to X-rays and other waves, Bragg's and Snell's laws govern these processes. All the total elastic processes highly depend on wavelength. A beam of neutrons with a spectrum of wavelengths enter a material; some wavelengths are reflected, others satisfy the Bragg condition (see below) and is diffracted into a set of specific angles, and the rest will disperse through refraction. Total elastic scattering is very important for instruments and experiments, such as in the reflective processes in neutron mirrors and also refractive processes in supermirrors. Neutron diffraction is also a major discipline in neutron-scattering experiments, since it is an efficient method for probing the structures of a condensed material.

From a moderator neutronics perspective, Bragg scattering, or diffraction, is the most important total elastic scattering process. Bragg scattering is scattering of a neutron wave on a crystal lattice and is governed by Bragg's law:

$$2d \sin\theta = n\lambda, \tag{4.2.2.1}$$

where d is the lattice's plane distance, θ is the incident angle and n is an integer. In a polycrystal or powder, Bragg scattering is observed as a series of sawtooth-like spikes in the cross-section: Bragg edges (Figure 4.2). In a single crystal, the Bragg scattering cross section is a set of delta function–like spikes. For long enough wavelengths ($\lambda > 2d$), no n or θ fulfills the Bragg condition; thus, Bragg scattering becomes impossible and the cross-section becomes 0.

Although total elastic scattering is very important to neutron-scattering experiments and in neutron instrument design, it is less important in moderator neutronics, since it by definition does not transfer energy. This means that these processes cannot alter the neutron wavelength distributions inside a moderator. However, total elastic scattering does change the mean free path of neutrons, and thus it might affect the neutron spectrum indirectly, in two ways.

First, total elastic scattering increases the scattering rate; the neutrons change directions more often and thus random walk for longer inside the moderator. This increases the average path length of the neutron inside the moderator, which in turn increases the likelihood of other non–total elastic scattering processes, leading to change of the neutron wavelength.

Second, the neutron spectrum observed from some point outside the moderator is not the same as the neutron spectrum inside the moderator. This can be intuitively understood by imagining neutrons being emitted from inside the moderator toward the point of observation. The number of neutrons reaching the observation point is attenuated (see section 4.2.1) depending on their macroscopic cross-section. Since neutrons of different wavelengths have different cross-sections, their likelihood of reaching the observation point depends on their wavelength. For many materials, the total elastic cross-section, especially for Bragg scattering, changes dramatically in the thermal or cold wavelength regime.

On the other hand there is a significant drawback here. The spatial distribution of neutrons inside a moderator system is highly isotropic, and the second law of thermodynamics therefore dictates that the entropy, and thus isotropy, cannot be reduced without transferring energy. Since total elastic scattering does not transfer energy, the example above is too simple. In the central region of the moderator where the neutron spatial distribution is isotropic, the likelihood of a neutron being scattered out of the beam through total elastic scattering, equals the likelihood that another neutron of the same wavelength will be scattered into the beam, and thus the attenuation cancels.

When the neutrons approach the edge of the moderator, the distribution becomes less isotropic, and attenuation from total elastic scattering becomes relevant. An interesting material to mention in this context is aluminum, which is typically used as a structural material in moderators and is dominated by total elastic scattering in the thermal or cold neutron wavelength regime (Figure 4.2).

The final reason why total elastic scattering is important in moderator neutronics comes from Liouville's theorem [74], which is considered fundamental in neutron science: "the phase-space density is constant when following its trajectories in conser-

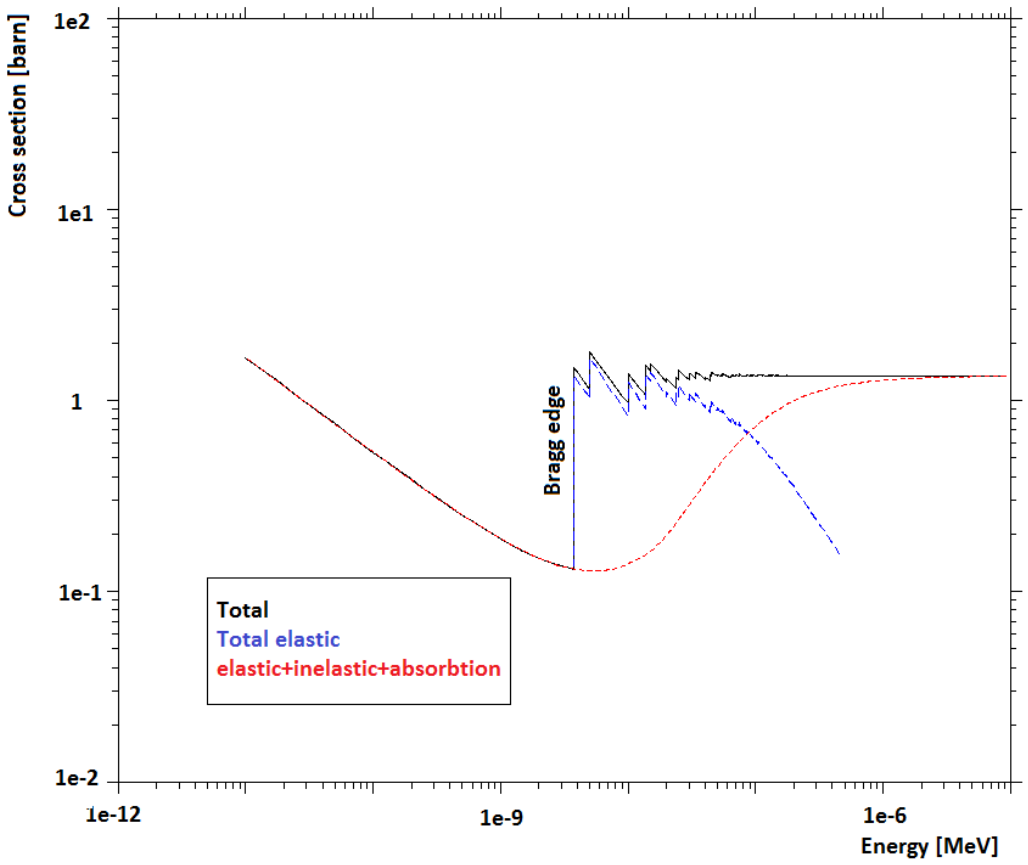

Figure 4.2: The Bragg edges in polycrystalline aluminum. From MCNPX, based on [66].

vative force fields", or $\frac{d}{dt}\rho(q_i, p_i) = 0$. Total elastic scattering can be considered a conservative force on the neutron distribution. This is one of the main motivational factors in the choice of brightness as a figure of merit for the ESS (explained in section 5.1). This is based on two elements, firstly instruments transport neutrons using total elastic scattering processes, and secondly, brightness is a measure of phase-space density. Thus, as a consequence of Liouville's theorem, brightness is conserved during transport in a perfect guide system. Therefore, in the perfect world, the brightness at the moderator surface is identical to the brightness at the sample.

Inelastic scattering

In inelastic scattering mass is converted to energy or vice versa. For fast neutrons, inelastic scattering is nuclear scattering, where the neutron and the nucleus form a compound state that almost instantaneously decays into an excited nucleus and a neutron [57]. In this process, the neutron leaves behind an amount of energy corresponding to the excitation of the nucleus. For neutrons in the lower-energy end of the fast neutron spectrum (i.e. with an energy in the eV range), most nuclei cannot be considered free particles. Since they are typically bound in molecules, when the neutron scatters, it must either scatter elastically on the entire molecule or "knock" the nucleus out of the molecule, which is an inelastic process. Inelastic scattering is incoherent for fast neutrons. But the more interesting regime from a moderator neutronics perspective is

the thermal and cold energy regime, in which inelastic scattering processes are both coherent and incoherent.

According to the theory of thermodynamics, heat in a material is stored in the form of random motion of particles plus a list of quantum mechanical states, such as molecular vibrations, rotations and intermolecular vibrations, known as phonons. These states are typically modeled with the Debye model [75]. When neutrons are slowed down to thermal and cold energy, they scatter on these quantum states.

Besides vibrational, rotational states and phonons, other inelastic scattering processes exist. Only one of these is important to the work described in this thesis: spin excitation in parahydrogen – due to the use of parahydrogen for the ESS cold moderator. Section 4.2.4 explains inelastic scattering on the spin excitation mode of parahydrogen in more detail.

A molecule consisting of N atoms typically has $3N-6$ or $3N-5$ vibrational modes, each with a set of quantum excitation states [76]. When a neutron interacts with a molecule, the neutron might change the vibrational state of the molecule and thereby gain or lose energy in the interaction in addition to the energy gained and lost from the kinematics of the collision. Similarly, a neutron can interact with and change a phonon state and thereby gain or lose energy.

As a material gets colder, fewer of the higher-energy states are occupied. This means that a higher-energy neutron will be more likely to excite a state into a higher-energy state thereby lose energy. As neutrons gets colder, they do not have the energy required for this excitation, and the state effectively becomes unavailable for scattering.

The different available states in a material differ significantly from the solid phase to the liquid, especially regarding the phonon states. The scattering properties of a solid and a liquid therefore differ significantly – but the principle is the same: neutrons interact inelastically and gain or lose energy from the interactions.

In solids, the direction of the lattice becomes important, since phonons travel in specific lattice directions and thus only interact with the neutron if the neutron's energy and direction match the occupied or available phonon excitation state. However, on the macroscopic level, most materials are so polycrystalline that a neutron effectively will travel through a series of small crystal regions each with a new "random" orientation. After traveling a few millimeters, the neutrons have effectively been through a region of each possible orientation. Thus, the directional dependence of the phonon scattering can be ignored in most polycrystals and powders. However, this approximation cannot be used for materials with a larger crystalline structure, and especially not in single crystals.

Moderator neutronics modeling is typically carried out in Monte Carlo codes, such as MCNPX [15]. In fact, MCNPX is used for all the neutronics work presented in this thesis. By default, MCNPX models all scattering as a free gas model, as described in section 4.1, except that MCNPX includes thermal smearing of cross-sections and the kinematics of the thermodynamically moving atoms (modeled as an free ideal gas). The scattering of thermal neutrons is added in by connecting materials to thermal treatment libraries. These libraries are based on dynamic structure factor $S(\mathbf{Q},\omega)$. Without going into detail, the dynamic structure factor is the part of the scattering intensity $I(\mathbf{Q},\omega)$ that involves structure. Figure 4.3shows the difference in cross-section from a free gas to thermal neutron-scattering treatment.

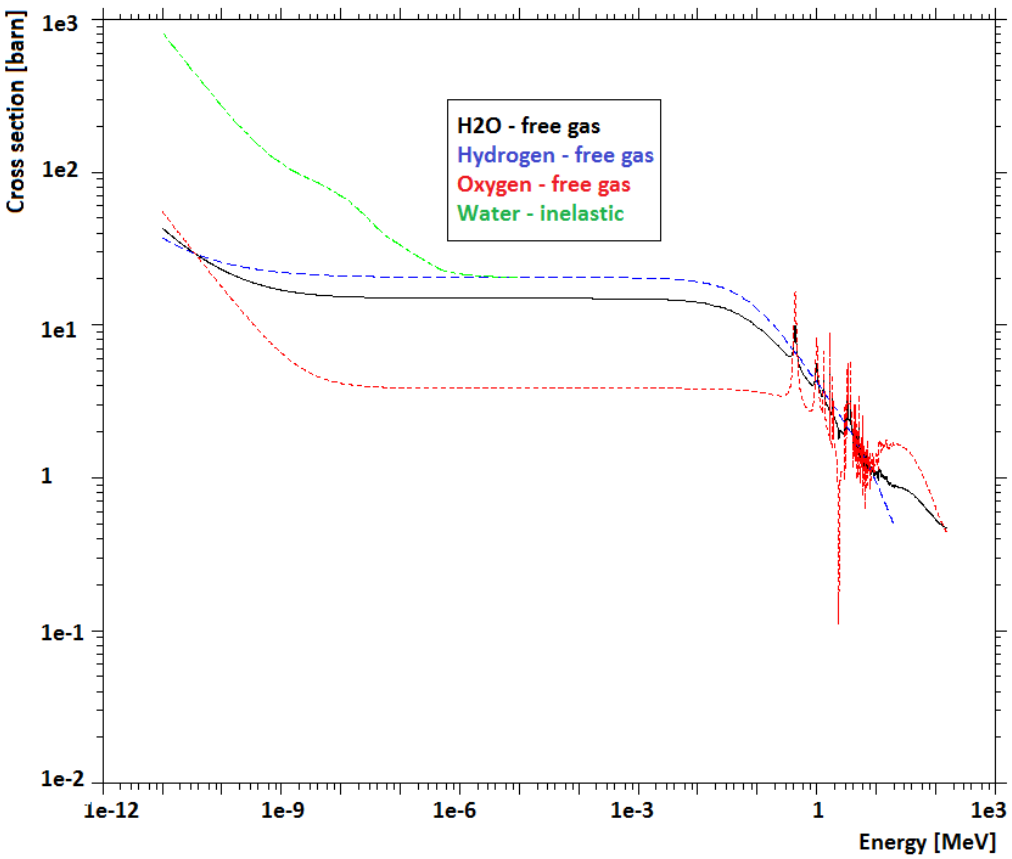

Figure 4.3: Free gas total cross-section model for hydrogen, oxygen and water (2×H+1×O), with the inelastic scattering cross-section extension of water at 300 K. For Monte Carlo technical reasons, the inelastic water cross-section is coupled to hydrogen and will be adjusted to the hydrogen fraction in the water in MCNPX while running but appears to start off wrongly in this plot. From MCNPX based on [66].

MCNPX omits all orientation of materials. This creates some implications that are clarified in the publication presented in Chapter 10. However, the neutron distributions inside neutron sources in moderator and in reflector systems are largely isotropic. For this reason, it can be assumed that a neutron is flying in each direction. MCNPX was therefore built on the assumption that all possible orientations can be averaged over. This makes modeling easier and computer time much faster, but it also makes modeling of single crystals impossible in the standard version of MCNPX. Most ray tracing codes, such as McStas [77] handles crystal effects accurately, however, most ray tracing codes does not provide the Monte Carlo particle transport capabilities necessary to simulate the other effects of a target-moderator-reflector system, and as such cannot be used to simulate the problem in details either. There exist modified versions of MCNPX which can handle some of the directional dependent cross section effects, one is being developed by F.X. Gallmeier et al., which is for example used to simulate the crystal effects in a convoluted moderator in [78]. Another method is to integrate McStas and MCNPX, which has been done by E.B. Klinkby el al. in [16].

4.2.3 Thermalization

Up- and down-scattering of neutrons in a medium results in equilibration around the thermal energy of the medium: thermalization of neutrons. This section focuses on the effects that dominate in the thermal regime. The next section I dig a bit deeper into the more complicated effects that dominate at longer wavelengths.

The average energy of atoms or molecules in a material can be derived from the Maxwell-Boltzmann speed distribution. Since the neutrons equilibrate around the same energy as the medium, they usually assume the same spectrum. The Maxwell-Boltzmann distribution is typically formulated as a distribution of speed v, which gives:

$$M(v) = \left(\frac{m}{2\pi k_B T}\right)^{\frac{3}{2}} \cdot 4\pi v^2 e^{-\frac{mv^2}{2k_B T}}, \tag{4.2.3.1}$$

where m is the mass of the particles, k_B is the Boltzmann constant and T is the temperature. Based on the de-Broglie matter–wave relationship, the neutron speed can be formulated as $v = \frac{2\pi\hbar}{m\lambda}$. Based on this, the Maxwell-Boltzmann distribution can be rewritten into a distribution of wavelengths: a Maxwellian distribution:

$$M(v) = M(\lambda) \cdot \frac{dv}{d\lambda} \downarrow M(\lambda) = \frac{2k_{Th}^2}{T^2\lambda^5} e^{-\frac{k_{Th}}{T\lambda^2}}, \tag{4.2.3.2}$$

where $k_{Th} = \frac{2\pi^2\hbar^2}{mk_B} \approx 949$ KÅ^2. The Maxwellian distribution resembles the neutron spectrum in an infinite, zero-absorption, thermal medium.

The Maxwellian distribution alone is not entirely descriptive, as numerous second order effects play a role. For instance, in the thermal regime, the absorption cross-section rises proportional to the wavelength. As a result a 0.9-Å neutron, near the thermal maximum, is half as likely to be absorbed as a 1.8-Å neutron on the tail of the distribution. Therefore the spectrum shifts towards a higher temperature than the actual temperature of the medium.

The actual neutron spectrum inside a moderator is almost Maxwellian. The deviation can be modeled by a shifted temperature from T to T'. For water, the shift is typically about 25°C, since $T' = T + 25^\circ$ and the spectrum inside a moderator is

$$M(\lambda) = \frac{2k_{Th}^2}{(T')^2\lambda^5} e^{-\frac{k_{Th}}{(T')\lambda^2}}. \tag{4.2.3.3}$$

One thing is the spectrum inside the moderator; another is the observed spectrum off a moderator surface – due to wavelength dependent attenuation, as exemplified and explained in section 4.2.2. Thus when a moderator is observed from a distance, the observed spectrum is also associated with a spectral shift from the spectrum present in the moderator. I have found it a effective to model the observed spectrum is by dividing the modified Maxwellian spectrum by some power of the wavelength,

$$M(\lambda) = \frac{2k_{Th}^2}{(T')^2\lambda^{5+\chi}} e^{-\frac{k_{Th}}{(T')\lambda^2}}, \tag{4.2.3.4}$$

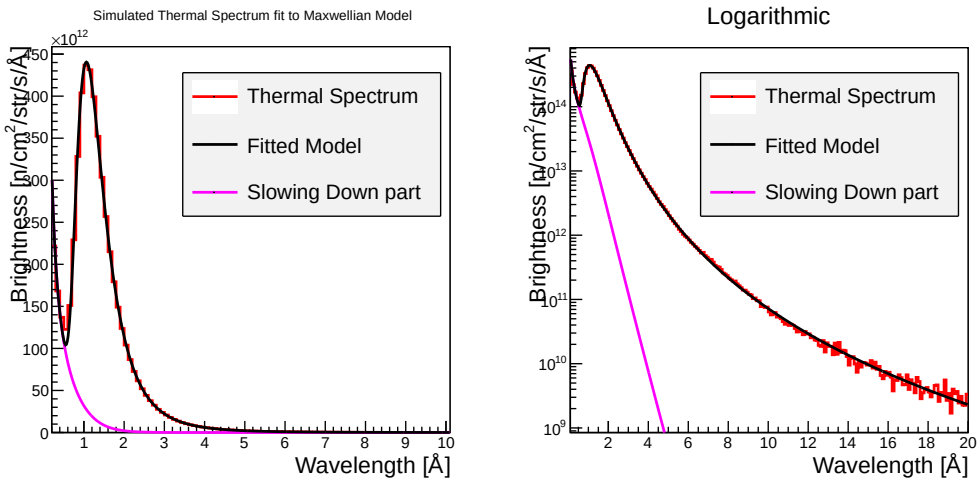

Figure 4.4: Fit of the thermal moderator spectrum observed from a central beamline: data simulated in the ESS TDR [4] geometry. Source: Schönfeldt et al. [20].

where χ has been between 0 and 1 on the distributions I have modeled.

Schönfeldt et al. [20] describe how a slowing-down term can be added to the Maxwellian spectrum to describe the full spectrum. The final model for the spectrum from a thermal moderator is:

$$M(\lambda) = I_{Th}\frac{2k_{Th}^2}{(T+25°\mathrm{C})^2\lambda^{5+\chi}}e^{-\frac{k_{Th}}{(T+25°\mathrm{C})\lambda^2}} + I_{SD}\frac{1}{\lambda}\frac{1}{1+e^{\alpha(\lambda-\lambda_{SD})}}, \qquad (4.2.3.5)$$

where I_{SD} and I_{Th}, respectively, describe the intensities of the slowing-down part and the Maxwellian part and α and λ_{SD} control the slowing-down cut-off function. α is typically set to 2.5Å^{-1} and λ_{SD} is typically set to 0.88Å. Figure 4.4 shows a fit of this function to the ESS TDR spectrum [4].

In summary: the effective observed spectrum from a thermal moderator can be modeled as a Maxwellian spectrum with three modifications.

- The effective temperature should be increased to compensate for incomplete moderation and premature leakage from the system, to T', typically the temperature of the medium plus 25°Cto 50°C.
- Longer-wavelength neutrons should be reduced to compensate for the reduced leakage probability and increased absorption of long-wavelength neutrons. This can be done by dividing the distribution by some power of λ, typically a power between 0 and 1.
- A slowing-down term, proportional to $\frac{1}{\lambda}$, with a cut-off should be added to describe the non-thermalized neutrons leaking from the system.

Schönfeldt et al. [20], Schönfeldt et al. [19] and section 7.1 provide much more on thermal spectra, modeling and fitting and geometrical effects.

4.2.4 Cold moderators

To produce cold neutrons, cold moderators are applied. As the moderator material cools down, the higher-energy excited states in the material become more and more scarce – a consequence of the thermal equilibrium in the material. This means that the upscattering cross-section is reduced and that the average upscatter transfers less energy to the neutrons. Unfortunately, this effect goes both ways. Cold neutrons scatter by exciting and de-exciting quantized vibrational and rotational states and phonons. As their energy drop below the excitation energy of the different states, interaction becomes impossible. For this reason, the downscattering probability of cold neutrons decreases for longer wavelengths as fewer and fewer downscattering interactions are permitted.

Cold neutrons still leak from the moderator. But since the absorption cross-section is high for cold neutrons and since the up- and downscattering cross-section is small, they leak as a non-equilibrating spectrum – the neutrons simply do not "exist" in the system for long enough to equilibrate. Baxter et al. [79] observed one such a spectrum, from the LENS 6 K solid methane moderator, as seen in Figure 4.5. The observed spectrum fits well to three Maxwellian spectra in this case.

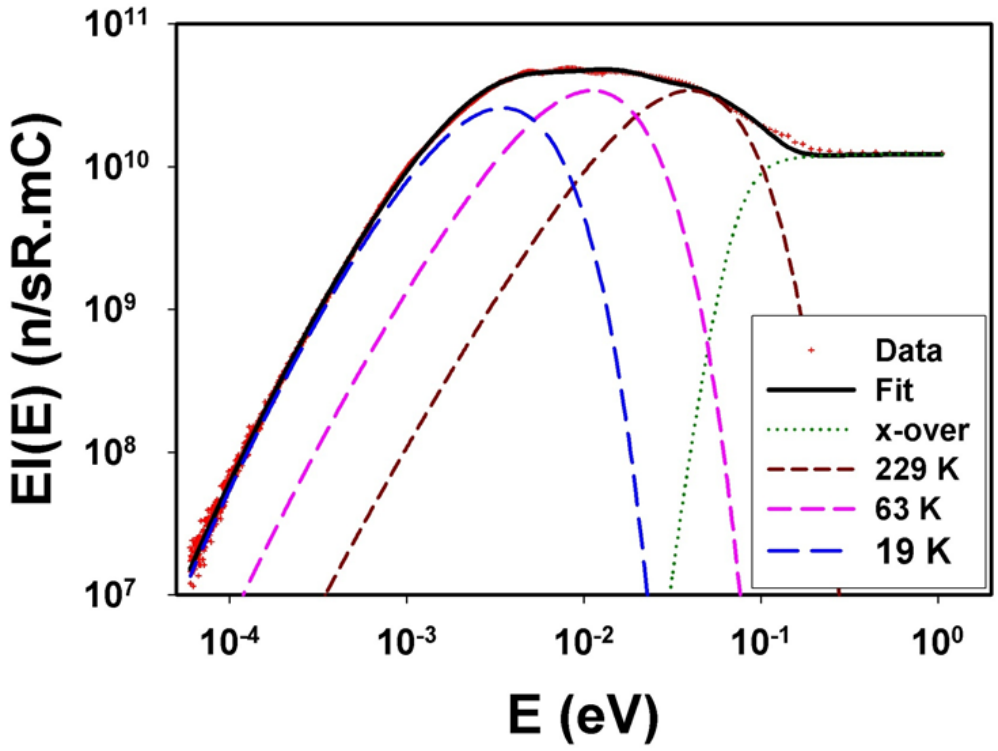

Figure 4.5: Triple-Maxwellian fit to the spectrum observed at the 6 K methane moderator at LENS. Source: Baxter et al. [79].

Cold moderators do not store neutrons in the ambient temperature range for very long, since they are either emitted or downscattered. Thus, short-pulse spallation sources for cold moderators are sometimes applied instead of thermal moderators for instruments requiring ambient room-temperature neutrons (thermal neutrons), since these have a very short emission time from a cold moderator, which increases the

instrument wavelength resolution, and this can be favorable despite the decrease in number of neutrons available.

The optimal (non-advanced) cold moderator material is one with low absorption and plenty of low-energy excitation states to scatter on. One such material is the commonly used solid methane, CH_4. The four hydrogen atoms around a carbon atom result in plenty of vibrational and rotational modes.

One drawback of methane is however that, it contains considerable amounts of hydrogen, which has a significant absorption cross-section for cold neutrons. This problem can be overcome by using heavy methane, CD_4, which has a very low absorption cross-section. But neutrons in deuterium have a very long mean free path compared with hydrogen, and the moderator therefore must be huge to be efficient. This disperses the neutron distribution over a large area, resulting in reduced flux off the moderator and ultimately reducing brightness (see section 5.1).

Having a large moderator not only disperses the hotspot but also results in a longer moderation time, which is very unfavorable for pulsed and especially short-pulsed spallation sources, since wavelength resolution is proportional to time resolution. For these reasons, deuterated materials are rarely favorable as moderator materials for spallation sources.

Nevertheless, the cold moderator at the Swiss Spallation Neutron Source (SINQ) at the Paul Scherrer Institut is a liquid deuterium moderator. This results in a high-intensity moderator (intensity being the brightness integrated over the moderator surface – a measure of how many neutrons leave the moderator in the direction of an instrument). Further, in reactors that are typically continuous, neutrons originate from a large area, and thus compactness matters less, and deuterated materials can be favorable.

Solid methane is hard to cool, as it cannot be circulated out of the system. This problem can be overcome by using liquid methane, which is still an efficient cold moderator material. Solid and liquid methane have different neutron spectra, first because solid methane is typically operated at 20 K, or even 6 K at LENS, whereas liquid methane is operated around 100 K, resulting in a significantly different spectral temperature, but also because of the significant difference in the thermal quantum states of a solid and a liquid.

Further, liquid methane causes problems at high-power facilities, since it forms carbon-hydride chains when irradiated and becomes tar. This slowly clogs up the cooling loop, effectively rendering liquid methane useless at high-power facilities.

At the ESS, the cold moderator experiences a heat load of about 10 kW. Keeping any material at cryogenic temperatures at this heat flux is problematic. The solution is to use a liquid that can be circulated through the moderator. However, finding liquids with good moderator qualities at low temperatures is difficult. In fact, the only cold moderator material currently available for high-power sources is liquid hydrogen.

Parahydrogen and orthohydrogen

Liquid hydrogen comes in two forms, parahydrogen and orthohydrogen. Orthohydrogen is the spin-1 triplet:

- $|\uparrow\uparrow\rangle$,

- $|\downarrow\downarrow\rangle$, and
- $\frac{1}{\sqrt{2}}(|\uparrow\downarrow\rangle + |\downarrow\uparrow\rangle)$,

and parahydrogen is the spin-0 singlet:

- $\frac{1}{\sqrt{2}}(|\uparrow\downarrow\rangle - |\downarrow\uparrow\rangle)$.

It is more favorable for the H_2 molecule to be in the para-spin state, and thus parahydrogen has a lower binding energy than orthohydrogen, about 14.7 meV lower. Since the energy difference between the two states is lower than the characteristic energy at room temperature, hydrogen comprises three parts orthohydrogen and one part parahydrogen at room temperature. When hydrogen is cooled below 14.7 meV (∼170 K), the hydrogen molecules start exchanging spin, and the parahydrogen fraction increases.

Spin exchange is a slow process, and thus reaching equilibrium takes months if no catalyst is present. This means that the ortho-/para- ratio in a system can be controlled between the thermal equilibrium, 3:1, and the cold equilibrium, 99.8% parahydrogen at 20 K, by constructing the correct hydrogen loop applying the correct amount of catalyst [80, 59, 81]

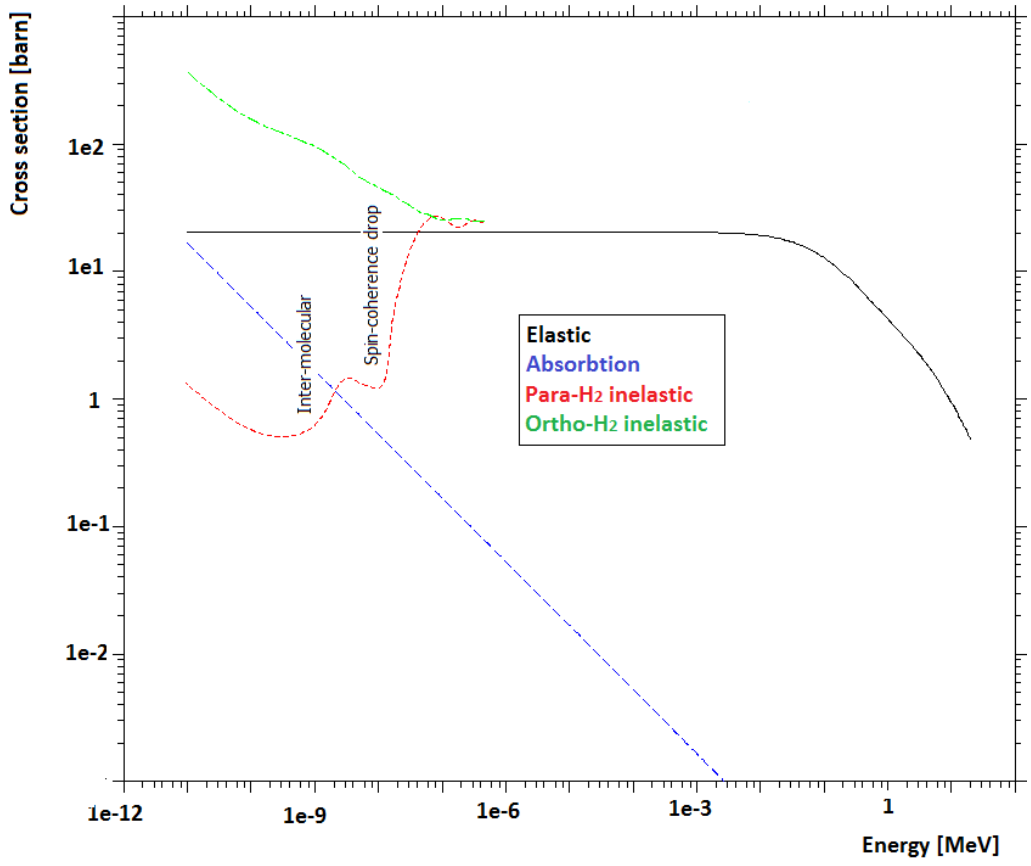

Figure 4.6: Free gas, absorption and inelastic (spin interaction) cross-section of para- and orthohydrogen. From MCNPX based on [66].

From a neutronics perspective, the 14.7 meV spin state energy difference is very interesting. Neutron–hydrogen interactions exchange spin; thus, in the interaction between

a neutron molecule and a parahydrogen molecule, the hydrogen becomes orthohydrogen, which has 14.7 meV more binding energy. As a result, this interaction becomes impossible if the neutron energy has less than 14.7 meV energy, and the total cross-section falls off by more than an order of magnitude, thus increasing the mean free path by more than an order of magnitude. Another lower cross-section spin mode is hidden in the intermolecular spin correlation in hydrogen, which has a lower threshold (a few meV). Figure 4.6 shows the cross-section falloff of the two spin modes.

I previously claimed that a good moderator material is one with a rich excitation spectrum. Hydrogen only has two dominant scattering modes: intermolecular spin at 14.7 meV and a much less intense intermolecular spin state [82]. In the coming two chapters it will be argued that parahydrogen is an inherent advanced moderator, and that such rules of thumb does not always apply to advanced moderators. Orthohydrogen, or hydrogen with a significant orthohydrogen fraction, can be considered the only available non-advanced moderator material for high-power sources – the SNS cold moderators are orthohydrogen moderators [81]. Orthohydrogen still has significant moderator potential but is not as good as methane would have been, due to the lower hydrogen density in hydrogen (70.9 gram hydrogen per litre at 20 K) compared to methane 106 gram hydrogen per litre at 110 K) and the reduced richness of excitation states.

Chapter 5

Designing advanced moderators

Fermi et al. noted the concept of moderation in the mid 1930'. They bombarded uranium and thorium with neutrons from a radon-beryllium source and observed that the neutrons induced more radioactivity in the elements when the experiment was conducted on a wooden table than on a marble table ([83]). This led to the discovery of the thermal neutron reactions and the Nobel Prize in 1938 [84]. Remarkably, wood is not only better than marble; in fact, it is an excellent moderator. It comprises mainly low-absorbing oxygen and carbon and moderating hydrogen and has a rich excitation spectrum, which is exactly what is needed according to the golden rules in moderator neutronics, as outlined by Muhrer [9]. There are better materials than wood, and there are also better geometrical configurations than a tabletop.

This chapter discusses the figure of merit as defined by the ESS and the basic role of and principles behind a moderator. The chapter also provides a brief guide to moderator design based on my interpretation of conceptual moderator design.

5.1 Figure of merit

Figure of merit is subject to an element of choice and is thus always difficult to encompass all desired features. For a neutron source, the only two things that matter are how many neutrons of interest reach the experiments and the ratio between signal and background. Examining the TMR system alone is insufficient to determine these values. In fact, neutrons should be simulated from when they are created in the target and all the way to being detected in the detectors to fully understand what is signal and what is background. Such full simulations are very complex and demanding, and defining an intermediate figure of merit between the TMR system and the instruments is typically preferred.

The ESS has officially chosen brightness (see below) as the figure of merit for moderator efficiency [4]. Thus, it is "blindly" used as the figure of merit for this work. Brightness can be used to decouple the efficiency of the TMR system from the instruments and experiments, such that the TMR system can be optimized independently of the instrument.

There are other good figures of merit for neutron sources. For instance, for short pulsed sources, the time distribution of neutrons is very important, and brightness as the sole figure of merit would therefore be insufficient. The following section argues

why brightness is a good figure of merit for the ESS. However, I do not intend to claim that brightness is the only or the best figure of merit, especially for other neutron sources than the ESS.

The efficiency of most experiments is assessed by the number of useful neutrons [4]. The definition of a useful neutron varies from experiment to experiment and determine the requirements to the neutron optics of the deployed extraction system. A neutron experiment typically uses less than one millionth of the neutrons created at the neutron source, for several reasons [5]. Moderator systems are imperfect: not all the source neutrons cool, and many of those that cool are absorbed before emission. Further, most moderators emit a spectrum of neutrons that is several angstroms wide (see section 4.2.3), and experiments typically require a specific wavelength or set of wavelengths [41, 42, 43], so that much of the produced spectrum is discarded or even considered background.

Most scattering processes in a moderator can be considered isotropic, and neutrons are therefore emitted in all directions. The isotropic processes result in the thermal neutron distribution covering large volumes, even if they originated at a point when they were fast. As a result, the moderator system will emit neutrons from anywhere and in all directions. This is not very compatible with the limited size of neutron instruments. Instruments extract neutrons from a area some distance from the moderator. Moreover, neutron guides can only reflect, and thus transport, neutrons in a narrow angular span, and with less-than-perfect efficiency. In addition, there is a wide array of different effects depending on the extraction instrument, neutron optics and experimental requirements.

Simply counting the number of neutrons emitted by a moderator does not say much about the usefulness of the system. Neutron current or neutron flux at the moderator surface has often been used as a figure of merit, typically with some reduction in the range of neutron energy to accommodate the instruments' need for neutrons with a specific wavelength. However, moving from the flux or current at the moderator surface to the flux or current at the guide entrance involves complex modeling. To illustrate the complexity, first consider the moderator as an isotropic point source; in this case, the flux at the guide entrance would be the flux at the source divided by the square of the distance. Now consider the moderator as an infinite surface; in this case, the flux on the guide entrance would be equal to the flux on the moderator – given isotropic emission. In reality, moderators are neither point sources nor infinite but something in between. Further, an instrument cannot directly extract the moderator surface flux or current because of the requirements on angular distribution imposed by the instruments neutron transport system.

One consequence of Liouville's theorem ([74]) is that the neutron phase-space density is transport invariant (see section 4.2.2). This means that the neutrons phase-space density at the moderator is the same as the neutron phase-space density at the guide entrance. Further, the phase-space density can be transported through a guide system, which uses totally elastic processes. By using, for instance, elliptical guides, the shape of the phase space can be transformed in the process: the neutron beam size can be reduced at the cost of increased divergence or vice versa (except for inefficiencies) – very similar to a common optical lens. Modern instruments apply a curved, parabolic and elliptical super-mirror guide system to optimally exploit this principle.

Given this, the neutrons from a moderator system should be measured through the

phase-space density, since this is what will end up on the sample in theory. One such measure is the brightness, B, also known as the angular flux Φ_Ω [22]. The angular flux can be defined as $\Phi_\Omega = v\rho(\overline{q}, \overline{p})$, where $\rho(\overline{q}, \overline{p})$ is the phase-space density and v is the particle speed [57]. Since no energy is transferred in total elastic scattering, v is constant and thus Φ_Ω is proportional to the phase-space density, i.e.: **brightness is transport invariant.**

Because Liouville's theorem impose transport invariance, the brightness yields the same value at any distance from the moderator. The brightness should typically be measured at least a couple of meters away to account for the fact that the moderator does not emit neutrons perfectly isotropically. Moreover, if the moderator surface emits neutrons homogeneously across the surface, the same brightness will be observed from any selected region of the moderator. Similar to flux and current, brightness is often divided into different wavelength regimes – typically cold, thermal and fast.

The ESS uses brightness as the official figure of merit for moderator efficiency. The ESS divides it into thermal and cold brightness. Thermal brightness is defined as the brightness of neutrons between 20 and 100 meV. Cold brightness is defined as neutrons with energy either 0 to 5 meV or 0 to 20 meV. The limit was officially changed from the former to the latter during the design process for the flat moderators presented in Chapter 7. This thesis uses both definitions. However, brightness measured with the different definitions are more or less proportional. The results obtained using either definition are consistent for all the moderator concepts covered in this thesis, except the reflector filter, in which the gain exists only for neutrons with energy below the Bragg edge, which is usually 5–10 meV depending on the material.

Brightness as a measure for source strength is widely disputed, since it not easily measured experimentally, whereas flux can be measured fairly easily. Despite the dispute, the ESS uses brightness as the official figure of merit, and this work therefore uses it consistently as the figure of merit throughout.

Schönfeldt et al. [22], included in Chapter 8, discuss brightness in more depth, and extends the concepts from the usual brightness spectrum.

5.2 The basics of moderators

The role of a moderator is to deliver useful neutrons to experiments: that is, to maximize brightness in the relevant wavelength range used by scattering instruments. Simplified, this can be divided into three tasks for a moderator:

- accumulate neutrons from the source;
- cool them to the correct spectrum; and
- emit them towards the experiments.

This is an optimization task. The moderator should be large enough to cover as large an area of the source as possible – to maximize the number of neutrons entering. It should also be large enough that neutrons are cooled before they leave, while small enough that the cooled neutrons are not absorbed before they leave. The optimal size depends on the moderating material.

The choice of material and the temperature of that material can solve the challenge of neutron cooling. According to Muhrer [9], the tribal knowledge in neutronics has resulted in two golden rules for moderator material.

- The total thermal neutron flux of a moderator scales with the hydrogen density of the material used as the moderator.
- The richer the excitation spectrum of a moderator material, the higher the flux generated by the moderator.

Water is typically used for thermal moderators and methane for cold moderators [8]. Unfortunately, materials are also constrained by other requirements, such as cooling demand and lifetime. At high-power facilities, only hydrogen is available as a cold moderator, and hydrogen does not have high hydrogen density (70.8 gram per litre - less than that of water, 111 gram hydrogen per liter, or methane, 106 g hydrogen per liter), nor does it have a rich excitation spectrum (two spin excitation states). However, being the only available cold material for high-power sources makes the competition trivial.

Deuterated materials, such as heavy water (D_2O) or deuterium (D_2), can be used to reduce absorption. However, they have lower slowing-down power and longer mean free paths (see section 4.1), so these materials tend to disperse the neutrons over a larger area, which reduces brightness (although reducing brightness might increase the total number of neutrons emitted, since fewer neutrons are absorbed). This also results in slower moderator response, which broadens the emission time and then ultimately reduces the energy resolution in the instruments. In general, deuterated materials are not preferred as moderator materials at spallation sources, especially the pulsed ones.

In summary, a good moderator is a thin enough slab covering a large area over the target hotspot made from a material with high hydrogen density and a rich excitation spectrum. A 3 to 4 cm slab of methane or 4 to 6 cm of orthohydrogen has typically been used for cold moderators, and a 3 to 5 cm thick slab of water has been used for thermal moderators [8]. For low-power sources, polyethylene is an excellent substitute for water, especially to avoid dealing with a (radioactive) liquid.

5.2.1 Pre-moderators and reflectors

The hydrogen cross-section drops for fast neutrons: above 10 keV (Figure 4.6). Since neutrons from both spallation and reactor sources far exceed this energy at birth [6], they tend to fly straight through hydrogen. This is a problem when using pure hydrogen moderator: unlike water and methane, hydrogen does not have any other nuclei that can scatter the fast neutrons. This can be solved by applying pre-moderators. A pre-moderator is typically a water layer 1–3 cm thick covering the sides of the moderator that are not observed by instruments. This water layer slows down or even thermalizes some of the neutrons before they enter the cold moderator, which increases the efficiency of cold moderators and reduce cooling requirements. For pure hydrogen moderators, a pre-moderator significantly increase the neutron yield.

In a simple geometrical configuration with a moderator next to a target, many neutrons are lost from the target in directions not covered by the moderator. Further, many fast neutrons will simply fly through the moderator (and pre-moderator) and escape the system or scatter a few times and leave the system before thermalization. By

placing some low-absorbing, high-scattering cross-section material around the target-moderator system – a reflector – many of these "lost" neutrons can be rescattered for a second chance in the moderator. Graphite is an inexpensive and readily available material with a very low absorption cross-section (0.0035 barn for a 2200 m/s neutron [61]) and moderate (coherent) scattering cross-section (5.551 barn for a 2200 m/s neutron [61]) and thus a good reflector. Water can also be used; despite its fairly high absorption cross-section (0.22 barn for a 2200 m/s neutron [61]), water can be used as reflector, with excellent inherent pre-moderator capabilities. For more expensive sources, low absorbing beryllium (0.0076 barn for a 2200 m/s neutron [61]) is typically used; this material is better than graphite because of its shorter mean free path, beryllium also have a significant (n,2n) cross-section which results in an increase in the number of available neutrons. Diamond would be slightly better than beryllium, since the high-density carbon has an even shorter mean free path (due to the roughly 50-60% increase in density over graphite). The production price for diamonds has been declining in recent years, and these might soon become viable for high-power sources.

	Cold brightness (E<20 meV) [A.U.]	Thermal brightness (20 meV<E<100 meV) [A.U.]
Full system	1	1
No pre-moderator	0.303	0.400
No reflector	0.574	0.583
No pre-moderator or reflector	0.076	0.137

Table 5.1: The effect of replacing the beryllium reflector and/or water pre-moderator with void. MCNPX simulations in the ESS butterfly geometry. The water disc, explained in Chapter 7.1, is here interpreted as a pre-moderator. The brightness declines drastically, especially when neither reflector nor pre-moderator are present. Note that the system is a flat moderator system, which is somewhat more sensitive to pre-moderators and reflectors than many other moderator systems.

To some extent, reflectors serve as pre-moderators, and pre-moderators serve as reflectors; thus, measuring the effects of one or the other separately is difficult. Further, structural and shielding materials and the target itself also serve as reflectors and pre-moderators. In addition, a source typically has more than one moderator, and these cross-talk and act as pre-moderators and reflectors for each other. In conclusion, target-moderator-reflector systems are complex and require vast optimization to yield the optimal brightness. Table 5.1 shows the drastic effect of removing pre-moderators and/or reflectors in the ESS butterfly geometrical configuration.

5.2.2 Quick guide for moderator designers

Based on my experience, a few rules of thumb should be followed when designing a moderator system.

- Maintain compactness: maximize the amount of reflective material near the moderator and minimize gaps and structural material. When possible, minimize the distance between moderator and target.
- Only use pre-moderators (or thermalizing reflectors) very close to the moderator. Do not thermalize fast neutrons too far from the moderator: thermal neutrons

get "stuck" (they have a shorter mean free path).

- Always reoptimize: every little change in your system changes the global neutron distribution, and your intuition might fail you. In particular, reoptimize the moderator and pre-moderator dimensions and position relative to the target. These can be significant even on a millimeter scale.
- Carefully consider the advanced moderator concepts, found in the next Chapter, for each concept: remember to reoptimize - an advanced modearator concept might be better in its optimal configuration, but the optimal configuration might not be trivial to find.
- Moderator systems are complex and you should rely on Monte Carlo simulations. Use conventional wisdom and intuition, but rely on the simulations.
- Consider your engineering constraints: the system needs cooling; liquids needs casings; regions of different temperature needs separation – keep these constrains in mind when designing.

5.2.3 Cooling and engineering

The principles described so far in section 5.2, and in this thesis in general, focus on the physics side of moderator design. However, engineering and cooling moderators, especially cold moderators at high-power facilities, is challenging.

A moderator at a high-power facility is cooled by pumping the moderator fluid through the moderator container, typically made from aluminum. Since much of the heating of the moderator system comprises heating of the aluminum container, and since heat is transported from the system in the liquid, the container heats up. The hottest part of the moderator is therefore typically the container itself, which can result in boiling on the container surface. This boiling results in bubble formation, or voiding, on the container surface, which in effect results in the moderating volume becoming smaller than the available cavity in the container. Such effects can be taken into account in the moderator design, and the aluminum container can be made slightly larger than the optimal thickness of the moderating material. Voiding also results in heating of the container, if it is cooled by the liquid, due to loss of thermal contact near the bubbles, and also the moderating material will be hotter in the region near the void formation, these effects can have an impact on the neutron spectrum.

This thesis revolves around the ESS, in which the moderator is made from parahydrogen, which is effectively transparent to cold neutrons [82]. For this reason, parahydrogen moderators are typically very deep (observed from the instrument). As a result, the potential void build-up on the moderator surface minimally affects the total depth. Also, parahydrogen is an advanced moderator which emits its neutrons prior to full thermalization, therefore temperature effects are minimal. for these reasons voiding does not affect the emitted spectrum significantly.

In a liquid moderator, the flow pattern needs to be controlled, which often requires putting some wings of structural material inside the moderator, and this reduces the amount of moderating material in the moderator.

Further, the reflector system has to be cooled. As a result, a beryllium reflector is not made from a solid block of pure beryllium. It must have cavities through which

a coolant can flow, and these cavities may or may not require a special coating or an aluminum pipe. All these reduce the efficiency of the reflector.

Lastly, all these cooling systems need pipes connected to a cooling facility. The position of these pipes can drastically affect the brightness of the moderator system, since they take up space and also need void gaps for thermal separation. Further, these cooling systems will generate heat in the pipes and cooling material.

Another factor to account for is the fact that components at different operating temperatures need to be thermally separated, typically by a vacuum gap. Such a vacuum gap strains the structural containers, since many components, such as the cold moderators, operate at high pressure to achieve the needed flow for cooling and to ensure that they are liquid at the operating temperature. This facilitates the structural thickness of containers being typically a few millimeters wide. At the ESS, the aluminum thickness, at the time of this study, was about 3 mm, and the vacuum gaps were about 5 mm thick. This results in a separation distance between components of about 1.1 cm, which substantially affects the systems compactness and thus brightness. This should be integrated into the moderator design.

In addition to all the cooling-related engineering issues, there are many non-cooling-related issues. For instance, the system needs to have excess spacing for swelling and structural deformation from radiation damage.

In conclusion, a conceptual moderator design differ significantly from an actual implemented moderator. In the conceptual design phase for the ESS moderator system (first the flat moderator and then the butterfly), we operated with an expected loss in brightness of 25% because of engineering and cooling implementation. This was later shown to be a good estimate, consult Batkov [85].

5.2.4 Wing versus slab geometry

Geometry is clearly essential to a moderator system. The most basic important geometrical configurations are the wing and slab geometry, as illustrated in Figure 5.1. The ESS is designed in wing geometry.

In the slab geometry, the target is "viewed" through the moderator, resulting in significant high-energy and fast neutrons – which are typically considered background. The proton and neutron beamlines are typically perpendicular, and thus only a small, yet still significant, fraction of the high-energy neutrons migrates in the direction of the neutron beamline. This is due to the high-energy neutrons are mainly directed forward relative to the proton beam [34].

In the wing geometry, fast and high-energy neutrons must scatter to end up in a beamline, as there is no direct line of flight from the target hotspot to the neutron beamline. This significantly reduces the fast neutron background. However, the geometry of the wing-type moderator is not as optimal as that for the slab, mostly due to reduced coverage area over the target, see section 5.2. The wing geometry therefore experiences reduced thermal and cold brightness compared to the slab geometry. Especially in the wing geometry, the reflector becomes very important, as it can regain some of the neutrons that are lost to the reduced target coverage.

Despite the reduced useful brightness, the reduction in background is large enough that this geometry is often favorable. The ESS has wing geometry. A third geometry

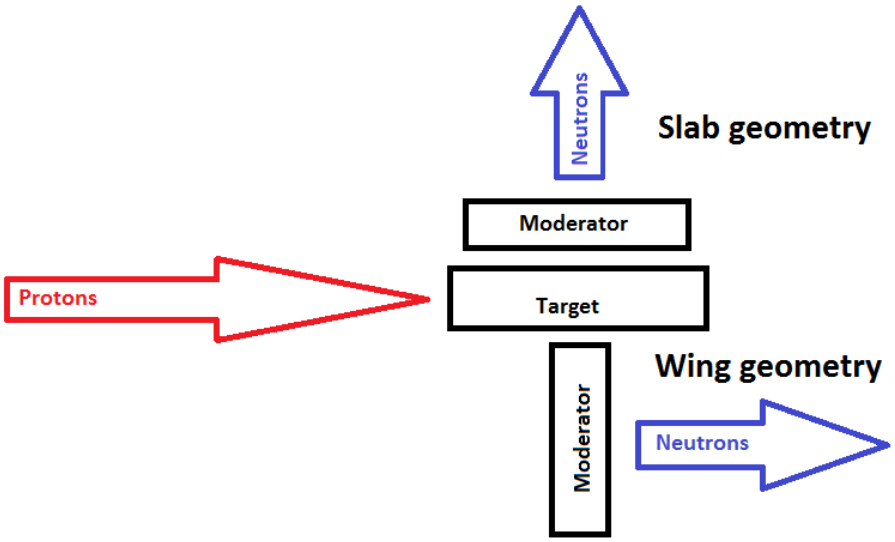

Figure 5.1: Slab geometry above and wing geometry below a target. In the slab geometry there is a line of sight from the neutron beamline, through the moderator, to the target hotspot. In the wing geometry, there is no line of sight from the neutron beamline to the target hotspot. In the figure the neutron beamline and the proton beamline are illustrated as parallel, which they can be in the wing geometry, but the neutron beamline can be rotated around the vertical axis in the figure, to any desired orientation and there will still not be a line of sight from the neutron beamline to the target hotspot.

option, the flux trap geometry, also exists and is explained later -. for more on basic target-meoderator configurations I recommend consulting [86].

5.3 Cavities, grooves and re-entrant holes

As neutrons leak through the moderator surface, the neutron population in a moderator must be reduced near the surface, and thus the neutron density must be highest near the center of the moderator. The observed neutron brightness must be somewhat proportional to the neutron density near the moderator surface ("near" being a few mean free paths, which is about 1 cm in water, methane and orthohydrogen).

Drilling holes (grooves) or one larger hole (a re-entrant hole) into the moderator (see Figure 5.2) facilitates entrance into the region with higher neutron density and thus increases brightness. These types of geometry usually significantly increases brightness, typically about 50% [8]. Many operating moderator systems successfully use grooves and re-entrant holes [8].

A similar concept is the cavity-type moderator, also seen in Figure 5.2, where liquid orthohydrogen is typically shaped as a shell forming an internal cavity inside the moderator. Neutrons are scattered around inside the cavity, with an increased likelihood of ending up leaving the moderator through the hole in the shell. For more, see Carpenter [8].

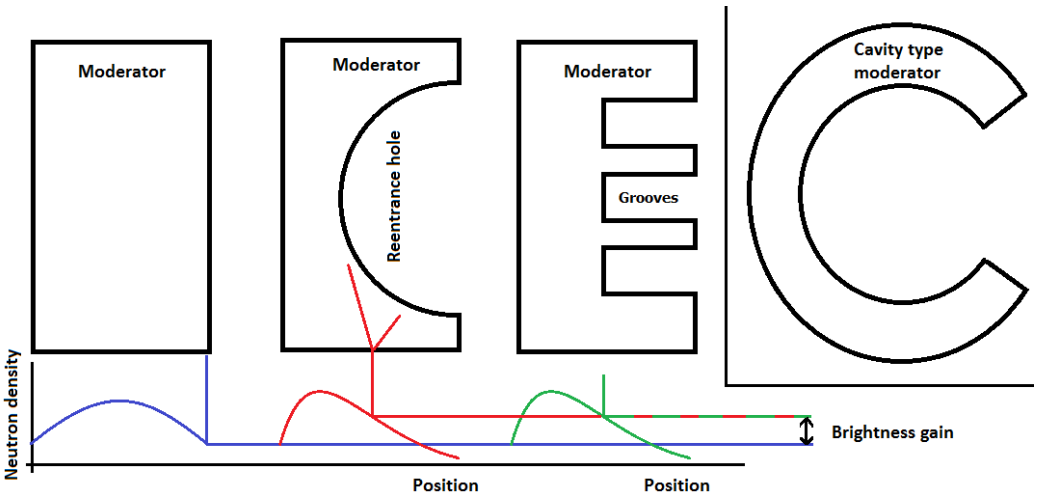

Figure 5.2: Sketch of grooves, reentrant hole and a cavity type moderator.

Chapter 6

State-of-the-art moderator concepts

This chapter examines the major advanced moderator concepts that have been developed historically. The explanation is based on my conceptual interpretation of the principles behind the concepts.

This chapter does not contain any information on ultracold moderators, but Golub et al. [87] provide information on ultracold neutrons, and Nesvizhevsky et al. [88] is recommendable reading. A nanodiamond collaboration was formed under the IAEA CRP framework in which I played a leading role. The collaboration aims at assessing the high-albedo properties of nanodiamonds, which potentially can be used to greatly increase the ultracold neutron yield from ultracold neutron sources. However, ultracold neutrons and nanodiamonds are not a topic of this thesis and no results are presented here.

6.1 Convoluted moderator

Grooves, re-entrant holes and cavities are so widely used and have been used for so long that they almost cannot be considered an advanced moderator concept [8]. However, one similar concept, the convoluted moderator, is definitely considered advanced. The convoluted moderator consist of alternating thin layers of moderating material (with a short mean free path) and transparent material (with a long mean free path), as suggested by Stuart Ansell [89]. This can be imagined as a stack of very thin grooves. Figure 6.1 shows a sketch of a convoluted moderator (taken from Gallmeier et al. [90]). Iverson et al. [91] describe this in more detail, including experimental results.

The basic idea is that the moderator has more scattering power in one direction than in the other, see Figure 6.1. Neutrons will therefore be more likely to be emitted at narrow angles relative to the transparent planes. Note in Figure 6.1 that the brightness is reduced in the direction parallel to the plane. This is because almost no neutrons scatter in the transparent planes – because they are transparent. For this reason, the moderator is expected to emit most of the neutrons slightly skewed from the moderator surface normal (a few degrees from the planes), as observed in Figure 6.1.

I have earlier argued that total elastic scattering has no or little relevance inside a moderator because of the second law of thermodynamics and the isotropic nature of

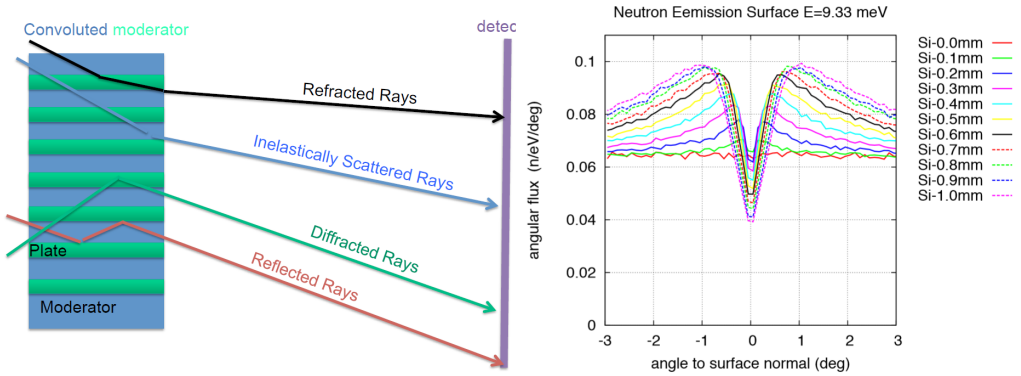

Figure 6.1: Illustration of the convoluted moderator and simulations with different silicon layer thicknesses using the modified version of MCNPX described by Gallmeier et al. [90].

the neutron distribution inside the moderator. However, in a convoluted moderator, the distribution is directional. A total elastic effect and the directionality of scattering therefore cannot be ignored. In fact, as seen in Figure 6.1, total elastic effects, in the form of reflection, refraction and diffraction, can potentially significantly increase the moderator's efficiency. A convoluted moderator mock-up is hard to simulate using conventional Monte Carlo codes, such as MCNPX, since reflection and refraction are not included and since diffraction is considered isotropic (or has too few discrete steps). MCNPX therefore cannot simulate single crystal scattering. Attempts have been made to implement material orientation and total elastic in MCNPX. Gallmeier et al. [90] made one such implementation based on the crystal scattering algorithms from McStas. This implementation has been used to study a convoluted moderator in the LENS geometry.

The LENS collaboration conducted a series of experiments on convoluted moderators using polyethylene-silicon and watersingle-crystal silicon. Iverson et al. [91] present the results of the polyethylene-silicon experiments. The latest experiment, water-silicon, was carried out in November–December 2012 within this PhD project. However, since no publications have yet been produced, the data are not shown or analyzed here. Here it is sufficient to say that the angular distributional effect has been observed, but the observed gain was not impressive, probably because of the unoptimized geometry. Thus, this does not detract from the quality of the concept. Finding optimal geometry can only be investigated in practice through extensive simulations, which requires developing and validating correct total elastic scattering implementation into Monte Carlo codes such as MCNPX, i.e. more work similar to that of Gallmeier et al. [90] is needed.

6.2 Reflector filters

A very successful concept for cold (less than 5 meV) neutron moderators is the concept of a reflector filter, as suggested by Carpenter [92]. This concept exploits the Bragg edge in cold beryllium.

Placing a thick (10–20 cm) block of beryllium in front (the side facing the instruments) of the cold moderator significantly increases the neutron density in the moder-

ator, especially near the front face. This is due to neutrons from the moderator or the surrounding reflector are likely to scatter in the beryllium and thus might enter the moderator from the moderator front phase. Naturally, placing a thick piece of beryllium between the moderator and the experiments reduces the brightness drastically. The trick is in the Bragg edge of cold beryllium, which results in a drop in cross-section of several orders of magnitude around 5 meV (∼4 Å) (the Bragg edge of beryllium at 20 K and 300 K can be seen in Figure 1 of the paper attached in Chapter 9 [28]). Beryllium is effectively transparent to neutrons below this energy. The increased neutron density in the moderator results in significantly increased brightness below this cut-off energy – roughly a factor of 2 at the Manuel Lujan, Jr. Neutron Scattering Center at the Los Alamos Neutron Science Center, where the first operational reflector filter has been successfully installed [93].

Schönfeldt et al. [28], included as Chapter 9, discuss the use of a few-centimeter-thick slab of enriched ^{208}Pb as an advanced reflector filter. Although this is less effective than beryllium for very-long-wavelength neutrons, this type of reflector filter can serve as both a reflector filter and a broad-spectrum moderator. This thesis returns to broad-spectrum moderators in section 6.8, under bispectral moderators, and Chapter 9 explains more about advanced lead reflector filters.

6.3 Single-crystal reflector filters

A reflector filter has a gain below (in energy) the Bragg edge and suppression above it. For many experiments, the neutrons in the thermal energy range are also very important. To resolve Muhrer [31] suggested the concept of a single-crystal reflector filter.

In a polycrystal, the crystal grains are oriented randomly, and thus a neutron (with the appropriate wavelength) will most likely fulfill the Bragg condition in at least one of these crystal grains while traversing the crystal - given that the crystal is large enough. However, in a single crystal only neutrons with very specific wavelength and direction fulfill the Bragg condition. For this reason, single crystals do not have Bragg edges. Instead, a single crystal has delta-function-like spikes in cross-section where the Bragg condition is fulfilled, but this effect is evened out if the neutron distribution is sufficiently isotropic, which is the case near a moderator.

Gain similar to the gain in a reflector filter below the (non-existing) Bragg edge would be expected if a single-crystal reflector filter is placed in front of a moderator. Nevertheless, since there is no Bragg edge, the gain above this limit should also be similar. As a result, a single crystal reflector filter can be used to regain some of the lost neutrons in the thermal range.

The LENS collaboration produced experimental proof of concept of a single-crystal reflector filter at LENS, with promising results, as part of this PhD project. A paper was recently published in "Nuclear Instruments and Methods in Physics Research A" [94] and is included in Chapter 10 of this thesis.

6.4 Decoupled and poisoned moderators

6.4.1 Note on time resolution

For continuous sources, Bragg scattering is sometimes used to select a neutron's wavelength or energy using monochromators. One problem with this method (although this can be an advantage in some cases) is that Bragg scattering is highly discrete, and thus only a specific energy level will be selected (or a set of energy levels fulfilling the Bragg condition). A neutron's energy, or wavelength, can also be determined with high precision from its time of flight. For continuous sources, the time of flight can be determined by imposing a time structure, for example, by using a chopper (see section 2.3).

For pulsed sources, the time structure is inherent, but slowing down a neutron takes a short, but non-zero, time. This results in a blurring of the time structure of the neutron beam compared with the proton beam. But worse, thermal and cold neutrons are stored in the moderator reflector system for a while before they are emitted, which results in a long tail (hundreds of microseconds) on the time structure. This ultimately reduces wavelength resolution. The Ikeda-Carpenter function [95] describes well the emission time structure for a short pulsed source and is given by:

$$\begin{aligned} IC(t) = &\frac{\alpha^3}{2}(1-R)t^2e^{-\alpha t} \\ &+ \alpha^3 R\frac{\beta}{(\alpha-\beta)^3}\left(e^{-\beta t} - e^{-\alpha t}\left((\alpha-\beta)^2\frac{t^2}{2} + (\alpha-\beta)t + 1\right)\right) \end{aligned} \tag{6.4.1.1}$$

Where R is the thermalization ratio, which determines the ratio of neutrons that are thermalized and stored, to neutrons that are slowed down, cooled and emitted directly without a delay. α relates to the slowing-down time and is typically in order of 5^{-1} μs^{-1} to 20^{-1} μs^{-1} [96]depending on the moderator-reflector system and the wavelength of interest: it is the inverse characteristic of the slowing-down time. β is the inverse characteristic storage time, which differs significantly between reflectors and moderators and from system to system.

A conventional moderator system, which is not decoupled (as explained in a moment) is normally denoted a "coupled" moderator system. For a coupled moderator system, the Ikeda-Carpenter function should be expanded, since it does not have a single characteristic storage time (as is assumed in the derivation of the function) but several storage times connected to different components of the system; reflector, pre-moderator and even shielding and structural materials. Nevertheless, in my experience from modeling coupled moderators at ESS and LENS, the Ikeda-Carpenter function can fairly well describe even coupled systems to the first order, with a β that is typically in the range of $200^{-1}s^{-1}$ to 400^{-1} μs^{-1}. In reality, all three parameters depend on energy, and thus $IC(t)$ should be $IC(t, E)$ with parameters given as $R(E)$, $\alpha(E)$ and $\beta(E)$.

This thesis is centered around a long pulsed coupled source, the ESS, where the time structure has largely been omitted. At the ESS the pulse is almost 3 ms long, and thus a tail of a few hundred microseconds is not important. At ESS, most instruments will apply choppers to subdivide the long pulse into several short pulses, which gives the time resolution of the instruments [4]. The long pulse structure can still be used

to reduce background, especially from fast and high-energy neutrons.

6.4.2 Decoupling and poisoning

Decoupled moderators are moderators that are wrapped in a layer of a material with a high thermal neutron absorption cross-section on all sides except the viewed surface. Cadmium is a good candidate for a decoupling material, since it has very high thermal absorption (2520 barn for a 2200 m/s neutron [61]) and a fairly low fast neutron absorption cross-section, and it is for instance used as decoupling material for experiments at LENS [94]. This decoupling layer prevents cold and thermal neutrons from bouncing back and forth between the moderator and reflector, which takes time, and it also prevents neutrons that have been thermalized and stored in the reflector from entering the moderator. These neutrons are the main contribution to the long tail of the neutron emission time distribution; thus, absorbing them significantly shortens the neutron pulse length. In terms of the Ikeda-Carpenter function, decoupling reduces the number of neutrons that are thermalized and stored in the system to those that are thermalized and emitted right away, or "prompt". This results in the prompt peak of the emission time distribution being larger compared with the tail. It also reduces the characteristic storage time from being dominated by the long storage time in the reflector to being dominated by the short storage time in the moderators, thus reducing the characteristic storage time of the system from several hundred microseconds to less than 100 μs.

Decoupling clearly does not result in extra neutrons, since it simply absorbs neutrons. Hence such an absorbing layer is unfavorable in terms of brightness (both time integrated and peak). However, decoupling significantly increases the time resolution for experiments, which benefits many experiments.

Another trick that can be used to increase time resolution, again at the cost of brightness, is applying a neutron poison to the moderator: mixing an absorbing material into the moderator material. The poison reduces the lifetime of a cold or thermal neutron inside the moderator, resulting in an even shorter tail of the time distribution.

The short pulsed sources SNS and J-PARC, have both a decoupled, and sometimes poisoned, moderator for high-wavelength-resolution experiments and a coupled moderator for maximum brightness. However, decoupling and poisoning is only meaningful at short pulsed sources, and thus of no interest at the ESS.

6.5 Backscattering moderator

In a total backscatter collision (a 180° scattering angle) between neutron and hydrogen, the neutron loses nearly 100% of its energy, which kicks it into the cold or thermal energy regime in a single collision. Positioning the moderator in a backscattering geometry exploits this principle (see Figure 6.2) [86].

A backscattering moderator is quite effective at long wavelengths. However, the moderator is not in an optimal position, and overall brightness is thus not favorable [86].

Both a thermal and a cold backscattering moderator are installed at the Manuel Lujan, Jr. Neutron Scattering Center at the Los Alamos Neutron Science Center [86],

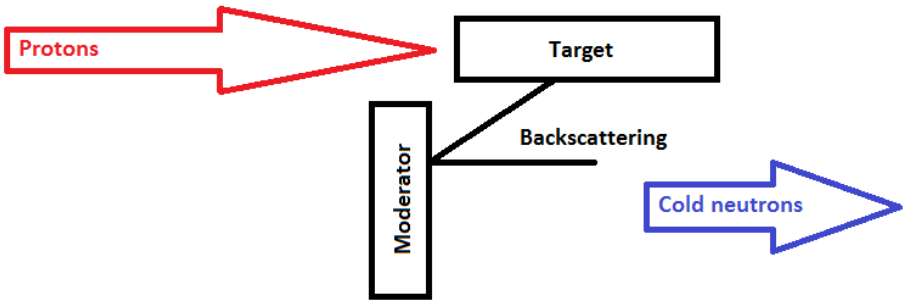

Figure 6.2: Simplified sketch of a backscattering moderator.

where the geometry is in fact quite favorable because of the application of a flux trap, see 6.7.

6.6 Pellets

Recent development at the IBR-2 fast pulsed reactor at the Joint Institute for Nuclear Research (JINR) in Dubna, Russia has produced proof of the concept of the pellet moderator [97]. Lucas et al. [98] originally suggested the system.

The concept is based on small pellets of solid material that are circulated through the moderator. This enables the use of materials that would be uncoolable in the heat load of the neutrons source if it was a static solid. A pellet moderator potentially enables the use of cold solid moderator materials at high-power facilities, even materials that are liquid or gas at room temperature.

This concept is being considered for SNS target station 2 [99], but the demonstration at Dubna was not produced in time for the concept to be viable for the ESS.

If the technique matures it will drastically expand the list of available moderator materials for high-power sources.

6.7 Flux trap

Another advanced feature of the Manuel Lujan, Jr. Neutron Scattering Center at the Los Alamos Neutron Science Center is the flux trap geometry, as illustrated in Figure 6.3 [86]. Although the flux trap is not really an advanced moderator but more of an advanced target geometry, it deserves a mention here.

At high energy (above 100 MeV), an impinging proton beam produces a high-energy particle shower in the target, which builds up over some distance. After traversing enough target material, the impinging beam and the shower are stopped as the particles in the shower lose their energy. Because of the shower formation distance and the finite penetration depth, the neutron production hotspot in the target is typically about 10 cm into the target (depending on target density and material and proton energy). Since most target materials have a high absorption cross-section, some neutrons are absorbed before they escape from the target – or if they scatter back into the target from the moderator-reflector system.

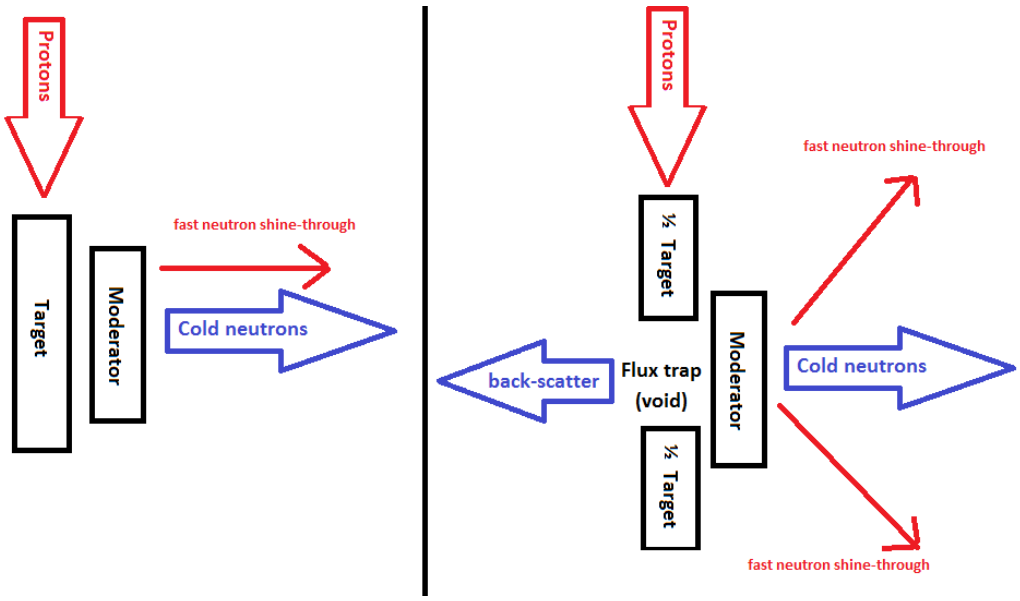

Figure 6.3: Sketch of a flux trap geometry and a moderator in transmission (left) and backscattering mode (right).

The flux trap geometry can overcome some of this problem: the target is split in two, cut over near the neutron production hotspot (Figure 6.3). Flux trap geometry is especially favorable in a slab-like geometry, where the shine-through of fast neutrons would end up in the neutron beamlines in the conventional slab geometry. Flux traps are also especially suited for a backscattering moderator or a combined backscatter and transmission moderator, as shown in the figure. Such a mock-up is installed at the Manuel Lujan, Jr. Neutron Scattering Center at the Los Alamos Neutron Science Center [86].

6.8 Bispectral moderators

For some neutron experiments, using both thermal and cold neutrons is desirable: broad or bispectral experiments. As seen in Figure 4.5, solid methane has a very broad spectrum. It fits to three Maxwellian spectra with 19 K, 63 K and 229 K (in the LENS 6 K moderator case). For this reason, a methane moderator can satisfy many such experiments. However, some require an even broader spectrum (including the thermal part), and most require higher brightness, which can only be achieved with high-power sources – where methane is unavailable.

A conventional orthohydrogen moderator has a spectrum that is close to a Maxwellian spectrum, and Figure 6.4 shows (part of the next section) that parahydrogen's spectrum is narrower than a Maxwellian spectrum, and thus these moderators alone are not well suited as bispectral moderators. Nevertheless, the parahydrogen moderator system at the ESS is promised to deliver bispectral neutrons for bispectral experiments [4].

At the ESS, bispectral neutrons are planned to be achieved using mirrors, via a method known as bispectral extraction, patented by Mezei & Russina [100]. A bispectral instrument requires a thermal moderator and a cold moderator positioned close to

each other. The instrument focuses the guide on the thermal moderator and positions a mirror in the flight path. The mirror transmits neutrons below a certain wavelength, depending on the mirror material, thus letting thermal neutrons through. The mirror totally reflects neutrons with long enough wavelength, and by orienting the mirror appropriately reflects cold neutrons from the cold moderator down the guide alongside the thermal neutrons transmitted through the mirror. This configuration is considered bispectral, since it transports some of the thermal neutrons from the thermal moderator and some of the cold neutrons from the cold moderator.

One problem with bispectral extraction is that a mirror reflects less than 100% of cold neutrons and transmits less than 100% of thermal neutrons (typically around 90% for both [24, 25]). Further, mirrors are placed near the extraction entrance in the instrument, where radiation is high, and accessing it is difficult, if not impossible: it is a critical component.

Producing a broad-spectrum moderator could avoid the use of mirrors. One such concept has previously been suggested: the composite moderator [26]. The composite moderator places a layer (3–5 mm (about 1 mean free path)) of cold moderator in front of a thermal moderator. Thus, some neutrons from the thermal moderator can shine through the cold moderator, and some neutrons scatter in the cold moderator and produce a cold spectrum on top of the shine-through thermal spectrum. Although the composite moderator successfully produces a bispectral spectrum, this mock-up clearly yields significantly less thermal brightness than the thermal moderator by itself (because of "blocking" by the cold moderator). Further, the cold moderator has less than optimal thickness, and the composite moderator also therefore produces significantly fewer cold neutrons.

The composite moderator was never installed. The challenge of producing a bispectral moderator therefore remains.

Schönfeldt et al. [28], included in Chapter 9, suggest another candidate for a bispectral moderator. This concept produces a bispectral spectrum by exploiting the poor ability of lead to thermalize neutrons. It is a moderator based on a material's inability to moderate. The concept investigates enriched ^{208}Pb, but most low-absorbing heavy elements (such as bismuth, enriched platinum or simply natural lead) could be used with varying efficiency. One can imagine placing five moderators with different spectral temperatures on five of the six sides of a lead cube. Neutrons from the different moderators entering the lead cube can scatter with little energy transfer (lead is a poor moderator). As scattering is more or less isotropic, about one sixth of the scattered neutrons from each of the five moderators will leave the lead block through the sixth surface but with almost unaltered wavelength. Thus, the lead will emit part of the spectrum of each of the five surrounding moderators through the sixth surface, producing a bispectral moderator. Since enriched lead also serves as a reflector filter, the geometry should be optimized to optimally exploit this. Schönfeldt et al. ([28], included in Chapter 9) have shown that this concept has promising results in simulation.

6.9 Parahydrogen moderators

As mentioned many times by now, for high-power sources the only currently viable moderator material is hydrogen. Luckily, hydrogen comes in two forms: para- and

orthohydrogen. All the concepts above can use orthohydrogen. In contrast, parahydrogen can be considered an advanced moderator by itself, and many of the concepts above have little or no effect [101].

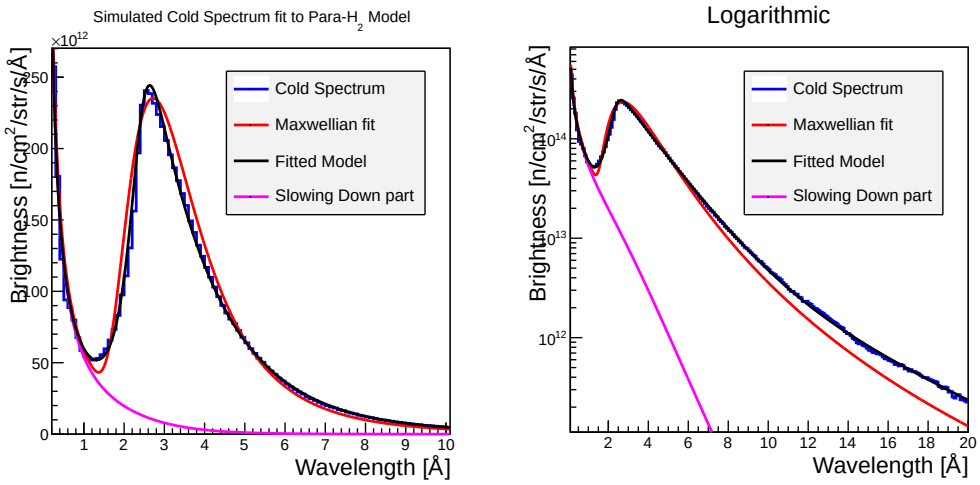

Figure 6.4: Fit of a Maxwellian spectrum and Equation 6.9.0.1 to the non-Maxwellian parahydrogen spectrum observed from a central beamline, with data simulated in the ESS TDR geometry. Source: Schönfeldt et al. [20].

Parahydrogen has a lower binding energy than orthohydrogen: about 15 meV difference in binding energy. The spin excitation mode is the dominant scattering mode in hydrogen, and thus the cross-section drops significantly for neutrons below the excitation energy – see Figure 4.6. As a result, the mean free path increases from some millimeters to more than 10 cm, and the material becomes transparent to cold neutrons.

In contrast to moderators using other hydrogenous materials, parahydrogen moderators are optimal when they are very thick, typically about 10–20 cm (methane or orthohydrogen moderators are typically 3–5 cm thick). This makes parahydrogen moderators particular favorable in wing geometry (Figure 5.1), since they cover a larger area over the target, resulting in more neutrons entering the moderator and thus higher brightness.

Because of the transparency, parahydrogen moderators are characterized by high cold neutron brightness. Due to their size they capture many neutrons from their surroundings and emit basically every neutron that becomes cold. However, most advanced moderator concepts do not work in parahydrogen moderators. For instance, grooving a parahydrogen moderator is almost meaningless, since cold neutrons are emitted from deep inside the moderator already. The grooves only help thermal and fast neutrons to escape, which in turn reduces the neutron density in the moderator and thus, ultimately, the cold brightness. Parahydrogen absorbs neutrons, especially the cold ones, and thus grooving might result in a small gain in certain geometrical configurations. Also reflector filters have little effect on parahydrogen moderators, since parahydrogen moderators can be considered inherent reflector filters because of their size and the transparency effect. Parahydrogen can be considered an advanced moderator, which inherently includes some of the most successful advanced moderator concepts: grooving and reflector filters.

In a pure (more than 99%) parahydrogen moderator, cold neutrons are emitted and do not further up- or downscatter once they are below the threshold energy. For this reason, the spectrum is not thermalized, and thus a parahydrogen moderator does not emit a Maxwellian spectrum. Schönfeldt et al. [20] present a pseudo-phenomenological formula that describes the spectrum of a parahydrogen moderator. Schönfeldt et al. ([22], included in Chapter 8) successfully applied this equation to parahydrogen moderators of different geometrical configurations. The equation describes the tail of the spectrum as the sum of two exponentials with different intensity, I_1 and I_2, and different decay constants, α_1 and α_2. The observed tail is cut off for wavelengths below the spin excitation threshold ∼2.3 Å (14.7 meV) by some power of a logistic function. The equation reads:

$$\begin{aligned} &S_{cold}(\lambda) = \\ &\frac{1}{(1+e^{\alpha_l(\lambda-\lambda_l)})^{\frac{1}{\gamma}}}(I_1 e^{-\alpha_1\lambda} + I_2 e^{-\alpha_2\lambda}) \\ &+ I_{SD}\frac{1}{\lambda}\frac{1}{1+e^{\alpha_{SD}(\lambda-\lambda_{SD})}}. \end{aligned} \tag{6.9.0.1}$$

The last term describes the slowing-down part and is the same as the one used for the Maxwellian spectrum, as described in section 4.2.3. Schönfeldt et al. [20] and Schönfeldt et al. [22] provide more detail on this function, along with fit parameters.

6.9.1 Flat moderators

Kai et al. [102] noted that the voluminous parahydrogen moderator installed at the J-PARC emits many of its neutrons near the edge of the moderator. To first order, the reason is that hydrogen is a very good moderator, and thus most of the thermal neutron feed-in from the surrounding pre-moderator and reflector will scatter to cold energy near the point where they entered. Since parahydrogen is transparent to cold neutrons, these will be observed from the point where they were cooled – i.e. where they entered, which is near the edge.

Since the central part of the moderator emits fewer neutrons than the edge, one can imagine making the moderator smaller such that it does not have this central region with lower brightness. This will increase the overall moderator brightness. A smaller moderator also enables the pre-moderator and reflector to be moved closer to the target, which results in a higher feed-in of thermal neutrons, increasing the brightness further. Gallmeier [103] initially studied this concept and concluded that gain of more than a factor of 2 can be achieved by reducing the parahydrogen moderator size, such that the viewed area is 3×3 cm^2 versus 10×10 cm^2.

Batkov et al. [10] published the first study and concluded that a disc-shaped moderator with a height of 1.4 cm maximized brightness. In [10] an unperturbed moderator geometry was studied, i.e. the moderator is packed in reflectors on all sides to reduce the bias from changes in reflector geometry. Shortly after publication, it was realized that the gains observed were even larger than anticipated when the reflector was opened up to enable a view of the moderator. The cause is that a large moderator requires a larger opening, which results in removing a larger block of reflector, and removing reflectors reduces brightness (Table 5.1). Figure 6.5 shows the relationship between brightness and moderator height.

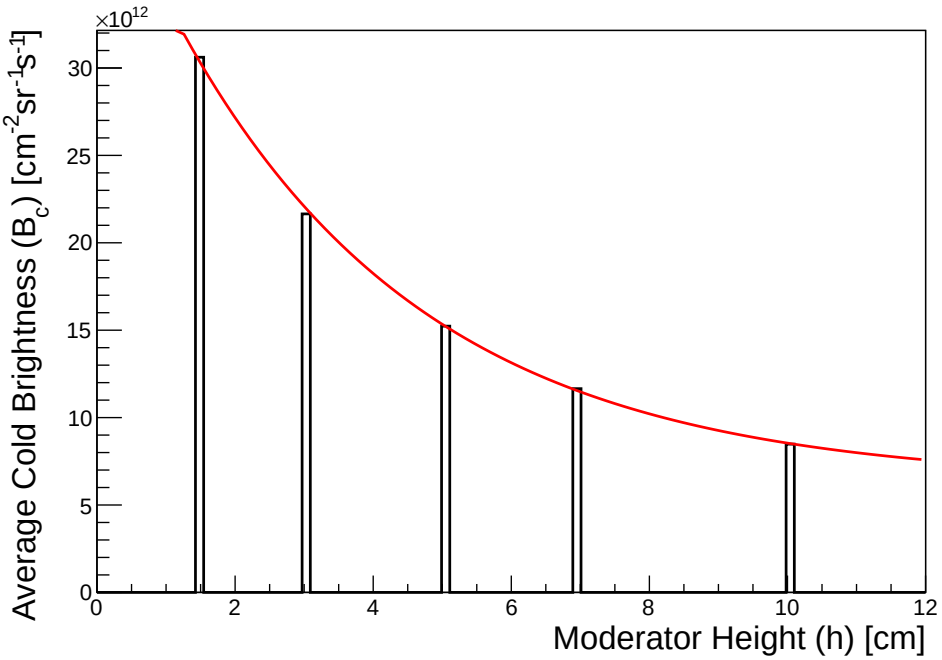

Figure 6.5: Functional fit of cold brightness (E <5 meV) of a pancake moderator of different heights. A 10 cm tall moderator resembles a conventional non-flat configuration similar to the ESS TDR geometry (which was 12 cm tall in the viewing area). "Average" refers to time average. (Schönfeldt et al. [22]) also present this figure.)

Similar studies of flat moderators had been carried out previously, such as for a 4 cm tall moderator [21]. This study found no significant gain. One reason is that moderators depend highly on geometry, and thus a flat moderator only works in certain geometrical configurations. Further, the gain can depend on several variables at once. This applies to flat moderators, as shown in Figure 6.6, which demonstrates that reducing the moderator height alone produces no remarkable gain.

Based on Batkov et al. [10] and Takibayev et al. [104], the ESS decided to open up for a potential baseline change into a flat or pancake moderator. It was later found that the large disc-shaped pancake moderator was unfavorable for extracting thermal neutrons, partly because of the great distance between the thermal wings next to the pancake and the high cold brightness area of the pancake. This distance is unfavorable because of the wide angle between the cold and thermal neutrons when observed from the instrument extraction point. This is not optimal for bispectral extraction, which is a basic requirement of the ESS.

One way to overcome this is through butterfly geometry, which is still a flat moderator but with the thermal moderator positioned centrally over the target hotspot next to two cold parahydrogen moderator (butterfly) wings. This significantly increases thermal brightness [105, 106] (included in Chapter 7), without losing cold brightness, compared with the disc-shaped moderator geometry. On March 6, 2015, the butterfly moderator baseline change request at ESS was accepted. [11, 12, 13] The ESS will thus be the first facility to use a flat parahydrogen moderator. Furthermore, it will do so in a geometrical configuration conceptualized by me under the scope of this thesis.

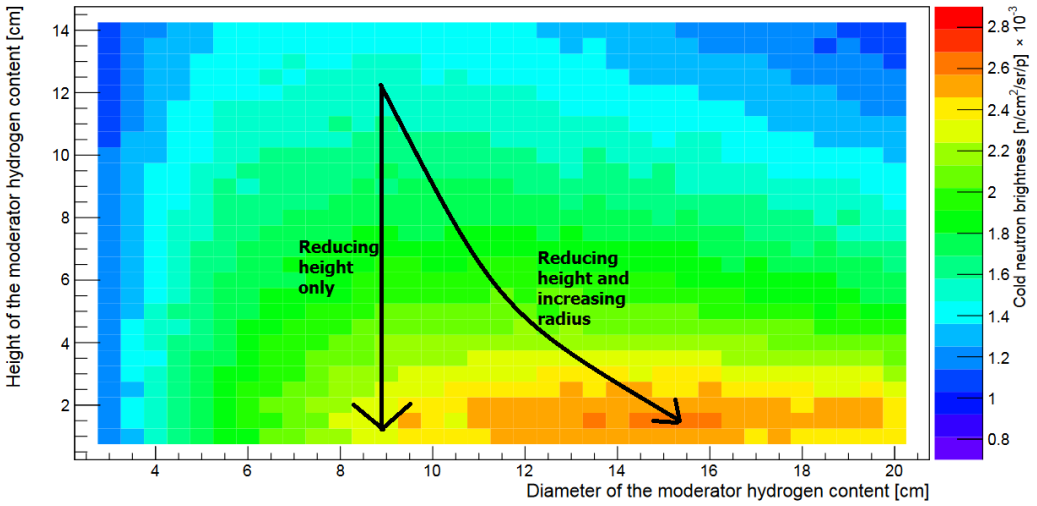

Figure 6.6: "Unperturbed" brightness emitted from a cylindrical moderator. Unperturbed refers to the moderator being packed in reflector material on all sides, and thus no open surface from which neutrons can be emitted. The gain from having an opening in the moderator surface is in fact greater than the gain observed in the unperturbed case, since the opening is smaller and thus has less impact for the smaller moderators [104]. Source: modified based on a figure from Batkov et al. [10].

Chapter 7

Disc-shaped and butterfly moderators

This chapter comprises two conference proceedings. The first proceedings are from ICANS XXI (2014) and describe the development from the moderator system suggested in the ESS technical design report (TDR) [4] into the disc-shaped flat, or pancake, moderator system. This moderator was being investigated as a potential new ESS baseline in 2014. Flat parahydrogen moderators significantly increase cold neutron brightness.

The second proceedings are from the Twelfth International Topical Meeting on Nuclear Applications of Accelerators (AccApp 15, Washington, DC, November 2015) and describe the butterfly moderator. The butterfly has the thermal water moderator placed centrally between two cold parahydrogen "wings". This increases the thermal neutron brightness compared with the pancake design without compromising the cold neutron gain. The butterfly moderator can be configured to increase the cold neutron brightness over the flat moderator at the cost of some of the thermal neutron gain. The ESS accepted the butterfly moderator as the new baseline in March 2015, and this is currently the ESS moderator baseline. The numbers and figures presented in the article are not final, since the moderator system is still being developed.

This chapter also includes a small section outlining the development history of the butterfly moderator after the first conference proceedings. Finally, after the second conference proceedings is a small section on the fast neutron background from the moderator system – which is partly based on the work presented in the next chapter.

Moderator Configuration Options for ESS

Luca Zanini[1], Konstantin Batkov[1], Esben Klinkby[1,2], Ferenc Mezei[1], Eric Pitcher[1], Troels Schönfeldt[1,2] and Alan Takibayev[1]

1) European Spallation Source ESS AB, Box 176, S-221 00 Lund, Sweden
2) DTU Nutech, Technical University of Denmark, DTU Risø Campus, Frederiksborgvej 399, DK-4000 Roskilde, Denmark

E-mail: luca.zanini@esss.se

Abstract. The current, still evolving status of the design and the optimization work for the moderator configuration for the European Spallation Source is described. The moderator design has been strongly driven by the low-dimensional moderator concept recently proposed for use in spallation neutron sources or reactors. Quasi-two dimensional, disc- or tube-shaped moderators, can provide strong brightness increase (factor of 3 or more) with respect to volume para-H_2 moderators, which constitute the reference, state-of-the-art technology for high-intensity coupled moderators. In the design process other, more conventional, principles were also considered, such as the importance of moderator positioning, of the premoderator, and beam extraction considerations.

Different design and configuration options are evaluated and compared with the reference volume moderator configuration described in the ESS Technical Design Report.

1. Introduction

The European Spallation Source (ESS), which entered the construction phase in 2013 in Lund, Sweden, aims at starting operations and delivering the first neutrons in 2019 [1]. At 5 MW time-average power, and 125 MW peak power (to be achieved by 2022), ESS will be the most powerful neutron source in the world for neutron scattering studies of condensed matter. Neutrons will be produced by a 2 GeV proton beam impinging on a target made of tungsten. ESS will be the first high-power long pulse source [2], the pulse length of the beam will be of 2.86 ms, with 14 Hz repetition rate.

A key for a highly performing neutron source is the optimisation of the configuration of the target, moderator and reflector assembly [3]. The use of tungsten as spallation material will ensure a high neutron yield per incoming proton; the high density of tungsten favours the production of neutrons in a small volume, increasing the probability that neutrons will eventually be slowed down by the moderators placed next to the target. The presence of a reflector surrounding the moderators is essential to increase the slow-neutron intensity from the moderators. For a long pulse facility such as ESS, the recommended cold moderator type is a coupled, pure para-H_2 moderator [4], because it delivers the highest brightness per proton. The coupling between moderator and reflector (i.e. the absence of any neutron absorbing material to shape the pulse length) guarantees the highest peak flux from the moderator surface; pulses are shaped in time by choppers placed in the beam lines.

An extensive effort from the ESS neutronic team has been carried out to design high-brightness moderators; the current, still evolving status of the work is described in this paper.

2. The baseline of the Technical Design Report

In April 2013 the ESS Technical Design Report (TDR) was issued[1]. The TDR design was based on the best available state-of-the-art technology, which for high intensity moderators is the J-PARC coupled volume para-H_2 moderator [4]. In the TDR baseline configuration [1], there are two volume moderators filled with pure para-H_2. The MCNPX model shown in Fig. 1 reproduces the engineering design developed during the target station design update phase. The moderators have a diameter of 16 cm and a height of 13 cm, see Fig. 1. The moderators are surrounded by light water premoderators (except for the cold neutron extraction window), of which the most important part, from the neutronic point of view, is the layer between target and moderator, which is 2 cm thick. The window surface on the cold moderators for beam extraction is of 12 $\times$ 12 cm^2. On the sides of the cold moderators, thermal moderators are placed for bispectral beam extraction. The openings in the reflector for beam extraction are of 60°, with two openings per moderator, as shown in the figure. More information is available in Ref. [5].

The absolute brightness was calculated at a distance of 10 m from the moderators, using collimators to view only the moderator surfaces. The calculated peak cold brightness is a factor of 75 larger that in ILL yellow book [6] at 4 Å, a factor of 60 larger at 6 Å, and a factor of 65 larger at 10 Å.

This paper describes the work carried out after the TDR was issued, in an attempt to improve the neutronic performance of the ESS moderators beyond best established practice.

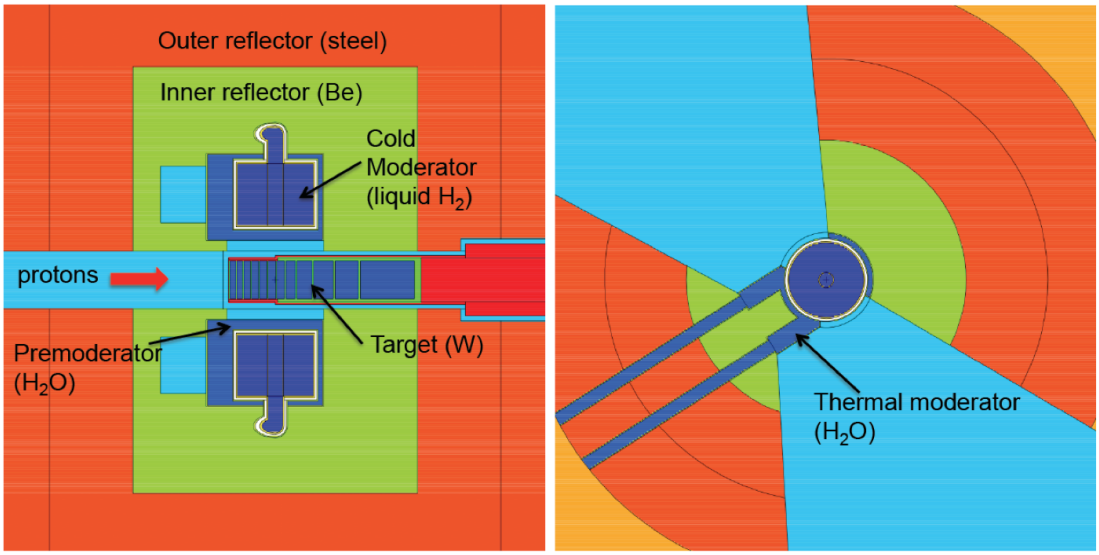

Figure 1. MCNPX[7, 8] geometry of the reference TDR moderator configuration.

3. Low-dimensional moderators

Much of the work was based on the concept of low-dimensional moderators for increased brightness, which are explained in details in Refs.[9, 10]. The basic principles of low-dimensional moderators is explained by the single-collision model [10]: the mean free path of thermal neutrons in para-H_2 is of about 1 cm, while is of about 11 cm for cold neutrons. Assuming that one collision only is needed to bring a thermal neutron to the cold regime, it is shown that the

moderator brigthness is increased for quasi two dimensional (flat) or quasi one-dimensional (tube) moderators. The brightness distribution map in the moderator face is shown in Fig. 2 for a 10 cm and a 1.5 cm tall moderator, showing the presence of regions of higher brightness in the tall moderator, while a flat moderator essentially has a single hot spot of neutron emission. In order to work, it is required that the moderators are filled with close to pure para-H_2; this can be achieved in high-power facilities by use of catalyzers.

The resulting brightness as a function of moderator height is shown in Fig. 3. Note that brigthness increase corresponds to a decrease in total neutron emission (red curve) as well as of the total heat load in the moderator. Therefore a high intensity moderator is not the brightest one; however, it is worth noting that, for the cylindrical shape used for the calculations in Fig. 3, already for 3 cm thickness the total neutron emission is about 80 % of the maximum reached at 10 cm.

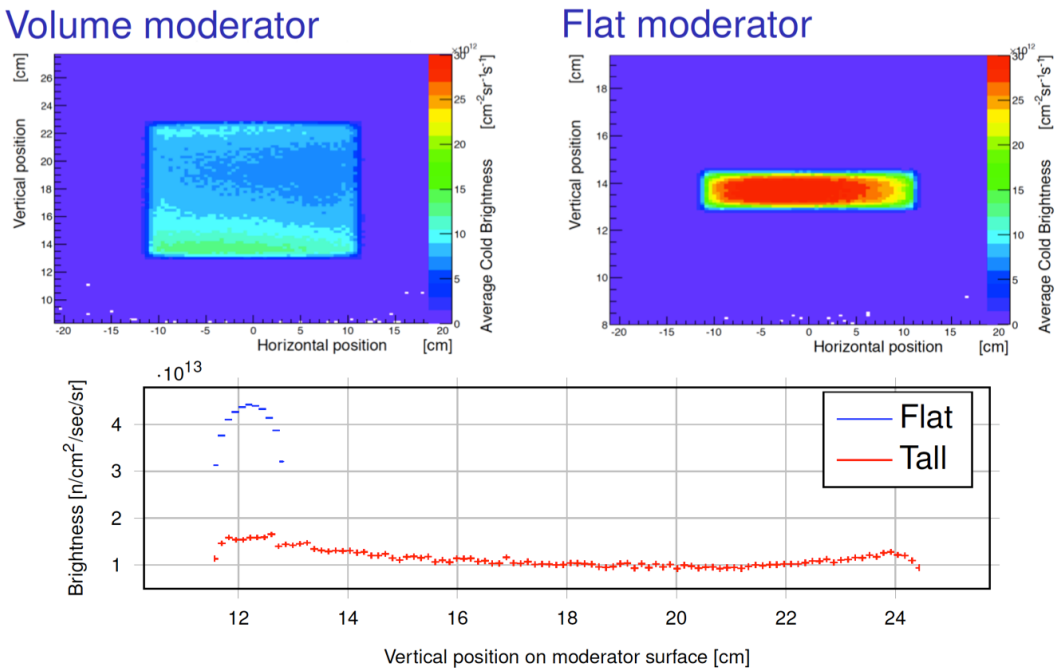

Figure 2. *Top:* Calculated brightness map from volume moderator (left) and flat moderator (right). *Bottom:* Brightness distribution along the moderator height for volume and flat moderator.

3.1. Other design principles

- Perturbation effect: in addition to the moderator shape effects, a brigthness increase is observed in low-dimensional moderators by the simple fact that being more compact, less reflector materials is removed around the moderators for beam extraction.
- Premoderator: the importance of the premoderator is well established and premoderators are widely used for cold neutron sources. The premoderator gives a spectral shaping, bringing neutron energies down from 1 MeV range to thermal. We have found that this

plays a crucial role not only for the cold moderator, but also for the thermal one (in which case the thermal moderator can be considered more as a scatterer than a moderator). As a result, we found that an extended premoderator, with dimensions practically equal to the Be reflector, and thickness of about 3 cm, gives a substantial gain in both thermal and cold moderator brightness.

- Position optimization: even though in a coupled moderator many of the neutrons reaching the moderator have been scattered by the inner reflector, we found that the positioning of the moderators close to the neutron production hotspot is quite important for brightness optimization. Additionally, it may be advantageous to place the thermal moderator above the target hotspot, rather than the cold moderator, because the thermal moderator is more compact, making it possible to place both thermal and cold moderators very close to the hotspot.
- Extraction optimization: a single moderator will not necessarily be able to serve the whole ESS instrument suite. However, we have found that in some cases this is possible; this is the case for the 3 cm pancake; if two moderators are installed, the ability to serve all the instruments by one or the other moderator is an advantage for maximum availability/flexibility.

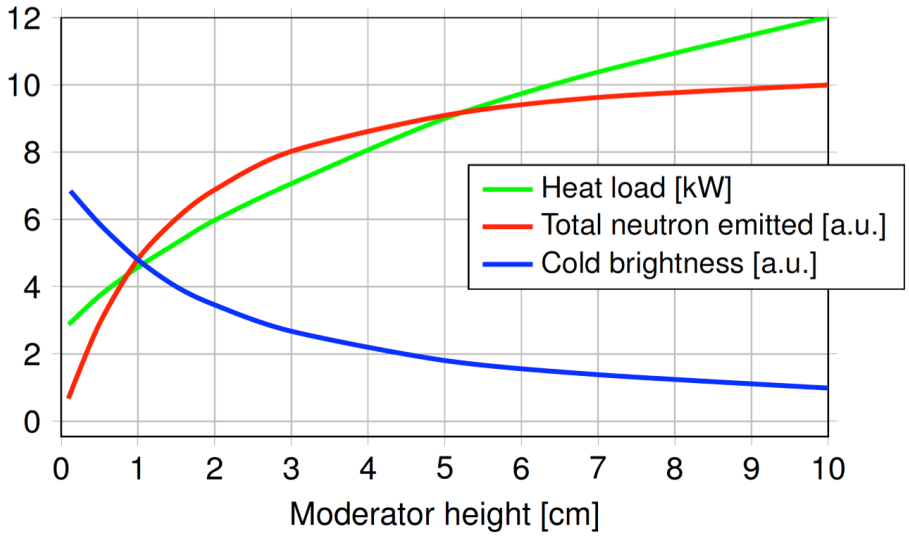

Figure 3. The integral cold brightness ($0 < E < 20$ meV) increases with decreasing height of the flat moderator (blue curve). On the contrary, the total number of emitted neutrons (brightness multiplied by the viewed area of the emitting surface) increases (red curve) with increasing moderator height, as well as the heat load (green curve).

4. The pancake moderator

The pancake design makes use of most of the concepts and findings described above. The resulting model is shown in Figure 4. The important features of this design are the following:

- 3 cm tall, 20 cm diameter cylindrical vessel containing pure para-H_2; the viewed surface can be up to 3 cm (Height) × 20 cm (Width), even though usually neutrons are extracted from a window 3 cm (H) × 6 cm (W). The choice of the diameter is considered a good balance between cold and thermal brightness, in the sense that it gives near maximum cold performance, while allowing a higher thermal brightness since the water wings are moved a bit closer to the neutron hotspot (Fig. 5).
- Neutron extraction for 2 × 120° angular openings.
- Water wings on the side of the cold moderator, for thermal neutron extraction. The viewed surface can be up to 3 cm (H) × 12 cm (W), or even more, even though usually neutrons are extracted from a window 3 cm (H) × 6 cm (W) or smaller.
- Extended premoderator between target and cold and thermal moderators, making use of findings described in section 5, for increased thermal brightness, with the additional advantage of reduction of the amount of Be close to the target.

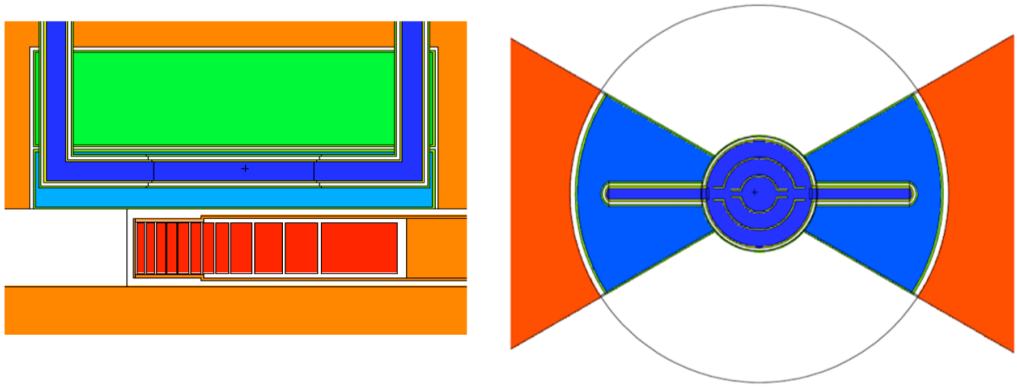

Figure 4. Reference geometry for the pancake configuration. See explanation in the text.

The pancake moderator is designed for increased cold brightness. The cold brightness is on average a factor of 2.4 the brightness delivered by the TDR moderators. For extraction of thermal neutrons, the thermal brightness is a factor of 1.5 the TDR. Thermal neutrons are extracted from the sides of the cold moderator. The thermal brightness can be increased by bringing the water closer to the neutron hotspot, but this can be obtained only at the expense of reduced cold brightness.

5. The second moderator

The pancake moderator brings not only an increased performance with respect to the TDR design, mainly in the cold brightness, and partially also in the thermal brightness, but also the fact that a flat moderator can serve the whole ESS instrument suite covering 2 × 120° beam extraction sector. This gives the opportunity to use the slot for the second moderator (the bottom moderator) to add flexibility to the facility. In other words, a second moderator can be used to supplement top pancake with either: *i*) a larger emission surface, resulting in a high intensity moderator, or *ii*) a moderator with a different overall wavelength spectrum, i.e.

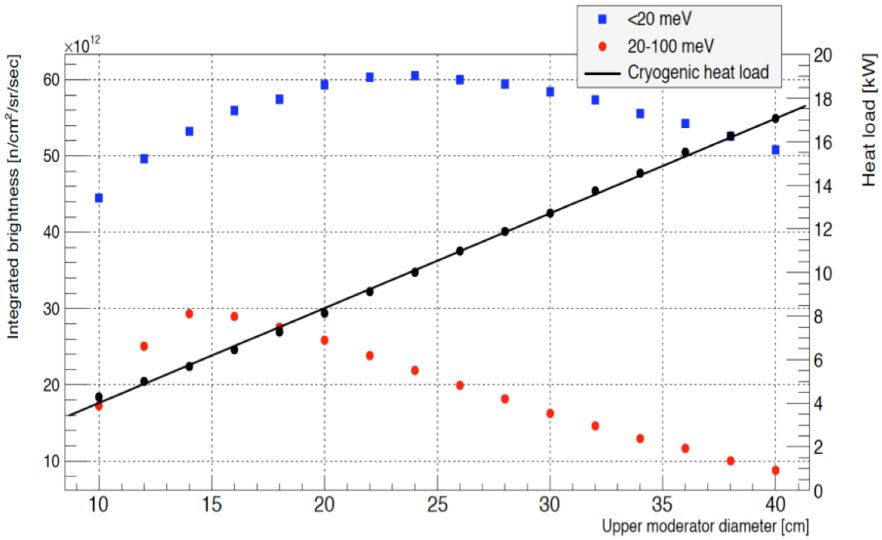

Figure 5. Integrated cold and thermal brightness for a pancake moderator, and heat load on the cryogenic parts (structure and hydrogen), as a function of the moderator diameter. The model (see Fig. (4)) includes some structure and pipes.

with increased thermal brightness with respect to the cold brightness, or *iii*) a combination of both things. The increased emission surface was discussed thoroughly. Essentially the gain in intensity with the moderator height is a balance between reduced brightness and increased area, and is seen in Figure 3; calculations for a 6 cm tall cold moderator were performed; its brightness is reduced with respect to the 3 cm pancake by about a factor of 1.5. Effort was particularly focussed on designing a moderator that would improve the thermal component of the spectrum.

6. The Optimized Thermal (OT) moderator

For maximum performance, the moderator should be placed near the hot spot of neutron production in the spallation target. In tungsten, because of its high-density, this is an area extended only a few cm starting about 10 cm from the target edge. The effect is mitigated by the presence of the Be reflector, however it is significant: the effect on vertical placement was calculated to be of about 3%/cm, while for horizontal placement is of about 1-2%/cm.

The thermal brightness can be improved if a moderator is specifically designed to improve this part of the spectrum. It was found that brightness of the thermal moderator increases if a water layer, approximately 3 cm thick, is placed between target and moderator, in a similar way to what happens to the top pancake (Fig. 6). The combination of optimal placement of the moderator with respect to the neutron production hot spot, and of the presence of this water layer, is found to give an increase up to a factor of 1.7 with respect to the brightness of the top pancake, for the same moderator height. The cold moderator next to the water moderator, shown in Fig. 6 is similar to a tube moderator and will provide high cold brightness; however it is highly directional and its brightness will decrease with the angle of beam extraction with respect to the tube axis.

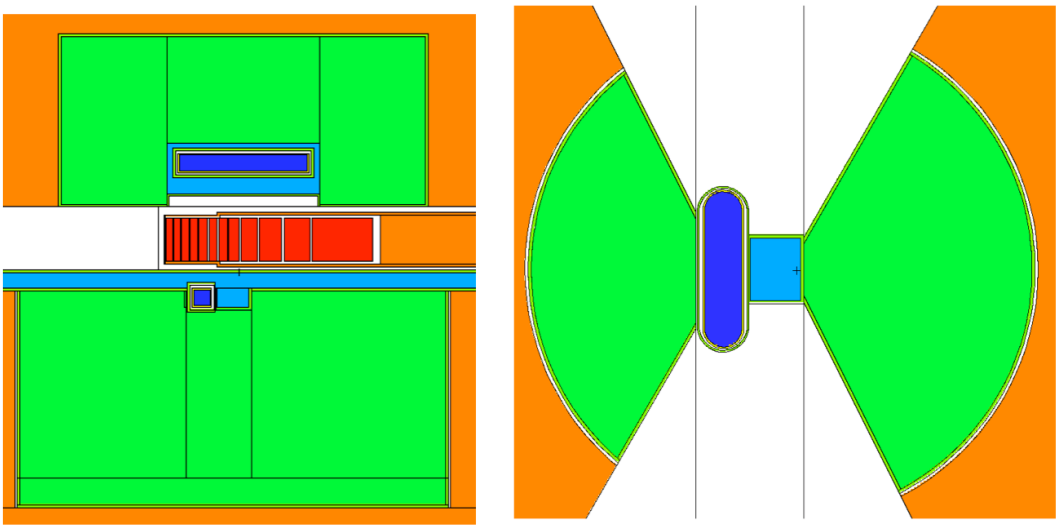

Figure 6. Geometry with a pancake 3 cm top moderator, and an optimized thermal moderator (3 cm tall) on bottom. *Left*: side view showing the 3 cm water layer between target and moderators. *Right*: top view showing the thermal moderator (light blue) and the cold moderator (dark blue), surrounded by the beryllium reflector (green).

7. Results and next steps

In Fig. 7 calculated wavelength spectra for the TDR, pancake and OT moderators are shown. Flat moderators offer a clear brightness increase with respect to the original TDR design based on volume moderators. Cylindrical pancake moderators are excellent cold moderators with a brightness about 2.5 times higher than the TDR moderators. The increase in thermal brightness is however limited, only a factor of 1.5: the thermal brightness remains the weak part of this moderator configuration. It is important to note that the TDR design suffers also from this drawback, as the peak thermal brightness is only a factor of 7 higher than the ILL yellow book, as opposed to the cold brightness which is 60 to 75 times higher than the yellow book. In an attempt to increase the thermal brightness we have developed the Optimized Thermal design. The OT is capable of delivering a thermal brightness higher than the pancake for a bigger emission surface. This increase is due to both optimal positioning of the water moderator (close to the neutron production hotspot) and to the optimal use of the extended premoderator (3 cm water layer between target and moderator). In order to deliver a good cold brightness, the OT has a cold tube moderator of its side. The resulting thermal-cold performance is enhanced (there is also come increase in cold brightness compared to the pancake). However, it is limited to a sector of about 60°, because of the strong directionality of the cold moderator, which means that this optimized thermal moderator must be used in conjunction with a top moderator.

The combination of a top pancake and an OT at the bottom, is a valid possibility for ESS. However, other possibilities are currently under consideration, and different designs are on the table exploting the design approach developed in the last two years and discussed in this paper.

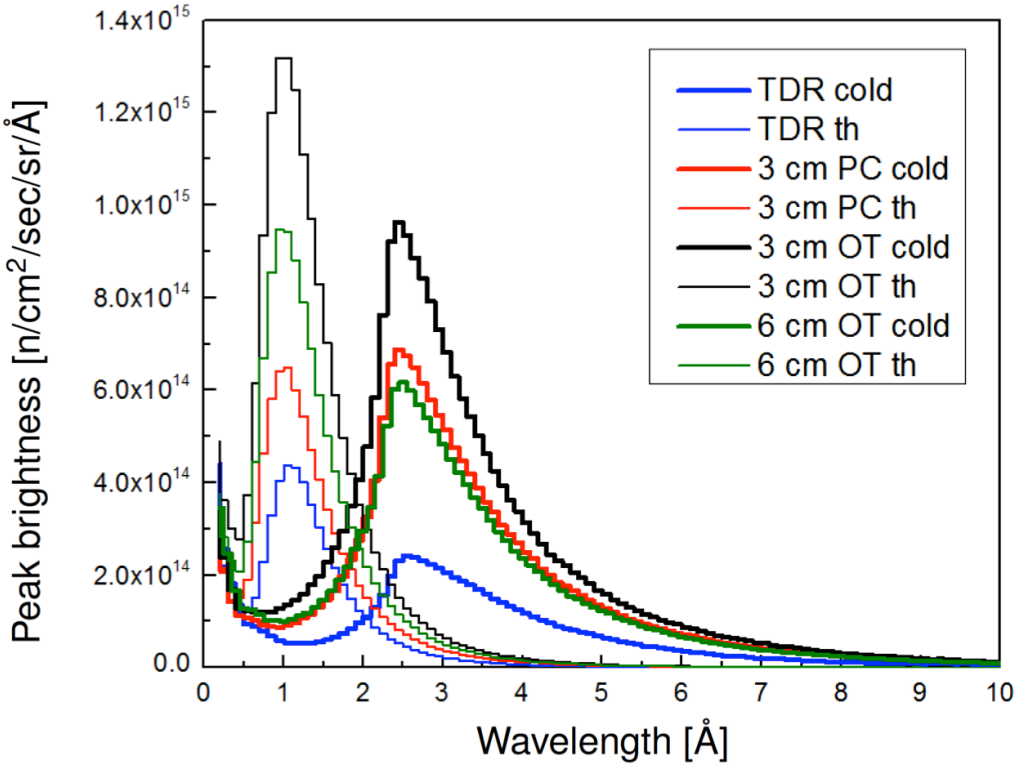

Figure 7. Calculated wavelength spectra from TDR, pancake (PC) and Optimized Thermal (OT) configurations. See explanation in the text.

Acknowledgments

The authors acknowledge Ken Andersen (ESS) for suggesting the study of a second moderator optimized for thermal neutron brightness.

References

[1] ESS Technical Design Report, S. Peggs editor, ISBN 978-91-980173-2-8, 2013, http://europeanspallationsource.se/scientific-technological-documentation
[2] F. Mezei, Long pulse spallation sources, Physica B 234-236 (1997) 1227.
[3] N. Watanabe, Neutronics of pulsed spallation neutron source, Rep. Prog. Phys. 66 (2003) 339381, and references therein.
[4] T. Kai, M. Harada, M. Teshigawara, N. Watanabe, Y. Ikeda, Nuclear Instrum. Methods A 523 (2004) 398.
[5] M. Magán et al., Neutronic analysis of the bi-spectral moderator such as that proposed for ESS Nucl. Instrum. Methods A729 (2013) 417425.
[6] Institut Laue-Langevin. 'ILL Yellow Book 2008.' http://www.ill.eu/?id=1379 , 2008.
[7] Waters L. S. et al. 2007. The MCNPX Monte Carlo radiation transport code. *AIP Conf.Proc.* **896**, 81-90.
[8] X-5 Monte Carlo Team 1987, MCNP – A General Monte Carlo N-Particle Transport Code, Version 5, *LA-UR-03-1987*.
[9] K. Batkov, A. Takibayev, L. Zanini and F. Mezei, Unperturbed moderator brightness in pulsed neutron sources, Nucl. Instrum. Methods, A729 (2013) 500.
[10] F. Mezei et al., Low dimensional neutron moderators for enhanced source brightness, Journal of Neutron Research 17 (2014) 101105 101.

7.1 Development of the butterfly moderator

The realization of Batkov et al. [10] that a disc-shaped parahydrogen moderator was superior to the parahydrogen volume moderators historically used led to the possibility of a potential baseline change at the ESS. The conference proceedings above presented the neutronic part of this investigation. As the conference proceedings indicated, flat moderators are not the most optimal for brightness. A tube or quasi-one-dimensional moderator increase the brightness over a flat or quasi-two-dimensional moderator. Takibayev et al. [104] first published this observation; the reactor modeling and simulations for this publication were part of the work carried out within this thesis but will not be explained further here.

The realization that a tube moderator was better than a flat moderator resulted in considerable development work within the ESS neutronics group. In fact, the tube moderator should have been called a caterpillar moderator, since it evolved into a butterfly moderator, as explained below.

Takibayev et al. [104] showed that tube moderators have the highest brightness but have a smaller emission angular span. In fact, a single tube only performs better than a flat moderator within about 10–15° of the central tube axis. At the time, the ESS required that each of the two moderators serve two 60° of instruments. In this way, the moderator system could cover a total of 240° of instruments. However, with the flat moderator, the opening angle has less impact on brightness, and thus one moderator could serve the entire 240° of instruments through two 120° openings. The ESS therefore considered having two moderators, one very flat and one somewhat larger, each able to serve all instruments. This would facilitate any instrument choice between a flatter or a taller moderator.

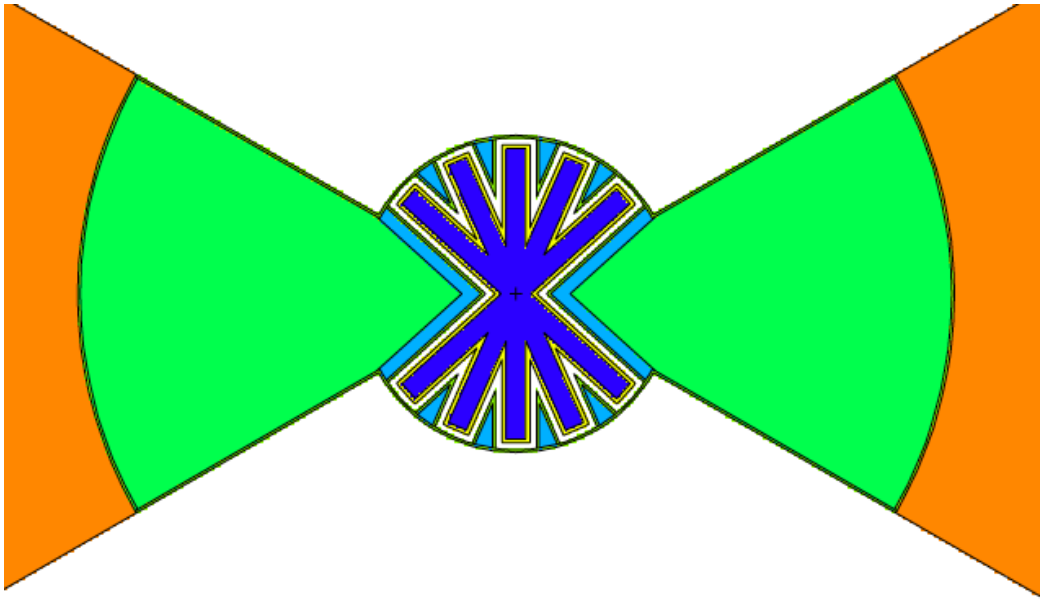

Figure 7.1: The starfish moderator. By Alan Takibayev.

As part of the collaborative effort to investigate the possibilities of a tube-like moderator, Alan Takibayev came up with the idea to have a series of tubes intersect: the starfish moderator, illustrated in Figure 7.1. Although the starfish could potentially

outperform the flat moderator conceptually, even simple engineering implementation significantly reduces brightness because of the many gaps and small volumes of pre-moderator between the "legs" of the starfish. Further, the cooling system and other engineering requirements for such a moderator system are probably strictly non-trivial. In the end, the concept of a starfish moderator was abandoned.

Around the same time, Esben Klinkby was working on a single-tube moderator to serve only a few instruments and then let the flat moderator serve the rest. Figure 6 of the above conference proceedings shows this concept. In this process, it was discovered that, if the end of the tube was cleared of pre-moderator, instruments could observe the tube from a slightly wider angle and still obtain a gain on the flat moderator. Thus, fewer tubes could serve all 240° of instruments.

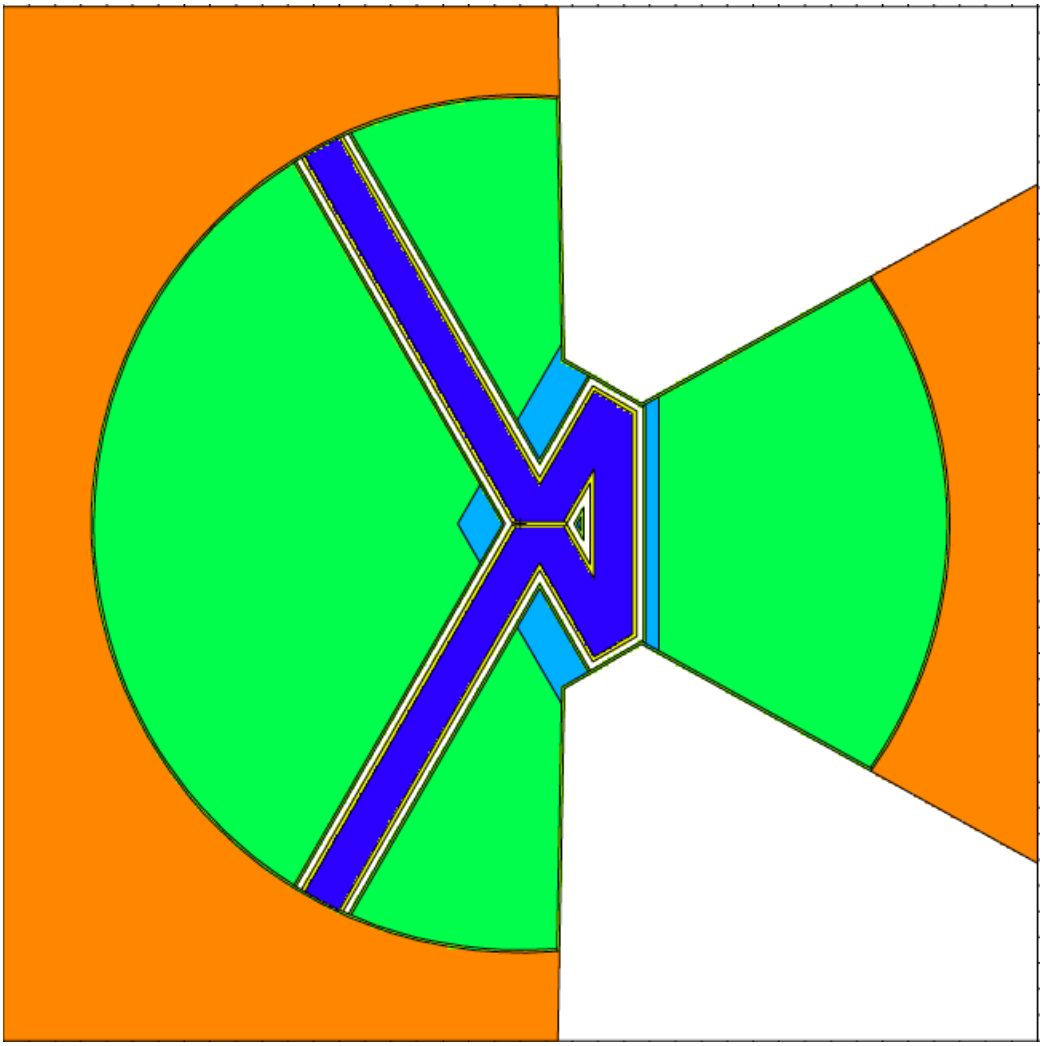

Figure 7.2: The scarf moderator. By Alan Takibayev.

However, with a tube serving about 20–30° in each end, one could imagine that three tubes would be sufficient for each of the two moderators, which would each cover two times 60° of instruments. Again, Alan Takibayev came up with an idea for such a mock-up, the Scarf moderator (Figure 7.2). The cooling of the Scarf moderator can be imagined as a flow through the loop of the Scarf and is fairly easily to implement. However, the scarf only serves two 60° openings and, unlike the TDR moderator, the

openings are not back to back as was planned for ESS. Further, although the cold moderator part is easily cooled, the gaps and the aluminum structure needed for the small pre-moderator in the center of the loop cause engineering headaches and reduce the brightness significantly. Ultimately, the scarf proved inadequate as a moderator concept.

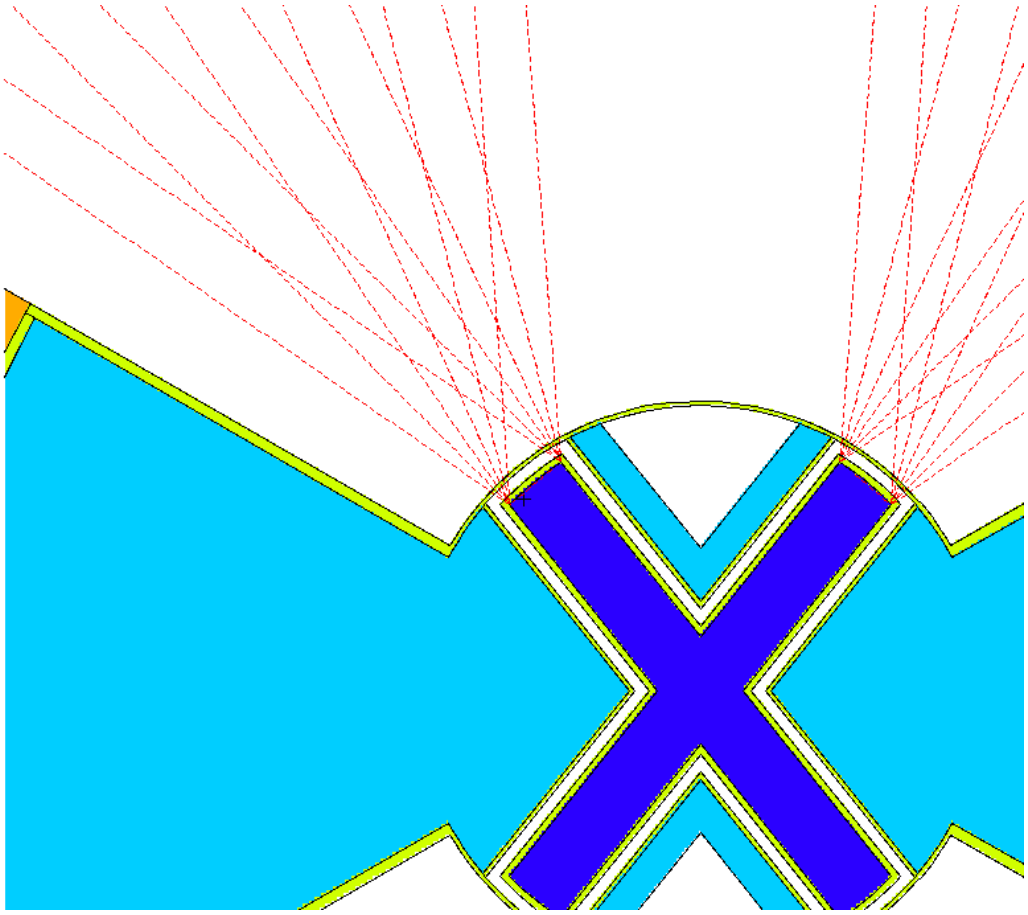

Figure 7.3: The cross-moderator, with colimators for F5 tallying in MCNPX

Meanwhile, I decided to examine a concept I called the cross-moderator. The cross-moderator has only two tubes (Figure 7.3). The tubes are made wider and the openings are cleared of pre-moderator. The idea was that this would enable each tube to serve all instruments at wide angles (from the center of the beam opening or in front of the tubes). Then thermal instruments could be positioned centrally and view the pre-moderator for the tubes as the thermal moderator. One novel thing here is that the thermal moderator is positioned centrally in the moderator system. All other previous concepts used a dedicated room-temperature water wing next to the moderator system and had the cold moderator placed centrally in the system. The neutronics community did not accept the concept of rearranging instruments such that thermal instruments were placed where the thermal brightness was optimal, the cold instruments where the cold brightness was optimal and bispectral instruments where both cold and thermal brightness were good. Ultimately the cross-moderator was also abandoned.

I then came up with the idea for the butterfly moderator. I see this as combining the scarf, the starfish and the cross-moderator. Figure 7.4 shows one of the first models of the butterfly moderator. This concept quickly proved to achieve excellent cold and

thermal brightness for all instruments in a 120° opening on each side and became the first real competitor to the pancake moderator.

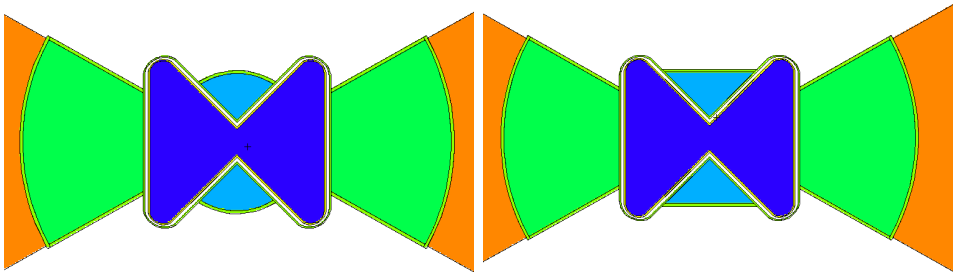

(a) Cylinder (b) Flat slab

Figure 7.5: Some of the various thermal moderator configurations tested. The original wedge-like geometry proved to be the best.

In the next months, I spent my time optimizing and implementing engineering requirements into the butterfly moderator, such as rounding corners. As an example, Figure 7.5 shows various configurations tested in optimizing the central thermal moderator. In the end, the butterfly moderator had evolved to the concept presented in the following conference proceedings, which was accepted as the new ESS baseline in March 2015.

THE NEUTRON MODERATORS AT THE EUROPEAN SPALLATION SOURCE

L. Zanini, K. Batkov, F. Mezei and A. Takibayev
European Spallation Source ERIC, Lund, Sweden
P.O. Box 176, SE-221 00 Lund, Sweden
luca.zanini@esss.se; konstantin.batkov@esss.se; ferenc.mezei@esss.se; alan.takibayev@esss.se

E. Klinkby and T. Schönfeldt
DTU Nutech, Technical University of Denmark, DTU Risø Campus,
Frederiksborgvej 399, DK-4000 Roskilde, Denmark
esbe@dtu.dk; trsch@dtu.dk

ABSTRACT

The moderator design for the European Spallation Source is based on the low-dimensional moderator concept recently proposed for use at spallation neutron sources or reactors. Quasi-two dimensional, disc- or tube-shaped moderators, can provide strong brightness increases (more than a factor of 2) with respect to high-intensity volume parahydrogen moderators, which constitute the reference, state-of-the-art technology for high-intensity coupled moderators. In the design process other aspects were also considered, such as the importance of moderator positioning, the premoderator and beam extraction angular range. Different design and configuration options were evaluated. The adopted "butterfly" configuration has the advantage of simultaneously offering high thermal and cold brightness or the bi-spectral combination of both for each beam line position in the full 2×120° beam extraction sectors of the instrument suite.

KEYWORDS
Spallation source, neutron moderators, parahydrogen

1. INTRODUCTION

The European Spallation Source (ESS) is a long pulse facility (2.86 ms pulses at 14 Hz repetition rate) currently under construction in Lund, Sweden. It will start operation in 2019 and it aims at becoming the brightest neutron source in the world for condensed matter studies using neutrons. This will be achieved by the high power proton beam (2 GeV protons with 2.5 mA average current, for 5 MW beam power) impinging on a spallation target made of tungsten.

Beam lines for neutron beam extraction start at 2 m from the moderators (Figure 1). Spallation neutrons in the MeV range will be cooled down to the desired energies by means of thermal and cold moderators. Because of the high power, and of the long pulse structure, at present the choice of moderator material for cold neutron production is limited to liquid hydrogen (as liquid deuterium would broaden too much the time pulse). Light water is used for thermal neutrons.

The neutronic design of the ESS moderators is based on the optimization of the brightness, i.e., the flux per unit solid angle averaged over the surface of the moderator. This optimization work used the recent

findings on low-dimensional moderators [1,2,3], according to which high brightness gains (factor 2-3 for realistic moderator heights) can be obtained for liquid parahydrogen moderators. As discussed in Ref. [2], the thermal neutrons from the water premoderator get primarily slowed down to the cold regime by the first collision close to the moderator wall after entering the parahydrogen, and they can escape with large probability from the moderator volume without any further collision.

By low-dimensional moderators we mean:

- Flat moderators (quasi two-dimensional shape). The height of such moderators are reduced with respect to conventional volume moderators, such as the coupled moderator used at J-PARC [4], ideally reducing it to a quasi-two-dimensional shape.
- Tube moderators: quasi-one-dimensional, tube-shaped moderators, in which one additional dimension is essentially removed with respect to the flat moderators (see Ref. [2], which includes some examples of application in an ILL-type reactor).

This classification refers to cold moderators. However, a requirement for ESS is the possibility to allow bi-spectral (thermal-cold) beam extraction, therefore a thermal neutron source must also be designed.

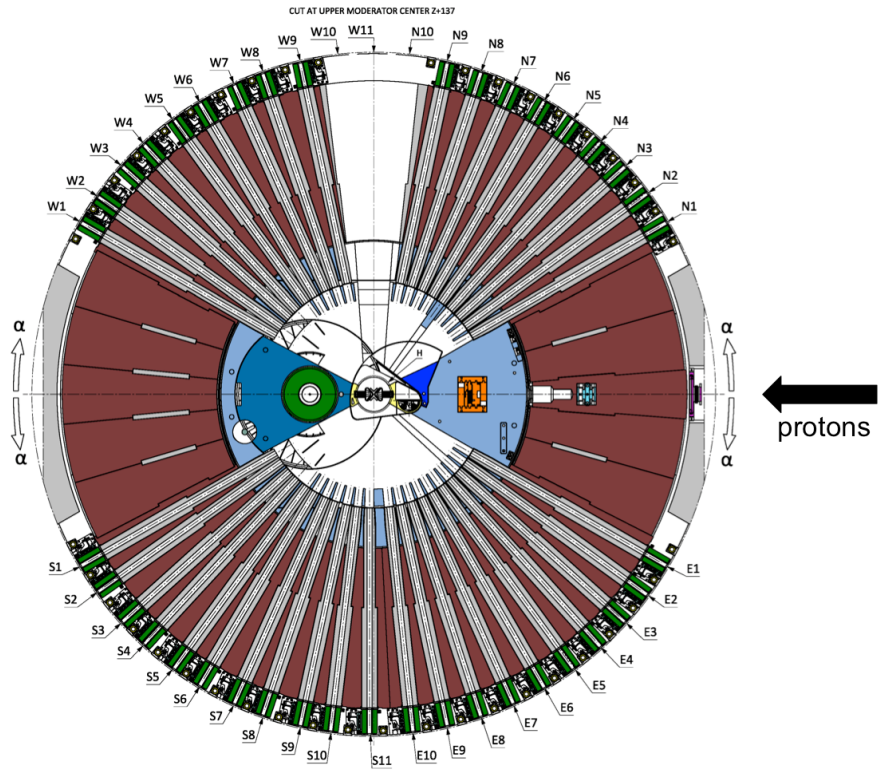

Figure 1. Horizontal section cut of the monolith structures, at the level of the upper moderator position above the target wheel. The moderators in the center are surrounded by the void cut-outs (white) in the reflector and innermost shielding blocks. Neutron beam extraction optics start at 2 m and extend out to 5.5 m in the form of inserts (grey) installed horizontally into the beam ports (brown). Shutters (green) fill the space from 5.5 m to 6 m. Courtesy R. Linander.

2. DESIGN CRITERIA AND MODERATOR CHOICE

At ESS bi-spectral extraction is needed for a significant number of instruments. The surface of the moderator viewed by instruments is required to be at least 3 cm (height)×6 cm (width) for both thermal and cold moderators, for all the instruments in the 2×120° sectors.

A design that places the cold moderator in the hotspot of neutron production is the pancake design [3], consisting of a cylindrical (20-cm diameter) Al container filled with parahydrogen. The weak point of this design is that thermal neutrons are extracted from the sides, resulting in a lower brightness thermal moderator.

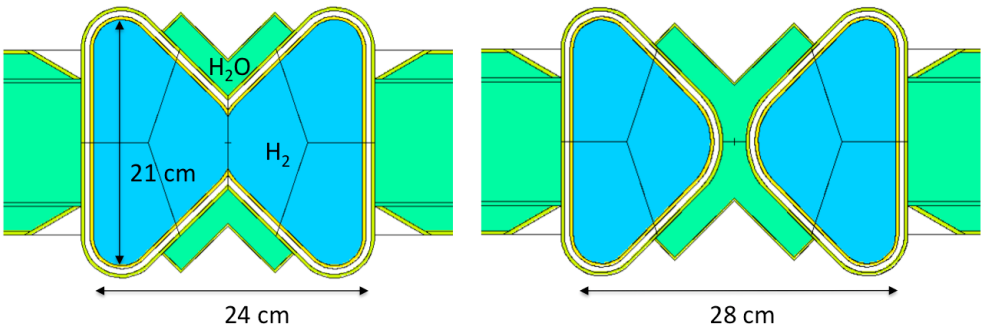

Figure 2. MCNPX models of the two "butterfly" concepts.

The need of bi-spectral extraction, and therefore the need to place, if possible, both thermal and cold moderators above the hotspot of neutron production (location of highest flux exposure to high energy neutrons created by the proton beam in the target), suggested the use of different moderator shapes, as shown in Figure 2. Such "butterfly" shapes on one hand place cold and thermal moderators closer on the hotspot. On the other hand, they exploit to some extent the concept of tube moderators, because of the presence of straight walls corresponding to the cold neutron extraction, adjacent to thermal premoderators. Finally, such moderators are also ideally fit for beam extraction in wide 120° sectors. The balance between thermal and cold brightness shifts within 10-15% between the two concepts of Figure 2; i.e., the moderator in Figure 2 (left), has higher cold brightness, but lower thermal, than the moderator in Figure 2 (right).
Butterfly moderators with two different heights have been studied in full engineering details for initial installation at ESS: a 3 cm high, and a 6 cm high, less bright (see Figure 3) but offering an about 1/3 higher integrated intensity emitted by the 2 times larger surface viewed by the beam lines. The choice of the height of the 3 cm moderator was done after an extensive simulation of the flux deliverable to the sample by state-of-the-art (focusing) neutron optical guide systems, for a large set of instruments considered for ESS [6].

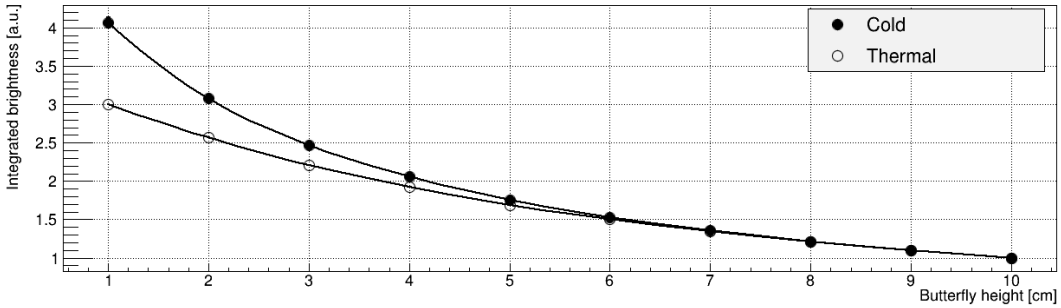

Figure 3. Calculated integrated time average cold (E < 20 meV) and thermal (20 < E < 100 meV) brightness as a function of moderator height for a butterfly configuration of Figure 2, right.

In Figure 3 the dependence of the cold and thermal brightness as a function of the moderator height is shown. The cold brightness of a 3 cm high moderator is 2.5 times the one of a 10 cm moderator, viewing 2×120° (equivalent in brightness to a 12 cm moderator viewing 2×60°), consistent with previously found results for the pancake moderator [3]. For the thermal brightness, the difference between 3 cm and 10 cm is a factor of 2, higher than previously found for the pancake.

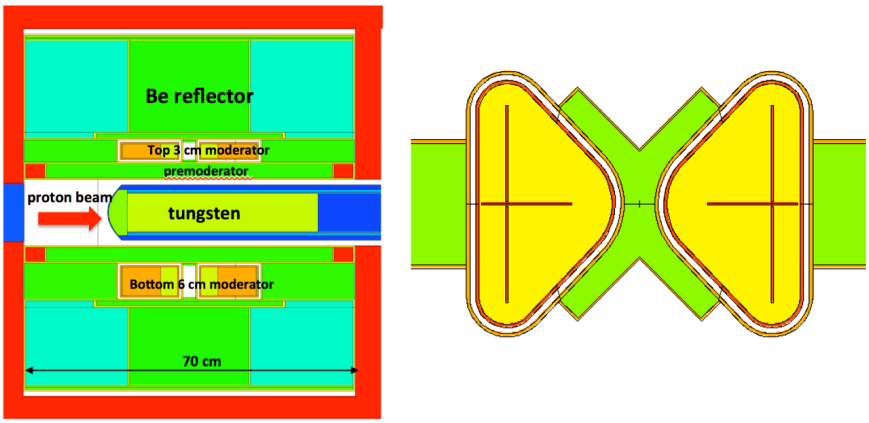

Figure 4. MCNPX model of an ESS target-moderator-reflector assembly with two butterfly moderators with different heights. *Left*: side view. *Right*: top view.

It is important to stress that the lifetime of the moderator-Be reflector assemblies at ESS will be limited to about 1 year by the high radiation load and they will be exchanged with this frequency. Moderators + Be reflectors can be replaced/removed independently on the top and bottom positions. The regular replacements also offer an opportunity to improve the design, by taking operational experience and adequate new developments into account.

2.1. Premoderator

The importance of the premoderators is well established and they are widely used at cold neutron sources. The premoderator provides a spectral shaping to the neutron spectrum from the spallation target, bringing

neutron energies down from the MeV range to thermal. We have found that this plays a crucial role not only for the cold moderator, but also for the thermal one. As a result, an extended premoderator (water disk, Figures 4 and 5), with diameter almost equal to the Be reflector, and thickness of about 3 cm, gives a substantial gain in both thermal and cold brightness.

2.2. Effect of orthohydrogen on the brightness

Best performance of the low dimensional moderators requires pure parahydrogen. Figure 6 (left) shows that for a 99.5 % parahydrogen fraction the brightness loss is of about 4%. Such a high fraction of parahydrogen can only be achieved by using catalyzers. Recent experimental results [7] indicate that the ENDF-VII measured cross section did not account for an impurity of orthohydrogen of 0.5%. Therefore in our calculations we assumed pure parahydrogen.

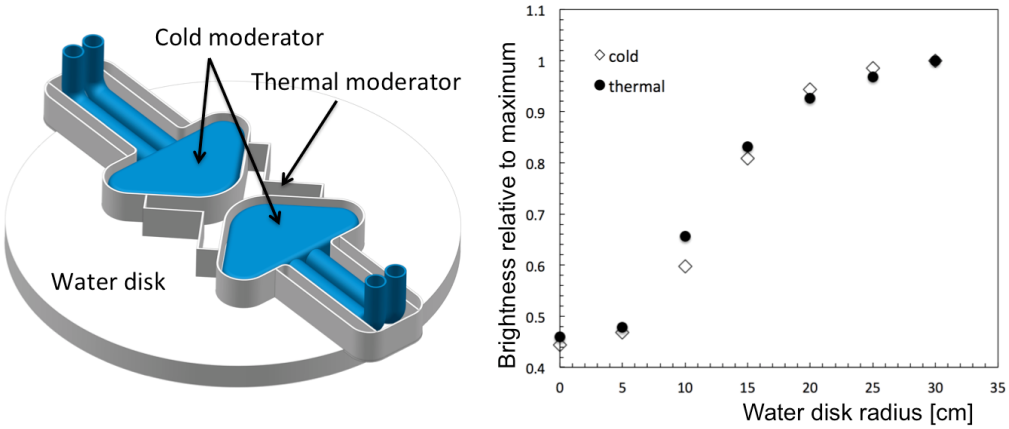

Figure 5. Left: schematic drawing of the top moderators and water disk premoderator. Right: relative change in average thermal and cold brightness as a function of the water disk diameter.

2.3. Source brightness

Figure 6 (right) shows the performance of the 3-cm high butterfly moderator in terms of cold and thermal brightness. The brightness spectra are shown for a beam line placed at 50° with respect to the incoming proton beam direction; the brightness variations as a function of the angle are within 10%. Calculations are performed with the MCNPX [5] model of Figure 4, corresponding to a model with the current available level of engineering details at the time of this writing. For the 6-cm high moderator the cold and thermal brightness are, respectively, a factor 1.60 and 1.45 lower than for the 3-cm high moderator.

With the presently adopted design, we found that the penalty in brightness, by implementing engineering details in the model, is independent of the height of the moderator, i.e., the relative performance of the 3 cm and 6 cm moderators are the same in the physics and engineering MCNPX models; this indicates that both moderators are equally affected in absolute brightness (about a 20% decrease, including design changes) going from the physics to engineering models.

The design in Figure 4 privileges the thermal component over the cold component. However, in the future a moderator of type “1” (on the left of Figure 2) giving a further increase in cold brightness of 10-15%, at

the cost of an equivalent loss in thermal brightness could be considered using a regular moderator replacement.

The calculated spectra in Figure 7 are compared with the official ILL yellow book values [8]; the ESS peak brightness is compared to the ILL time independent brightness. For the 3-cm high configuration the ESS thermal moderator is on average a factor of 10 brighter than the nominal ILL thermal brightness. The cold brightness at 4 Å is more than 100 times the nominal ILL brightness.

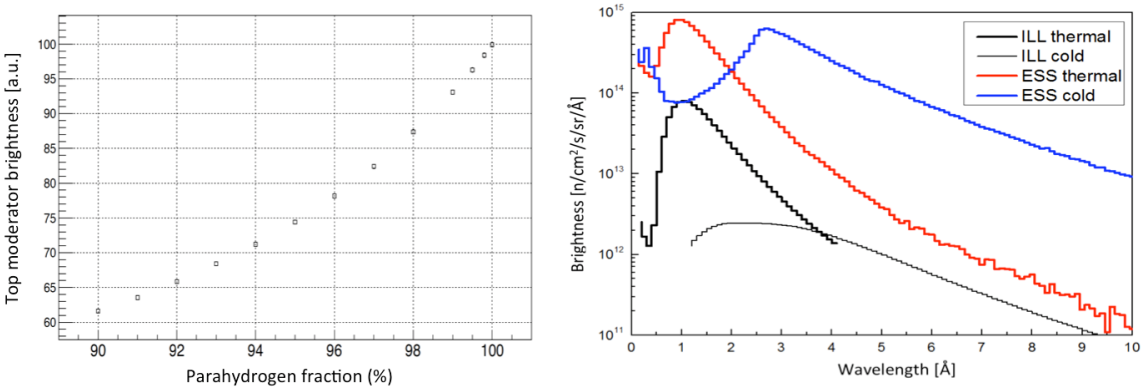

Figure 6. *Left*: dependence of the brightness of the 3-cm high cold moderator on the parahydrogen fraction, calculated using the ENDF-VII cross section at 19 K. *Right*: representative calculated brightness spectra for 3 cm high moderator of Figure 4, compared with ILL official curves [4]. See explanation in the text.

3. CONCLUSIONS

The neutron moderators for ESS have been designed, based on the high-brightness properties of low-dimensional moderators. After several options were considered, the adopted configuration for the moderators is the "butterfly" shaped, for increased bi-spectral performance and improved neutron extraction. The engineering design and manufacturing of the moderators is in progress.

REFERENCES

1. K. Batkov, A. Takibayev, L. Zanini and F. Mezei, "Unperturbed moderator brightness in pulsed neutron sources", *Nuclear Instrum. Methods in Physics Research* **A 729** (2013) 500 - 505.
2. F. Mezei, L. Zanini, A. Takibayev, K. Batkov, E. Klinkby, E. Pitcher, T. Schönfeldt, "Low dimensional neutron moderators for enhanced source brightness", *Journal of Neutron Research* 17 (2014) 101105.
3. L. Zanini, K. Batkov, E. Klinkby, F. Mezei, E. Pitcher, T. Schönfeldt, A. Takibayev , "Moderator configuration options for ESS", *Proceedings of the ICANS XXI conference*, Mito, Japan, 2014.
4. T. Kai, M. Harada, M. Teshigawara, N. Watanabe, Y. Ikeda, "Coupled hydrogen moderator optimisation with ortho/para hydrogen ratio", *Nuclear Instrum. Methods in Physics Research* **A 523**, 398 (2004).
5. D. Pelowitz, editor, MCNPX Users Manual, Version 2.7.0, Number LA-CP-11-0438, 2011.
6. K. Andersen, private communication, 2015.
7. L. B. Grammer et al., "Measurement of the scattering cross section of slow neutrons on liquid parahydrogen from neutron transmission", *Phys. Rev.* B **91**, 180301(R) (2015).
8. Institut Laue-Langevin. `ILL Yellow Book 2008.' http://www.ill.eu/?id=1379 , 2008.

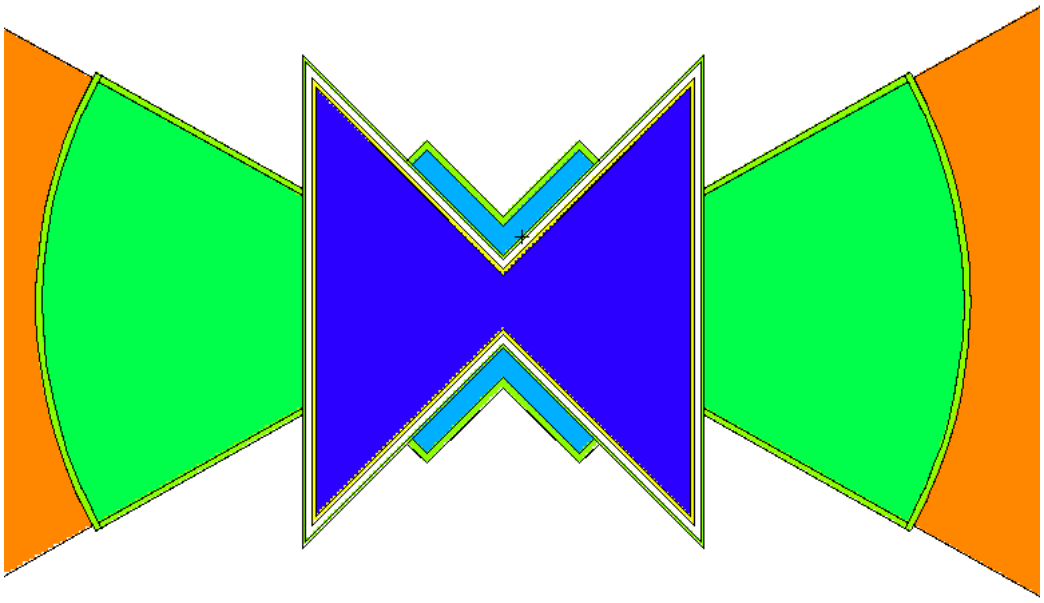

Figure 7.4: An early MCNPX model of the butterfly moderator

7.2 Estimating the neutron background

"Background" is very hard to define, since it strongly depends on both the instruments and experimental requirements. At the ESS, the neutron optics group led by P. Bentley is investigating the background at the ESS. However, this group has yet to define a figure of merit for the background, and the ESS does not yet have a working definition.

However, during the study of disc-shaped moderators, many neutron scientists asked about the expected background. One way of determining this is by examining the spectrum as a function of energy instead of wavelength, which is shown in Figure 7.6 for a 10 cm tall and a 1.5 cm flat disc-shaped moderator. The background from a smaller region of the tall moderator might be expected to have another signal and background profile than the entire moderator surface, and Figure 7.6 therefore also shows the spectrum from two different 1.5 cm belts over the tall moderator. One belt is over the cold hotspot, the 1.5 cm closest to the target, where the brightness of both the cold and fast neutrons is highest. The other belt is from the side farthest from the target, where there is also a cold hotspot but the fast brightness is significantly lower – denoted a coldspot. Note on the plot that the increase in the brightness of the fast neutrons in the flat moderator is smaller than the increase in the brightness of the cold neutrons, which indicates that the flat moderator not only has higher cold brightness but also has a better signal-to-background ratio.

Another plot (Figure 7.7) was also produced in the baseline change assessment at the ESS in 2014. This figure is based on an early version of the image projection technique, which I will discuss in details in Chapter 8. The neutrons that hit the extraction area are projected backwards along their trajectory, and their origin in the vertical direction near the moderator is plotted. Figure 7.7 shows that the gain in cold neutrons from a flat moderator is significantly larger than the gain in fast neutrons, again indicating

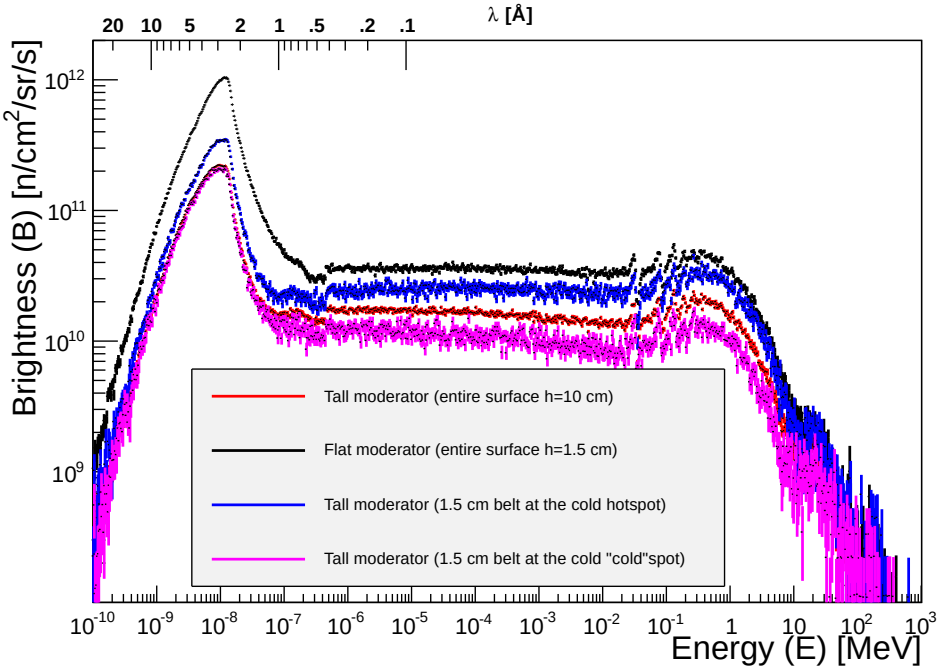

Figure 7.6: The spectrum from a 1.5 cm flat moderator and from a 10 cm tall moderator. Along with the spectrum from the bottom and top 1.5 cm of the tall moderator.

that the flat moderator has a better signal-to-background ratio.

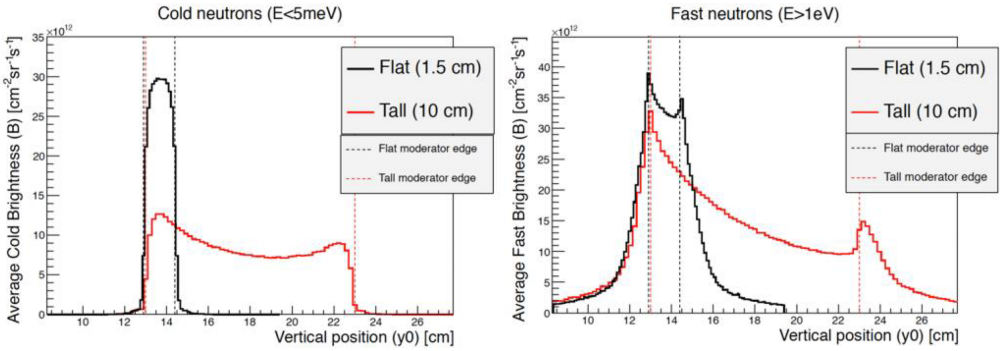

Figure 7.7: An early plot of the neutron origin position of fast and cold neutrons. The moderator is slightly out of focus, and the extraction position spans a 12×12 cm^2 guide opening, which is used in the study presented in the next chapter.

Another way to study the neutron background is through the spectral fits, which is discussed in the manuscript in Chapter 8. This manuscript shows that the cold brightness of an ESS moderator of height h can be described as:

$$B^c(h) = (3.6 \times 10^{13} e^{-0.28\ cm^{-1} \cdot h} + 6.3 \times 10^{12})\ \text{cm}^{-2}\text{sr}^{-1}\text{s}^{-1} \tag{7.2.0.1}$$

and the thermal brightness as:

$$B^t(h) = (2.7 \times 10^{13} e^{-0.14\ cm^{-1} \cdot h} + 5.6 \times 10^{12})\ \text{cm}^{-2}\text{sr}^{-1}\text{s}^{-1}. \tag{7.2.0.2}$$

Further, the fast part of the spectrum (from both cold and thermal moderator), as a function of height, can be described by a slowing-down term of the form:

$$B^t(\lambda;h) = I_{SD}\frac{1}{\lambda}\frac{1}{1+e^{\alpha(\lambda-\lambda_{SD})}}, \tag{7.2.0.3}$$

where only I_{SD} depends on height. In the cold case, $I_{SD,c}(h) = (4.1\times10^{12}e^{-.13cm^{-1}h} + 8.5\times10^{11})$ cm^{-2}sr^{-1}s^{-1}; in the thermal case, $I_{SD,t}(h) = (4.7\times10^{12}e^{-0.18cm^{-1}h} + 1.74\times10^{12})$ cm^{-2}sr^{-1}s^{-1}.

Simply dividing these "signal" and "background" terms produces:

$$\frac{B^c(h)}{I_{SD,c}} = \frac{3.6\times10^{13}e^{-0.28\ cm^{-1}\cdot h} + 6.3\times10^{12}}{4.1\times10^{12}e^{-0.13cm^{-1}\cdot h} + 8.5\times10^{11}} \tag{7.2.0.4}$$

for the cold ratio and for the thermal ratio we get:

$$\frac{B^t(h)}{I_{SD,c}} = \frac{2.7\times10^{13}e^{-0.14\ cm^{-1}\ h} + 5.6\times10^{12}}{4.7\times10^{12}e^{-0.18\ cm^{-1}\ h} + 1.74\times10^{12}}. \tag{7.2.0.5}$$

These functions both decrease with increasing h, and thus the more flat moderators are expected to have a better signal-to-background ratio. The functions presented in the next chapter enable fairly good estimates to be calculated for signal-to-background ratios from the moderator surface by defining a signal and a background region on the spectrum and dividing the integral values.

Chapter 8

Neutron extraction at the ESS

This chapter presents a study in which MCNPX simulations are translated into ROOT and analyzed. A method is developed that reconstructs the full brightness emission distribution, spatial and spectral, from a moderator system. In particular, the ESS pancake and butterfly (see the Appendix of the paper) moderators are studied. The distributions are fitted to analytical functions that have been implemented into McStas (and other simulation tools). This enables the expectations from the ESS to be much more precisely predicted. Predictions are not only a key requirement for experiments at the ESS but also enable significantly better optimization of neutron instruments before construction. In turn, this study is expected to contribute significantly to improving the overall quality of the ESS.

The method development presented in the following paper represents the culmination of much of the work carried out within this PhD project. The work was developed based on Esben Klinkby and Konstantin Batkovs SSW (a MCNPX method) to ROOT (data analysis software) method [16, 18].

My first use of the method was to better describe the neutron spectrum from the ESS. This functional description was implemented into McStas in 2013, and the results [19] were presented at AccApp 13. The first spatial distributions from the TDR moderator system [4] were presented at ICNS in 2013 at a poster session.

The method was further developed and was used to study many details in the ESS moderator system through 2014 and 2015. The method was also used to produce the spectral description of the "new" flat and tall moderators that were implemented into McStas in spring 2014 and formed the basis of the studies by the instrument groups at ESS, which ultimately resulted in the baseline change in 2015.

Later in 2014, the method was developed to a state in which it could produce a "full" spatial and spectral distribution for the flat moderator. This was the first non-flat spatial distribution of the ESS implemented into McStas. The following paper describes the method and fits used for this implementation and was presented at ICANS XXI in 2014. Further, the paper describes the spatial and spectral distribution from the butterfly moderator, obtained using the same method. This distribution was implemented into McStas in 2015.

The manuscript have been submitted to Journal of Neutron Research.

Functional description of the thermal and cold brightness distribution at ESS

T. Schönfeldt[d,e], K. Batkov[e], E. B. Klinkby[d,e], B. Lauritzen[d], G. Muhrer[e], A. Takibayev[e], P. K. Willendrup[f], L. Zanini[e]

[a] *Center for Nuclear Technologies, Technical University of Denmark, Roskilde, Denmark*
[b] *European Spallation Source, Lund, Sweden*
[c] *Department of Physics, Technical University of Denmark, Lyngby, Denmark*

Abstract

The present paper provides a functional description of the full phase-space distribution of cold and thermal neutrons emitted from the flat moderator, the so called pancake, planned for the European Spallation Source (ESS) as of April 2014, and for the butterfly moderator, the new ESS baseline design as of March 2015. Neutron distributions at the beam extraction surface are tallied from detailed MCNPX proton-on-target simulations and mapped onto the moderator surface. Assuming that the neutron brightness distribution can be factorized into horizontal, vertical, and spectral components, a functional description of the brightness is obtained. The functional forms, fitted to the cold and thermal regions of the flat moderator at different heights and to the butterfly design. The functional description employs 74 free parameters, and 8 predefined parameters, hence is not intended as a physics model of the moderator but rather an effective description of the neutron distribution of the moderator system. The functional description has been implemented in McStas.

Functional description of the thermal and cold brightness distribution at ESS

T. Schönfeldt[d,e], K. Batkov[e], E. B. Klinkby[d,e], B. Lauritzen[d], G. Muhrer[e], A. Takibayev[e], P. K. Willendrup[f], L. Zanini[e]

[d] *Center for Nuclear Technologies, Technical University of Denmark, Roskilde, Denmark*
[e] *European Spallation Source, Lund, Sweden*
[f] *Department of Physics, Technical University of Denmark, Lyngby, Denmark*

1. Introduction

For cold and thermal neutron sources, the neutron brightness provides a measure for the intensity of the source. The brightness is invariant under transportation according to Liouville's theorem. Therefore the neutron flux at a sample can be estimated by multiplying the source brightness by the efficiency of the neutron extraction instrument, the so called brilliance transfer. For this reason brightness is a key quantity at neutron sources, and it is used as a figure of merit of the European Spallation Source (ESS) [1].

Brightness is usually given as a function of wavelength, i.e. the neutron wavelength spectrum, or given as the integral over a specific wavelength range, e.g. the cold or thermal brightness, where the spatial dependencies have been suppressed. Though the variation of the neutron flux over the moderator surface is usually small, there are exceptions. For instance, at the high power Japanese spallation source J-PARC the cold brightness varies by a factor of two over the coupled para-hydrogen moderator surface [2]. In Ref. [3] the neutron flux from the ESS moderator surface and its surroundings is estimated in the TDR geometry [1]. This study finds that for certain planned instruments the highest intensity thermal emission point, often referred to as the thermal neutron hot-spot, is not even on the thermal moderator surface itself but on the reflector surface on the opposite side of the cold moderator.

Advanced neutron optical systems are used to guide neutrons from the moderator and transport them to the experimental samples. In neutron scattering experiments, Monte Carlo ray tracing codes such as McStas [4] are used to design instruments prior to construction and to predict experimental results. Alignment of these instruments is challenging, thus instruments are rarely realigned during their lifetime. At J-PARC a factor two increase in brightness near the edge of the moderator was only discovered after the first instruments were aligned [2]. These instruments had been aligned to the center of the moderator where the peak brightness was expected, while a gain in brightness could have been obtained by aligning the instruments to the edge of the moderator.

In addition to the potential gain related to the better optimization of instruments, at ESS it is a key principle that all experiments should be modelled in details prior to actual beam time. This in turn requires that the neutron source distribution is modelled in details.

Previous attempts have been made to map an inhomogeneous neutron distribution over the moderator surface into ray tracing codes. One example is at the Spallation Neutron Source (SNS) where neutrons from MCNPX Monte Carlo simulations were tallied using point detectors in 2x2 cm^2 regions of the moderator surface. The values were smoothed using a finite element technique and implemented into ray tracing codes [5]. While this method is robust it is not optimal, as the use of point detectors limits the method to a fairly low resolution of the moderator surface (maximum of 20 point detectors per run).

Different methods have been developed in [6, 7] which couples MCNPX simulations directly to McStas via a SSW/PTRAC cards. However, these methods require massive data storage capacity (several TB) and is computationally demanding, even using super computers.

The present study provides an efficient method for extracting phase-space information on the neutron brightness, based on tools developed in [7]. With the geometry of the ESS moderator system, the brightness to a first approximation factorizes into components depending on the horizontal and vertical coordinates of the moderator surface, respectively. The method is used to evaluate the

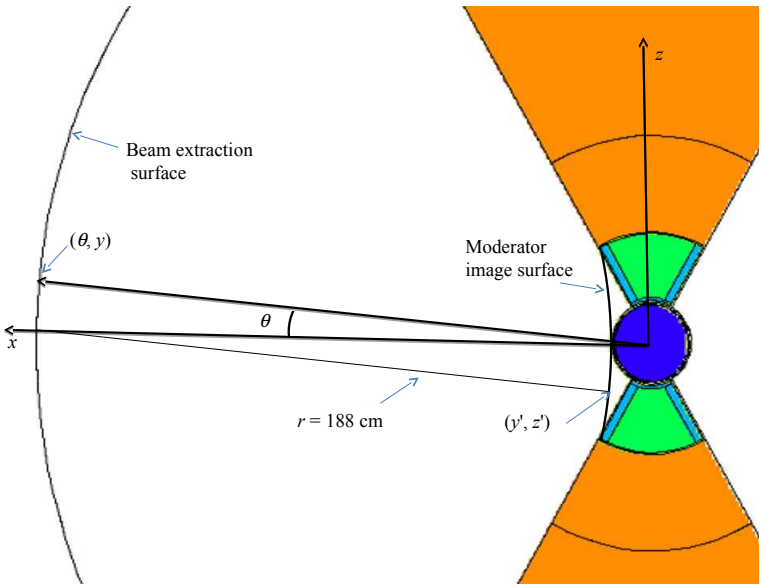

Figure 1: (x, z) cross section of the MCNPX model of the ESS flat moderator. The beam extraction surface is a cylindrical surface with cylinder radius 2 m and axis crossing the moderator center in the y direction. The moderator image surface is a sphere of radius 188 cm with the center on the beam extraction surface at (θ, y)=(0,0).

expected brightness at the European Spallation Source (ESS) for flat moderators of different heights, as suggested in [8]. In the appendix the method is used to evaluate the expected brightness from the so called butterfly moderator, which is the current ESS baseline design. The results of this study were used to develop McStas source components which enable fast optimization of the proposed ESS instruments. The flat moderator study is included as a source component in McStas 2.1 and the butterfly source component is included in McStas 2.2/2.2a [9].

A less detailed geometrical mapping of the old ESS baseline design is given in Ref. [3] using the geometry described in the ESS Technical Design Report (TDR) [1].

2. Brightness

The brightness can be calculated as: $B = NA^{-1}\Delta\Omega^{-1}\Delta t^{-1}$, where N the number of neutrons entering a sphere with cross section A in a solid angle $\Delta\Omega$ over the time Δt. Brightness is given in units of $cm^{-2}sr^{-1}s^{-1}$ or $cm^{-2}sr^{-1}s^{-1}\text{Å}^{-1}$ when expressed as a wavelength spectrum, $B(\lambda)$.

Brightness is equivalent to the angular flux, $\Phi(\overline{r}, E, \Omega, t)$, given by the neutron phase-space density at the position $\overline{r}$, with energy E, and direction Ω, multiplied by the neutron speed [10]. Processes with no energy transfer out of the neutron system, here defined as total elastic scattering, such as reflection, refraction or Bragg scattering, do not change the speed of the particle. The brightness is therefore transport invariant for such interactions according to Liouville's theorem.

The fact that the brightness is transport invariant is used to estimate the neutron flux on an experimental test sample. Brilliance transfer is defined as the probability that a particle is successfully transported through a neutron optics system. The number of neutrons at a sample can then be estimated by multiplying the source brightness with the brilliance transfer, integrated over the sample size, angular acceptance, wavelength range, and timing requirements.

Brightness is often provided as the average value over the entire moderator surface observed from a specific direction (or a small detector) some distance from the source, e.g. 5 m or 10 m from the moderator surface. The brightness spectrum $B(\lambda)$ can be further reduced to the integral value, $B^{ab} = \int_a^b B(\lambda)d\lambda$ over some wavelength region $a < \lambda < b$. At ESS the cold and thermal brightness are defined as $B_c^{\text{CM}} = \int_{4.05\text{ Å}}^{\infty} B(\lambda)d\lambda$ and $B_t^{\text{TM}} = \int_{0.9\text{ Å}}^{2.02\text{ Å}} B(\lambda)d\lambda$, respectively [1]. Equivalently these integration limits can be expressed in terms of energy; [20 meV, 100 meV] for the thermal brightness and [0, 5 meV] for the cold brightness.

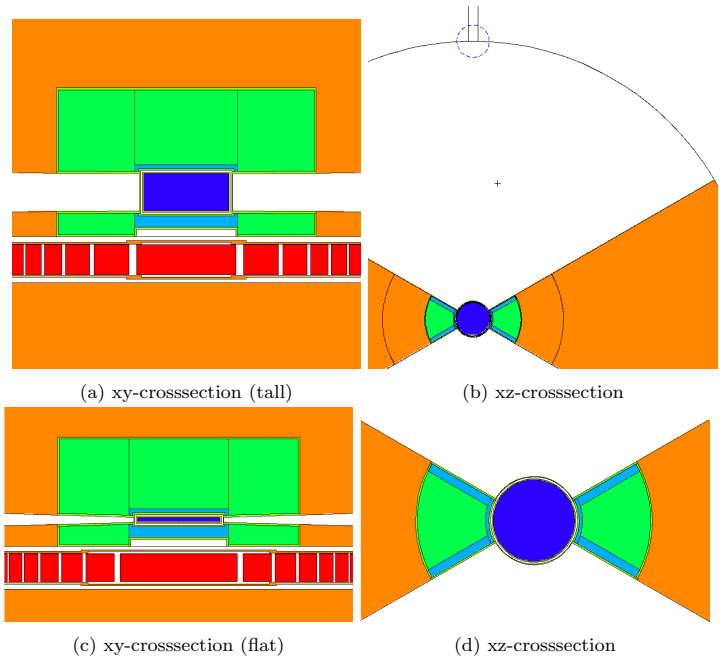

(a) xy-crosssection (tall) (b) xz-crosssection

(c) xy-crosssection (flat) (d) xz-crosssection

Figure 2: Vertical and horizontal cross sections of the 10 cm tall moderator (a, b and d) and the 1.5 cm flat moderator (b, c and d) of the ESS TMR system. The cold moderator (blue) is surrounded by water pre-moderator (light-blue) which in turn is surrounded by beryllium (green) and steel (orange). The entire system is situated above the rotating tungsten target wheel (red), and aluminium casings (light-green). The panels (b) and (d) show the water extensions next to the moderator from where thermal neutrons can be extracted. The small dashed sphere in the top of (b) is the DXTRAN sphere, see text, situated on the 2 m extraction surface (the black line).

3. Method

This study is based on a series of full proton-on-target simulations of the ESS target moderator reflector geometry, in the pancake geometry shown in Figure 2. The calculations are carried out using the Monte Carlo code MCNPX [11]. The MCNPX geometrical model itself constitutes a simplified design, where details related to e.g. cooling system and mechanical design are disregarded and where information on vacuum gaps, moderator tank thickness, and tungsten density is based on the conceptual ESS target-moderator-reflector (TMR) design [1].

The protons are initiated using the expected beam footprint on the target

surface in a 2.857 ms square pulse resembling a single ESS proton pulse. The time-averaged brightness B_a is derived from the peak brightness B_p as $B_a = f\delta t B_p$, where $f = 14$ Hz is the pulse frequency and δt is the pulse length.

In the MCNPX simulations the brightness is calculated using a point detector tally (F5) measuring the neutron flux, and a perfect collimator positioned such that the point detector only records neutrons arriving from the surface of the moderator, see [11].

The MCNPX simulations are carried out using an importance biasing (weight-windows) to gain higher statistics in the region of the moderator to optimally exploit computational efforts [11]. Furthermore neutrons are forced to the extraction area of interest using a DXTRAN sphere, see [11]. The importance biasing and the DXTRAN method effectively reduce the simulations needed by four to six orders of magnitude.

A Source Surface Write (SSW) card, see [11], is applied to the cylindrical beam extraction window surface 2 m away from the moderator center. The DXTRAN sphere is positioned centrally in this window, to gain statistics in this particular region of the surface, cf. Figure 2. The SSW data is analysed using ROOT [7, 12].

Neutron coordinates are described by the position (z', y') on the moderator surface image (the view of the moderator surface, observed from beam extraction position), the position (θ, y) on the beam extraction surface, located 2 m away from the center of the moderator, the neutron wavelength λ, as well as the emission time t from the moderator surface, see Figure 1.

Using the above method it is possible to calculate the full brightness distribution $B(\theta, y, z', y', \lambda; t)$. However, numerical evaluation of this distribution is not computationally feasible with present days computer power. Instead we will seek an analytical approximation to the full brightness distribution. We assume that the brightness can be factorized into the form,

$$B(\theta, y, z', y', \lambda; t) \approx \frac{1}{N} B_\theta(\theta) B_y(y) B_{z'}(z') B_{y'}(y') B_\lambda(\lambda; t), \qquad (1)$$

where the factors B_i attain simple analytical forms and N is a normalization

	Variable	Range
Cold Moderator (CM)		
- Vertical	y'	$[y_c - \frac{h}{2.5\ \mathbf{cm}}, y_c + \frac{h}{2.5\ \mathbf{cm}}]$
- Horizontal	z'	$[-5\ \text{cm}, 5\ \text{cm}]$
Thermal Moderator (TM)		
- Vertical	y'	$[y_c - \frac{h}{2.5\ \mathbf{cm}}, y_c + \frac{h}{2.5\ \mathbf{cm}}]$
- Horizontal	z'	$[-15\ \text{cm}, -12\ \text{cm}] \cup [12\ \text{cm}, 15\ \text{cm}]$
Beam extraction surface		
- Vertical	y	$[y_c - 1.5\ \text{cm}, y_c + 1.5\ \text{cm}]$
- Horizontal	θ	$[-0.432°, 0.432°]$
Spectrum		
- Cold neutrons (c)	λ	[4.05 Å, ∞]
- Thermal neutrons (t)	λ	[0.90 Å, 2.02 Å]

Table 1: Integration limits. h is the moderator height and y_c is the vertical moderator center position.

factor.

Due to the rather different characteristics of the cold and thermal moderators, separate factorizations of the brightness distribution will apply to the cold and thermal regions of the coordinate space.

The factorization (Eq. 1) implies that each of the functions B_i, e.g. $B_y(y)$, describes the distribution of the brightness along the associate coordinate (y), irrespective of the values of the remaining coordinates. While the brightness is assumed to factorize in the four spatial coordinates (y, θ, y', and z'), the emission time distribution will be highly correlated with the wavelength.

For each variable, i, the functions B_i is obtained by integration over the remaining coordinates, e.g.:

$$B_\theta(\theta) = \int B(\theta, y, z', y', \lambda; t) \frac{dy}{\Delta y} \frac{dz'}{\Delta z'} \frac{dy'}{\Delta y'} \frac{dt}{\Delta t} d\lambda, \tag{2}$$

with integration limits provided in Table 1. The integration limits cover the central region of the cold and thermal moderators (y', z'), the cold and thermal wavelength range (λ), and small beam extraction angles (θ, y). The integration range in time (Δt), covers the full neutron pulse to yield the time averaged brightness.

The integration limits are chosen such that a sufficient number of neutrons

from the moderator is obtained in the simulations, while boundary effects from the moderator-reflector interface are avoided. Hence, the one-dimensional distributions B_i will be representative for instruments aligned to the central region of the moderator surfaces (cold and thermal).

The one-dimensional distributions B_i were obtained from the MCNPX Monte Carlo simulations using the data analysis framework ROOT [12]. For each of the distributions B_i an analytical function was found to fit the simulated distributions for a range of moderator heights h, and the distributions were fitted to the simulated data using a maximum likelihood method [12]. All functions were chosen with the aim of keeping these including the parameter dependencies on h simple.

For convenience, the subscript i will be omitted from the one dimensional distributions in the following, e.g. $B(\theta) \equiv B_\theta(\theta)$.

4. Results

4.1. Cold and thermal brightness, B_c^{CM} and B_t^{TM}

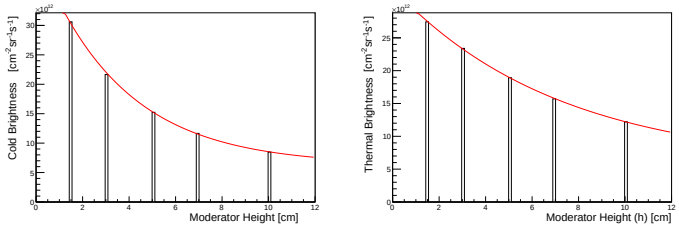

(a) Cold brightness B_c^{CM} (b) Thermal brightness: B_t^{TM}

Figure 3: Time averaged brightness of cold neutrons from the cold moderator B_c^{CM} and thermal neutrons from the thermal moderator B_t^{TM}. Curves (red) are analytical approximations to the Monte Carlo simulations (black).

The cold (c) neutron brightness from the cold moderator (CM) and thermal (t) neutron brightness from the thermal moderator (TM) are defined as,

$$B_c^{\mathrm{CM}} = \int_{\mathrm{CM},c} B(\theta, y, z', y', \lambda; t) \frac{d\theta}{\Delta\theta} \frac{dy}{\Delta y} \frac{dz'}{\Delta z'} \frac{dy'}{\Delta y'} \frac{dt}{\Delta t} d\lambda, \tag{3}$$

and

$$B_t^{\mathrm{TM}} = \int_{\mathrm{TM},t} B(\theta, y, z', y', \lambda; t) \frac{d\theta}{\Delta\theta} \frac{dy}{\Delta y} \frac{dz'}{\Delta z'} \frac{dy'}{\Delta y'} \frac{dt}{\Delta t} d\lambda, \tag{4}$$

where the integration ranges are provided in Table 1. Similarly, we may define the thermal neutron brightness from the cold moderator, B_t^{CM}, and the cold neutron brightness from the thermal moderator, B_c^{TM}, by appropriate change of integration limits.

The cold and thermal brightness B_c^{CM} and B_t^{TM}, for different moderator heights h are both well fitted by the simple exponential function $ae^{\alpha h} + b$. This is shown in Figure 3, where

$$B_c^{\mathrm{CM}} = (3.6 \times 10^{13} e^{-0.28\mathrm{cm}^{-1} h} + 6.3 \times 10^{12}) \ \mathrm{cm}^{-2}\mathrm{sr}^{-1}\mathrm{s}^{-1}, \tag{5}$$

and

$$B_t^{\mathrm{TM}} = (2.7 \times 10^{13} e^{-0.14\mathrm{cm}^{-1} h} + 5.6 \times 10^{12}) \ \mathrm{cm}^{-2}\mathrm{sr}^{-1}\mathrm{s}^{-1} \tag{6}$$

With the integration limits provided in Table 1, B_c^{CM} is estimated for the central region (35%) of the cold moderator surface, and B_t^{TM} is estimated for the thermal wings, cf. Figure 2.

4.2. Wavelength spectra

4.2.1. Thermal moderator spectrum

The thermal spectrum from the thermal moderator is described as a sum of a slowing down function and a Maxwellian with temperature T (Eq. 8) [13]. The slowing down function can be deduced from an epithermal ($E > 1$ eV) neutron distribution that is flat in lethargy $B(\ln(E)) = c$,

$$B(\lambda) = B(\ln(E)) \left| \frac{d\ln(E)}{d\lambda} \right| = c \times \left| \frac{d}{d\lambda} \ln(2\pi^2 \hbar^2 m_n^{-1} \lambda^{-2}) \right| = 2c\lambda^{-1} \tag{7}$$

where c is a constant. The λ^{-1} dependency is only valid for non-thermalized neutrons, hence the slowing down function should be cut off at a wavelength λ_{SD}. A logistic cut-off function, $\frac{1}{1+e^{\alpha(\lambda-\lambda_{SD})}}$ [13] has previously been applied at ESS [14] and is also chosen for this study.

As neutrons with low energy have a high absorption cross-section and as neutrons of higher energy may leak from the system before being fully thermalized, there are corrections to the simple Maxwellian distribution. A simple way of describing this is by increasing the effective temperature of the Maxwellian. In this study the Maxwellian model is further modified by a correction factor λ^{χ}, where χ is determined from the fitting procedure.

Hence, the thermal moderator spectrum is written as:

$$B^{\mathrm{TM}}(\lambda) = I_t \frac{2k_{th}^2}{T^2\lambda^5}\left(\frac{\lambda}{\lambda_0}\right)^{\chi} e^{-\frac{k_{th}}{T\lambda^2}} + I_{SD}\frac{1}{\lambda}\frac{1}{1+e^{\alpha(\lambda-\lambda_{SD})}} \tag{8}$$

Here $\lambda_0 = 1$Å, $k_{th} = \frac{2\pi^2\hbar^2}{m_n k_B} \approx 949$ KÅ^2, I_t and I_{SD} are the intensities of the Maxwellian distribution and the slowing down functions respectively, and α determines how fast the cut-off sets in around λ_{SD}.

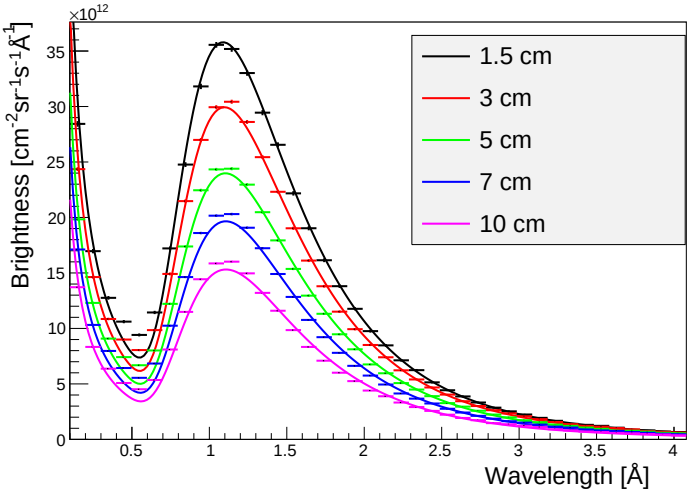

Figure 4: Thermal moderator spectra from MCNPX simulations in the ESS flat moderator geometry. Analytical forms from Eq. 8.

The parameters of the cut-off function are set to $\lambda_{SD} = 0.88$ Å and $\alpha = 2.5$ Å^{-1}, which are values historically used at ESS [14]. Figure 4 shows the functional fits to the thermal brightness spectra for different moderator heights h, with the parameters given in Table 2.

Parameter	Value	Unit
I_t	$3.5 \times 10^{13} e^{-0.166\text{cm}^{-1}h} + 8.1 \times 10^{12}$	$\text{cm}^{-2}\text{sr}^{-1}\text{s}^{-1}$
I_{SD}	$4.7 \times 10^{12} e^{-0.18\text{cm}^{-1}h} + 1.74 \times 10^{12}$	$\text{cm}^{-2}\text{sr}^{-1}\text{s}^{-1}$
T	325	K
χ	$-0.31\left(1 - e^{-0.35\text{cm}^{-1}h}\right) - 0.092$	-
α	2.5	Å^{-1}
λ_{SD}	0.88	Å

Table 2: Model parameters for $B^{\text{TM}}(\lambda)$ (Eq. 8)

4.2.2. Cold moderator spectrum

The pancake moderator is a cylindrical tank of pure para-hydrogen at 20 K. At neutron energies less than 14.7 meV the para-hydrogen cross-section falls off by more than one order of magnitude and as a result the mean free path increases drastically for cold neutrons (from ∼1 cm to ∼10 cm [15]). As a result neutrons below this energy experience the moderator as transparent and are emitted from the system with no further collisions. In [16] a formula describing a cold para-hydrogen spectrum has been suggested, and it is shown to fit the spectrum from the para-hydrogen geometry described in the ESS TDR [1]. In this study a slightly rearranged form is applied,

$$B^{\text{CM}}(\lambda) = \frac{1}{\left(1 + e^{\alpha_{cf}(\lambda - \lambda_{cf})}\right)^{\frac{1}{\gamma}}} I_c \left(e^{-\alpha_1 \lambda} + \kappa e^{-\alpha_2 \lambda}\right) + I_{SD} \frac{1}{\lambda} \frac{1}{1 + e^{\alpha_{SD}(\lambda - \lambda_{SD})}} \tag{9}$$

The phenomologically determined parameters are provided in Table 3. The cold moderator spectra are shown in Figure 5 as function of the moderator height, with the fitted parameters given in Table 3. The model is seen to fit quite well, both in the tall and the flat moderator geometry.

As in the case of the thermal moderator spectrum the parameters λ_{SD} and α_{SD} are not fitted but fixed to historically used cut-off values [14].

4.3. Time distribution

For a long pulsed source as ESS, the time distribution can be modelled as a square pulse modified by saturating exponential build up and a exponential

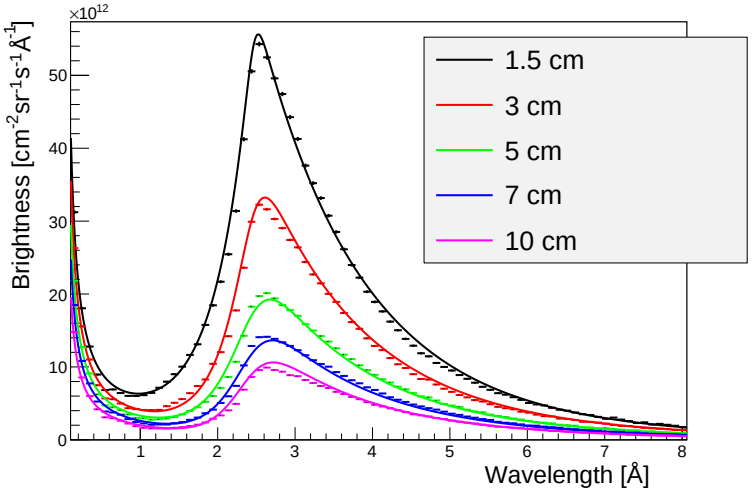

Figure 5: Cold moderator spectrum fitted to Eq. 9. The model parameters are provided in Table 3.

Parameter	Value	Unit
λ_{cf}	$2.5 - 0.0073\text{cm}^{-1}h$	Å
α_{cf}	$-78e^{-h\text{cm}^{-1}} - 5.5$	Å^{-1}
γ	$1.2e^{-.253\text{cm}^{-1}h} - 0.93$	-
I_c	$5.2 \times 10^{14}e^{-0.39\text{cm}^{-1}h} + 7.2 \times 10^{13}$	$\text{cm}^{-2}\text{sr}^{-1}\text{s}^{-1}\text{Å}^{-1}$
α_1	0.77	Å^{-1}
α_2	0.32	Å^{-1}
κ	$-0.050e^{-0.58\text{cm}^{-1}h} + 0.057$	-
I_{SD}	$4.1 \times 10^{12}e^{-0.13\text{cm}^{-1}h} + 8.5 \times 10^{11}$	$\text{cm}^{-2}\text{sr}^{-1}\text{s}^{-1}$
λ_{SD}	2.2	Å
α_{SD}	2.5	Å^{-1}

Table 3: Parameters for $B^{\text{CM}}(\lambda)$

decay as the proton beam is on or off, respectively. This model can be written as

$$B(t,\lambda) = B(\lambda) \times \frac{1}{\delta t f} \begin{cases} \left(1 - e^{-\frac{t}{\tau(\lambda)}}\right) & \text{for } t < \delta t \\ \left(1 - e^{-\frac{\delta t}{\tau(\lambda)}}\right) e^{-\frac{t-\delta t}{\tau(\lambda)}} & \text{otherwise} \end{cases} \tag{10}$$

Here $\delta t = 2.857$ ms is the proton pulse length and $f = 14$ Hz is the ESS pulse frequency. The approximation is only valid for long pulses, while for short

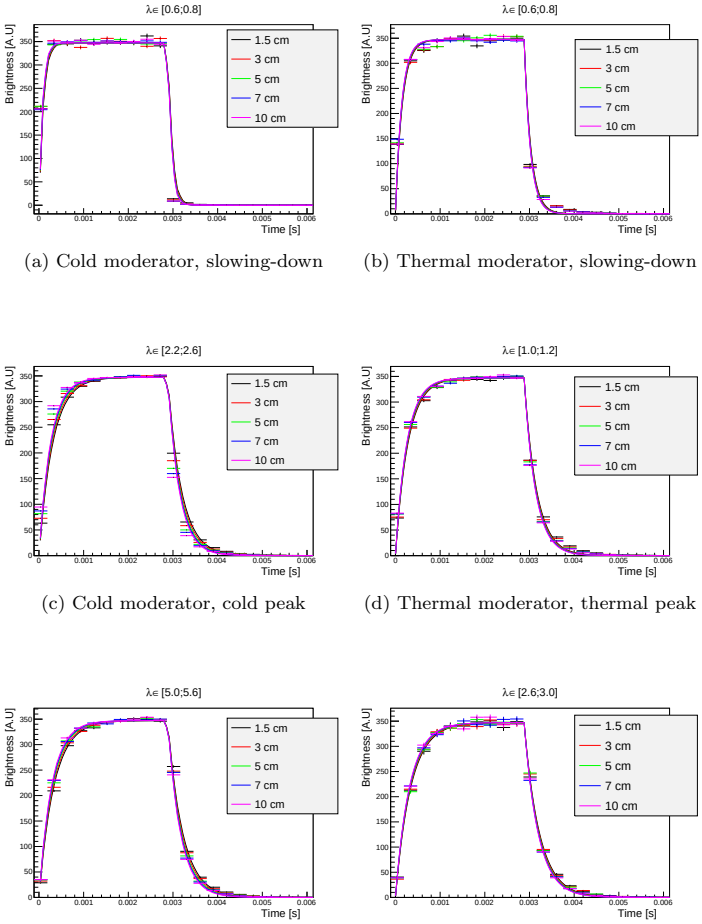

(a) Cold moderator, slowing-down (b) Thermal moderator, slowing-down

(c) Cold moderator, cold peak (d) Thermal moderator, thermal peak

(e) Cold moderator, distribution tail (f) Thermal moderator, distribution tail

Figure 6: Fit of simulations for cold (left) and thermal (right) time distributions, in different wavelength regions; corresponding to the slowing down part (top), the region near the spectral maximum (middle) and the region on the tail of the distribution (bottom). The units on the y-axis are arbitrary.

pulses the time distribution should be described by Ikeda-Carpenter function (see [17]).

In Eq. 10 the decay time $\tau(\lambda)$ depends on the wavelength. Fast neutrons will be emitted almost instantaneous while thermalized neutrons will be delayed

(or "stored") in the TMR system before being emitted. Thus one would expect the characteristic storage time τ to increase with wavelengths. Note that there is a small difference between the emission time from the moderator surface and from the moderator surface image - see Figure 1.

The distribution Eq. 10 has been fitted for different wavelengths intervals and moderator heights, some examples are shown in Figure 6. In Figures 7 and 8 the parameter $\tau(\lambda)$ is shown as a function of wavelength. $\tau(\lambda)$ can be modelled as,

$$\tau(\lambda) = 3 \times 10^{-4} \times (a\lambda^2 + b_\tau) \times \begin{cases} e^{\alpha(\lambda - S)^\gamma} & \text{for } \lambda > S \\ 1 & \text{otherwise} \end{cases} \quad (11)$$

The model fits are provided in Figure 7. The parameters of the model are given in Table 4 for the cold moderator time distribution and in Table 5 for the thermal moderator time distribution.

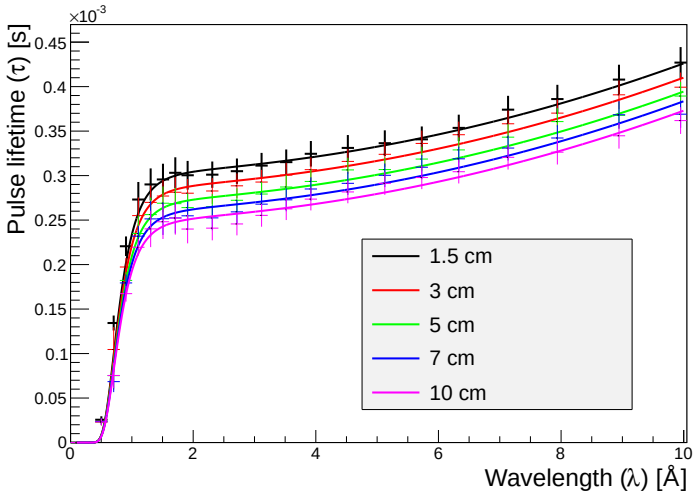

Figure 7: Fit of storage time constants, Eq. 11, for cold neutrons. Parameters as a function of height h are given in Table 4.

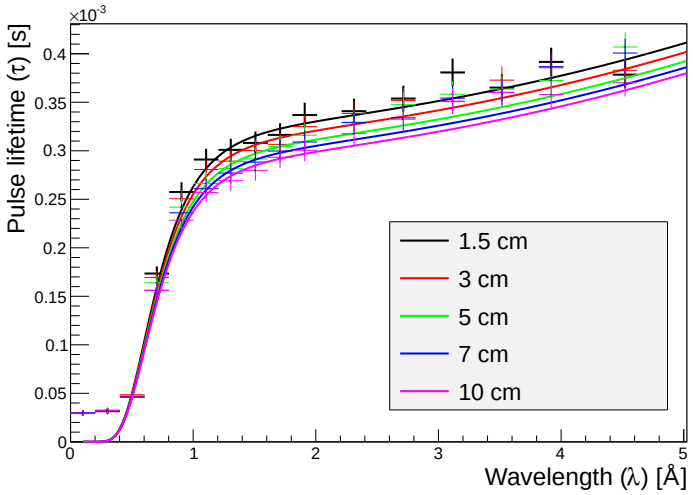

Figure 8: Fit of storage time constants, Eq. 11 thermal neutrons. Parameters as a function of height h are given in Table 5.

Parameter	Value	Unit
a	4.2×10^{-3}	sÅ^{-2}
b	$0.30e^{-0.178\mathrm{m}^{-1}h} + 0.78$	s
α	-6.6	Å$^{-\gamma}$
γ	-8.7	-
S	-0.90	Å

Table 4: Parameters for characteristic time constant $\tau^{\mathrm{CM}}(\lambda)$ for cold neutrons

Parameter	Value	Unit
a	1.2×10^{-2}	sÅ^{-2}
b	$0.176e^{-0.183\mathrm{m}^{-1}h} + 0.93$	s
α	-39	Å$^{-\gamma}$
γ	-7.7	-
S	-0.99	Å

Table 5: Parameters for characteristic time constant $\tau^{\mathrm{TM}}(\lambda)$ for thermal neutrons.

4.4. Brightness distribution over the moderator surface

In Figure 9 and 10 the cold and thermal neutron brightness distribution over the moderator image surface $B_c(y', z')$ and $B_t(y', z')$ are shown for the flat and the tall moderator, respectively.

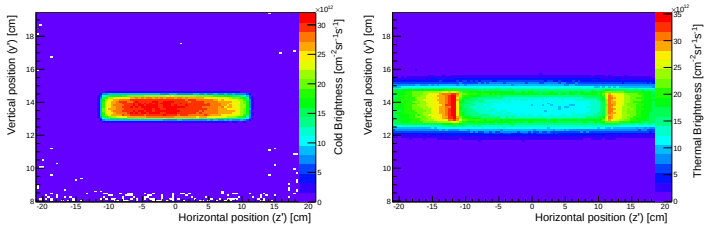

(a) Cold neutrons (b) Thermal neutrons

Figure 9: Moderator surface image of the 1.5 cm flat moderator for cold neutrons, $B_c(y', z')$ (left), and thermal neutrons, $B_t(y', z')$ (right). Note that the brightness color scales refer to different spectral regions.

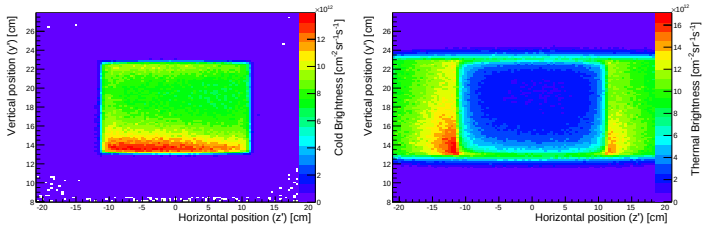

(a) Cold neutrons (b) Thermal neutrons

Figure 10: Moderator surface image of the 10 cm tall moderator. Cf. Figure 9.

4.4.1. Vertical cold distribution, $B_c^{\mathrm{CM}}(y')$

Thermal neutrons enter the cold moderator with a mean free path of the order of a centimetre or less and quickly scatter to a lower energy. The cold moderator consists of cold para-hydrogen which is transparent to cold neutrons below the spin excitation energy of hydrogen (around 14.7 meV). Cold neutrons are therefore emitted from the cold moderator without further scattering. This means that the majority of neutrons are emitted from the bottom of the moderator, facing the target wheel, or from the top of the moderator facing the reflector, as seen in Figure 10.

In the vertical direction (y') this can be modelled by two feed-in terms which decrease exponentially. More neutrons are fed-in from the target side than from the reflector side, which can be described by an asymmetry factor. On the moderator surface the distribution should thus be on the form: $e^{-\beta y' - y_c} +$

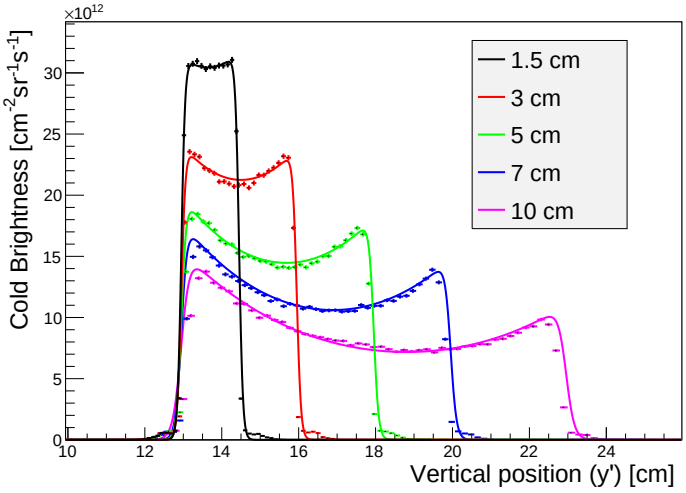

Figure 11: $B_c^{\mathrm{CM}}(y')$ distribution.

$\kappa e^{\beta y' - y_c}$.

Parameter	Value	Unit
A	$-0.12e^{-0.30\mathrm{cm}^{-1}h} + 1.0$	-
α	$36e^{-0.42\mathrm{cm}^{-1}h} + 4.6$	cm^{-1}
β	$0.38 - 0.014\mathrm{cm}^{-1}h$	cm^{-1}
κ	$1.14e^{-0.0544\mathrm{cm}^{-1}h}$	-

Table 6: Parameters for $B_c^{\mathrm{CM}}(y')$

The thermal neutrons entering in the cold moderator are mainly down-scattered by the para-hydrogen spin excitation mode. This inelastic scattering mode reduces the energy of the neutron with 14.7 meV per scatter. The thermal feed-in spectrum can, to first order, be assumed to be a Maxwellian distribution around 25 meV (300 K). This means that a significant fraction of the feed-in neutrons have energy above 30 meV and thus need two or more scattering events before their energy is below 14.7 meV, where they experience the full transparency effect of the moderator. This can be modelled with a couple of cut-off functions near the edge of the moderator. Logistics functions are used,

$(1+e^{\pm\alpha\left(y'-y_c\mp\frac{h}{2}\right)})^{-1}$, where α is a model parameter.

The y' distribution is given by,

$$B_c^{\mathrm{CM}}(y') = B_c^{\mathrm{CM}} \times A \times \left(e^{-\beta(y'-y_c)} + \kappa e^{\beta(y'-y_c)}\right) \times \left(1+e^{\alpha\left(y'-y_c-\frac{h}{2}\right)}\right)^{-1} \times \left(1+e^{-\alpha\left(y'-y_c+\frac{h}{2}\right)}\right)^{-1} \quad (12)$$

The fitted parameters for this function are given in Table 6, the cold neutron brightness $B_c^{\mathrm{CM}}(y')$ is shown in Figure 11.

4.4.2. Vertical thermal distribution, $B_t^{\mathrm{TM}}(y')$

In contrast to the vertical cold distribution, the thermal neutrons are distributed more uniformly in the vertical direction. In this study it is found that the form $a(y'-y_c)+1$ provides a good description of the vertical distribution from the thermal moderator.

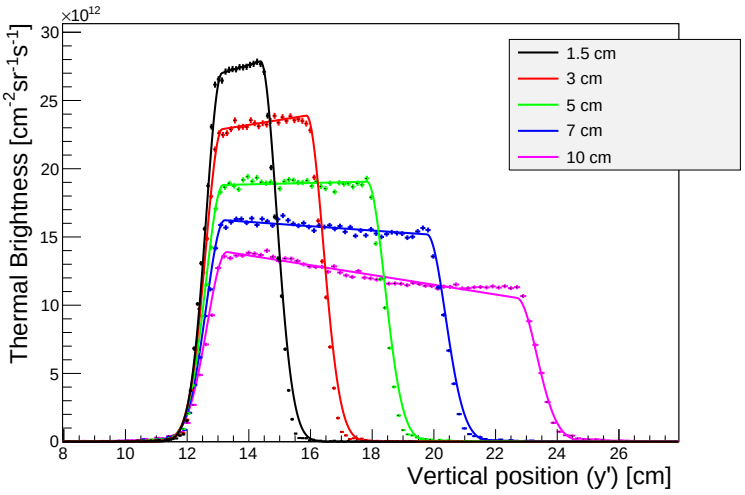

Figure 12: $B_t^{\mathrm{TM}}(y')$ distribution.

The reflectors above and below the thermal moderator operate at room temperature and emit a significant amount of thermal neutrons, hence the cut-off function should extend outside the moderator. The cut-off function is well

described by a Gaussian and the thermal brightness distribution $B_t^{\mathrm{TM}}(y')$ can be written as

$$B_t^{\mathrm{TM}}(y') = B_t^{\mathrm{TM}} \times (a(y'-y_c)+1) \begin{cases} e^{-\frac{(y'-y_c+\frac{h}{2})^2}{\sigma^2}} & \text{for } y'-y_c < -\frac{h}{2} \\ e^{-\frac{(y'-y_c-\frac{h}{2})^2}{\sigma^2}} & \text{for } y'-y_c > \frac{h}{2} \\ 1 & \text{otherwise} \end{cases} \quad (13)$$

The fit is shown in Figure 12 and the fitted parameters are given in Table 7.

Parameter	Value	Unit
a	$0.035 - 0.0064\mathrm{cm}^{-1}h$	cm^{-1}
σ	$0.70 + 0.022\mathrm{cm}^{-1}h$	cm

Table 7: Model parameters for $B_t^{\mathrm{TM}}(y')$

4.4.3. Horizontal cold distribution, $B_c^{\mathrm{CM}}(z')$

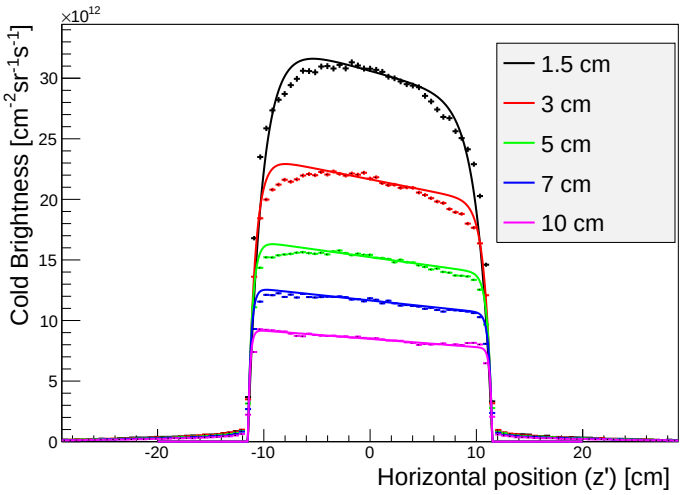

Figure 13: $B_c^{\mathrm{CM}}(z')$ distribution. Note that the MCNPX simulations extend into the region of the thermal moderator, while the analytical forms are restricted to the z'-values of the cold moderator.

The center of the flat moderator is positioned right above the spallation hot-spot in the target wheel. The horizontal cold distribution is shown in Figure 13. From this figure it can be seen that especially the flat moderators emit more

neutrons near the center of the moderator, while tall moderators have more homogeneous neutron distributions. This implies that flat moderators are more influenced by the target neutron hot-spot than tall moderators. The slight asymmetry in the horizontal distribution is due to a misalignment of the target position in the MCNPX model, which will not be present in the final design. The model function makes use of an asymmetry parameter, a, which accounts for the target misalignment. The horizontal cold neutron distribution is modelled by,

$$B_c^{\mathrm{CM}}(z') = B_c^{\mathrm{CM}} \times (az' + 1) \times \left(e^{\alpha(z' - \frac{w}{2})} - 1\right) \times \left(e^{-\alpha(z' + \frac{w}{2})} - 1\right) \text{ for } z' \in [-\tfrac{w}{2}; \tfrac{w}{2}] \tag{14}$$

Here w is the width of the moderator surface image, which is 23 cm. Eq. 14 only applies to the cold moderator range ($-\frac{w}{2} < z' < \frac{w}{2}$). The fit is shown in Figure 13 and the fitted parameters are given in Table 8. Cold neutrons originating from the thermal moderator are not modelled here.

Parameter	Value	Unit
α	$\frac{h}{2\mathrm{cm}}$	cm^{-1}
a	-0.008	cm^{-1}

Table 8: parameters for $B_c^{\mathrm{CM}}(z')$.

4.4.4. Horizontal thermal distribution, $B_t^{\mathrm{TM}}(z')$

The neutron brightness from the thermal moderator falls off quite fast in the horizontal direction. The model for the horizontal distribution of thermal neutrons from the thermal moderator is chosen as,

$$B_t^{\mathrm{TM}}(z') = B_t^{\mathrm{TM}} \times \left(a|z'| + b + ce^{\beta|z'|}\right) \times \begin{cases} \left(e^{\alpha(z' + \frac{w}{2}\cdot)} - 1\right) & \text{for } z' < -\frac{w}{2} \\ \kappa\left(e^{-\alpha(z' - \frac{w}{2}\cdot)} - 1\right) & \text{for } z' > \frac{w}{2} \end{cases} \tag{15}$$

This model is fitted to the simulated data, as shown in Figure 14. The parameters are provided in Table 9. In addition to the thermal neutrons from the thermal moderator there is a significant contribution of thermal neutrons from the cold moderator.

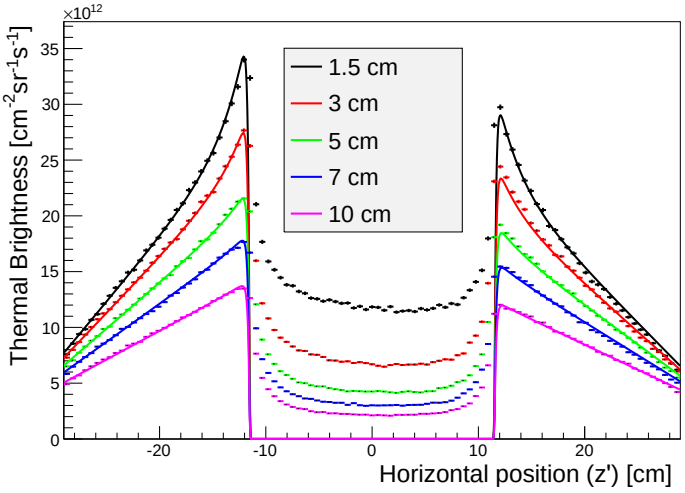

Figure 14: $B_t^{\mathrm{TM}}(z')$ distribution. Note that there are quite a few thermal neutrons originating from the cold moderator. These are described by the slowing down part of the cold moderator spectrum, cf. Figure 5.

Parameter	Value	Unit
α	7.0	cm^{-1}
β	-0.45	cm^{-1}
a	0.053	cm^{-1}
b	$-1.8 - 0.019h$	-
c	$-150e^{-.41\mathrm{cm}^{-1}h}$	cm^{-1}
κ	$0.84 + 0.0030\mathrm{cm}^{-1}h$	-

Table 9: Model parameters for $B_t^{\mathrm{TM}}(z')$

4.5. Distributions on the beam extraction surface

4.5.1. Beamport angle, $B_c^{\mathrm{CM}}(\theta)$ and $B_t^{\mathrm{TM}}(\theta)$

Due to statistical limitations this study only investigated a narrow span around $\theta = 0°$. However, in the model implemented into McStas the vertical distribution on the extraction surface is assumed to be flat for cold neutrons, i.e. $B_c^{\mathrm{CM}}(\theta) = const.$ as well as for the thermal neutrons, $B_t^{\mathrm{TM}}(\theta) = const.$

4.5.2. Vertical distributions, $B_c^{\mathrm{CM}}(y)$ and $B_t^{\mathrm{TM}}(y)$

As para-hydrogen is transparent to cold neutrons, many of the neutrons entering a neutron guide will originate from deep inside the cold moderator, thus the observed brightness will depend on the depth of view into the moderator. As the viewing depth of the moderator will be reduced when viewing the moderator at an inclination w.r.t. the moderator plane, one would expect a reduction in cold brightness. In other words, the ESS flat moderator is going to be a directional moderator, due to internal collimation. This effect can be modelled by,

$$B_c^{\mathrm{CM}}(y) = B_c^{\mathrm{CM}}(1 - a|y|) \tag{16}$$

The distribution, Eq. 16, is shown in Figure 15a, with the parameter $a = 0.05\mathrm{cm}^{-1}e^{-0.39\mathrm{cm}^{-1}h}$.

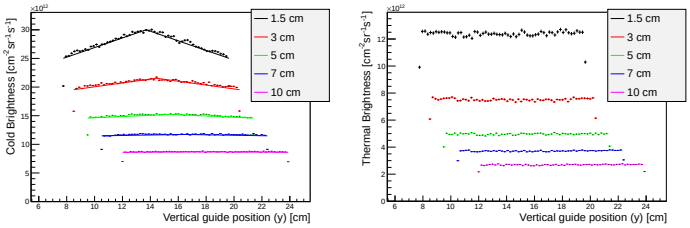

(a) Cold distribution (b) Thermal distribution

Figure 15: The vertical cold distribution ($B_c^{\mathrm{CM}}(y)$) and thermal distribution ($B_t^{\mathrm{TM}}(y)$) on a 12 cm high beam extraction slot. The cold distribution $B_c^{\mathrm{CM}}(y)$ is not flat indicating a directional moderator.

The thermal moderators are not directional, and the inclination angle distribution should be modelled as a constant, i.e. $B_t^{\mathrm{TM}}(y) = 1$.

4.5.3. Brightness factorization

To investigate the validity of the factorization (1) we compare the simulations to the factorized form, where analytical functions for the one-dimensional distributions are employed.

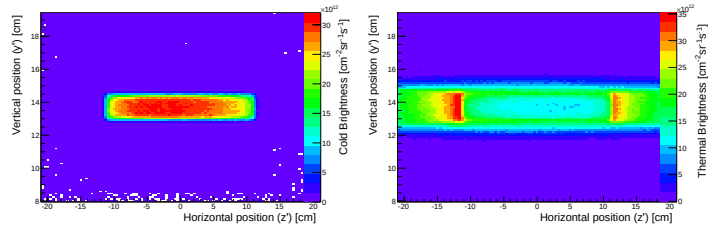

(a) Cold neutrons from MCNPX (b) Thermal neutrons from MCNPX

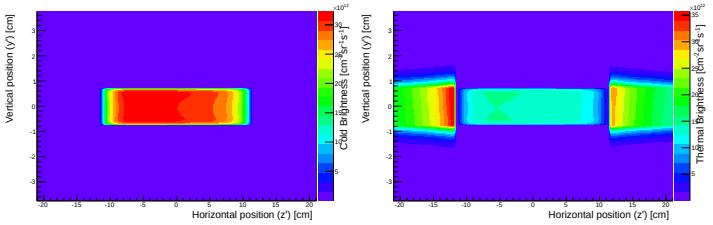

(c) Cold neutrons from functions (d) Thermal neutrons from functions

Figure 16: Comparison between the MCNPX simulations (top) and the factorized and fitted functions for a flat moderator.

In the following we consider only the moderator surface image and wavelength coordinates, i.e. (z', y', λ). We seek factorizations of the form

$$B(z', y', \lambda) \approx \frac{1}{(B_c^{\mathrm{CM}})^2} B_c^{\mathrm{CM}}(z') B_c^{\mathrm{CM}}(y') B^{\mathrm{CM}}(\lambda), \tag{17}$$

for z' in the cold moderator region ($z' \in [-\frac{w}{2}, \frac{w}{2}]$), and

$$B(z', y', \lambda) \approx \frac{1}{(B_t^{\mathrm{TM}})^2} B_t^{\mathrm{TM}}(z') B_t^{\mathrm{TM}}(y') B^{\mathrm{TM}}(\lambda). \tag{18}$$

for z' outside the cold moderator region ($z' \notin [-\frac{w}{2}, \frac{w}{2}]$).

Hence it is assumed that the one-dimensional distributions of cold neutrons $B_c^{\mathrm{CM}}(y')$ and $B_c^{\mathrm{CM}}(z')$ describe the brightness of the cold moderator, similarly $B_t^{\mathrm{TM}}(y')$ and $B_t^{\mathrm{TM}}(z')$ describe the brightness of the thermal moderator.

From the distributions Eq. 17 and 18 it follows that

$$B_c^{\mathrm{CM}}(y', z') = \frac{1}{B_c^{\mathrm{CM}}} B_c^{\mathrm{CM}}(z') B_c^{\mathrm{CM}}(y') \tag{19}$$

for cold neutrons from the cold moderator,

$$B_t^{\mathrm{CM}}(y',z') = \frac{B_t^{\mathrm{CM}}}{(B_c^{\mathrm{CM}})^2} B_c^{\mathrm{CM}}(z') B_c^{\mathrm{CM}}(y') \tag{20}$$

for thermal neutrons from the cold moderator, where $B_t^{\mathrm{CM}} = \int_t B^{\mathrm{CM}}(\lambda) d\lambda$,

$$B_t^{\mathrm{TM}}(y',z') = \frac{1}{B_t^{\mathrm{TM}}} B_t^{\mathrm{TM}}(z') B_t^{\mathrm{TM}}(y') \tag{21}$$

for thermal neutrons from the thermal moderator, and

$$B_c^{\mathrm{TM}}(y',z') = \frac{B_c^{\mathrm{TM}}}{(B_t^{\mathrm{TM}})^2} B_t^{\mathrm{TM}}(z') B_t^{\mathrm{TM}}(y') \tag{22}$$

for cold neutrons from the thermal moderator, where $B_c^{\mathrm{TM}} = \int_c B^{\mathrm{TM}}(\lambda) d\lambda$.

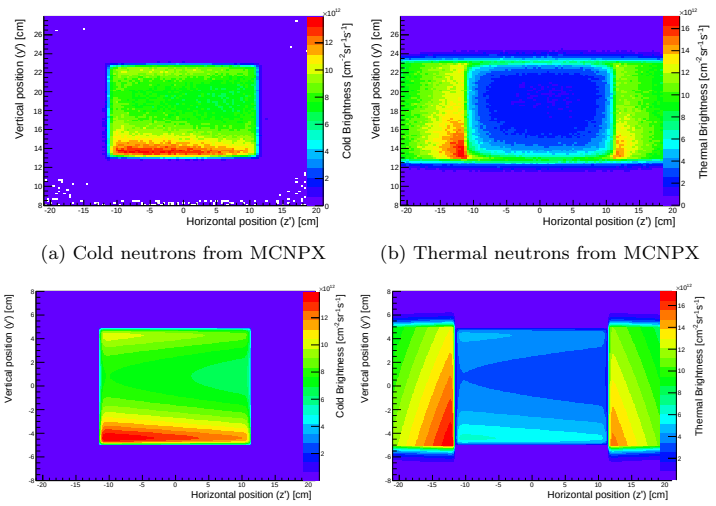

(a) Cold neutrons from MCNPX (b) Thermal neutrons from MCNPX

(c) Cold neutrons from functions (d) Thermal neutrons from functions

Figure 17: Comparison between the MCNPX simulations (top) and the factorized and fitted functions for a tall moderator.

Figures 16 and 17 show the MCNPX simulations of $B_t(z',y')$ and $B_c(z',y')$ next to the factorized functional description of flat and tall moderators, respectively. Similarly Figures 18, 19 and 20 show $B^{\mathrm{TM}}(y',\lambda)$, $B^{\mathrm{CM}}(y',\lambda)$ and $B(z',\lambda)$, respectively.

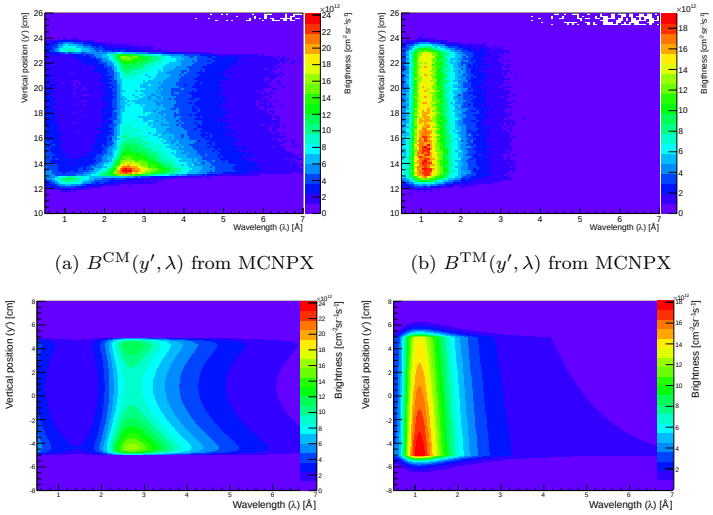

(a) $B^{\mathrm{CM}}(y', \lambda)$ from MCNPX (b) $B^{\mathrm{TM}}(y', \lambda)$ from MCNPX

(c) $B^{\mathrm{CM}}(y', \lambda)$ from functions (d) $B^{\mathrm{TM}}(y', \lambda)$ from functions

Figure 18: Comparison between the MCNPX simulations (top) and the factorized and fitted functions for a tall moderator.

The model is limited to fitting cold neutrons emitted from the cold moderator and thermal neutrons emitted from the thermal moderator, hereby neglecting the contribution of cold neutrons emitted from the thermal moderators, and thermal neutrons from the cold moderator. This limitation implies that in regions of Figures 17, 18, 19 and 20 there are deviations between model and simulation. Despite these differences, the method is superior to implicitely assuming a flat distribution, which was previously done for the ESS moderator system [4, 18].

5. Conclusion

A method for extracting full brightness information on a moderator system has been developed. Full phase-space information is extracted from MCNPX proton-on-target simulations using a SSW card, this information is then translated into brightness phase-space using ROOT.

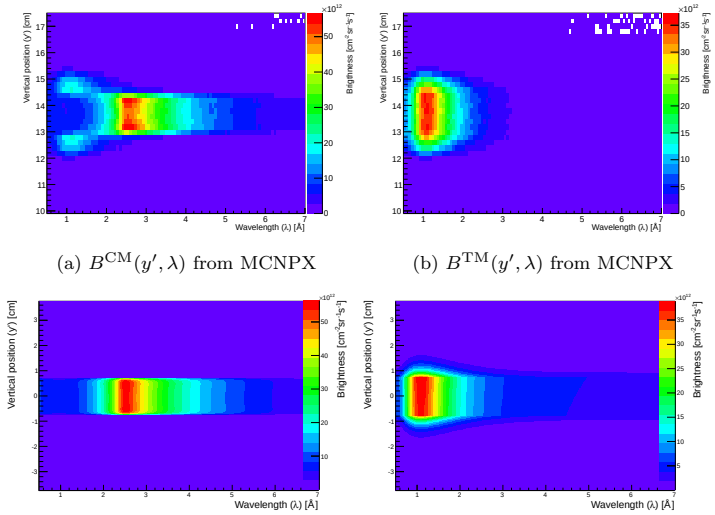

(a) $B^{\mathrm{CM}}(y', \lambda)$ from MCNPX (b) $B^{\mathrm{TM}}(y', \lambda)$ from MCNPX

(c) $B^{\mathrm{CM}}(y', \lambda)$ from functions (d) $B^{\mathrm{TM}}(y', \lambda)$ from functions

Figure 19: Comparison between the MCNPX simulations (top) and the factorized and fitted functions for a flat moderator.

The SSW method facilitates post-simulation analysis of moderator hot-spots, neutron beam directionality, and time and wavelength distributions.

By studying the ESS para-hydrogen moderator and thermal extensions, it is shown that the neutron distribution on the moderator surface is not flat. For the taller moderators the emission distribution of cold neutrons varies substantially, as much as a factor 2 over a 5 cm range for a 10 cm tall moderator, which is consistent with results observed at J-PARC [2]. This effect diminishes for flatter moderators, and is almost negligible for 1.5 cm to 3 cm high moderators. For thermal neutrons from the thermal water extensions the brightness falls off rapidly with the distance from the cold moderator, the effect seems to increase for smaller heights of the moderator.

All one-dimensional brightness distributions, have been fitted to simple functions, using ROOT. Assuming that the full brightness distribution can be factorized into these one-dimensional forms enables a full functional description of

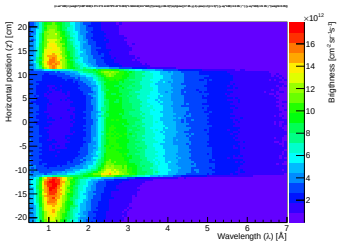

(a) $B(z', \lambda)$ for a tall moderator from MCNPX

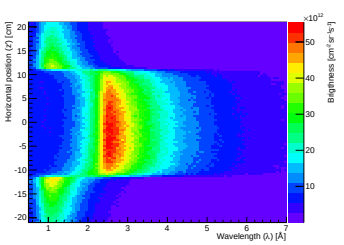

(b) $B(z', \lambda)$ for a flat moderator from MCNPX

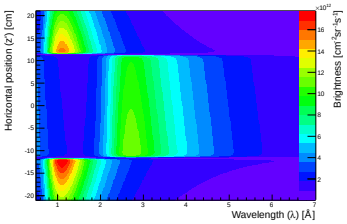

(c) $B(z', \lambda)$ for a tall moderator from functions

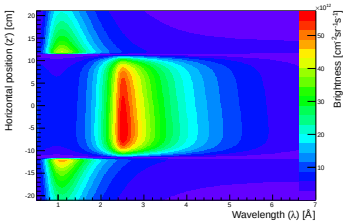

(d) $B(z', \lambda)$ for a flat moderator from functions

Figure 20: Comparison between the MCNPX simulations (top) and the factorized and fitted functions for a flat (left) and a tall (right) moderator.

the expected brightness from flat moderators at ESS.

Obviously this approach only provides an approximate description of the full phase space distribution. To assess the accuracy of the factorization 2-d brightness model distributions are compared to MCNPX calculations. Overall, the modelling is successful in the sense that the functional description captures the main features of the full simulation. It should be noted, that the functional description is not intended as a physics model, and it does contain many parameters. In fact for a given height of moderator, the functional description contains a total of 38 free parameters, and for the functional description for all heights it contains 74 parameters. Furthermore, the model makes use of thermal moderator temperature, the moderator height, pulse frequency, pulse length, and four cut-off function parameters. The modelling is phenomenological providing a tool to aid instrument developers optimizing their neutron guides for optimal

neutron extraction, which in turn will result in an overall increase in the quality and efficiency of the entire ESS facility. The functions have been implemented in McStas and has already been released with the release of McStas 2.1 for the pancake geometry, and is part of McStas 2.2/2.2a for the butterfly geometry described in the appendix.

References

[1] S. Peggs (Ed.), ESS Technical Design Report, 2013.

[2] T. Kai, M. Harada, M. Teshigawara, N. Watanabe, and Y. Ikeda, Coupled hydrogen moderator optimization with ortho/para-hydrogen ratio, Nuclear Instruments and Methods A 523 (2004) 398414.

[3] T. Schönfeldt et. al., Optimization of cold neutron beam extraction at ESS, AccApp Conf. Proc. (2013).

[4] P. Willendrup, E. Knudsen, E. Farhi and K. Lefmann, User and Programmers Guide to the Neutron Ray-Tracing Package McStas, Version 1.12c ((2011)).

[5] F. X. Gallmeier, Private communication.

[6] E. Farhi, C. Monzat, R. Arnerin, T. van Vuure, C. Castn-Guerrero, C. Hennane, P.A. Harraud, G. Campioni, S. Fuard, J. Ollivier, P. Willendrup, Advanced sources and optical components for the McStas neutron scattering instrument simulation package, Journal of Neutron Research 17 (2014) 63.

[7] E. Klinkby et al, Developing an interface between MCNPX and McStas for simulation of neutron moderators, Nuclear Instruments & Methods In Physics Research A 700 ((2013)) 106.

[8] K. Batkov, A. Takibayev, L. Zanini and F. Mezei, Unperturbed moderator brightness in pulsed neutron sources, Nucl. Inst. Meth. 729 (0) (2013) 500.

[9] P. Willendrup, E. Farhi, E. Knudsen, U. Filges, K. Lefmann, McStas: Past, present and future, J. Neutr. Res. 17 ((2014)) 35–43.

[10] D. Filges, F. Goldenbaum, Handbook of Spallation Research: Theory, Experiments and Applications, Wiley-VCH Verlag GmbH and Co. KGaA.

[11] L. S. Waters, G. W. McKinney, J. W. Durkee, M. L. Fensin, J. S. Hendricks et. al., The MCNPX Monte Carlo radiation transport code, AIP Conf.Proc. 896 (2007) 81. doi:10.1063/1.2720459.

[12] R. Brun, F. Rademakers, ROOT - An Object Oriented Data Analysis Framework, Nuclear Instruments and Methods A 389 (1997) 81.

[13] R.A. Robinson, and J.M. Carpenter, On the use of switch functions in describing pulsed neutron moderators, Nuclear Instruments and Methods in Physics Research A 307 (1991) 359-365.

[14] Mezei, F., ESS report: ESS target - moderator performance estimates (2010).

[15] F. Mezei, L. Zanini, A. Takibayev, K. Batkov, E. Klinkby, E. Pitcher, T. Schnfeldt, Low dimensional neutron moderators for enhanced source brightnessarXiv:1311.2474.

[16] T. Schönfeldt et. al., Analytical fits to the ESS cold and thermal moderator spectra, conf. proc. ICANS XXI, Mito, Ibaraki, Japan.

[17] S. Ikeda, J.M. Carpenter, Wide-energy-range, high-resolution measurements of neutron pulse shapes of polyethylene moderators, Nuclear Instrument and Methods A 239 (3) (1985) 536.

[18] P. Willendrup, E. Knudsen, K. Lefmann and E. Farhi, Component Manual for the Neutron Ray-Tracing Package McStas, Version 1.12 ((2011)).

Appendix A. The butterfly moderator

Following the same procedure as described above, the brightness distribution for the ESS butterfly moderator is evaluated. The horizontal MCNPX cross section of the butterfly moderator is shown in Figure A.21.

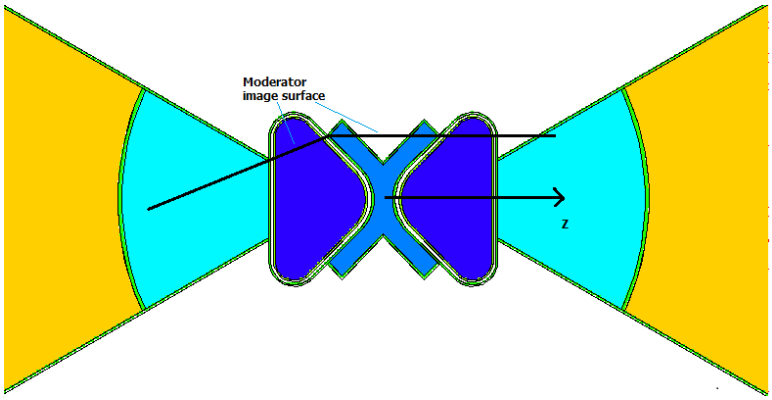

Figure A.21: (x, z)-cross-section of the butterfly moderator, the ESS baseline moderator design as of March 2015. A cross shaped thermal water moderator is positioned centrally over the neutron hotspot in the target wheel with a cold para-hydrogen moderator wing at each side. The butterfly is 28.0 cm across and 21.2 cm deep and yields an increase in brightness over the pancake moderator, especially in thermal brightness.

In the butterfly design the moderator height is fixed to 3 cm for the top moderator and 6 cm for the bottom moderator, placed above and below the target wheel respectively. In the following, the 3 cm tall butterfly moderator is considered.

We define, the moderation image surface as two planes described by: $x = 8.27$ cm for $z' > -7.16$ and $x = 0.45z' + 11.5$ cm otherwise, cf. Figure A.21.

Appendix A.1. Wavelenght spectra

The cold and thermal spectra from the butterfly moderator is well described by the same functional forms as used for the flat moderator. The cold moderator brightness spectrum is modelled by Eq. 9. The fit is shown in Figure A.22 and parameters are given in Table A.10. Similarly, the thermal moderator brightness

spectrum is modelled by Eq. 8. The fit is shown in Figure A.23 and parameters are provided in Table A.11.

Parameter	Value	Unit
λ_{cf}	2.5	Å
α_{cf}	$\frac{5°-\theta}{2°} - 13$	$Å^{-1}$
γ	$-0.048 - 0.16e^{-0.45\frac{\theta-5°}{10.}}$	-
I_c	2.3×10^{14} for $\theta = 5°$	$cm^{-2}sr^{-1}s^{-1}$
	2.4×10^{14} for $\theta = 15°$	$cm^{-2}sr^{-1}s^{-1}$
	2.4×10^{14} for $\theta = 25°$	$cm^{-2}sr^{-1}s^{-1}$
	2.5×10^{14} for $\theta = 35°$	$cm^{-2}sr^{-1}s^{-1}$
	2.4×10^{14} for $\theta = 45°$	$cm^{-2}sr^{-1}s^{-1}$
	2.4×10^{14} for $\theta = 55°$	$cm^{-2}sr^{-1}s^{-1}$
α_1	$0.79 + 0.0085\frac{\theta-5.°}{10°}$	$Å^{-1}$
α_2	0.33	$Å^{-1}$
κ	$0.046 - 0.0016 * \frac{\theta-5.°}{10°}$	-
I_{SD}	3.4×10^{12}	$cm^{-2}sr^{-1}s^{-1}$
λ_{SD}	2.2	Å
α_{SD}	2.5	$Å^{-1}$

Table A.10: Parameters for $B^{\mathrm{CM}}(\lambda)$ (Eq. 9)

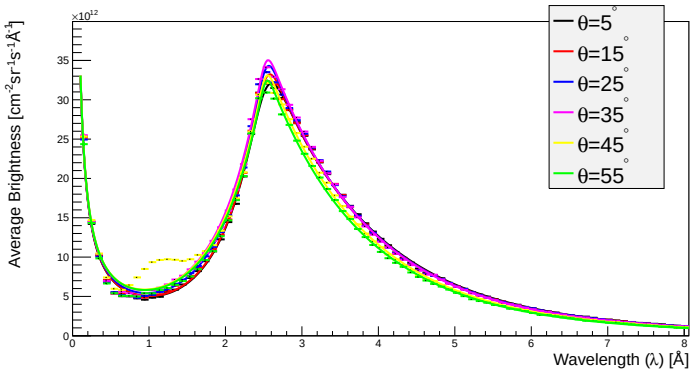

Figure A.22: Cold moderator spectrum. The thermal bump at 45° is due to the collimator extending into the thermal moderator regime.

Appendix A.2. Vertical brightness distribution

The vertical brightness distribution of the moderator surface can be described by the same model as used for the pancake moderator. The thermal

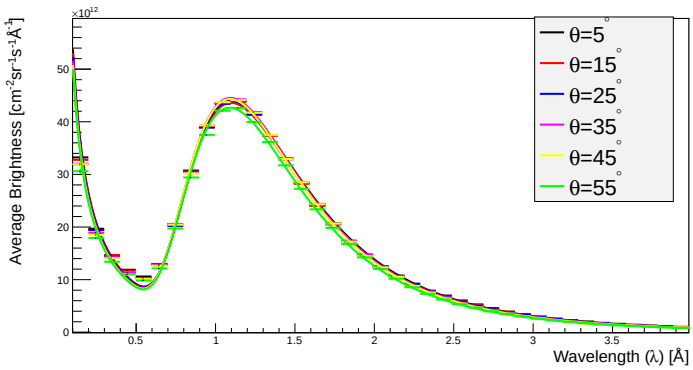

Figure A.23: Thermal moderator spectrum.

Parameter	Value	Unit
I_t	$4.3 \times 10^{13} - 9.3 \times 10^{10} \frac{\theta-5^\circ}{1^\circ} + 8.0 \times 10^9 \left(\frac{\theta-5^\circ}{1^\circ}\right)^2 - 1.3 \times 10^8 \left(\frac{\theta-5^\circ}{1^\circ}\right)^3$	$\mathrm{cm}^{-2}\mathrm{sr}^{-1}\mathrm{s}^{-1}$
I_{SD}	$6.2 \times 10^{12} - 8.8 \times 10^9 \frac{\theta-5^\circ}{1^\circ}$	$\mathrm{cm}^{-2}\mathrm{sr}^{-1}\mathrm{s}^{-1}$
T	325	K
χ	$0.31 + 2.2 \times 10^{-3} \frac{\theta-5^\circ}{1^\circ}$	-
α	2.5	$\mathrm{Å}^{-1}$
λ_{SD}	0.88	Å

Table A.11: Parameters for $B^{\mathrm{TM}}(\lambda)$, (Eq. 8)

distribution $B_t^{\mathrm{TM}}(y')$ is described by Eq. 13, the fit is shown in Figure A.24 with parameters given in Table A.12 and the cold distribution $B_c^{\mathrm{CM}}(y')$ is described by Eq. 12, the fit is shown in Figure A.25 with parameters given in Table A.13.

Parameter	Value	Unit
h	3.2	cm
a	0	-
σ	0.37	cm

Table A.12: Parameters for $B_t^{\mathrm{TM}}(y')$ (Eq. 13). Note that the height is here modelled as slightly larger than the actual moderator height.

Parameter	Value	Unit
h	3	cm
A	$\frac{1}{2}$	-
α	30	cm^{-1}
β	.35	cm^{-1}
κ	1	-

Table A.13: Parameters for $B_c^{\mathrm{CM}}(y')$ (Eq. 12)

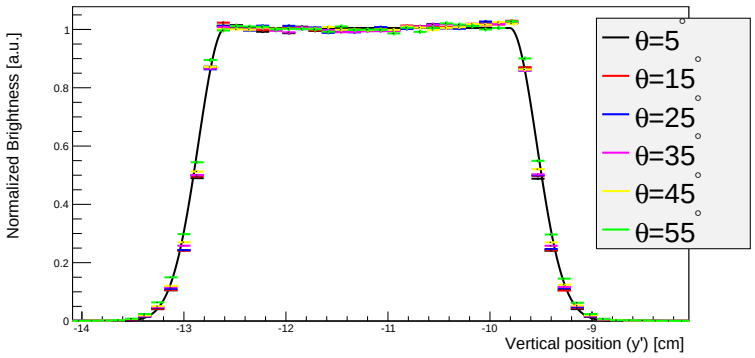

Figure A.24: Thermal neutron distribution from the thermal moderator surface.

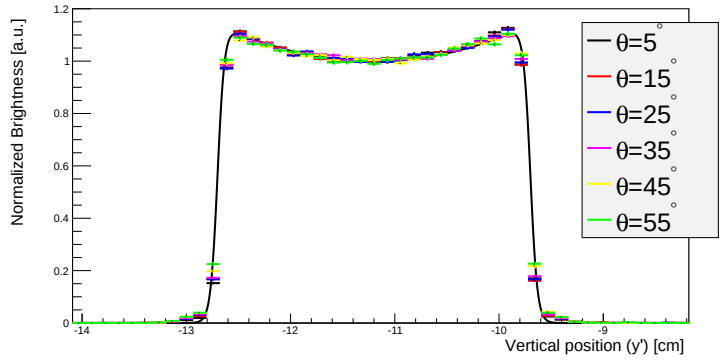

Figure A.25: Cold neutron distribution from the cold moderator surface in the vertical direction.

Appendix A.3. Horizontal brightness distribution

The butterfly is significantly different from the pancake in the horizontal direction, thus new models have been written for the horizontal brightness dis-

tribution.

The cold moderator brightness distribution $B_t^{\mathrm{CM}}(z')$ is well modelled by the function

$$B_c^{\mathrm{CM}}(z') = (a + b(z' + 12\text{ cm}))(1 + e^{\alpha(z'-A)})^{-1}(1 + e^{\beta(z'-B)})^{-1} \tag{A.1}$$

The model parameters are provided in Table A.14, and the fit is shown in Figure A.26.

Parameter	Value	Unit
a	0.98 for $\theta = 5°$	-
	0.97 for $\theta = 15°$	-
	0.98 for $\theta = 25°$	-
	1.01 for $\theta = 35°$	-
	1.12 for $\theta = 45°$	-
	1.16 for $\theta = 55°$	-
b	$1.46 \times 10^{-2} + 8.0 \times 10^{-4}(\theta - 5) - 2.8 \times 10^{-5}(\theta - 5)^2$	cm^{-1}
α	-20 for $\theta = 5°$	cm^{-1}
	$-4.0 - .075\frac{\theta-5°}{1°}$ otherwise	cm^{-1}
A	-14.27 for $\theta = 5°$	cm
	$-15 - 1.8 \times 10^{-2} + 3.7 \times 10^{-4}\frac{\theta-5°}{1°}$ otherwise	cm
β	-3.5 for $\theta = 35°$	cm^{-1}
	-1.9 for $\theta = 55°$	cm^{-1}
	-15 otherwise	cm^{-1}
B	-8.1 for $\theta = 45°$	cm
	$-7.1 + 8.4 \times 10^{-3}\frac{\theta-5°}{1°} - 5.5 \times 10^{-4}\left(\frac{\theta-5°}{1°}\right)^2$ otherwise	cm

Table A.14: Parameters for $B_c^{\mathrm{CM}}(z')$ (Eq. A.1)

The thermal neutron distribution $B_t^{\mathrm{CM}}(z')$ is modelled by,

$$\begin{aligned} B_t^{\mathrm{TM}}(z') = {} & (1 + e^{-8\mathrm{cm}^{-1}(z'-A)})^{-1} \times (1 + e^{-8\mathrm{cm}^{-1}(z'-B)})^{-1} \times \Bigg[\\ & \left(a(z' - A) + c + 1.2e^{-(z'+7.55\mathrm{cm})^2/(.35\mathrm{cm})^2}\right) \times \left(1 + e^{8\mathrm{cm}^{-1}(z'-C)}\right)^{-1} \\ & + \left(\frac{c-d}{C-D}(z' - C) + c\right) \times \left(1 - \left(1 + e^{8\mathrm{cm}^{-1}(z'-C)}\right)^{-1}\right) \\ & + (b(z' - D) + d) \times \left(1 - \left(1 + e^{8\mathrm{cm}^{-1}(z'-D)}\right)^{-1}\right) \Bigg] \end{aligned} \tag{A.2}$$

The model parameters are provided in Table A.15, and the fit is shown in Figure A.27.

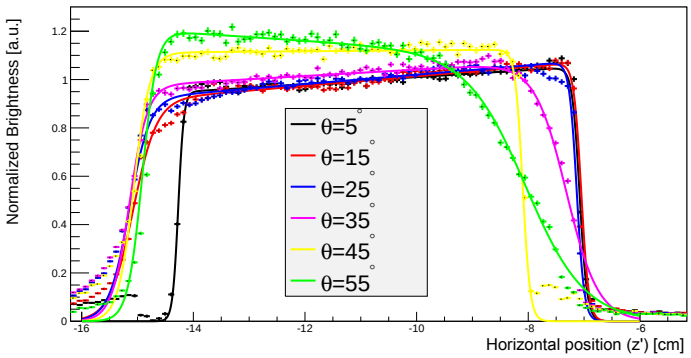

Figure A.26: Cold neutron brightness in the horizontal direction.

Parameter	Value	Unit
A	7.5 for $\theta = 45°$	cm
	8.2 for $\theta = 55°$	cm
	7.2 otherwise	cm
B	-8.2 for $\theta = 45°$	cm
	-7.7 for $\theta = 55°$	cm
	-7.2 otherwise	cm
C	$-5.6 + 4.93 \times 10^{-2}(\theta - 5°)$	cm
D	-2.6 for $\theta = 55°$	cm
	$-2.7 \times 10^{-1} - 7.11 \times 10^{-2}(\theta - 5°)$ otherwise	cm
a	-3.5×10^{-2}	cm^{-1}
b	$-8.2 \times 10^{-2} + 8.07 \times 10^{-4}(\theta - 5°)$	cm^{-1}
c	$-8.2 \times 10^{-1} + 9.15 \times 10^{-4}(\theta - 5°)$	cm
d	1.2 for $\theta = 55°$	cm
	$1.3 - 7.0 \times 10^{-4}(\theta - 5°)$ otherwise	cm

Table A.15: Parameters for $B_t^{\mathrm{TM}}(z')$ (Eq. A.2)

The functional forms of the horizontal distribution of thermal neutrons $B_t^{\mathrm{TM}}(z')$ next to the distribution of cold neutrons $B_c^{\mathrm{CM}}(z')$ are shown in Figure A.28.

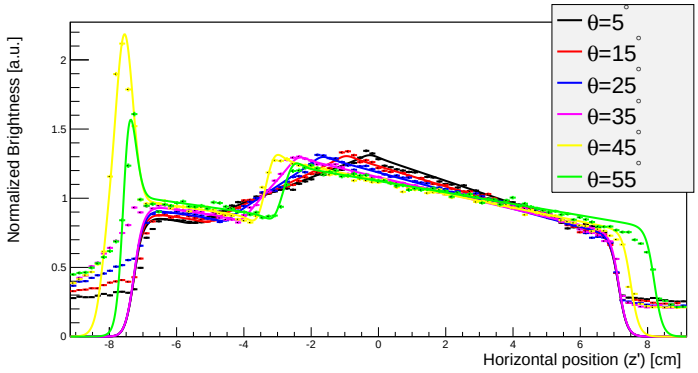

Figure A.27: Thermal neutron brightness in the horizontal direction. Note the bump at $\theta = 45°$ and $\theta = 55°$ stemming from the gab between the cold and thermal moderator.

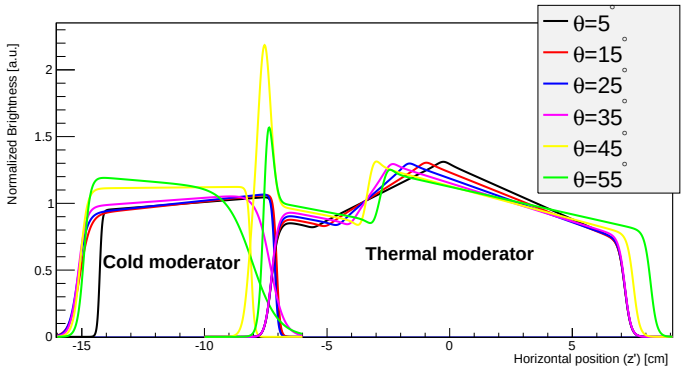

Figure A.28: Functional forms from of Figure A.27 and Figure A.26 plotted next to each other.

Chapter 9

A bispectral moderator using lead

This chapter suggests a novel type of moderator: a broad-spectrum moderator. This moderator concept is based on the idea that heavy metals, such as lead and bismuth, are horrible moderator materials. The article investigates this idea through enriched ^{208}Pb. It shows that the inability of these materials to moderate can be exploited to design a moderator that reflects neutrons from the surrounding moderators of different spectral temperatures, with little change in energy. This results in the emission of a broad spectrum (or multi-spectrum) from the lead. Since lead can also serve as a reflector filter, the geometry can be configured such that the lead broad-spectrum moderator acts as a reflector filter for a cold moderator positioned behind it, thus increasing the neutron yield below the Bragg edge.

This moderator concept is not as goof a reflector filter as beryllium. However, it does provide more neutrons than a beryllium reflector filter in the region above the Bragg edge, especially in the thermal neutron region (about 25 meV).

The article has been published in Nuclear Instruments and Methods in Physics Research A (2015), issue 769.

Nuclear Instruments and Methods in Physics Research A 769 (2015) 1–4

Contents lists available at ScienceDirect

Nuclear Instruments and Methods in Physics Research A

journal homepage: www.elsevier.com/locate/nima

Broad spectrum moderators and advanced reflector filters using ^{208}Pb

T. Schönfeldt [a,b,*], K. Batkov [b], E.B. Klinkby [a,b], B. Lauritzen [a], F. Mezei [b], G. Muhrer [d], E. Pitcher [b], A. Takibayev [b], P.K. Willendrup [c], L. Zanini [b]

[a] Center for Nuclear Technologies, Technical University of Denmark, Roskilde, Denmark
[b] European Spallation Source, Lund, Sweden
[c] Department of Physics, Technical University of Denmark, Lyngby, Denmark
[d] Los Alamos National Laboratory, Los Alamos, New Mexico, United States

ARTICLE INFO

Article history:
Received 19 December 2013
Received in revised form
4 July 2014
Accepted 16 September 2014
Available online 26 September 2014

Keywords:
Spallation
Neutron
Moderators
Reflector filter
Bispectral
Neutronics

ABSTRACT

Cold and thermal neutrons used in neutrons scattering experiments are produced in nuclear reactors and spallation sources. The neutrons are cooled to thermal or cold temperatures in thermal and cold moderators, respectively. The present study shows that it is possible to exploit the poor thermalizing property of ^{208}Pb to design a broad spectrum moderator, i.e. a moderator which emits thermal and cold neutrons from the same position. Using ^{208}Pb as a reflector filter material is shown to be slightly less efficient than a conventional beryllium reflector filter. However, when surrounding the reflector filter by a cold moderator it is possible to regain the neutrons with wavelengths below the Bragg edge, which are suppressed in the beryllium reflector filter. In both the beryllium and lead case surrounding the reflector filter with a cold moderator increases the cold brightness significantly compared to a conventional reflector filter.

1. Introduction

In neutron scattering experiments cold and thermal neutrons are used for a wide range of applications. In some of these experiments the main limitation, apart from intensity, is the wavelength range of neutrons which the neutron moderator and extraction system can deliver to a sample. The wavelength spectrum of interest often extends beyond the spectrum of a single temperature Maxwellian distribution. For this reason the possibility of bispectral extraction has been considered for neutron scattering instruments, e.g. at the European Spallation Source, see [1]. A method for bispectral extraction is aiming an extraction instrument (a neutron guide) at a thermal moderator positioned next to a cold moderator. Then by placing a neutron supermirror in front of the neutron guide, cold neutrons from the cold moderator are reflected into the guide, while the thermal neutrons from the thermal moderator are transmitted through the mirror and into the guide [2], some examples of this are found in [1,3,4]. However, at high intensity sources the strong radiation field might pose a risk for a mechanical component, such as a mirror. In case of a mirror failure a bispectral instrument will lose its entire cold neutron spectrum, which to most experiments is considered the most valuable part. This motivates an interest in moderators which emit neutrons of several spectral temperatures (i.e a broad spectrum moderator) from the same position and in the same direction. Such moderator systems, however, are difficult to design. Previously, in [5], a composite moderator has been suggested. The composite moderator exploits the property that neutrons from a thermal moderator can shine through a cold moderator (given that the cold moderator is sufficiently thin), which enables instruments to see both thermal and cold neutrons simultaneously. This leads to a flux reduction compared to a dedicated cold or thermal moderator, as the composite moderator divides the intensity of the thermal spectrum into a cold and a thermal spectrum.

The present study takes a different approach to the concept of moderation. By exploiting ^{208}Pb's poor ability to moderate and low neutron absorption cross-section, it is possible to design a broad spectrum moderator, which combines thermal and cold neutron fluxes from conventional thermal and cold moderators. The heavy material will in this case emit both thermal and cold neutrons. As this type of broad spectrum moderator (or bispectral moderator) requires the presence of nearby moderators, it can easily be used in conjunction with bispectral extraction via mirrors, providing the maximal cold intensity from the cold moderator. The advantage of such a design over bispectral extraction using a mirror from conventional cold and thermal moderators is the limited consequences if the mirror fails, as cold neutrons can still be extracted directly from the lead broad spectrum moderator. However, a disadvantage of a lead bispectral moderator is the reduced thermal neutron flux compared to a dedicated thermal moderator.

Before studying the details of a broad spectrum moderator, a reflector filter (RF) system is studied and modified. This shows that even if pure ^{208}Pb is not as efficient a reflector filter as beryllium,

* Corresponding author.

http://dx.doi.org/10.1016/j.nima.2014.09.048
0168-9002/

in lead it is possible to regain the neutrons below the Bragg edge (Fig. 1). In this modified reflector filter geometry (Fig. 2b) both beryllium and lead show a significant brightness increase, compared to the more conventional reflector filter geometry (Fig. 2a).

2. Moderation in lead

^{208}Pb is a double magic nuclide with a very low neutron absorption cross-section, even lower than that of beryllium, carbon or deuterium. Lead is a common material in nature, where it is found in two forms, natural lead, with 52.3% ^{208}Pb, and radiogenic lead, where the isotope composition strongly depends on the uranium and thorium content of the ore it is extracted from. According to [8] natural lead can be enriched to 99.0% ^{208}Pb in gas centrifuges for an estimated price of 1000–2000 USD/kg or at a much lower price be extracted from ancient thorium ore, with 85–93% ^{208}Pb depending on the ore quality.

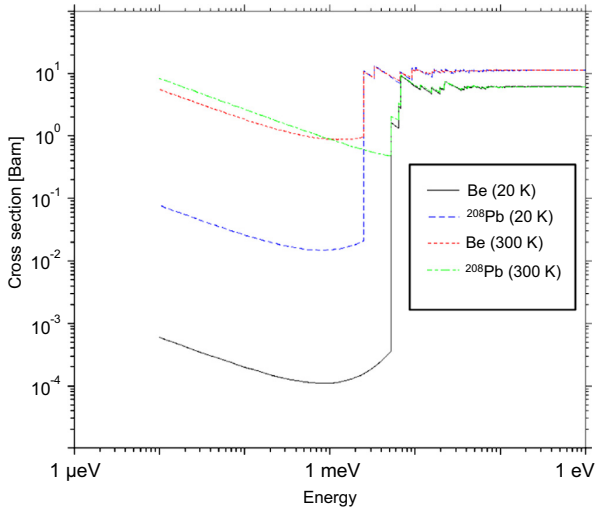

Fig. 1. Cross-section ($S(\alpha,\beta)$) of thermal Be (green) thermal ^{208}Pb (red) and cold Be (black) and cold ^{208}Pb (blue). (^{208}Pb cross-sections are from [6] and Be cross-sections are generic to MCNPX [7]). (For interpretation of the references to color in this figure caption, the reader is referred to the web version of this article.)

This study is focused on ^{208}Pb, due to its exceptionally low neutron absorption cross-section (thermal neutron capture: $\sigma_a < 1$ mbarn). It should be mentioned that similar results could be obtained using natural lead ($\sigma_a = 0.171$ barn) or bismuth ($\sigma_a = 0.034$ barn), but with a reduction in flux due to increased absorption and possibly some changes for cold neutrons in cold materials, from differences in vibrational modes and material structure ($S_{\alpha,\beta}$).

In a free gas model, there is almost no energy transfer in a collision between a fast neutron and a lead nucleus, due to the very high mass of the lead nucleus compared to the neutron, hence lead is only weakly thermalizing. However, for low energy neutrons ($E < 1$ eV) the free gas model breaks down as neutrons start scattering inelastically with phonons. For cold neutrons the maximal energy transfer in a material is then given by Debye temperature. The Debye temperature of lead (at 298 K) is roughly 87 K, where for example beryllium has a Debye temperature of 1031 K and carbon (graphite) has 1550 K [9], which means that the maximal energy transfer in lead is low compared graphite or beryllium.

3. Reflector filter

The concept of a cold beryllium reflector filter was first suggested by Carpenter et al. [10]. The concept exploits the fact that cold beryllium becomes transparent to neutrons of energies below the lowest Bragg edge, see Fig. 1, around 5 meV (Fig. 1). When a slab of beryllium is positioned in front of a moderator, it scatters some of the fast and thermal neutrons back into the moderator system, which increases the neutron density in the moderator, while transmitting neutrons below the Bragg edge through the filter.

Fig. 1 shows that lead might be a good reflector filter material. This is investigated using MCNPX, with the geometry shown in Fig. 2a. The results of this study are seen in Fig. 3 and show that beryllium is a slightly better reflector filter material than lead. This is likely due to the longer mean free path for fast neutrons in lead, which makes a lead reflector filter less efficient at increasing the moderator neutron density, hence not as good a reflector filter as beryllium (even at wavelengths above the Bragg edge). Fig. 3 also shows that lead is less temperature sensitive than beryllium, which might be a useful feature.

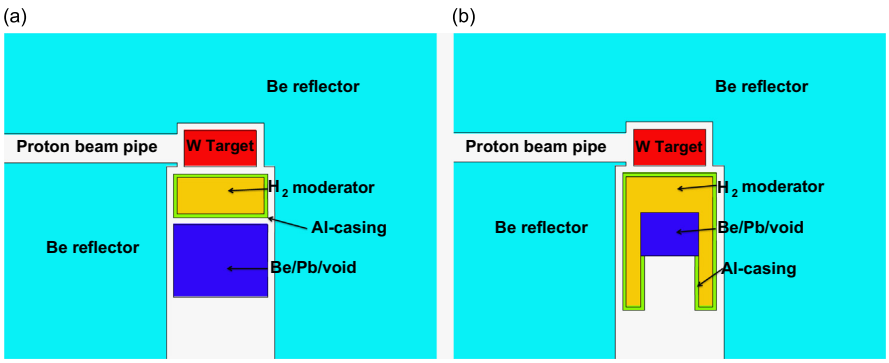

Fig. 2. Geometry of the MCNPX model of a reflector filter mockup (left) and a reentrant reflector filter (right). A common reflector filter is shown to the left and a smaller reflector filter in a reentrant hole geometry is shown to the right. A 2 GeV proton beam is impinging on a $5 \times 5 \times 10$ cm^3 tungsten target (red). Next to the target there is a slab of $5 \times 12 \times 12$ cm^3, 20 K cold, 75% ortho and 25% para H_2 moderator (yellow). In the slab reflector filter case, a 10 cm thick reflector filter, filled with a test material, is positioned in front of the moderator (blue). In the reentrant geometry the outer 2 cm of the slab has been extended forward such that it surrounds a block of test material (blue) which has been reduced to a thickness of 6 cm. In both cases the central 8×8 cm^2 part of the 12×12 cm^2 moderator surface is viewed from 5 m distance using a point detector (f5:n) and a perfect collimator (imp:n=0). The hydrogen has been packed in a 5 mm aluminium layer (green). The entire system is surrounded by a in a $60 \times 60 \times 60$ cm^3 beryllium cube (cyan). 1 cm vacuum layers are used in between the different volumes, to allow for some engineering freedom. Results are seen in Figs. 3 and 4. (For interpretation of the references to color in this figure caption, the reader is referred to the web version of this article.)

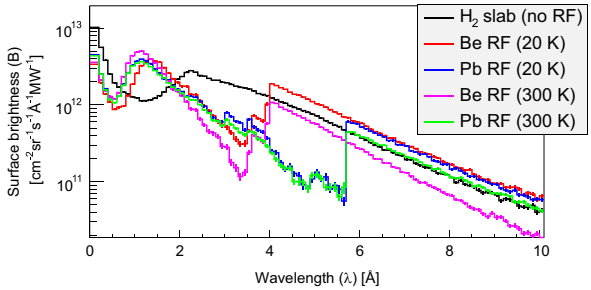

Fig. 3. Results on reflector filter simulation in the geometry are explained in Fig. 2a, using Be and pure ^{208}Pb at 20 K and 300 K and void (H_2 slab) for reference. It is clear that cold beryllium is a better reflector filter than lead (even above leads Bragg edge at 2.5 meV), however lead is less temperature sensitive and a 300 K ^{208}Pb filter is better than a 300 K Be filter.

One of the problems with a reflector filter is the huge suppression of thermal and semi-cold neutrons ($\lambda < 4$ Å or $\lambda < 5.7$ Å), which are interesting to many experiments. Exploiting the poor ability of lead to moderate neutrons, placing a cold moderator around the reflector filter would scatter some neutrons from the cold moderator into the detector (or back into the moderator). Such a geometry is seen in Fig. 2b, and the results are shown in Fig. 4. The study shows that the cold moderator extensions result in a significant increase in cold brightness, even without the lead or beryllium piece present, simply because this geometry resembles a reentrant hole, which is well known to increase the cold brightness. However, adding the piece of pure ^{208}Pb or a piece of cold beryllium, there is a gain from the reflector filter effect on top of the gain from the (reentrance hole like) geometry, but more importantly the cold neutrons below the Bragg edge are regained in the lead case. From Fig. 4 it is also clear that lead is less sensitive to temperature changes than beryllium.

From the results in Figs. 3 and 4 two important conclusions can be drawn: pure ^{208}Pb is slightly less efficient as reflector filter material than beryllium in the regime above the Bragg edge. However, in certain geometries lead can regain the brightness in the region below the Bragg edge and still serve as a quite efficient reflector filter material in the region above the Bragg edge; and surrounding at reflector filter with a cold moderator can increase the brightness.

4. Broad spectrum moderator

One important observation from Fig. 4 is that the reflector filter has a significant amount of thermal neutrons (wavelengths around of 1 Å) in the slab like geometry but almost no thermal neutrons in the reentrant geometry. The reason for this is that these thermal neutrons originate from re-scattering of thermal neutrons from the surrounding thermal beryllium reflector. One can exploit this to construct a broad spectrum moderator, by placing moderators with different neutron spectra around the lead, allowing their spectra to be mixed into one spectrum and emitted from the lead.

One possible configuration of such a broad spectrum moderator is a modification of the reentrant reflector filter shown in Fig. 2b, where some of the surrounding cold hydrogen moderator is replaced with a thermal water moderator. This will allow part of the neutrons from the water and part of the neutrons from the hydrogen to scatter in the lead. Such a geometry is shown in Fig. 5 and the results are shown in Fig. 6.

From Fig. 6 it is seen that the spectrum from the lead piece can be modified by changing the amount of water surrounding it, i.e. it is possible to get more thermal neutrons at the cost of fewer cold neutrons.

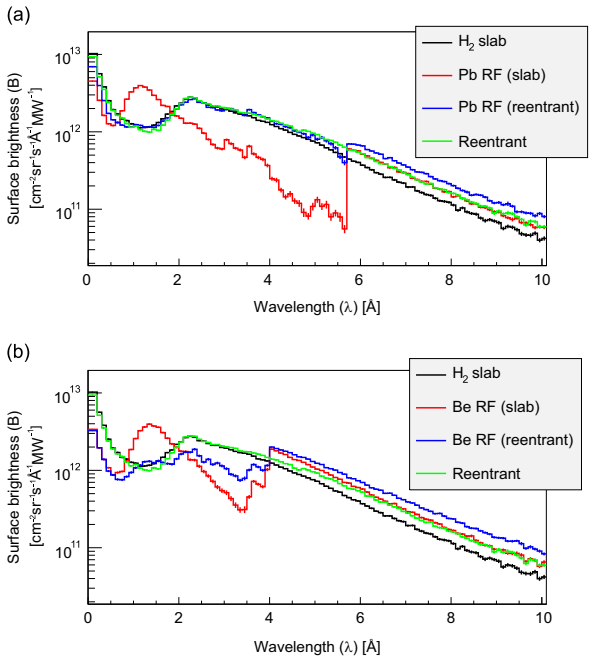

Fig. 4. Results on simulations on reentrant hole combined with a reflector filter, for lead (upper) and beryllium (lower). The black and red distributions are the made in the slab geometry shown in Fig. 2a and the blue and green curves are from the geometry shown in 2b. The black and green curves are the same in the two figures. The first thing to note is that the H_2 extensions resemble a reentrant hole by them self, which yield a significant gain of cold neutrons; this gain results in an additional gain when adding a piece of lead or beryllium into the reentrant hole. The important thing to note is that in the lead case enough of the cold neutrons from the surrounding moderators are reflected in the detector direction that the brightness in the region below the Bragg edge is comparable between the reentrant hole itself and the lead filled reentrant hole. (For interpretation of the references to color in this figure caption, the reader is referred to the web version of this article.)

Instead of replacing all four side extensions, one could imagine a geometry where one side is left as a cold moderator while the others are replaced; this would allow for bispectral extraction aiming the neutron guide at the lead piece and using a mirror aimed at the cold wing. In theory, this would yield extraction of the full cold spectrum from the wing, while allowing transmission of the thermal part of the lead spectrum. The resulting spectrum would have fewer thermal neutrons than if a dedicated thermal moderator was used, but the same cold spectrum in both the lead and the water case, as this originates from a dedicated cold moderator. Extracting the same amount of cold neutrons but fewer thermal neutrons do not sound very attractive at first, but one should remember that mirror failure in a conventional bispectral instrument will result in the loss of the entire cold spectrum. In the case of a lead broad spectrum moderator next to a cold moderator, mirror failure will result in the full lead spectrum being retained. This spectrum still contains quite a significant amount of cold neutrons, and even more cold neutrons above the Bragg edge at 5.7 Å.

Another potential application of lead arises from the fact that lead is a good choice of target at a spallation source and the observation that the temperature of the lead has insignificant impact on the neutron spectrum. One could imagine a simple system where the proton beam impinges on a lead piece cooled by liquid hydrogen on all sides, except for the beam pipe side and a side which should be opened up for neutron extraction. Such a geometry would benefit from the fact that the neutron density is highest in the target, as the target also serve as the moderator. This could potentially lead to a significant gain in brightness.

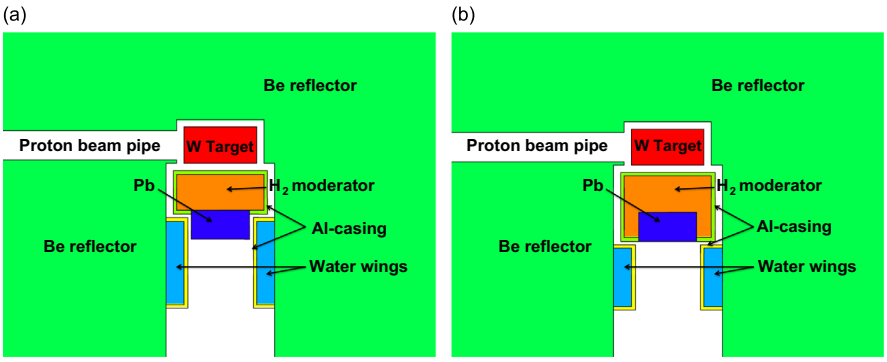

Fig. 5. Geometry of the MCNPX model of a broad spectrum moderator. Water wings replace parts of the hydrogen extensions from the geometry in Fig. 4b. In the simulations, shown in Fig. 6 this has been done in 4 steps: full hydrogen extensions (as shown in Fig. 2b); front replaced (right) where the cold extensions in front of the moderator have been replaced with water slabs; and sides replaced (left) where both the hydrogen on the sides of the moderator and in front of it have been replaced with water slabs. Note that the water extensions have been packed in 5 mm aluminium and a gab of 5 mm has been modelled between the water extensions and the $^{208}Pb/H_2$.

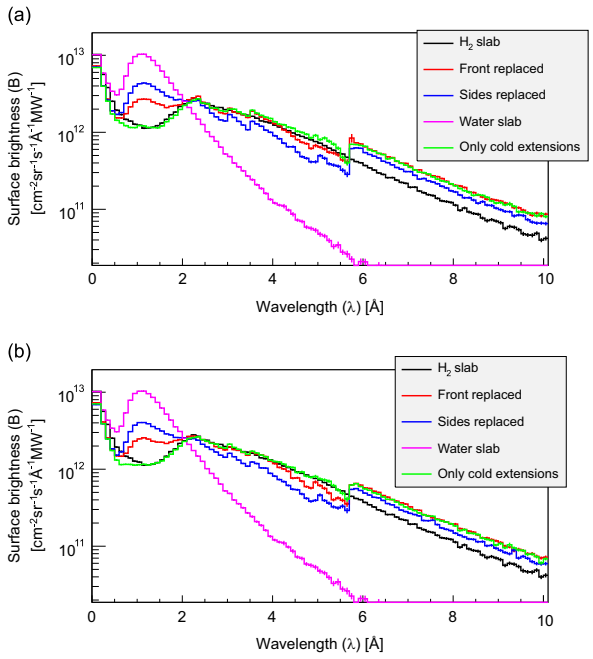

Fig. 6. Results on simulations on a broad spectrum moderator, using the geometry shown in Fig. 5. The ^{208}Pb piece was simulated at 20 K (upper) and at 300 K (lower). Simulations on a 3 cm water slab and a 5 cm thick hydrogen slab are shown as reference. It is apparent that the more water surrounds the lead the more thermal neutrons are emitted from the lead, however, this comes at the cost of loss of cold neutrons. Note that the temperature of the lead piece does not have a large impact on the spectrum.

5. Conclusion

It has been shown that a broad spectrum moderator can be designed utilizing the poor thermalizing property of ^{208}Pb. An example mockup has been studied using MCNPX which showed that such a moderator system can increase the brightness compared to a dedicated cold moderator, in the regime above 5.7 Å (the Bragg edge), while maintaining a large portion of the cold neutron below 5.7 Å and adding a significant amount of thermal neutrons.

The broad spectrum moderator concept can be applied at small scale facilities to produce a simple and inexpensive bispectral neutron source. At larger facilities a ^{208}Pb broad spectrum moderator could be used by itself or in conjunction with a conventional bispectral extraction system, using mirrors. This enables extraction of cold neutrons from the cold moderator and thermal neutrons from the lead broad spectrum moderator. The advantage of such a design is that in the case of mirror failure, the instrument will retain the cold neutron spectrum from the lead bispectral moderator, while a conventional system would suffer the loss of the entire cold spectrum.

It is shown that pure ^{208}Pb is not as efficient a reflector filter material as beryllium for neutrons above the Bragg edge. However, if the reflector filter is surrounded by a cold moderator the lead piece retains the cold neutrons below the Bragg edge, which are suppressed in a conventional reflector filter. Furthermore, both for beryllium and for ^{208}Pb, placing a cold moderator around the reflector filter increases neutron brightness significantly above the Bragg edge, compared to a conventional reflector filter.

It is shown that the neutron spectrum is not sensitive to the lead temperature. This indicates that the target itself could be made from pure ^{208}Pb packed in cold and/or thermal moderator to facilitate neutron extraction from the position of highest neutron density.

Acknowledgements

The work has received funding from the European Commission in the frame of the Cluster of Research Infrastructures for Synergies in Physics (CRISP) under the 7th Framework Programme Grant Agreement 283745.

References

[1] S. Peggs (Ed.), ESS Technical Design Report, 2013.
[2] F. Mezei, M. Russina, Neutronenoptische Bauelementenanornung zur gezielten spektralen Gestaltung von Neutronenstrahlen oder Pulsen. German Patent: 102 03 591.1 (US 7030397 B2).
[3] H. Jacobsen, K. Lieutenant, C. Zendler, K. Lefmann, Nuclear Instruments and Methods in Physics Research Section A 717 (2013) 69.
[4] C. Zendler, K. Lieutenant, D. Nekrassov, L.D. Cussen, M. Strobl, Nuclear Instruments and Methods in Physics Research Section A 704 (2013) 68.
[5] L.L. Daemen, G.J. Russell, E.J. Pitcher, Moderator materials and neutronic performance, in: Proceedings of the ICANS XII Conference, 1994.
[6] G. Muhrer, T. Hill, F. Tovesson, E. Pitcher, Nuclear Instruments and Methods in Physics Research Section A 572 (2007) 866.
[7] L.S. Waters, G.W. McKinney, J.W. Durkee, M.L. Fensin, J.S. Hendricks et al., The MCNPX Monte Carlo radiation transport code, AIP Conference Proceedings, vol. 896, 2007, pp. 81–90. doi: http://dx.doi.org/10.1063/1.2720459.
[8] G.L. Khorasanov, A.I. Blokhin, A.A. Valter, New Coolant from Lead Enriched with the Isotope Lead-208 and Possibility of Its Acquisition from Thorium Ores and Minerals for Nuclear Energy Needs, 2012, ISBN: 978–953–51–0018–8 http://cdn.intechopen.com/pdfs-wm/28075.pdf.
[9] C.Y. Ho, R.W. Powell, P.E. Liley, Journal of Physical and Chemical Reference Data 3 (1974) 1.
[10] J.M. Carpenter, R. Kleb, T.A. Postal, R.H. Stefiuk, D.F.R. Mildne, Nuclear Instruments and Methods in Physics Research Section A 189 (1981) 485.

Chapter 10

Single-crystal reflector filter experiment

This chapter is an experimental article carried out under the LENS collaboration. The experiments investigated the concept of a single-crystal reflector filter – a reflector filter that also transmit neutrons in the thermal energy range because of the non-existent Bragg edge. The experiment compared void, single-crystal sapphire and sapphire powder. Sapphire was used since no other single-crystal candidates (e.g. diamond, pyrolytic graphite or lithiumfluoride) could be obtained within the cost and time constraints of the experiment. Unfortunately, but not unexpectedly, sapphire does not notably increase neutron yield, but the experiment proves the viability of a single-crystal reflector filter and indicates the potential to regain the thermal neutrons lost to a conventional reflector filter, with little or no loss of the cold neutrons below the Bragg edge.

This experiment was my third participation in an experiment with the LENS collaboration at LENS. Besides contributing to the planning of the experiment, I was also the only person present throughout the entire experiment and thus had the leading role.

The data taken at LENS are logged into a set of log files in different formats. For instance, proton pulse profiles are logged in Excel files, temperature is logged in text files and neutron detector counts are logged as sets of 8 ASCII characters (time stamp, detector ID, background flags etc.) in continuous charter streams. During my participation in the series of LENS experiments, I coded numerous C++-based ROOT tools, to translate these data files into a single ROOT data file, making all information easy to access and rapid to analyze and making it easy to correlate various data and perform advanced analysis.

As the developer of these tools, I was naturally in charge of the data analysis process after the experiments at LENS. In particular, for the experiment that resulted in the following article, I carried out the entire data analysis and produced the data plots (Figures 3–7) in the article and wrote the first draft of the article.

The article was published in Nuclear Instruments and Methods in Physics Research A, (2016), issue 830.

Nuclear Instruments and Methods in Physics Research A 830 (2016) 454–460

Contents lists available at ScienceDirect

Nuclear Instruments and Methods in Physics Research A

journal homepage: www.elsevier.com/locate/nima

Demonstration of a single-crystal reflector-filter for enhancing slow neutron beams ☆

G. Muhrer [a,d], T. Schönfeldt [b,a], E.B. Iverson [c,*], M. Mocko [d], D.V. Baxter [e], Th. Hügle [c], F.X. Gallmeier [c], E.B. Klinkby [b,a]

[a] European Spallation Source, Lund, Sweden
[b] Center for Nuclear Technologies, Technical University of Denmark, Roskilde, Denmark
[c] Spallation Neutron Source, Oak Ridge National Laboratory, Oak Ridge, TN, USA
[d] Los Alamos Neutron Science Center, Los Alamos National Laboratory, Los Alamos, NM, USA
[e] Center for the Exploration of Energy and Matter, Indiana University, Bloomington, IN, USA

ARTICLE INFO

Article history:
Received 21 October 2015
Received in revised form
6 June 2016
Accepted 10 June 2016
Available online 14 June 2016

Keywords:
Moderator
Neutron
Beam
Reflector-filter

ABSTRACT

The cold polycrystalline beryllium reflector-filter concept has been used to enhance the cold neutron emission of cryogenic hydrogen moderators, while suppressing the intermediate wavelength and fast neutron emission at the same time. While suppressing the fast neutron emission is often desired, the suppression of intermediate wavelength neutrons is often unwelcome. It has been hypothesized that replacing the polycrystalline reflector-filter concept with a single-crystal reflector-filter concept would overcome the suppression of intermediate wavelength neutrons and thereby extend the usability of the reflector-filter concept to shorter but still important wavelengths. In this paper we present the first experimental data on a single-crystal reflector-filter at a reflected neutron source and compare experimental results with hypothesized performance. We find that a single-crystal reflector-filter retains the long-wavelength benefit of the polycrystalline reflector-filter, without suffering the same loss of important intermediate wavelength neutrons. This finding extends the applicability of the reflector-filter concept to intermediate wavelengths, and furthermore indicates that the reflector-filter benefits arise from its interaction with fast (background) neutrons, not with intermediate wavelength neutrons of potential interest in many types of neutron scattering.

1. Introduction

In moderators for slow neutron sources, a reflector-filter can be used to enhance the emission of cold neutrons while suppressing the fast neutrons comprising a major source of instrumental background. Some of the neutrons emitted with wavelength less than approximately 4 Å are reflected back into the moderator (reducing the fast neutron emission) and get another chance to be scattered down to desirable energies before being emitted once again. The reflector-filter has only recently been implemented at the Lujan Center [1], where its observed performance was documented. It increased the source emission above 4 Å by more than a factor of two, while reducing the (for these instruments) undesirable neutron intensity below 1 Å by a factor of four. Unfortunately, the reflector-filter also suppresses beam intensity between 1 Å and 4 Å—these neutrons are not necessarily background, but potentially very important. For many scattering instruments this is an acceptable trade-off, but for some scattering instruments, the loss of 1–4 Å neutrons is unacceptable. It has been theorized that a single crystal can also be used as an effective reflector-filter [2–4]. A single crystal does not have the same sharp Bragg edge associated with a polycrystalline filter—the effective cross section is the same at long wavelengths, but remains low through the 1–4 Å range as well. We therefore anticipate that a single-crystal reflector-filter will augment the neutron emission at long wavelengths just as the polycrystalline reflector-filter does, but will also enhance (or at least not decrease) the neutron emission at energies 1–4 Å relative to a conventional cold moderator without any reflector-filter.

Reflector-filters, both polycrystalline and single-crystal, were tested on an unreflected pulsed neutron source at the I.V.

* Corresponding author.
E-mail address: iversoneb@ornl.gov (E.B. Iverson).

http://dx.doi.org/10.1016/j.nima.2016.06.047
0168-9002/

Kurchatov Institute of Atomic Energy [3,4], indicating gains approaching a factor two at long wavelengths from 40 mm layers of beryllium and quartz, respectively, placed adjacent to the moderator, covering the viewed moderator area as well as significant additional solid angle. As such, the reflector-filters tested there did not distinguish between the gains arising from a (partial) reflector assembly, such as is now common [5], and a reflector-filter blocking only the outgoing beamline within the neutron reflector. Studies in Japan [6] and at the Lujan Center [7,8] on the beryllium (polycrystalline) reflector-filter reinforce this distinction. The optimum thickness for a polycrystalline beryllium reflector in the unreflected Kurchatov measurement is 20–40 mm, and gives a factor of two low-energy intensity gain [3]. An even thicker beryllium reflector filter (50 mm) was tested in Japan and found to provide no low-energy gain [6], which those authors attribute to the fact that their test assembly was already fully reflected. At the Lujan Center, the successful deployment of a beryllium reflector-filter in a fully reflected system, which did achieve that factor two gain at low energies, required a much thicker reflector-filter of 120 mm [7,8].

This study describes a set of experiments carried out at the Low Energy Neutron Source [9–11] (LENS) between 21 April 2014 and 11 May 2014. The aim of this campaign was to demonstrate the concept of a single-crystal reflector-filter on a reflected pulsed slow neutron source.

2. Single crystal reflector-filter concept

The concept of a cold beryllium reflector-filter on a reflected pulsed slow neutron source was first proposed in [12], and has later been implemented in the moderator system at the Lujan Center [1]. The concept of a reflector-filter is simple—by placing a thick block of material with high coherent scattering cross section but small incoherent and absorption cross sections on the front face of the moderator (nominally blocking the neutron beam-lines), many fast (energy greater than 1 MeV, wavelength less than 3×10^{-4} Å), slowing-down (energy between 1 eV and 1 MeV, or wavelength between 3×10^{-4} Å and 0.3 Å), and slow (energy below 1 eV, wavelength above 0.3 Å) neutrons which would have leaked out through the neutron beam-ports will have some chance of scattering in the filter, returning to the moderator, and increasing the neutron density in the moderator. Beryllium, with its large but predominantly coherent scattering cross section, is an ideal reflector-filter material. A cold beryllium reflector-filter will scatter many neutrons with wavelengths less than that of the so-called Bragg edge at 4 Å (5 meV), but it is very nearly transparent above that wavelength. This property of beryllium is frequently exploited as a beam-line filter [13], taking advantage of the change in the scattering cross section from some 6 barns per atom below 4 Å to less than 0.005 barns per atom above that wavelength (cross sections from ENDF/B-VII.0). As the reflector-filter returns neutrons below 4 Å to the moderator and increases the total neutron density therein, the neutrons have a much higher chance of being emitted at wavelengths above the Bragg edge than would otherwise be the case.

While the cold neutron emission increase at wavelengths above the Bragg edge is significant (as much as a factor two in the right geometry, such as at the Lujan Center [1,7,8]) the major problem with a polycrystalline reflector-filter is the suppression of neutrons with wavelengths below the Bragg edge at 4 Å but still within the slow neutron range useful for neutron scattering. These 1–4 Å neutrons are essential to many instruments, even those primarily considered to be “cold neutron instruments.”

The single-crystal reflector-filter [2] exploits the fact that, in a single crystal, only very narrow portions of wavelength-angle phase space meet the Bragg condition and will be scattered by the reflector-filter material. The transmission at long wavelengths (above the Bragg edge) will be just as high as in the polycrystalline case (if not higher, given the possibility of more small-angle scattering in the polycrystal), but the transmission between the Bragg edge and the wavelength at which inter-atomic effects become important (that is, around 1–4 Å) will also be high. This can be exploited in the same way as the conventional reflector-filter to scatter fast neutrons back into the moderator to increase the neutron density, while letting neutrons over the entire wavelength range of interest escape.

As a corollary, a comparison of the wavelength-dependent gain factors of the polycrystalline reflector-filter and the single-crystal reflector-filter (relative to a conventional moderator) should allow us to proportionally attribute the neutron emission gains from that polycrystalline reflector-filter to the wavelength ranges below 1 Å and from 1 Å to 4 Å:

- If the single-crystal reflector-filter provides a gain factor comparable to the polycrystalline reflector-filter at long wavelengths, and additionally provides a gain ($G(\lambda) > 1$) between 1 Å and 4 Å, then the reflector-filter benefit is coming primarily from the previously described process acting on fast and slowing-down neutrons ($\lambda < 0.5$ Å).
- If the single-crystal reflector-filter provides a reduced gain factor at long wavelengths, and imposes a loss ($G(\lambda) < 1$) from 1 Å to 4 Å as compared to a conventional moderator, then the reflector-filter benefit is coming primarily from the previously described process acting on slow neutrons below the Bragg edge ($1 < \lambda < 4$) Å.

In neutron scattering, it seems that there is no agreement as to whether one should use wavelength or energy for neutrons. In this work, we will use primarily wavelength, for its direct comparison to time-of-flight and easy identification of Bragg edges, even though discussing “fast neutrons,” which have energy greater than 1 MeV, in terms of wavelength (less than 3×10^{-4} Å) is unusual.

3. Experimental setup

3.1. LENS Moderator test facility

The Low Energy Neutron Source (LENS) is a small scale neutron facility, producing neutrons from a 13 MeV proton beam impinging on a beryllium target, which we use for moderator research and development [14]. For this experiment LENS was set up to produce 13 μs pulses at 40 Hz, resulting in a time-averaged beam power of 142 W. The beryllium target is embedded in a cylindrical reflector of 300 K light water, with a cavity where the moderator system can be lowered from above. The water reflector is surrounded by lead shielding, embedded in alternating layers of lead-epoxy and borax-epoxy-polyethylene. The water tank and shielding have an opening enabling four beam-lines to view the moderator location; see Fig. 1. When operated as a moderator test facility, the moderator usually used in LENS is removed, and test moderator assemblies can be sequentially installed.

3.2. Instrumentation

In addition to a proton beam current measuring device (the Q-box) used for normalization, our experimental instrument suite consists of two detectors: a low-efficiency beam monitor within the SANS beam-line and an emission time analyzer we add to the SANS beam-line for moderator tests.

The SANS beam-line beam monitor is a thin low-density ^{3}He

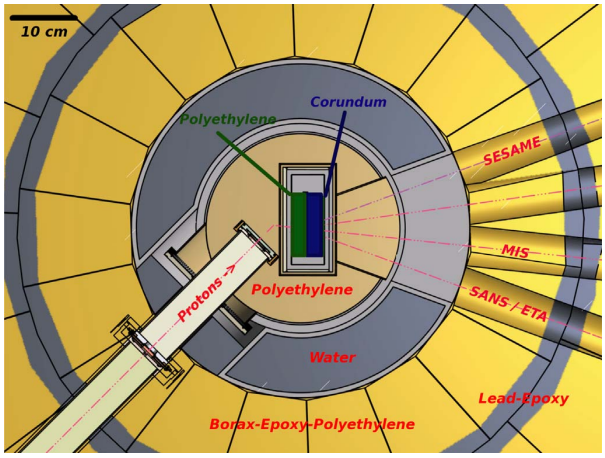

Fig. 1. Horizontal cross section through LENS target-moderator-reflector. The green box in the middle represents the polyethylene moderator, while the blue box represents the corundum (or empty) reflector-filter. (For interpretation of the references to color in this figure caption, the reader is referred to the web version of this paper.)

detector positioned (5.25 ± 0.01) m downstream from the moderator surface along the SANS beam line, which is 20° away from the moderator surface normal, as shown in Fig. 1. This detector provides neutron energy spectra via time-of-flight.

The emission time analyzer is positioned in the SANS sample area during moderator studies. A high mosaicity 10 K germanium single crystal in the SANS sample position at 8.50 m diffracts neutrons from the (*nnn*) series into a scintillator detector positioned in time focused geometry at a nominal Bragg angle of $2\theta \approx 112°$ [15]. The emission time analyzer provides the emission time distribution (sometimes called the pulse shape) for several different neutron energies simultaneously.

3.3. Test moderator/reflector-filter assemblies

For these experiments we used a moderator of 25 mm thick virgin high-density polyethylene, 110 mm by 110 mm on the face, transversely penetrated by 5 mm diameter thoroughgoing aluminum rods for thermal conductivity, shown in Fig. 2. The aluminum rods displace approximately 23% of the polyethylene volume, giving a full-density effective thickness of approximately 19 mm, while significantly flattening the temperature distribution within

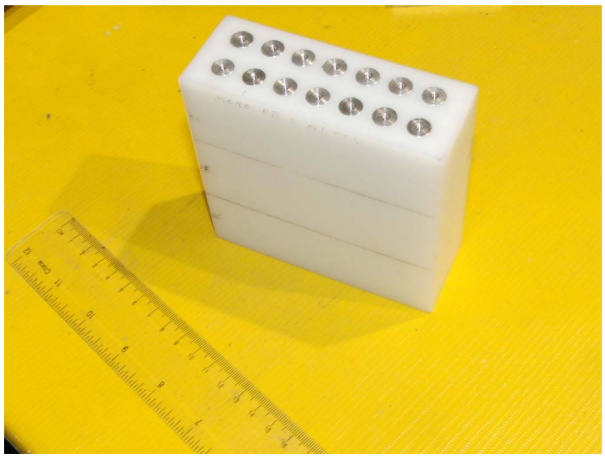

Fig. 2. Photograph of polyethylene moderator.

the moderator at low temperature. The reflector-filter test objects were mounted on the front face of the moderator, in identical aluminum vessels, each 51 mm by 102 mm by 102 mm. The reflector-filter mounting, on the same cold platform as the moderator itself, is not strictly necessary for the characterization of a reflector-filter. Indeed, it precludes separate control of the temperature of the moderator and the reflector-filter. However, in these studies we were primarily interested in achieving the lowest practical temperatures in both moderator and reflector-filter, so no separate control was necessary. The vacuum vessel containing the cryogenic apparatus can be wrapped with absorbing material to decouple the moderator from the long-lived thermalized neutron population within the reflector. For these studies, that decoupler was left off, as our tests were intended to understand the performance of the single-crystal reflector-filter for moderators optimized for long-wavelength intensity, which are typically coupled moderators.

The properties of an ideal material for a single-crystal reflector-filter are similar to those of a conventional reflector-filter: high coherent scattering cross section and low incoherent scattering and absorption cross sections. While beryllium, as used in the Lujan Center reflector-filter, meets these criteria, it is not easily available in large single crystals. Graphite also has a favorable cross section [2], but is quite expensive in the size and quality needed for our demonstration. We chose to use single crystal corundum (Al_2O_3) to test the single crystal reflector-filter concept. The test apparatus we used limited the total volume available for a reflector-filter (either single-crystal or polycrystalline) to some 50.8 mm thickness, well below optimum, but sufficient for this proof of concept. While corundum has a higher capture cross section than desirable, we believe we can correct for this effect.

The single crystal reflector filter was constructed from four single crystal corundum blocks, each 12.7 mm thick and 102 mm by 102 mm, which were stacked with the same crystal orientation and positioned at the front face of the polyethylene moderator. As previously stated, the physical constraints near the LENS target preclude a test with a filter of optimal thickness—we describe below how we extrapolate from this geometry-limited experiment to the expected performance of more optimized reflector-filters. The crystallographic orientation was confirmed, and the mosaic distribution measured, using the CG1B neutron diffractometer at HFIR [16]. The crystal blocks had mosaic of roughly 0.17°. Each crystal block was oriented with the *c*-axis (as measured by the ⟨006⟩ reflection) emerging within 1° of the normal to the large face. For each crystal block we identified the orientation of the $\langle \bar{3}30 \rangle$ reflection to be within 4° of one of the smaller side faces. We named this face the *y*-face. The ⟨110⟩ vector thus emerges nearly normal to the *x*-face, with the ⟨006⟩ vector (the *z*-face) toward the viewer.

We tested four cases—the actual single crystal corundum reflector filter was tested twice. In both configurations using the single-crystal reflector-filter, the crystal lattice was oriented with the *c*-axis emerging along the nominal moderator normal. In the configuration we describe below as *y*-up, the $\langle \bar{3}30 \rangle$ pointed up and the SANS beam-line used for characterization emerges approximately along the $\langle \bar{1}\bar{1}9 \rangle$ direction. In the configuration we describe as *x*-up, the ⟨110⟩ pointed up, and the SANS beam-line emerges approximately along $\langle \bar{1}110 \rangle$. The two remaining cases included one where the crystals were replaced with corundum powder (99.99% pure with particle size between 0.5 micron and 1 micron, loaded into an aluminum cell in a helium environment, packed to around 25% theoretical density), and one where the aluminum casing containing the crystal or powder was left empty (i.e. vacuum).

Each of the four different configurations was first measured at ambient room temperature (~300 K during these experiments)

and then at 75 K without modification to the experimental setup (only the temperature was changed). Only the low-temperature results are described below, as our primary interest for these experiments was in long-wavelength neutron intensity gains. We anticipated possibly significant differences between the *x*-up and *y*-up configurations as the mosaicity of the corundum might result in significant Bragg effects being visible in the transmitted spectra [17]. However, we saw no particular difference between the orientations, and as the *x*-up measurement suffered from poor statistics relative to the *y*-up measurement, we report below only the *y*-up results.

4. Analysis

4.1. Normalization

Our data normalization is based on the number of Q-pulses obtained by a measurement of the proton current by a transformer in the proton beam pipe. Each Q-pulse represents 10 nC of proton beam charge passing through the transformer. The recorded data (in counts per time-of-flight bin) from the 1/*v*-SANS beam monitor of known efficiency (4.5×10^{-4} counts per neutron at 1 Å), when normalized, provide wavelength spectra in neutrons per Å per nC. The recorded data from the emission time analyzer cannot easily be absolutely normalized, but can easily be normalized to counts per microsecond per nC enabling relative comparisons. It should be noted that the time in this representation is time-of-flight, not time of exposure, and we use microsecond rather than second to emphasize this distinction. Further details of data analysis can be found elsewhere [18].

4.2. Spectral gain

The measured spectra are shown in Fig. 3. The spectra shown in Fig. 3 from the single crystal and powder measurements, when divided by the spectrum from the empty reflector-filter measurement (that is, the spectrum from the bare moderator), produce the gain factors $G_p(\lambda)$ for the polycrystalline powder reflector-filter and $G_y(\lambda)$ for the *y*-up single-crystal reflector-filter shown in Fig. 4. Note that the (powder) polycrystalline reflector-filter has approximately one quarter of the neutronic thickness of the single-crystal reflector-filter, due to lower density. If the two samples had the same neutronic thickness, we would expect the suppression of short-wavelength neutron emission to be identical.

The gain factors shown in Fig. 4 show the effect of the

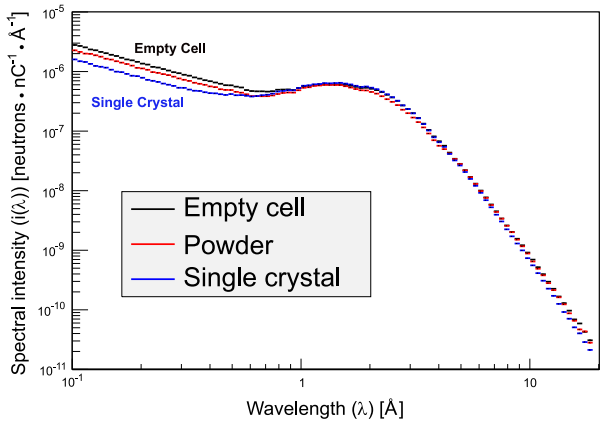

Fig. 3. Measured neutron spectra showing suppression of short wavelength neutrons by 75 K reflector-filters.

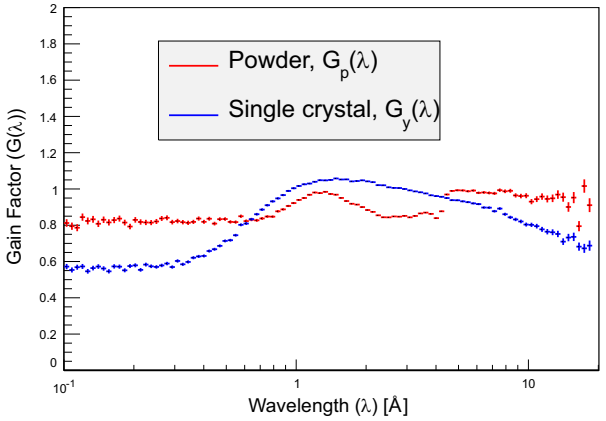

Fig. 4. Measured gain factors for the 75 K polycrystalline and single-crystal reflector-filters studied.

polycrystalline reflector-filter and the single-crystal reflector-filter. We do observe suppression of short-wavelength neutrons in the beam from the single crystal case, and transmission gradually sets in the range from 0.3 Å to 1 Å as expected. In the less dense powder sample there is still a suppression of fast neutrons and the transmission sets in suddenly at the Bragg edge around 4 Å. Another effect, previously observed from polycrystalline reflector-filters, is apparent in the powder case, namely the feature around 1.5 Å [1,8]. This feature appears in both calculated and measured polycrystalline reflector-filter results for the beryllium implementation at the Lujan Center and in our measured results here. We considered whether it might be related to some thermalized component in the reflector-filter itself, but this seems unlikely as the feature appears at too low of a wavelength (around 1.5 Å, implying a spectral temperature of around 400 K from a medium at 70 K), and is significantly narrower in wavelength spread than would be expected from a Maxwellian distribution in any event. Similarly, we do not think it related to a thermalized population in the reflector, appearing in the emitted beam after a single scattering within the reflector-filter. With these measurements, we have confirmed that it is not an artifact of either the Lujan Center geometry, or of beryllium itself, and we hope to address its origins in further studies, both experimental and computational.

The single-crystal and polycrystalline reflector-filters measured have significantly different neutronic thicknesses due to a large difference in density (approximately a factor four). To be able to compare the measurements we assume that, were the polycrystalline powder to have the same density as the single crystal, then it would behave identically at wavelengths below some 0.3 Å, that is, where structure and orientation effects are negligible. We correct the gain factor of the polycrystalline measurement by treating the gain factor as though it arises from a repeated series of filters, raising it to a power a such that $G_p^a(\lambda_0) = G_y(\lambda_0)$ for $\lambda \approx 0.1$ Å. We apply this correction over the entire wavelength range, assuming that the model of a repeated series of filters is uniformly valid.

By fitting constants to the gain factors at short wavelengths shown in Fig. 4, we find $G_y(\lambda_0) = 0.566 \pm 0.015$ and $G_p(\lambda_0) = 0.818 \pm 0.017$, such that $a = 2.83 \pm 0.02$, as applied in Fig. 5. Though we believe this to be a good approximation, we would only be able to verify the correction by redoing the experiment using a polycrystalline corundum reflector-filter of equal dimension *and density* as the single crystal reflector-filter. The apparent gain factor a short wavelength, $G_y(\lambda_0) = 0.566 \pm 0.015$, is

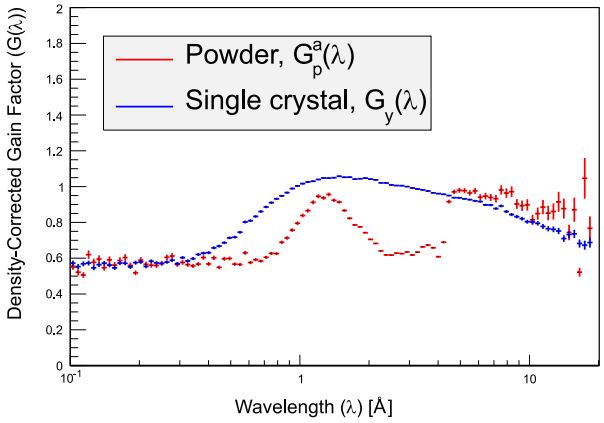

Fig. 5. Reflector-filter (75 K) gain factors corrected for different neutronic thicknesses.

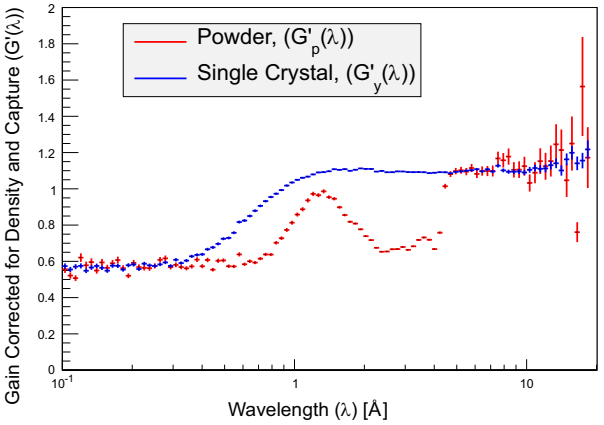

Fig. 6. Reflector-filter (75 K) gain factors corrected for density and capture.

significantly higher than the transmission of a comparable filter (as opposed to a reflector-filter), for which values from the literature range over 0.15–0.35 [19–22]. The significant variation in the literature is not something we can address at this point, but our apparent gain factor $G_y(\lambda_0)$ is larger yet, indicating that the reflector-filter does indeed boost the intensity within the moderator and at the moderator surface by a significant amount. Strictly speaking, while we can also assume that the reflector-filter provides in-scattering to the beam from the reflector itself, regardless of the intensity within moderator, as well as out-scattering from the beam, we cannot here distinguish among these effects.

It is worth noting that the above comparison also yields an effective estimate of the polycrystalline powder density relative to the single-crystal density; $\rho_p = \rho_y/a$. Using the corundum single-crystal density of 4.03 g/cm^3 we would estimate the effective powder density to be 1.42 g/cm^3, significantly higher than the measured density of 1.06 g/cm^3. That is, the powder appears to have *more* of an effect compared to the thicker single-crystal than its relative density would indicate. We note that the additional scattering power at 0.1 Å could be explained by this additional (unrealistic) 0.36 g/cm^3 of additional corundum, or equally by 0.02 g/cm^3 of water within the corundum powder. Water contamination seems much more plausible. However, that much water would represent an effective 0.1 cm thickness of water or water ice, which might be expected to have significant effect at long wavelengths.

Fig. 5 shows clearly the benefit (increased gain/reduced penalty) of the single-crystal reflector-filter relative to the polycrystalline reflector-filter in the 0.4–4 Å range, and their similarity at long wavelengths. What Fig. 5 also shows is that both reflector-filters are significantly compromised by capture in the corundum (primarily in the aluminum), as can be seen by the fall-off in the gain factor at long wavelengths for both reflector-filters. For a production reflector-filter (whether polycrystalline or single-crystal), one would choose a material with low absorption, such as graphite, diamond, enriched lithium fluoride, beryllium fluoride, enriched lead, or bismuth. To estimate the gain factor of an ideal reflector-filter, polycrystalline or single-crystal, we eliminate the absorption effects by dividing the adjusted gain factors shown in Fig. 5 for the single crystal reflector-filter and polycrystalline reflector-filter by the transmission factors (against capture) of a 50.8-mm slab of corundum of density 4.03 g/cm^3 and 1.06 g/cm^3 respectively. To do so, we assume $1/v$ behavior for both the aluminum and oxygen capture cross sections, with microscopic capture cross sections of 0.233 b and 0.0002 b, respectively [23]. These observed gain factors $G(\lambda)$, corrected for capture and for full density across 50.8 mm thickness and defined as $G'(\lambda)$, appear in Fig. 6.

Fig. 6 clearly shows that low-capture polycrystalline and single crystal reflector-filters would comparable in gain at long wavelengths, and in suppression at short wavelengths, while the single crystal reflector-filter regains the intermediate wavelength neutron emission lost in the polycrystalline reflector-filter. That is, the single-crystal reflector-filter retains all the long-wavelength advantages of the polycrystalline reflector-filter, without suppressing potentially important intermediate wavelength neutrons. Even without the scaling argument applied to $G_p(\lambda_0)$, the fact that $G_y(\lambda_0)$ is larger than a filter transmission at the same wavelength confirms our hypothesis that the gains from a reflector-filter, whether polycrystalline or single-crystal, accrue from effects on neutrons of wavelength less than 0.1 Å rather than on neutrons of 1–4 Å.

The magnitude of the gains shown in Fig. 6 are modest, around 10% at wavelengths longer than the Bragg edge. The LENS facility is somewhat constrained in the room available for a reflector-filter, precluding prototypical tests. However, the gains shown in Fig. 6 indicate that a single-crystal reflector-filter with the same (coherent) scattering cross section as 200 mm of corundum and negligible capture could provide gains of 50% at long wavelengths and intermediate wavelengths at the same time, while suppressing background fast neutrons. By extension, a single-crystal reflector-filter with the same scattering power as the beryllium reflector-filter implemented at the Lujan Center could extend the observed factor two gain in neutron intensity for greater than 4 Å to as low as 1 Å wavelength.

4.3. Emission time analysis

The previous section indicates that the single-crystal reflector-filter increases the wavelength-dependent intensity in a neutron beam in the desired 1–4 Å region as compared to an unfiltered beam, while retaining the long-wavelength gains we expect from the proven polycrystalline reflector-filter. This effect is exactly, if quantitatively, what is desired from the single-crystal reflector-filter. We can use the wavelength-dependent emission-time distributions, which we measured at the same time as the spectra, to further explore the nature and origins of the effect.

If we ignore the corrections for neutronic thickness and absorption made in the previous section, the gain factors $G_p(\lambda)$ for the polycrystalline reflector-filter and $G_y(\lambda)$ for the single-crystal reflector-filter are equal to 0.90 and 1.05, respectively, at the 1.81 Å wavelength corresponding to the third-order reflection measured in the emission time analyzer. The emission time

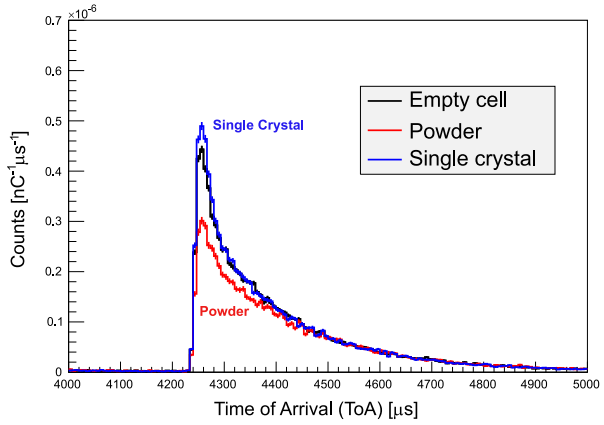

Fig. 7. Emission time distributions for 1.81 Å neutrons as measured (without density or capture correction) at 75 K.

distributions as measured at 1.81 Å appear in Fig. 7. The gain factors (0.90 and 1.05) mentioned above are the ratio of the spectra, and approximately corresponds to the ratio of the integrals of these emission time distributions. It is clear from Fig. 7 that the intensity change at 1.81 Å occurs primarily in the peak of that distribution. That is, the 5% gain from the single-crystal reflector-filter as integrated over the emission time distribution is really a 10% increase in the peak of the distribution. The long-time tails (around 200 μs after the peak) are unchanged. Similarly, the 10% loss imposed by the polycrystalline reflector-filter (as compared to the unfiltered system) is really a 30% loss in peak intensity. Again, the long-time tails are unchanged.

The uncorrected spectral gain at 1.81 Å, 5%, is not large. But all that gain occurs in the peak of the emission time distribution, and is therefore a gain not only in time-integrated intensity, but also in peak intensity and in available time-of-flight resolution. Instruments for which the only parameter of interest is integrated intensity at a given wavelength will see a modest gain (5%). Instruments (such as chopper spectrometers) for which the appropriate metric is instantaneous (peak) intensity will see a more significant gain (10%). Resolution-driven instruments (such as powder diffractometers) with more complicated figures-of-merit which increase with either peak or integrated intensity and also increase with *decreasing* pulse width will benefit more strongly yet. By looking at the emission time distributions, we can see that the benefit of the single-crystal reflector-filter is even greater than what is indicated solely by the ratios of spectral intensities shown previously. The emission time distributions at 1.35 Å and 1.08 Å show similar effects.

Additionally, the emission time distribution comparison indicates that the action of either reflector-filter does not change the storage time of the moderator-reflector system—further support that the single-crystal reflector-filter gain arises from short-lived epithermal and fast neutron populations being returned to the moderator rather than from a thermal neutron population bouncing back and forth. Finally, we also see that while the polycrystalline reflector-filter does not change the storage time of the moderator-reflector system, it does suppress the peak intensity. From this observation we conclude that the intermediate-wavelength neutrons "lost" from the effects of the polycrystalline reflector-filter are not returned to the moderator, and perhaps subsequently emitted at long wavelengths; they are simply lost to the emitted neutron beam.

5. Conclusion

We have successfully demonstrated single-crystal and polycrystalline reflector-filters at LENS. Comparative time-of-flight study reveals that the single-crystal reflector-filter augments intermediate wavelength neutrons as hoped. Our measurements show that the intermediate wavelength neutrons allowed through the single-crystal reflector-filter do not detract from the cold neutron intensity, indicating that the reflector-filter benefit (whether single-crystal or polycrystalline) derives primarily from suppressing fast neutrons of no use to the instruments viewing that moderator.

The reflector-filters we tested in the LENS facility do not provide significant gains for LENS itself. In the first place, corundum, with its high capture cross section, is not an ideal reflector-filter material. In the second place, the LENS geometry, in order to permit easy access to and rapid exchange of test moderators, does not provide sufficient space for an optimized reflector-filter. Our experiments were intended to demonstrate the concept prior to optimizing a single-crystal reflector-filter for a particular application.

Acknowledgments

Research sponsored by Oak Ridge National Laboratory, managed by UT-Battelle, LLC, for the U.S. Department of Energy. Work performed at Oak Ridge National Laboratory is managed by UT-Battelle, LLC, under contract DE-AC05–00OR22725 for the U.S. Department of Energy.

Construction of LENS was supported by the National Science Foundation grants DMR-0220560 and DMR-0320627, the 21st Century Science and Technology fund of Indiana, Indiana University, and the Department of Defense. Operation of LENS is supported by Indiana University, and the experiments described in this paper were supported with funds from the US Department of Energy.

This work was supported by Readiness in Technical Base and Facilities (RTBF) which is funded by the Department of Energy's Office of National Nuclear Security Administration. It has benefited from the use of the Manuel Lujan, Jr. Neutron Scattering Center at Los Alamos National Laboratory, which is funded by the Department of Energy's Office of Basic Energy Sciences. Los Alamos National Laboratory is operated by Los Alamos National Security LLC under DOE Contract DE-AC52–06NA25396.

References

[1] M. Mocko, G. Muhrer, Fourth-generation spallation neutron target-moderator-reflector-shield assembly at the manuel lujan jr. neutron scattering center, Nucl. Instrum. Methods Phys. Res. Sect. A: Accel. Spectrom. Detect. Assoc. Equip. 704 (2013) 27–35, http://dx.doi.org/10.1016/j.nima.2012.11.103.

[2] G. Muhrer, Cold crystal reflector filter concept, arxiv.org/abs/1402.6314, February 2014.

[3] S.N. Ishmaev, I.P. Sadikov, A.A. Chernyshov, The Choice and Optimisation of a Moderator for a Pulsed Slow-Neutron Source, Technical Report IAE 2019, I.V. Kurchatov Institute of Atomic Energy, in Russian, 1970.

[4] S.N. Ishmaev, I.P. Sadikov, A.A. Chernyshov, The Choice and Optimisation of a Moderator for a Pulsed Slow-Neutron Source; Neutron Moderation in Ice and Polyethylene at Low Temperatures, Technical Report RL 75129, Rutherford Laboratory, includes English translations of IAE 2019 and IAE 1954 from the I. V. Kurchatov Institute of Atomic Energy, 1975.

[5] J.M. Carpenter, High intensity, pulsed thermal neutron source, US Patent 3,778,627, URL ⟨http://www.osti.gov/doepatents/biblio/4326397⟩, December 11, 1973.

[6] Y. Kiyanagi, Y. Ogawa, N. Kosugi, H. Iwasa, M. Furusaka, N. Watanabe, Further optimization of coupled liquid-hydrogen moderator for intense pulsed neutron source, in: G.S. Bauer, R. Bercher (Eds.), Proceedings of ICANS-XIII, the 13th Meeting of the International Collaboration on Advanced Neutron Sources,

vol. II, 1995, p. 654, URL ⟨http://www.neutronresearch.com/proc/?y=1995;n=1;o=0⟩.
[7] G. Muhrer, M.A. Hartl, L.L. Daemen, J. Ryu, Benchmark test of the effectiveness of a nitrogen cooled beryllium reflector-filter, Nucl. Instrum. Methods Phys. Res. Sect. A: Accel. Spectrom. Detect. Assoc. Equip. 578 (3) (2007) 463–469, http://dx.doi.org/10.1016/j.nima.2007.06.004.
[8] G. Muhrer, E. Pitcher, G. Russell, The neutron performance of a pre-moderated beryllium reflector-filter hydrogen moderator system for the Manuel Jr. Lujan Neutron Science Center, Nucl. Instrum. Methods Phys. Res. Sect. A: Accel. Spectrom. Detect. Assoc. Equip. 536 (1–2) (2005) 154–164, http://dx.doi.org/10.1016/j.nima.2004.07.201.
[9] C.M. Lavelle, D.V. Baxter, A. Bogdanov, V.P. Derenchuk, H. Kaiser, M. B. Leuschner, M.A. Lone, W. Lozowski, H. Nann, B.V. Przewoski, N. Remmes, T. Rinckel, Y. Shin, W.M. Snow, P.E. Sokol, Neutronic design and measured performance of the low energy neutron source (LENS) target moderator reflector assembly, Nucl. Instrum. Methods Phys. Res. Sect. A: Accel. Spectrom. Detect. Assoc. Equip. 587 (2–3) (2008) 324–341, http://dx.doi.org/10.1016/j.nima.2007.12.044.
[10] D.V. Baxter, J. Cameron, M. Leuschner, H. Meyer, H. Nann, W. Snow, LENS-a pulsed neutron source for education and research, Nucl. Instrum. Methods Phys. Res. Sect. A: Accel. Spectrom. Detect. Assoc. Equip. 542 (1–3) (2005) 28–31, http://dx.doi.org/10.1016/j.nima.2005.01.007.
[11] D.V. Baxter, J.M. Cameron, V.P. Derenchuk, C.M. Lavelle, M.B. Leuschner, M. A. Lone, H.O. Meyer, T. Rinckel, W.M. Snow, Status of the low energy neutron source at Indiana University, Nucl. Instrum. Methods Phys. Res. Sect. B: Beam Interact. Mater. Atoms 241 (1–4) (2005) 209–212, http://dx.doi.org/10.1016/j.nimb.2005.07.027.
[12] J.M. Carpenter, R. Kleb, T.A. Postol, R.H. Stefiuk, D.F.R. Mildner, The liquid hydrogen moderator on the ZING – P′ pulsed spallation neutron source, Nucl. Instrum. Methods Phys. Res. Sect. A 189 (2–3) (1981) 485–501, http://dx.doi.org/10.1016/0029-554X(81)90435-3.
[13] A.D. Taylor, E.J. Wood, J.A. Goldstone, J. Eckert, Lineshape analysis and filter difference method for a high intensity time-of-flight inelastic neutron scattering spectrometer, Nucl. Instrum. Methods Phys. Res. Sect. A 221 (2) (1984) 408–418, http://dx.doi.org/10.1016/0167-5087(84)90012-7.
[14] D.V. Baxter, J. Leung, H. Kaiser, S. Ansell, G. Muhrer, E.B. Iverson, P.D. Ferguson, Neutron moderator development research at the low energy neutron source, Phys. Procedia 26 (0) (2012) 117–123, http://dx.doi.org/10.1016/j.phpro.2012.03.016.
[15] K.F. Graham, J.M. Carpenter, Pulsed moderator studies using a time focussed crystal spectrometer, Nucl. Instrum. Methods Phys. Res. Sect. A 85 (2) (1970) 163–171, http://dx.doi.org/10.1016/0029-554X(70)90236-3.
[16] L. Crow, L. Robertson, H. Bilheux, M. Fleenor, E.B. Iverson, X. Tong, D. Stoica, W. T. Lee, The CG1 instrument development test station at the high flux isotope reactor, Nucl. Instrum. Methods Phys. Res. Sect. A: Accel. Spectrom. Detect. Assoc. Equip. 634 (Suppl. 1) (2011) S71–S74, http://dx.doi.org/10.1016/j.nima.2010.06.213.
[17] A. Freund, H. Friedrich, W. Nistler, R. Scherm, Neutron transmission properties of perfect silicon crystals, Nucl. Instrum. Methods Phys. Res. Sect. A: Accel. Spectrom. Detect. Assoc. Equip. 234 (1) (1985) 116–121, http://dx.doi.org/10.1016/0168-9002(85)90815-0.
[18] E.B. Iverson, D.V. Baxter, G. Muhrer, S. Ansell, R. Dalgliesh, F.X. Gallmeier, H. Kaiser, W. Lu, Enhancing neutron beam production with a convoluted moderator, Nucl. Instrum. Methods Phys. Res. Sect. A: Accel. Spectrom. Detect. Assoc. Equip. 762 (2014) 31–41, http://dx.doi.org/10.1016/j.nima.2014.04.047.
[19] D.C. Tennant, Performance of a cooled sapphire and beryllium assembly for filtering of thermal neutrons, Rev. Sci. Instrum. 59 (2) (1988) 380–381, http://dx.doi.org/10.1063/1.1140212.
[20] D.F.R. Mildner, M. Arif, C.A. Stone, R.K. Crawford, The neutron transmission of single-crystal sapphire filters, J. Appl. Crystallogr. 26 (3) (1993) 438–447, http://dx.doi.org/10.1107/s0021889893000433.
[21] D.F.R. Mildner, G.P. Lamaze, Neutron transmission of single-crystal sapphire, J. Appl. Crystallogr. 31 (1998) 835–840, http://dx.doi.org/10.1107/S0021889898005846.
[22] F. Cantargi, J.R. Granada, R.E. Mayer, Thermal neutron scattering kernels for sapphire and silicon single crystals, Ann. Nucl. Energy 80 (2015) 43–46, http://dx.doi.org/10.1016/j.anucene.2015.01.020.
[23] V.F. Sears, Neutron scattering lengths and cross sections, Neutron News 3 (3) (1992) 26–37, http://dx.doi.org/10.1080/10448639208218770.

Chapter 11

Summary

Experiments at modern facilities use less than one millionth of the neutrons created in neutron sources. Much of this inefficiency can be attributed to the moderator system. The imperfections of moderator systems originate from the highly isotropic slowing-down and thermalizing processes, premature leakage (fast neutron escape), neutron absorption and suboptimal geometric configurations. The inefficiency of moderator systems implies a potential gain in efficiency for neutron sources. My work, as presented in this thesis, contributes to the striving for more thermal neutrons in five ways (details outlined below):

- development and optimization for the ESS;
- conceptualization of the new ESS baseline moderator system;
- development of a method for describing neutron emission distributions from moderator systems;
- invention of a new advanced moderator concept, based on heavy metals; and
- experimental verification of existing conceptual advanced modereator ideas.

Chapter 7 shows that the **development and optimization for the ESS** and the **conceptualization of the new ESS baseline moderator system** combined are expected to yield a factor of 2 in increased thermal brightness and a factor of 2.5 in increased cold brightness over the old baseline concept suggested in the TDR.

Chapter 8 presents the **development of a method for describing neutron emission distributions from moderator systems**. The improved understanding of neutron emission distributions from moderator systems is expected to be valuable to the neutron-scattering community. In particular, since the method is applied to the ESS pancake and butterfly moderator concepts, this study is expected to contribute significantly to optimizing and increasing the efficiency of neutron extraction instruments at the ESS and thus enabling improved neutron exploitation in experiments and increases in the quality of experiments.

The **invention of a new advanced moderator concept, based on heavy metals** presented in Chapter 9 enables a new class of moderators: broad-spectrum moderators. Although such a moderator cannot immediately be applied at current facilities nor experimentally verified, such a moderator is theoretically viable. The possibility of

bispectral extraction is required for all neutron experiments at the ESS, due to a general interest in a broad spectrum of neutron energies from many of the proposed experiment classes. If a direct bispectral moderator is constructed in the future, this would increase the quality of experiments demanding a broad spectrum of neutrons.

The **experimental verification of existing conceptual advanced modereator ideas**, the single-crystal reflector filter, presented in Chapter 10, proves the viability of such a moderator and strongly indicates a potential regain of neutrons in the thermal energy range above the Bragg edge that are normally lost in a conventional reflector filter. The single-crystal reflector filter holds great promise and potential and is a good candidate for an advanced moderator concept at a future facility.

Glossary

- AccApp – International Topical Meeting on Nuclear Applications of Accelerators
- CERN – European Organization for Nuclear Research
- ESS – European Spallation Source
- HFIR – High-Flux Isotope Reactor
- IBR-2 – The pulsed reactor at JINR.
- ICANS – International Collaboration on Advanced Neutron Sources
- ICNS – International Conference on Neutron Scattering
- ILL – Institut Laue-Langevin (High Flux Reactor)
- IPNS – Intense Pulsed Neutron Source
- J-PARC – Japan Proton Accelerator Research Complex
- JINR – Joint Institute for Nuclear Research
- LANCE – Los Alamos Neutron Science Center (at LANL)
- LANL – Los Alamos National Laboratory
- LENS – Low Energy Neutron Source
- MCNP – Monte Carlo N-Particle
- MCNPX – Monte Carlo N-Particle eXtended
- MLNSC – Manuel Lujan, Jr. Neutron Scattering Center (at LANL)
- ORNL – Oak Ridge National Laboratory
- SINQ – Swiss Spallation Neutron Source
- SNS – Spallation Neutron Source (at ORNL)
- SSW – Source Surface Write (MCNPX method)
- TDR – (ESS) Technical Design Report
- TMR – Target-Moderator-Reflector system

Bibliography

[1] Enrico Fermi. Motion of neutrons in hydrogenous substances. *Ricerca Scientifica*, 7(2):13–52, 1936.

[2] C. Bryan R. A. Crone. High flux isotope reactor operation and capabilities. *ORNL*, 2013.

[3] G. Cicognani et. al. The yellow book. *Institut Laue-Langevin*, 2008.

[4] S. Peggs, editor. *ESS Technical Design Report*. April 2013.

[5] F.X. Gallmeier. Source terms for neutron beamline shielding and activation calculations. *SNS-107030700-DA0002-R00*, 2005.

[6] D. Filges, F. Goldenbaum. Handbook of Spallation Research: Theory, Experiments and Applications. *Wiley-VCH Verlag GmbH and Co. KGaA*, (2009).

[7] John M. Carpenter and William B. Yelon. *Neutron scattering*, volume 23, pages 99–196. Academic Press, Inc., 1986.

[8] J. M. Carpenter. *Neutron Production, Moderation, and Characterization of sources*. Essay by J. M. Carpenter (2004).

[9] G. Muhrer. Urban legends of thermal moderator design. *Nuclear Instruments and Methods in Physics Research A 664 (2012) 3847*.

[10] K. Batkov, A. Takibayev, L. Zanini and F. Mezei. Unperturbed moderator brightness in pulsed neutron sources. *Nucl. Inst. Meth.*, 729(0):500, 2013.

[11] D. Lyngh. Target project change request - ess-0026843. *ESS report*, Approved Mar. 2015.

[12] E. Klinkby F. Mezei T. Schönfeldt A. Takibayev L. Zanini, K. Batkov. Neutronic design and optimization of ess moderators. *ESS report*, Jan. 2015.

[13] L. Zanini. Latest neutronic results for the ess moderators. *ESS report*, Feb. 2015.

[14] P. Willendrup, E. Knudsen, E. Farhi and K. Lefmann, (2011). User and Programmers Guide to the Neutron Ray-Tracing Package McStas, Version 1.12c.

[15] L. S. Waters, G. W. McKinney, J. W. Durkee, M. L. Fensin, J. S. Hendricks et. al. The MCNPX Monte Carlo radiation transport code. *AIP Conf.Proc.*, 896:81, 2007.

[16] E. Klinkby et al. Developing an interface between MCNPX and McStas for simulation of neutron moderators. *Nuclear Instruments & Methods In Physics Research A*, 700:106, (2013).

[17] R. Brun, F. Rademakers. ROOT - An Object Oriented Data Analysis Framework. *Nuclear Instruments and Methods A*, 389:81, 1997.

[18] N. Borghi, K., and Batkov. Abstract programming interface for MCTAL files. In *ICANS XXI*, 2014.

[19] T. Schönfeldt et. al. Optimization of cold neutron beam extraction at ESS. *AccApp Conf. Proc. (2013).*

[20] T. Schönfeldt, K. Batkov, E. B. Klinkby, B. Lauritzen, F. Mezei, A. Takibayev, P. K. Willendrup ,L. Zanini. A model for non-thermalized neutron spectra emitted from para-hydrogen. *ICANS XXI, conf. proc.*, 2014.

[21] T. Kai, M. Harada, M. Teshigawara, N. Watanabe, and Y. Ikeda. Coupled hydrogen moderator optimization with ortho/para-hydrogen ratio. *Nuclear Instruments and Methods A 523 (2004) 398414.*

[22] T. Schönfeldt et al. Functional description of the thermal and cold brightness distribution at ESS. *Submittet to Journal of Neutron Research*, 2016.

[23] F. Mezei. Instrumentation Concepts: Advances by Innovation and Building on Experience, The ESS Project Vol. II, New Science and Technology for the 21st Century. 2002.

[24] C. Zendler, K. Lieutenant, D. Nekrassov, L. D. Cussen and M. Strobl. Bi-spectral beam extraction in combination with a focusing feeder. *Nucl. Instr. Meth. Phys. Res. A*, 2013.

[25] H. Jacobsen, K. Lieutenant, C. Zendler and K. Lefmann. Bi-spectral extraction through elliptic neutron guides. *Nucl. Instr. Meth. Phys. Res. A*, 2013.

[26] L. L. Daemen, G. J. Russell and E. J. Pitcher. Moderator Materials and Neutronic Performance. *ICANS XII Conf. Proc.*, 1993.

[27] L. A. Charlton T. Tahara Y. Kiyanagi J. A. Crabtree E. B. Iverson, B. D. Murphy and A. T. Lucas. Hydrogen-water composite moderators at pulsed spallation neutron sources. In *Proceedings of the 4th International Topical Meeting on Nuclear Applications of Accelerator Technology, AccApp'00*, pages 101–108, 2000.

[28] T. Schönfeldt, K. Batkov, E.B. Klinkby, B. Lauritzen, F. Mezei, G. Muhrer, E. Pitcher, A. Takibayev, P.K. Willendrup, L. Zanini. Broad spectrum moderators and advanced reflector filters using (208)Pb. *Nuclear Instruments and Methods in Physics Research A (2015) 769.*

[29] M. Leuschner H. Meyer H. Nann W. Snow D.V. Baxter, J. Cameron. Lens-a pulsed neutron source for education and research. *Nucl. Instrum. Methods Phys. Res. Sect. A*, 2005.

[30] V.P. Derenchuk C.M. Lavelle M.B. Leuschner M.A. Lone H.O. Meyer T. Rinckel W.M. Snow D.V. Baxter, J.M. Cameron. Status of the low energy neutron source at indiana university. *Nucl. Instrum. Methods Phys. Res. Sect. B*, 2008.

[31] G. Muhrer. Cold Crystal Reflector Filter Concept. *Arxiv*, arXiv:1402.6314, 2014.

[32] https://europeanspallationsource.se/article/building-heart-ess-spain. *European Spallation Source*.

[33] H. Bethe. Zur theorie des durchgangs schneller korpuskularstrahlen durch materie. *Annalen der Physik*, 1930.

[34] B.R. Martin and G. Shaw. Particle physics. *Wiley*, 1992.

[35] E Pitcher. Private communication. 2016.

[36] M. Villa J. S. Beaumont, M. P. Mellor and M. J. Joyce. High-intensity power-resolved radiation imaging of an operational nuclear reactor. *Natuer commnuications*, 2015.

[37] ESS. https://europeanspallationsource.se/cryogenics.

[38] K. Andersen. Private communication. 2016.

[39] F. Mezei. *Very High Reflectivity Supermirrors and Their Applications*. Proc. SPIE 0983, Thin Film Neutron Optical Devices: Mirrors, Supermirrors, Multilayer Monochromators, Polarizers, and Beam Guides, 10 (1989).

[40] K. Yoshida. Neutronchoppers. *US 7820992 B2*, 2007.

[41] K. Andersen. Optimisation of instrument performance for pancake moderators. *Internal ESS report (Request from: ken.andersen@esss.se)*, 2014.

[42] K. Andersen. Instrument optimisation for the first and second moderator assemblies. *Internal ESS report (Request from: ken.andersen@esss.se)*, 2014.

[43] K. Andersen. Pancake and butterfly moderators. *Internal ESS report (Request from: ken.andersen@esss.se)*, 2015.

[44] K. Skold and D. L. Price. Neutron scattering. *Academic Press*, 1986.

[45] G. T. Seaborg. Interaction of fast neutrons with lead. *PhD dissertation, University of California, Berkeley.*, (1937).

[46] G. T. Seaborg and E. Seaborg. Adventures in the atomic age: From watts to washington. *Farrar, Straus and Giroux*, 2001.

[47] G. T. Seaborg. Scientific and luminary biography. *Argonne National Laboratory*, 2013.

[48] O. Hahn. From the natural transmutations of uranium to its artificial fission. *Nobel Lecture*, (1946).

[49] Ipns: Intense pulsed neutron source (operation: 1982 - 2008). *Argonne Accelerator History Document Collection*, 2013.

[50] H.W. Bertini M.P. Guthrie, R.G. Alsmiller Jr. Calculation of the capture of negative pions in light elements and comparison with experiments pertaining to cancer radiotherapy. *Nuclear Instruments and Methods, 66*, 1968.

[51] H. W. Bertini. Intra-nuclear-cascade calculation of the secondary nucleon spectra from nucleon-nucleus interactions in the energy range 340 to 2900 mev and comparisons with experiment. *Phys. Rev. 188*, 1969.

[52] H. W. Bertini and P. Guthrie. Results from medium-energy intra-nuclear-cascade calculation. *Nucl. Phys. A169*, 1971.

[53] G. Mank J. C. David S. Leray D. Filges M. U. Khandaker, A. Mengoni and Y. Yariv. Benchmark of nuclear spallation models . *nternational Atomic Energy Agency, Vienna, Austria.*

[54] N. Watanabe. Neutronics of pulsed spallation neutron sources. *Reports on Progress in Physics*, 66:339381, 2003.

[55] G.S. Bauer. Physics and technology of spallation neutron sources. *Nuclear Instruments and Methods in Physics Research A 463 (2001) 505543.*

[56] J. W. Hilborn J. C. D. Milton W. A. Gibson E. E. Gross J. S. Fraser, R. E. Green and A. Zucker. Neutron production in thick targets bombarded by high energy protons. *Physics in Canada*, 21(2):17–18, 1965.

[57] K. S. Krane. Introduction to nuclear phyiscs. *John Wiley and sons, inc.*, 1988.

[58] T. Broome. High power targets for spallation sources. *Rutherford Appleton Laboratory*, 1988.

[59] S. Hasegawa K. Ohtsu T. Uehara Y. Kawakami H. Sakurayama F. Maekawa M. Futakawa & I. Ushijima T. Aso, H. Tatsumoto. Commissioning of the cryogenic hydrogen system in j-parc: Preliminary operation by helium gas. *ICEC 22-ICMC conf. proc.*, 2008.

[60] J.R. Alonso. Status report on the spallation neutron source (sns) project. *ORNL report.*

[61] V.F. Sears. Special feature section of neutron scattering lengths and cross sections of the elements and their isotopes. *Neutron News*, 1992.

[62] A. Takibayev, (May 2015). ESS master deck: TSM141108.

[63] J. S. Hendricks, G. W. McKinney, T. A. Wilcox, M. R. James . MCNPX 2.7.4 Extensions. *Los Alamos National Security, LLC.*, (2012).

[64] B Guttek. Present state of the ESS tantalum target. *ICANS XIII conf. proc.*

[65] M. Ragheb. Neutron collision theory. *NPRE 402 ME 405 Nuclear Power Engineering - http://mragheb.com*, 2006.

[66] M. B. Chadwick et. al. ENDF/B-VII.1 Nuclear Data for Science and Technology: Cross Sections, Covariances, Fission Product Yields and Decay Data. 2011.

[67] R. Pynn. Introduction to neutron scattering, ch. 2. *Springer*, 1998.

[68] M. Born. Quantenmechanik der stossvorgnge. *Zeitschrift für Physik*, 1926.

[69] L. Van Hove. Correlations in space and time and born approximation scattering in systems of interacting particles. *Physical Review 95*, 1954.

[70] K. Leffman. Neutron Scattering: Theory, Instrumentation, and Simulation. *Lecture notes in neutron scattering, Niels Bohr Institute (2010).*

[71] C. G. Windsor. Pulsed neutron scattering. *Taylor and Francis*, 1981.

[72] A special issue on neutron scattering. *Physics Today*, 1985.

[73] G. L. Squires. Introduction to thermal neutron scattering. *Cambridge University Press*, 1978.

[74] J. Liouville. Source terms for neutron beamline shielding and activation calculations. *Journ. de Math., 3, 349*, 1838.

[75] P. Debye. Zur theorie der spezifischen waerme. *Annalen der Physik*, 1912.

[76] C. Kittel. Introduction to solid state physics, 8th edition. *Wiley*, 2004.

[77] P. Willendrup, E. Farhi, E. Knudsen, U. Filges, K. Lefmann. McStas: Past, present and future. *J. Neutr. Res.*, 17:35–43, (2014).

[78] W. Lu G. Muhrer D.V. Baxter E.B. Klinkby F.X. Gallmeier, E.B. Iverson. Simulating convoluted moderators. *AccApp11 Conf. Proc.*, 2013.

[79] D. V. Baxter, S. Ansell, P. D. Ferguson, F. X. Gallmeier, E. B. Iverson, H. Kaiser , W. Lu, G. Muhrer, T. C. Rinckel, T. Steinbach. Moderators at LENS: Performance and Development Research. *Physics Procedia 26 (2012) 153 160.*

[80] H. Tatsumoto T. Aso K. Ohtsu H. Takada M. Futakawa & Y. Ikeda M. Teshigawara, M. Harada. Experimental verification of equilibrium para-hydrogen levels in hydrogen moderators irradiated by spallation neutrons at j-parc. *Nuclear Instruments and Methods in Physics Research B*, 2016.

[81] J. M. Carpenter E. B. Iverson. Kinetics of irradiated liquid hydrogen. *Meeting of the Collaboration on Advanced Cold Moderators Conf. Proc.*, 2002.

[82] K.B. Grammer et al. Measurement of the scattering cross section of slow neutrons on liquid parahydrogen from neutron transmission. *Phys. Rev. B*, 2015.

[83] E Segr. Enrico fermi, physicist. *University of Chicago Press*, 1970.

[84] E. Fermi. Artificial radioactivity produced by neutron bombardment. *Nobel Lecture*, (1938).

[85] K. Batkov. Butterfly moderator studies. *Internal ESS report (Request from: konstantin.batkov@esss.se)*, 2015-2016.

[86] E. J. Pitcher J. D.Court G. J. Russell, P. D. Ferguson. Split-target neutronics and the mlnsc spallation target system. *AccApp Conf. Proc. (1996).*

[87] R. Golub, D.J. Richardson, and S.K. Lamoreaux. *Ultra-Cold Neutrons.* Taylor & Francis, 1991.

[88] V. Nesvizhevsky, H. G. Börner, A. K. Petukhov, H. Abele, S. Baeßler, F. J. Rueß, T. Stöferle, A. Westphal, A. M. Gagarski, G. A. Petrov and A. V. Strelkov. Quantum states of neutrons in the Earth's gravitational field. *Nature 415, 297-299 (2002).*

[89] G Muhrer S. Ansell R. Dalgliesh F.X. Gallmeier H. Kaiser E. Iverson, D. Baxter and W Lu. Target project change request - ess-0026843. *Nucl. Instr. Meth. A*, 2014.

[90] F. X. Gallmeier, E. B. Iverson, W. Lu, G. Muhrer, D. V. Baxter, E. Klinkby. Simulating Convoluted Moderators. *AccApp conf. proc. (2013).*

[91] E. B. Iverson, D. V. Baxter, G. Muhrer, S. Ansell, R. Dalgliesh, F. X. Gallmeier, H. Kaiser, W. Lu. Enhancing neutron beam production with a convoluted moderator. *Nuclear Instruments and Methods in Physics Research A 762, (2014), 3141.*

[92] J.M. Carpenter, R. Kleb, T.A. Postal, R.H. Stefiuk, D.F.R. Mildner. The liquid hydrogen moderator on the ZING-P pulsed spallation neutron source. *Nuclear Instrument and Methods A*, 189:485, 1981.

[93] E.J. Pitcher G. Muhrer and G.J. Russell. Implementation of the beryllium reflector filter concept in the lansce 1l target mark-iii upgrade. *ICANS-XVII*, 2005.

[94] E.B.Iverson M.Mocko D.V. Baxter Th.Hügle F.X.Gallmeier E.B.Klinkby G. Muhrer, T.Schönfeldt. Demonstration of a single-crystal refector-filter for enhancing slow neutron beams. *Nucl. Instr. Meth. A*, 2016.

[95] S. Ikeda, J.M. Carpenter. Wide-energy-range, high-resolution measurements of neutron pulse shapes of polyethylene moderators. *Nuclear Instrument and Methods A*, 239(3):536, 1985.

[96] J.M. Carpenter. Gaussian and Top-hat Broadened I-C Pulse Shape Functions, and a Conjecture. *ICANS XIX, conf. proc.*, 8. 12. March 2010.

[97] V. Ananiev, A. Belyakov, M. Bulavin, E. Kulagin, S. Kulikov, K. Mukhin, T. Petukhova, A. Sirotin, D. Shabalin, E. Shabalin, V. Shirokov and A. Verhoglyadov. The worlds first pelletized cold neutron moderator at a neutron scattering facility. *Nuclear Instruments and Methods in Physics Research B (2014) 320.*

[98] A. T. Lucas, G. S. Bauer, and C. D. Sulfredge. A pelletized solid methane moderator for a medium-to-high power neutron source. In *Proceedings of ICANS-XIII, the 13th Meeting of the International Collaboration on Advanced Neutron Sources*, volume II, pages 644–653. Paul Scherrer Institut, 1995.

[99] W. Lu P.D. Ferfuson R.K. Crawford F.X. Gallmeier, E.B. Iverson. Sns second target stating moderator performance update. *Conf. Proc. ICANS XIX*, 2010.

[100] F. Mezei, and M. Russina. Neutronenoptische Bauelementenanornung zur gezielten spektralen Gestaltung von Neutronenstrahlen oder Pulsen. German Patent: 102 03 591.1 (US 7030397 B2). 2002.

[101] T. Kai M. Teshigawara N. Watanabe, M. Harada and Y. Ikeda. Optimization of coupled and decoupled hydrogen moderators for a short-pulse spallation source. *Journal of Neutron Research*, 2003.

[102] T. Kai, M. Harada, M. Teshigawara, N. Watanabe, Y. Ikeda. Coupled hydrogen moderator optimization with ortho/para hydrogen ratio. *Nuclear Instruments and Methods A*, 523:398, 2004.

[103] F. X. Gallmeier. Moderator Studies for a SNS Short-Pulse Second Target Station. *SNS report: STS03-31-TR0004 - R00 (2013)*.

[104] A. Takibayev K. Batkov E. Klinkby E. Pitcher F. Mezei, L. Zanini and T. Schönfeldt. Low dimensional neutron moderators for enhanced source brightness. *Arxiv*, 2014.

[105] E. Klinkby F. Mezei E. Pitcher T. Schönfeldt A. Takibayev L. Zanini, K. Batkov. Thermal and cold moderators for ess. *Conf. Proc. AccApp15*, 2015.

[106] E. Klinkby F. Mezei E. Pitcher T. Schönfeldt A. Takibayev L. Zanini, K. Batkov. Moderator configuration options for ess. *Conf. Proc. ICANS XXI*, 2014.